DESIGN AND FABRICATION OF NOVEL MICROFLUIDIC SYSTEMS FOR MICROSPHERE GENERATION

A Thesis Submitted to the College of

Graduate Studies and Research

In Partial Fulfillment of the Requirements

For the Degree of Doctor of Philosophy

In the Division of Biomedical Engineering

University of Saskatchewan

Saskatoon, Canada

By

KI-YOUNG SONG

Keywords: uniformity, size-controllability, microsphere, axiomatic design theory

PERMISSION TO USE

In presenting this thesis in partial fulfilment of the requirements for a Postgraduate degree from the University of Saskatchewan, I agree that the Libraries of this University may make it freely available for inspection. I further agree that permission for copying of this thesis in any manner, in whole or in part, for scholarly purposes may be granted by the professor or professors who supervised my thesis work or, in their absence, by the Chair of the Division or the Dean of the College in which my thesis work was done. It is understood that any copying or publication or use of this thesis or parts thereof for financial gain shall not be allowed without my written permission. It is also understood that due recognition shall be given to be and to the University of Saskatchewan in any scholarly use which may be made of any material in my thesis.

Requests for permission to copy or to make other use of material in this thesis in whole or part should be addressed to:

Head of the Division of Biomedical Engineering

University of Saskatchewan

Saskatoon, Saskatchewan CANADA S7N 5A9

ABSTRACT

In this thesis, a study of the rational design and fabrication of microfluidic systems for microsphere generation is presented. The required function of microfluidic systems is to produce microspheres with the following attributes: (i) the microsphere size being around one micron or less, (ii) the size uniformity (in particular coefficient of variation (CV)) being less than 5%, and (iii) the size range being adjustable as widely as possible.

Micro-electro-mechanical system (MEMS) technology, largely referring to various micro-fabrication techniques in the context of this thesis, has been applied for decades to develop microfluidic systems that can fulfill the foregoing required function of microsphere generation; however, this goal has yet to be achieved. To change this situation was a motivation of the study presented in this thesis.

The philosophy behind this study stands on combining an effective design theory and methodology called Axiomatic Design Theory (ADT) with advanced micro-fabrication techniques for the microfluidic systems development. Both theoretical developments and experimental validations were carried out in this study. Consequently, the study has led to the following conclusions: (i) Existing micro-fluidic systems are coupled designs according to ADT, which is responsible for a limited achievement of the required function; (ii) Existing micro-fabrication techniques, especially for pattern transfer, have difficulty in producing a typical feature of micro-fluidic systems - that is, a large overall size (~ mm) of the device but a small channel size (~nm); and (iii) Contemporary micro-fabrication techniques to the silicon-based microfluidic system may have reached a size limit for microspheres, i.e., ~1 micron.

Through this study, the following contributions to the field of the microfluidic system technology have been made: (i) Producing three rational designs of microfluidic systems, device 1 (perforated silicon membrane), device 2 (integration of hydrodynamic flow focusing and crossflow principles), and device 3 (liquid chopper using a piezoelectric actuator), with each having a distinct advantage over the others and together having achieved the requirements, size uniformity (CV $\leq$ 5%) and size controllability (1-186 μm); (ii) Proposing a new pattern transfer technique which combines a photolithography process with a direct writing lithography process (e.g., focused ion beam process); (iii) Proposing a decoupled design principle for micro-fluidic

systems, which is effective in improving microfluidic systems for microsphere generation and is likely applicable to microfluidic systems for other applications; and (iv) Developing the mathematical models for the foregoing three devices, which can be used to further optimize the design and the microsphere generation process.

ACKNOWLEDGEMENTS

I would like to take this opportunity to express my sincere gratitude to my supervisor Professor Chris W.J Zhang, who provided me with an extraordinary amount of patience, encouragement, and enthusiasm during the development of the study. His invaluable guidance, stimulating discussion, dedication and expertise were immersed into any little progress of this study. His financial support was extremely important for the continuity of my study.

I would like to thank my co-supervisor Professor Madan M. Gupta for his invaluable support, guidance, suggestion and wisdom throughout my Ph.D. study. I would like to extend special thanks to the members of the advisory committee: Professor James D. Bugg, Professor Satyanarayan Panigrahi, and Dr. Qiang Liu. Their valuable advice and constructive suggestions have greatly improved the present work.

I would like to thank Professor Daniel X.B. Chen and Dr. Ramaswami Sammynaiken for kind offering of their laboratories to perform experiments.

My research was made possible by the generous support of the Natural Sciences and Engineering Research Council (NSERC) through a discovery grant program and the Division of Biomedical Engineering through the graduate scholarship.

DEDICATED TO

My wife Manika

My daughter Nara

My families in Korea and Thailand

TABLE OF CONTENTS

LIST OF FIGURES

LIST OF TABLES

1. INTRODUCTION

1.1. Trend of Drugs

A drug, in the context of medication, is a pharmaceutical product consumed externally or internally to diagnose, mitigate, treat, or prevent diseases. Also, a drug can affect the structure and thus, the function of the body. The drug is usually synthesized outside an organism, but introduced into the organism to initiate its action [1].

Traditionally, drugs come from one of several classes of small molecules such as amino acids, steroids, and small lipids. Such molecules are relatively easy to put into tablets and generally are not destroyed by acids in the stomach before they can be absorbed [2]. To date, modern medicine relies heavily on synthetically or chemically produced drugs to treat or prevent diseases. However, a special category of therapeutics and diagnostics, referred to as protein-based drugs, is promising [3]. The protein-based drugs contain naturally occurring proteins that perform the same function as the proteins in the human body. The new drugs can minimize the side effects caused by conventional chemically synthesized drugs.

1.2. Protein-Based Drug Delivery System (DDS)

Proteins are bio-molecules essential for ensuring the functions of living cells that make up all living organisms. A protein has a specific function which is determined by the structure of the protein and its environment. Some proteins are involved in structural support, while others are involved in defense against germs through bodily movement. With the great versatility and potential of phenotype, protein-based drugs provide two unique advantages. First, a protein-based drug performs the same function as already naturally-occurring proteins in the body. Second, a protein-based drug can be extremely target specific.

Related to the second unique advantage of protein-based drugs, there is a promising avenue to understand the structure of a protein and to design it so that it can play a different specific function in a different environment. For example, Cytokines activate immune system cells to carry out different immune functions. Hormones can elevate levels of certain hormones such as estrogen during menopause or growth deficiency, and they can also be used to treat certain diseases such as diabetes or unhealthy conditions such as infertility. Clotting factors regulate the clotting of blood, thereby alleviating hemophilia. Vaccines stimulate the immune system, producing specific antibodies to prevent or treat diseases. Monoclonal antibodies mark specific foreign materials, such as cancer cells, disease-causing bacteria, and viruses, for removal or destruction by other components of the immune system; they are also effective diagnostic tools for many specific genetic diseases and conditions such as pregnancy [3]. Below is a list of types of proteins and their functions [4]:

Antibodies - defend the body from antigens (foreign invaders). One way antibodies destroy antigens is by immobilizing antigens, so that anitgens can be destroyed by white blood cells.

Contractile Proteins - regulate muscle contraction and movement. Examples of the contractile proteins are actin and myosin.

Enzymes - facilitate biochemical reactions. They are often referred to as catalysts because they speed up chemical reactions. Examples include lactase and pepsin. Lactase breaks down the sugar lactose which is found in milk. Pepsin works in the stomach to break down proteins in food.

Hormonal Proteins - help to coordinate certain bodily activities as messenger proteins. Examples include insulin, oxytocin, and somatotropin. Insulin regulates glucose

metabolism by controlling the blood-sugar concentration. Oxytocin stimulates contractions in females during childbirth. Somatotropin is a growth hormone that stimulates protein production in muscle cells.

Structural Proteins – are fibrous and stringy substances which provide a protective or supportive role. Examples include keratin, collagen, and elastin. Keratins strengthen protective coverings such as hair, quills, feathers, horns, and beaks. Collagens and elastin provide a support for connective tissues such as tendons and ligaments.

Storage Proteins - act in storing amino acids. Examples include ovalbumin and casein. Ovalbumin is found in egg whites, and casein is a milk-based protein.

Transport Proteins - are carrier proteins which move molecules from one place to another around the body. Examples include hemoglobin and cytochromes. Hemoglobin transports oxygen through the blood. Cytochromes operate in the electron transport chain as electron carrier proteins.

There are already more than 75 protein therapeutics in the marketplace today and over 180 protein candidates waiting to be released in the market, leading to combined sales of $31.7 billion in 2003 in various research fields such as peptide mimetics, phage display, and antibody conjugates [5]. The field of peptide mimetics is one of the most active areas today for the drug discovery strategy. A molecule that mimics the biological activity of a peptide is called a peptide mimetic. Moreover, engineered peptide sequences can be used to substitute for the entire molecule. The peptide mimetic overcomes the poor bioavailability and short duration of action that characterize a real peptide. Furthermore, peptide mimetic is much more cost effective to produce than peptides [6]. Phage display, invented in 1985 by George Smith, has drawn attention over the last two decades in studying the interactions of protein-protein, protein-peptide, and

protein-DNA; it involves displaying peptides or proteins on the surface of bacteriophage (or phage) which is a virus that infects only bacteria. A new generic material is inserted into the phage gene to produce a new protein or peptide during the phage display process, as shown in Figure 1.1. This display has led to a variety of rational methods to select the protein of choice for many applications such as mapping epitopes of monoclonal and polyclonal antibodies, generating immunogenes, identifying peptide ligands, defining substrate sequences, directing evolution of proteins, isolating high-affinity antibodies, and defining protein-protein interactions [7]. Variations on the display technology (including yeast and ribosomal display) allow for optimization of protein drugs by improving their stability and ease of delivery [5].

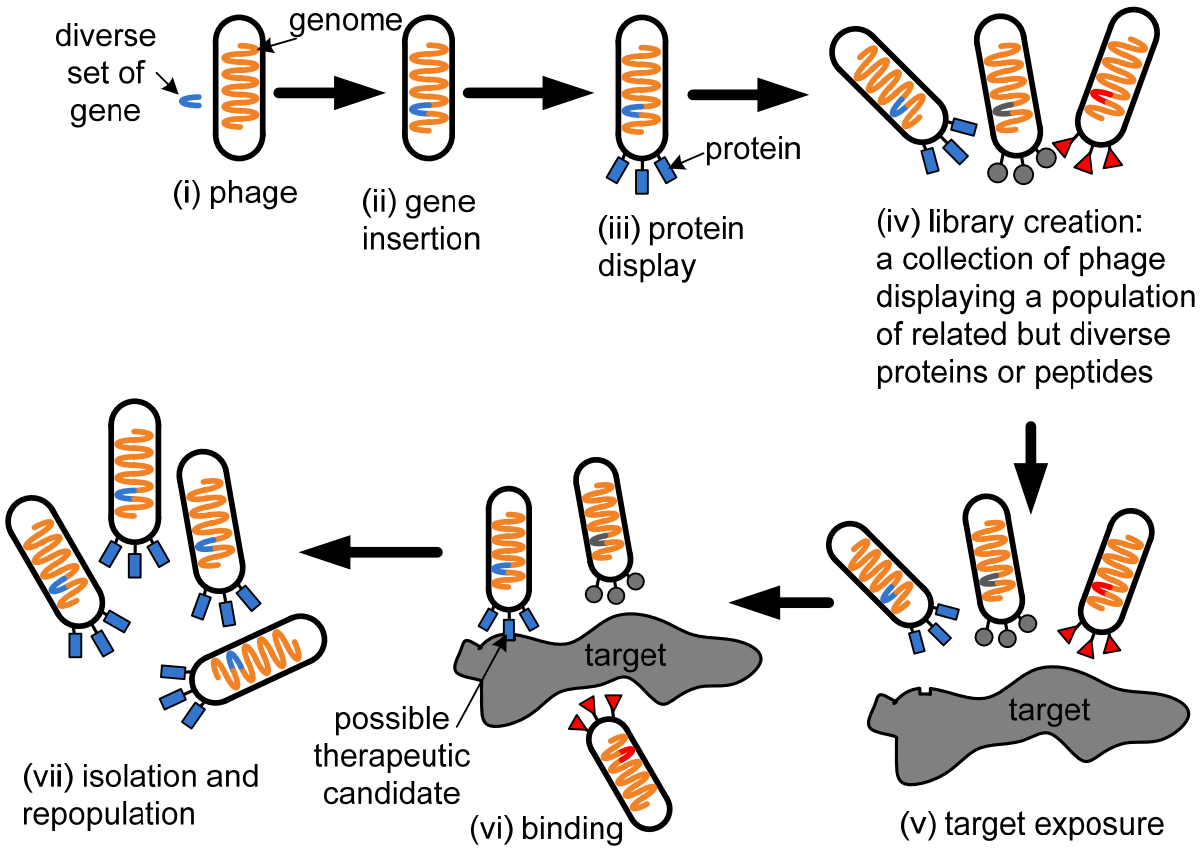

Figure 1.1 Schematic diagram of the process of phage display technique in drug discovery.

One of the potential therapeutic activities of peptides and proteins is antibody conjugate (drug-protein conjugate) as an anticancer agent. The interest of using the conjugated antibodies is increasing since the defenses of unconjugated antibodies are insufficient to defeat the tumors. Antibodies against certain cancer-specific ligands are considered as protein anticancer drugs for delivering a drug payload as illustrated in Figure 1.2.

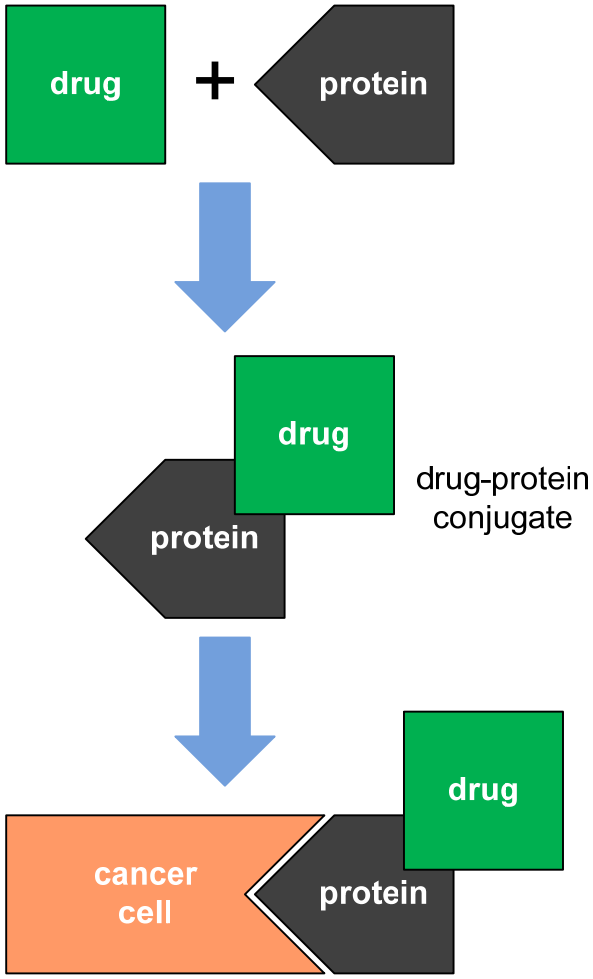

Figure 1.2 Schematic diagram of targeted drug delivery through drug-protein conjugate (antibody conjugate). The cancer cell is killed by the drug after the protein recognizes the cancer cell.

Furthermore, information from the human genome project, together with advances in proteomics, promises further progress in the identification and development of peptide- and protein-based anticancer drugs [8].

1.3. Limitation of Protein Drugs

Although these new drugs have revealed advantages for medical treatments, such as site specificity and minimal toxicity by reducing the consumption of the conventional chemically synthesized drugs, proteins present a challenge for pharmacologists. Proteins are large and bulky, which can prevent them from accessing the sites of interest. They are also unstable, lasting only in short-term storage. Once injected, proteins degrade rapidly. Additionally, proteins are very sensitive to the acid and digestive enzymes of the gut, which prevents them from being administered orally [2].

1.4. Drug Encapsulation: Microspheres

Since there is difficulty in oral administration, protein and peptide are normally injected into the blood stream. However, they easily degrade *in vivo,* causing short half-life time. In order to prevent the protein from degradating, polymer encapsulation of proteins by emulsion has been developed [9]. Emulsion produces a dispersed system of two (or more) insoluble liquids and is an important phenomenon widely used in the formation of foods, cosmetics, and pharmaceuticals. In an emulsion one liquid disperses in the other liquid, yielding two types of emulsions depending on which one of the two is the dispersed phase. For instance, two such fluids are water and oil, and two types of emulsions are thus oil-in-water (O/W) and water-in-oil (W/O). Microspheres are the droplets in micro-sizes that result from the emulsion of immiscible liquids [10-13]. Biodegradable and biocompatible polymeric microspheres created by microencapsulation techniques have brought researchers high attention for years, resulting in the

increased use of proteins and peptides as active therapeutic agents in pharmaceutical applications. These active agents should not be administered to the digestive tract because proteins lose their potency in such environments. The microsphere encapsulates the therapeutic agents and makes friendly environments for the agents; thus the agents stay stable over a prolonged period and are released as the microsphere degrades with very minimal toxicity [14-19]. The release of therapeutic agents from the polymer formulation occurs in three phases: burst effect, formation of pores in the matrix, and polymer degradation [20-22]. Since the release of the active agents in the microsphere is mainly controlled by the polymer degradation, a relatively lower molecular mass polymer is most appropriate for rapid degradation. As well, the ratio of monomers in a polymer changes the degradation rate [23, 24].

1.5. Materials and Formation of Drug Encapsulation

1.5.1. Poly(Lactic-co-Glycolic Acid) (PLGA)

Poly(lactic-co-glycolic acid) (PLGA) is a copolymer which is preferred in a host of therapeutic devices for its biodegradability and biocompatibility. PLGA is synthesized by means of random ring-opening co-polymerization of two different monomers, the cyclic dimers (1,4-dioxane-2,5-diones) of glycolic acid and lactic acid. During polymerization, successive monomeric units of glycolic or lactic acid are linked together in PLGA by ester linkages, thus yielding a linear, aliphatic polyester as a product [25].

PLGA is degraded by the hydrolysis of its ester linkages in the presence of water, so PLGA has been a successful biodegradable polymer because it produces the original monomers, lactic acid and glycolic acid, during hydrolysis in the body. Since the monomers are by-products of various metabolic pathways in the body which effectively deal with the two monomers, minimal systemic toxicity is associated with using PLGA for drug delivery or biomaterial

applications yielding biocompatibility [25-27]. Also, the possibility to tailor the polymer degradation time by altering the ratio of the monomers used during synthesis has made PLGA a common choice for producing a variety of biomedical devices such as grafts, sutures, implants and prosthetic devices [28]. The higher the content of glycolide units, the lower the time required for degradation. The physical characteristics of PLGA include strength, hydrophobicity, and pliability. All these features make PLGA desirable for use in drug delivery applications [29].

1.5.2. Concept of Conventional Drug Encapsulation

Microspheres have been prepared by various techniques that demonstrate partly competing and partly complementary characteristics. Conventionally, emulsion can be simply realized by three main approaches: solvent extraction / evaporation, phase separation and spray-drying by mixers, colloid mills, homogenizers and sonicators with immiscible fluids (dispersed phase and continuous phase) [24, 29-39]. The solvent extraction / evaporation method is commonly used because it requires neither elevated temperatures nor phase separation inducing agents. Controlled particle sizes in the nano- to micrometer range can be achieved, but careful selection of encapsulation conditions and materials is needed to yield high encapsulation efficiencies and low residual solvent content. In order to encapsulate drugs, two immiscible solutions are prepared. The first solution is considered as the dispersed phase including polymer and drugs dissolved in a volatile liquid, and the second solution is considered as the continuous phase, including an emulsifier or stabilizer dissolved in a stable liquid. Drug encapsulation by solvent extraction / evaporation with the two solutions basically consists of four major steps: (i) dissolution or dispersion of the bioactive compound often in an organic solvent containing the matrix forming material; (ii) emulsification of this organic phase in a second continuous (frequently aqueous) phase immiscible with the first one; (iii) extraction of the solvent from the

dispersed phase by the continuous phase, which is optionally accompanied by solvent evaporation, either one transforming the droplets into solid microspheres; (iv) harvesting and drying of the microspheres as shown in Figure 1.3 [30]. Increasing the concentration of the dispersed phase increases the frequency of collisions in, and the viscosity of a polymer solution. A higher rate of agitation results in smaller microspheres [38].

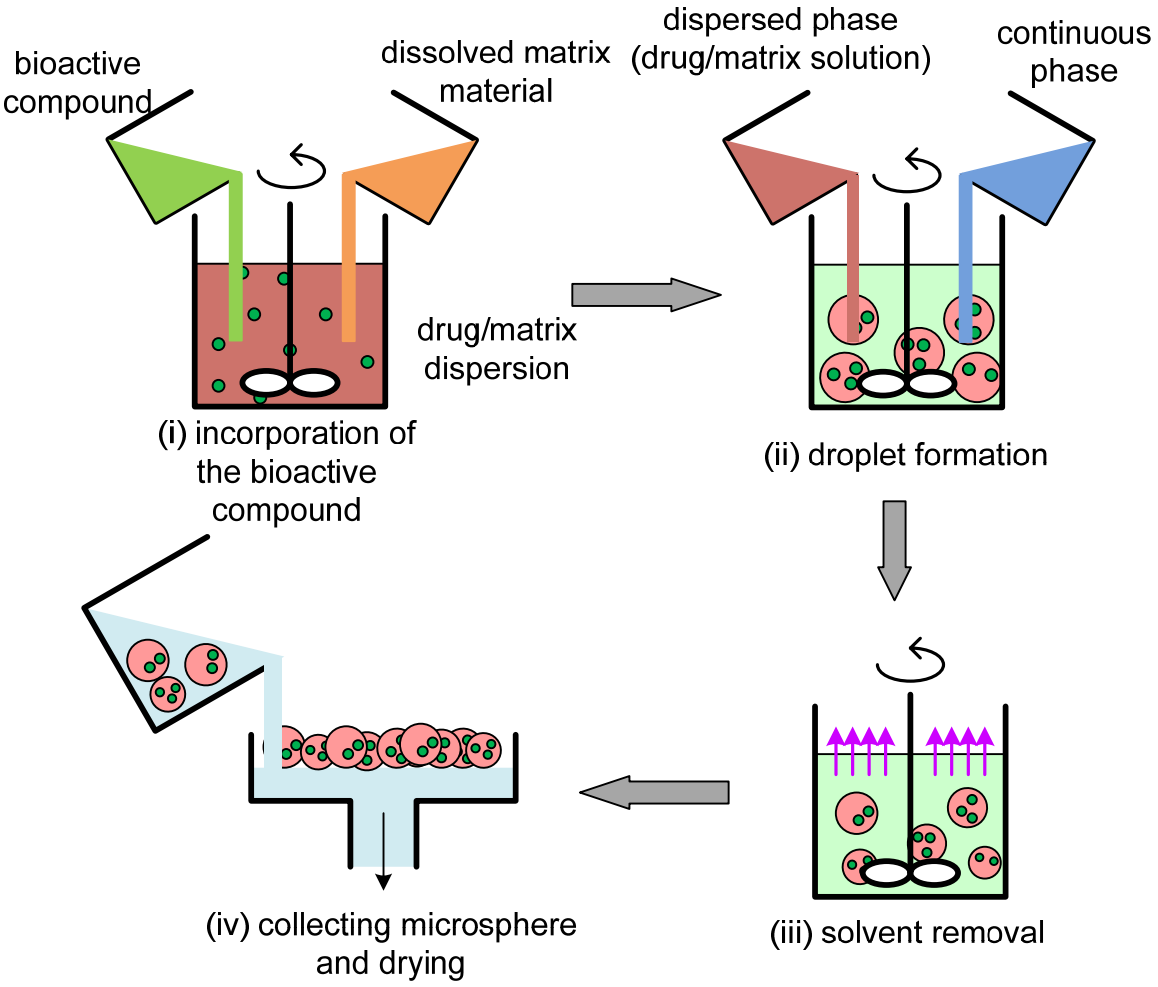

Figure 1.3 Schematic overview of the drug encapsulation process by solvent extraction / evaporation.

1.6. Issues concerning Microsphere Generation

One difficulty in all the conventional methods is achieving a desired size, as well as a narrow size distribution, of microspheres. Uniformity or mono-dispersity of microspheres is desirable because of the constant and predictable responses of microspheres to external fields; it is required in various industrial applications such as drug delivery devices, chromatographic packing materials, and dry and liquid tones for electrophotography [10, 40-43]. The size of microspheres from the conventional method ranges from 2 μm to 10 μm [44], which is very poor uniformity. Additionally, controllability of microsphere size is demanded for different applications [44-48]. For the preparation of microspheres, a microfluidic system made with the micro-electro-mechanical system (MEMS) technology seems to prevail for better uniformity and size controllability: the system is based on the principles such as membrane emulsification, hydrodynamic flow focusing, crossflow, and pneumatic chopper [49]. For the past decades, studies on chemical reactions have shown high interest in microfluidic devices since scaling down of a typical length to tens or hundreds of microns, reduction of a large amount of materials, and fabrication of a large array of units in one batch greatly increase efficiency in microsphere production [49, 50].

However, current membrane emulsification methods cannot meet the need to control microsphere size, and besides these methods produce relatively big sizes of microspheres. Active and precise size control is not achievable with hydrodynamic flow focusing and crossflow methods, although the size of the microsphere becomes smaller with these methods. This observation has become an important motivation for this thesis. In particular, the general philosophy here was to trace back to the origin of the existing microfluidic systems, i.e., design – especially conceptual design, as it is well known in general product design practices that

conceptual design is responsible for quality and cost of products significantly.

1.7. Research Objectives

The study reported in this thesis was motivated by a need to address the current issues in microsphere generation with the MEMS technology; this study aims to develop new theories and methodologies for designing microchannel systems for microsphere generation. In particular, there are three specific objectives for this study:

I. Uniformity or mono-dispersity: Uniformity or mono-dispersity of microspheres is desirable to allow constant and predictable responses of the microspheres to external fields [41]. Reliability of drug delivery increases by avoiding the peak-related toxic side effects which common drugs cause. Mono-dispersity can be achieved, as at least 90% of the distribution of microspheres lies within 5% of the median size [51] or defined by Coefficient of Variance ($CV = \frac{standard\ deviation}{average} \times 100\ \%$, mono-dispersity: CV < 5% [51-53]) .

II. Controllability of microsphere size: For different applications with microspheres, a range of sizes of microspheres is required. By controlling the size of microspheres from one microchannel, the cost of production is reduced.

III. Systematic design process: A general design methodology called Axiomatic Design Theory (ADT) is applied to analyze and to design microchannel systems, further improving the performance of microsystems.

1.8. Major contributions of the thesis

The following contributions have been made through the study reported in this thesis:

(1) A finding that the current microfluidic systems for microsphere generation are coupled designs, which are responsible for their restricted functions and performances.

(2) Proposal of three new designs of microfluidic systems for microsphere generation, which are improved designs and have upgraded the fulfillment of the functional requirements for microsphere generation.

(3) A new fabrication method based on micro-electro-mechanical system (MEMS) to fabricate perforated silicon membranes which have two competing features – the large size of an overall membrane, but the small size of individual holes on the membrane. In this fabrication process, two lithography techniques, photolithography and direct writing lithography (i.e., focused ion beam [FIB] in this study), were applied to overcome the disadvantages from each of them. In particular, the photolithography process opened wide windows in millimeters on a substrate surface to expose the embedded silicon dioxide membrane; it is, however, very difficult and inefficient to perform with FIB. FIB is effective at writing high resolution patterns on the silicon dioxide membrane, but it is incapable to cover a large area.

(4) A new principle for microsphere generation in a microfluidic system by integrating hydrodynamic flow focusing and crossflow methods. Conventionally, the two methods are operated for microsphere generation independently to achieve uniformity and size-controllability in microsphere generation. By integrating them based on ADT, the two requirements were fully satisfied in one step. Furthermore, satellite drop (which commonly appears from the conventional methods for microsphere generation) is significantly reduced and uniformity is improved with the new method. As a result, with the new method, uniformity and size-controllability of microspheres are achieved.

(5) A new principle for microsphere generation in a microfluidic system by utilizing a PZT actuator, namely liquid chopper; in particular, a PZT actuator is embedded to realize an improved microfluidic system for microsphere generation as well as to impose an external force which is further converted to an extra shearing force on a dispersed phase fluid. Furthermore, an adjustable oscillating flow, driven by the PZT actuator, realizes the size-controllability. This new method is the best for achieving uniformity and size-controllability.

1.9. Organization of the Thesis

To provide the background for the research conducted in this thesis, Chapter 2 presents a literature review on microsphere generation by the MEMS technology, in particular including MEMS fabrication processes for microchannel systems. The review focuses on such principles for microchannel systems as membrane emulsification, hydrodynamic flow focusing, crossflow, and pneumatic chopping. Chapter 3 presents analysis of current microfluidic methods for microsphere generation by applying a design theory and methodology called Axiomatic Design Theory (ADT). In this chapter, the ADT is discussed briefly. Further, improved designs of microfluidic devices are proposed.

Chapter 4 explains a microfluidic system based on the membrane emulsification principle, which has perforations built on a silicon membrane. The general idea with this method is such that a liquid phase containing the dissolved microsphere matrix material reaches a continuous phase after passing through a silicon membrane with micron-sized perforations, where microdroplets are formed. After the droplet is detached from the membrane, the solvent diffuses out of the droplets into a continuous phase leading to the formation of solid microspheres. It will be shown that through this method, about 90% of the microspheres range from 1 to 2 μm (CV =

7.9%).

Chapter 5 discusses the microfluidic system based on the integration of the hydrodynamic flow focusing and crossflow principles. It is supposed that by introducing immiscible fluids to the microfluidic device and varying the flow parameters, microspheres can be successfully controlled in various sizes (as opposed to the first system). Further, with a constant flow rate of the focused flow, the size of microspheres decreases as the velocity of the crossflow increases, and the production of microspheres increases as the velocity of the crossflow increases. Through this method, about 5% CV was achieved, and the nominal size of the microsphere can vary from 16 to 37 μm.

Chapter 6 presents the microfluidic system based on the liquid chopper principle. In particular, a piezoelectric actuator is embedded at the mouth of an external channel, and the external channel is connected to the downstream of the main channel. The focused flow is pinched off by the fluctuating external flows generated by the actuator, generating microspheres periodically. The piezoelectric actuator operates in varying frequencies responsible for varying microsphere sizes. It will be shown that with this method, under 5% CV was achieved, and the nominal size of the microsphere can vary from 78 to 186 μm.

Finally, Chapter 7 gives conclusions drawn from the results obtained, summarizes the contributions of the thesis, and outlines future research work.

2. LITERATURE REVIEW: MICROSPHERE GENERATION USING MICROFLUIDIC SYSTEMS

2.1. Introduction

In this chapter, state of the art developments in microsphere generation by four types of microfluidic systems (specifically microchannel systems) are reviewed to justify the significance of the research conducted in this thesis. Section 2.2 discusses basic principles of microencapsulation. Section 2.3 reviews current microfluidic devices fabricated by micro-electro-mechanical system (MEMS) technology: membrane emulsification by crossflow, T-junction, hydrodynamic flow focusing, and choppers. Section 2.4 addresses mathematical modeling of formation of microspheres in microchannels with the Lattice Boltzmann method (LBM) which is widely applied for simulation studies. Some concluding remarks are expressed in Section 2.5.

2.2. Microencapsulation

The most widely applied technique for preparation of microspheres is a process of emulsification by solvent evaporation / extraction [54-56] as explained in the previous chapter. The solvent evaporation / extraction method consists of two main stages: formation of droplets and solvent removal. A biodegradable and biocompatible polymer solution forms a droplet by emulsification in immiscible aqueous and oil phases. A variety of polymers are suitable candidates for biodegradable and biocompatible encapsulation such as Poly(methyl methacrylate) (PMMA) [57], Poly(lactide-co-glycolides) (PLGA) [24, 29, 31-34, 36-39], Poly(lactic acid) (PLA) [58, 59], Gelatin [56], Polyvinyl alcohol (PVA) [34], and combinations of sorbitan esters and polysorbates [22]. The emulsification is engaged with complex interactions between the

mechanical forces applied on the polymer solution and the viscosity of the emulsion medium. In particular, mechanical forces and viscosity affect the rheological behavior of the emulsion medium and change the shear stress of the polymer solution. This situation will further change the size of droplets (i.e., microspheres) [33]. During the first stage, droplets collide and combine continuously up to the point of steady-state at which the size of the droplets is stable. Then, an emulsifier or surfactant (i.e., stabilizer) in the emulsion medium covers the droplets and provides a thin protective layer to prevent coalescence of droplets. During the second stage, the solvent is evaporated from the droplets, gradually leading to microsphere hardening and precipitation [33, 60]. Traditionally, the emulsification has been realized by mixers, colloid mills, homogenizers, and sonicators, while researchers have focused on the homogeneity and stability of emulsion [61]. Later, membrane emulsification was introduced by Nakashima et al. [62, 63] applying membrane filtration with porous glass. It has been shown that the membrane filtration is an adequate method for homogeneity and narrow size distribution of microspheres, since the size of microspheres is controlled primarily by the pore size of a membrane [61, 64]. However, the methods mentioned above do not fully meet the requirements of microencapsulation. One of the most important properties of microencapsulation is the size controllability demanded in various therapeutic applications. In order to realize a controlled release of suitable active agents (i.g. antigens) from the polymeric microsphere, the control of particle size is essential [38]. Additionally, small sizes of microspheres are much more immunogenic than larger sizes of microspheres [46, 48]. For oral administration of microspheres with inserted proteins, particle size has been shown to be an important parameter. From the studies of mice [45] and rats [47], polymeric microspheres as large as 10 μm were apparently taken up by the mice; however, smaller sizes of polymeric microspheres less than 1 μm in size have shown optimal uptake. In the

field of mucosal immunity, Peyer's Patches (PPs) have been used for antigen uptake. In order to be taken by PPs, the sizes of particles must be smaller than 10 μm [45]. The other significant property of such microencapsulation is uniformity or mono-dispersity. Regarding efficiency of drug delivery, uniformity of microspheres is another most important property. The narrow size distribution, which represents uniformity, of polymeric microspheres is desirable for constant and predictable responses of the microspheres to the external fields [41]. Additionally, various industrial applications demand uniformity of microspheres. With the intention of overcoming these difficulties from conventional methods of microencapsulation, microfluidic devices fabricated by the micromachining technology called micro-electro-mechanical systems (MEMS) have been developed, in particular MEMS for microsphere generation.

2.3. Microchannel

Microfluidic devices have received great attention from researchers on chemical reactions because of the efficiency of handling micro-scaled structures. The systems of microfluidic devices have potential in broad fields of biology and chemistry such as biomolecular separations, enzymatic assays, polymerase chain reaction, and immunohybridization reactions [65]. Kawakatsu et al. [66] introduced a novel method of filtration by using microchannels formed in a silicon substrate. Then, the silicon based microchannel array was introduced by Kikuchi et al. [67, 68] to study the flow characteristics of human blood by using a microscope video system to observe microspheres in the microchannels.

The microchannels were fabricated by processes such as photolithography, etching, molding, and so on [69]. Generally, there are three major processes for the MEMS fabrication process: deposition, lithography and etching. Deposition is a process to deposit thin films of materials from several nanometers to several micrometers. The materials can be deposited by

chemical reactions or physical reactions in gas and/or liquid. Lithography (or photolithography) is a process to transfer a pattern to a photosensitive material by selective exposure to a radiation source such as light. Typically, a photoresist is used as a photosensitive material. The photosensitive material changes its physical properties when exposed to a radiation source. Etching is a process to form a functional MEMS structure on a substrate after or before thin film deposition. A chemical solution is used for the wet etching process, and reactive ions or vapor phase etchants are used for the dry etching process. These processes must be performed in clean environments.

A cleanroom with a low level of environmental pollutants such as dust, airborne microborne, aerosol particles and chemical vapors can provide the required environment. A cleanroom is separated into two rooms: a lithography room under yellow lights to protect from damage during the lithography process and a thin film room under white lights [70]. By the development of MEMS technology, microchannels gained attention for the preparation of microspheres [49]. Since most microfluidic devices operate at low Reynolds number regimes, the flow becomes laminar. Thus, the Navier-Stokes equation for fluid flow becomes the Stokes equation by neglecting the $\boldsymbol{u} \cdot \boldsymbol{\nabla u}$ term, which makes this equation linear [71, 72]. Overall, various configurations of microfluidic devices have been developed. In the next section, different mechanisms of the microencapsulation in microchannels are explained.

2.3.1. Membrane emulsification by crossflow

Kawakatsu et al. [66] introduced a microfiltration method by using grooved microchannels formed in a silicon substrate to filter certain sizes of microspheres generated by a homogenizer. Later, Kawakatsu et al. [61, 73] proposed an emulsification method using silicon microchannels as shown in Figure 2.1. This grooved microchannel method did not require any

strong turbulent mixing as a homogenizer. Regular-sized microspheres were produced by pressing a dispersed phase into a continuous phase through the microchannels. Further, Kawakatsu et al. [74] studied the effect of microchannel structures on the size of microspheres by changing the microchannel shape, equivalent diameter and terrace length.

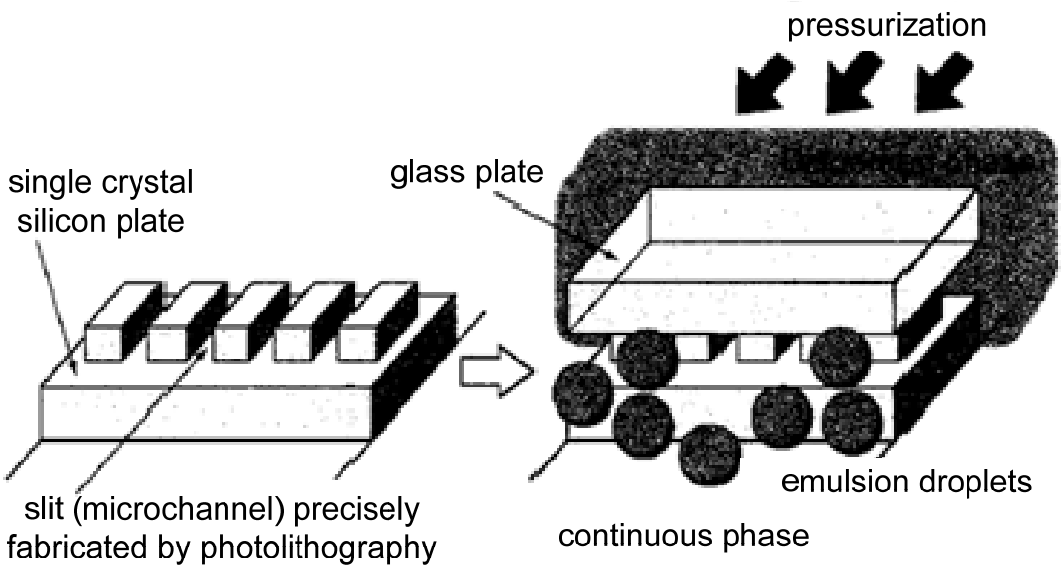

Figure 2.1 Scheme of microchannel emulsification [73].

Tong et al. [75] studied the effect of surfactants on the size of mono-dispersed oil-in-water (O/W) microspheres through microchannels. They found that the surfactant lowers the interfacial tension for emulsification, changes the contact angle for wetting and dispersion, and creates the gradient of interfacial tension for formation and stability of an emulsion [76]. These effects are considered to change the breakthrough pressure and the size of the microspheres. Since it is necessary to maintain the microchannel surface hydrophilic (i.e., low interfacial tension between water and solid wall) for O/W emulsion [77-79], it was found that in the oil phase liquid, the hydrophobic surfactant and oleic acid created higher interfacial tension than the hydrophilic surfactant. However, the hydrophilic surfactant makes the formation of O/W microspheres easier because the dynamic interfacial tension achieved by faster diffusion affects

the emulsification process of microspheres [80]. Further, it was found that nonionic and anionic surfactants assist in maintaining the microchannel hydrophilic by being repulsed from the negatively charged microchannel surface, but cationic surfactants are absorbed on the microchannel surface; they increase its wetting of microchannel surface and thereby worsen the emulsification process for O/W microspheres as shown in Figure 2.2.

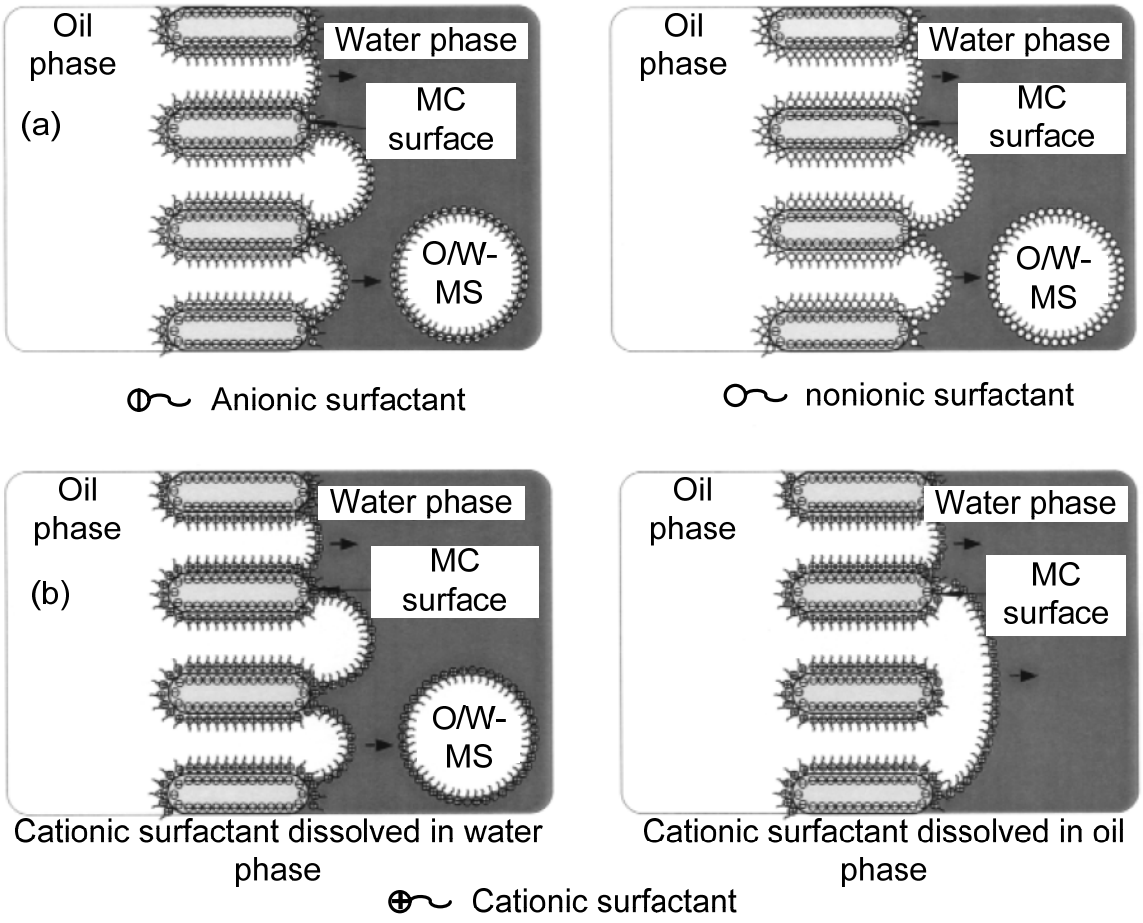

Figure 2.2 Schematic illustration of the function of surfactant in the microchannel emulsification process. (a) anionic and nonionic surfactants; (b) cationic surfactant. (MC: microchannel, MS: microsphere) [75].

Kobayashi et al. [81] introduced a microfabricated silicon membrane (see Figure 2.3) with oblong through-holes to generate mono-dispersed emulsion microspheres. A precise straight-through and highly integrated layout of microchannels with a high aspect ratio was

fabricated by the deep reactive ion etching (RIE) process in MEMS fabrication techniques. The thick membrane allowed for higher pressure yielding higher throughput.

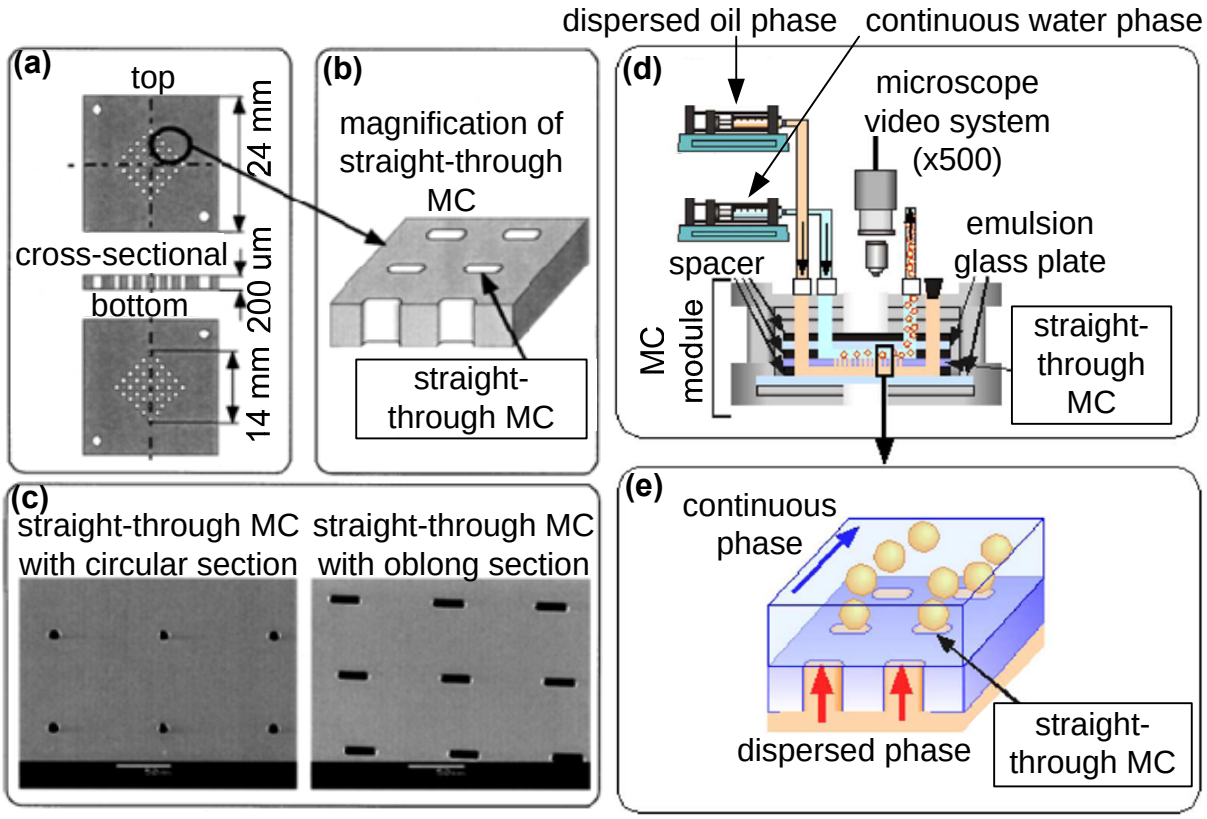

Figure 2.3 Straight-through microchannel plate and SEM images of straight-through microchannels [51, 81]. (a) The top view, cross-sectional view, and bottom view of the straight-through microchannel plate. (b) Magnification of an oblong straight-through microchannel. (c) Scanning electron microscope (SEM) images of straight-through microchannels. (the bar represents 50 μm) (d) Schematic diagram of the experimental setup. (e) Schematic of flow through the straight-through MC in the module. (MC: microchannel).

The oblong straight-through microchannel was compared with a circular straight-through microchannel for generating mono-dispersed microspheres. The circular microchannels yielded a similar behavior as that seen in a circular capillary studied by Peng et al. [43, 82, 83]. At the tip of the circular section, the main forces on growing droplets are primarily external forces, consisting of the drag force from the continuous phase flow, the interfacial tension force, the

buoyancy force, and the inertial force from the dispersed phase. The interfacial tension force acts against the detachment of droplets; however, the other forces act for detachment of droplets. The drag force works as a primary force for the detachment. However, the drag force is extremely sensitive to operating conditions such as the velocity of continuous phase liquid and the applied pressure of dispersed phase liquid, suggesting that it is very difficult to produce size-controlled mono-dispersed microspheres by circular straight-through microchannels. On the other hand, the oblong straight-through microchannels have shown mono-dispersed microsphere production with and without continuous phase flow. The interface along the oblong tip was elongated, causing instability at the tip. Thus, the growing droplets at the oblong tip were sheared and detached to be microspheres without any turbulent flow. As well, oblong tip aspect ratios (length to width) exceeding about 3 were suitable for the stable formation for mono-dispersed microspheres [84]. Further, with anionic surfactants such as sodium dodecyl sulfate (SDS), as well as with nonionic surfactants such as polyglycerol fatty acid ester (PGFE) and poly oxyethelene sorbitan monolaurate (Tween 20), mono-dispersed O/W microspheres with diameters of 30-50 μm can be stably formed below 3% of coefficient of variation (*CV*) in hydrophilic microchannels with to-be-dispersed flux of 10-100 $\mathrm{L/(m^2h)}$. The *CV* is calculated to provide the degree of the droplet size distribution as

$$CV = \frac{\sigma_{sd}}{d_{av}} \times 100\ (\%) \tag{2.1}$$

where σ_{sd} is the standard deviation (μm), and d_{av} is the average diameter of microspheres (μm) [51-53]. The formation of a microsphere from a single straight-through microchannel was analyzed with computational fluid dynamics (CFD): by the velocity at the neck and the increased pressure difference between the channel entrance and the neck, the neck of the oil phase inside

the microchannel was shrunken to form a microsphere as shown in Figure 2.4 [85, 86].

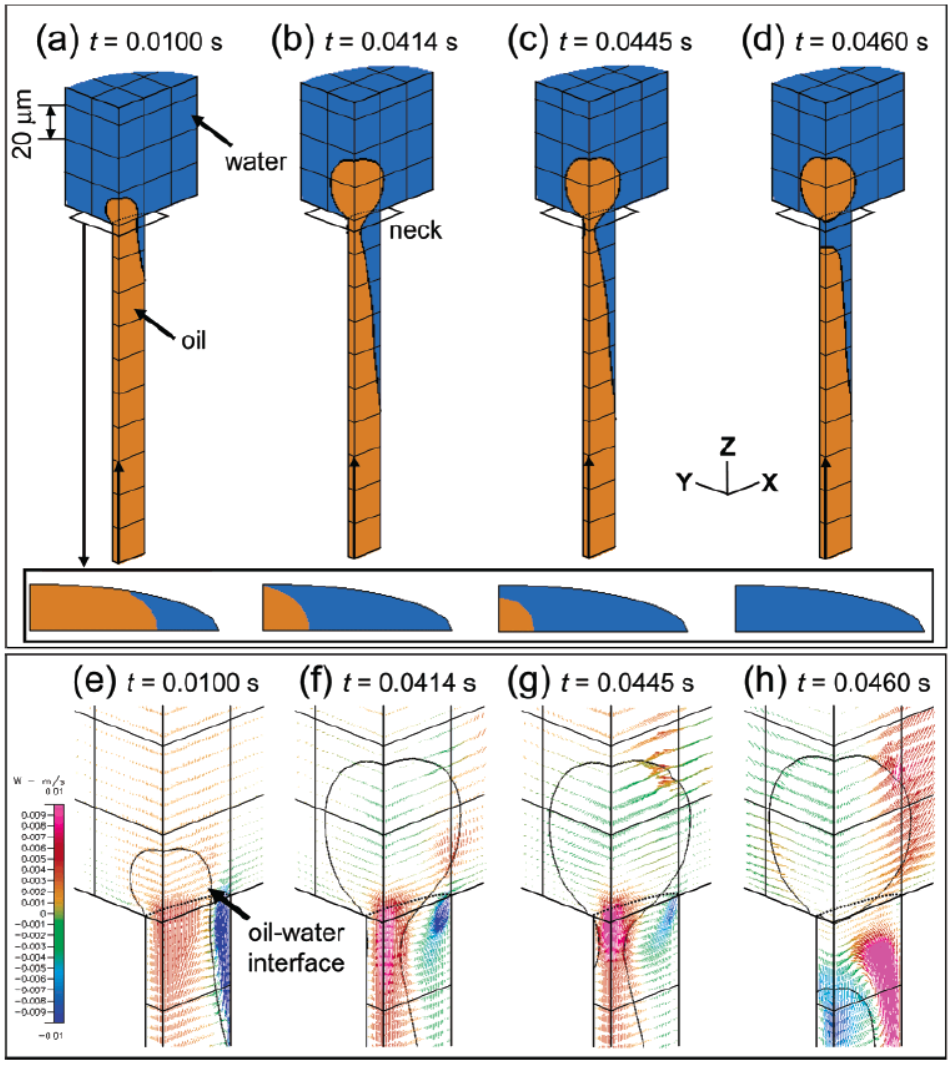

Figure 2.4 (a-d) Successful formation of a small droplet with elliptical channel cross section. (e-h) Shape of an oil-water interface and velocity vectors of both phases in the region around the channel exit as a function of time [85].

2.3.2. T-junction

Although silicon membrane methods can achieve the requirements of microencapsulation to some extent, they are still not suitable for producing variable volumes of chemical samples [49]. Thorsen et al. [72] introduced a microchannel with a T-junction structure for water-in-oil (W/O) microspheres as shown in Figure 2.5. A 9 µm high microchannel was patterned with

acrylated urethane after curing with a silicon wafer mold. Pressure was applied by an air compressor to introduce continuous phase and dispersed phase flows with a surfactant from the reservoirs.

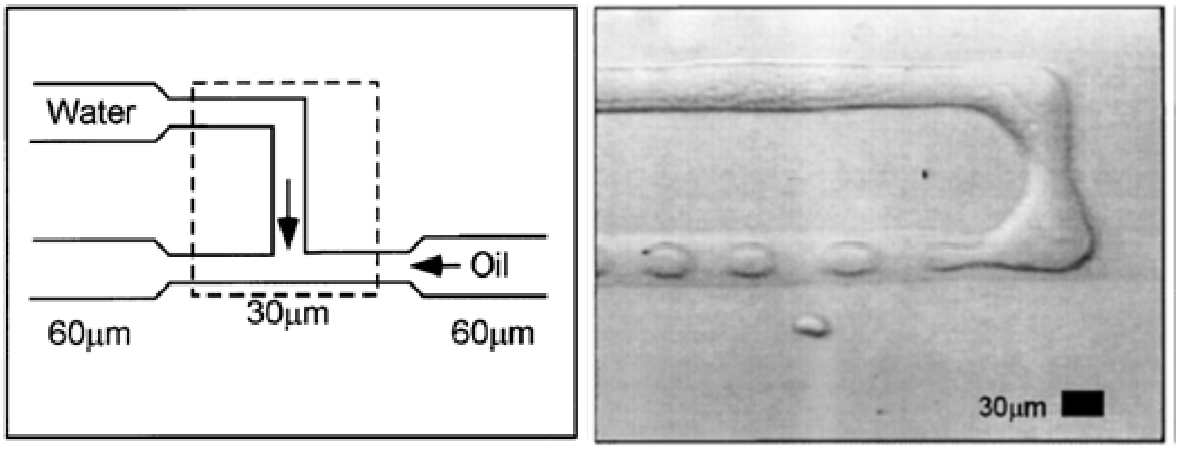

Figure 2.5 Microfabricated channel dimensions at the point of crossflow and photomicrograph of the discontinuous aqueous phase introduced into the continuous oil phase. Dashed rectangle indicates area in photomicrograph [72].

Nisisako et al. [49] fabricated a T-junction structure in a microchannel on polymethyl methacrylate (PMMA) plate with 100 μm of depth by an end mill (see Figure 2.6). Syringe pumps were used to inject the dispersed phase and continuous phase fluids without a surfactant. The wall of the microchannel was hydrophobic, and the hydrophobicity played an important role in generating W/O microspheres.

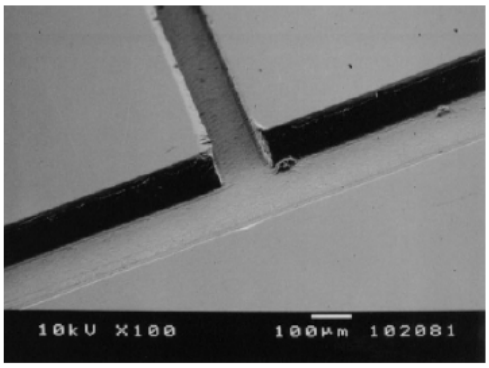

Figure 2.6 SEM image of top view of the microchannels fabricated on a PMMA plate [49].

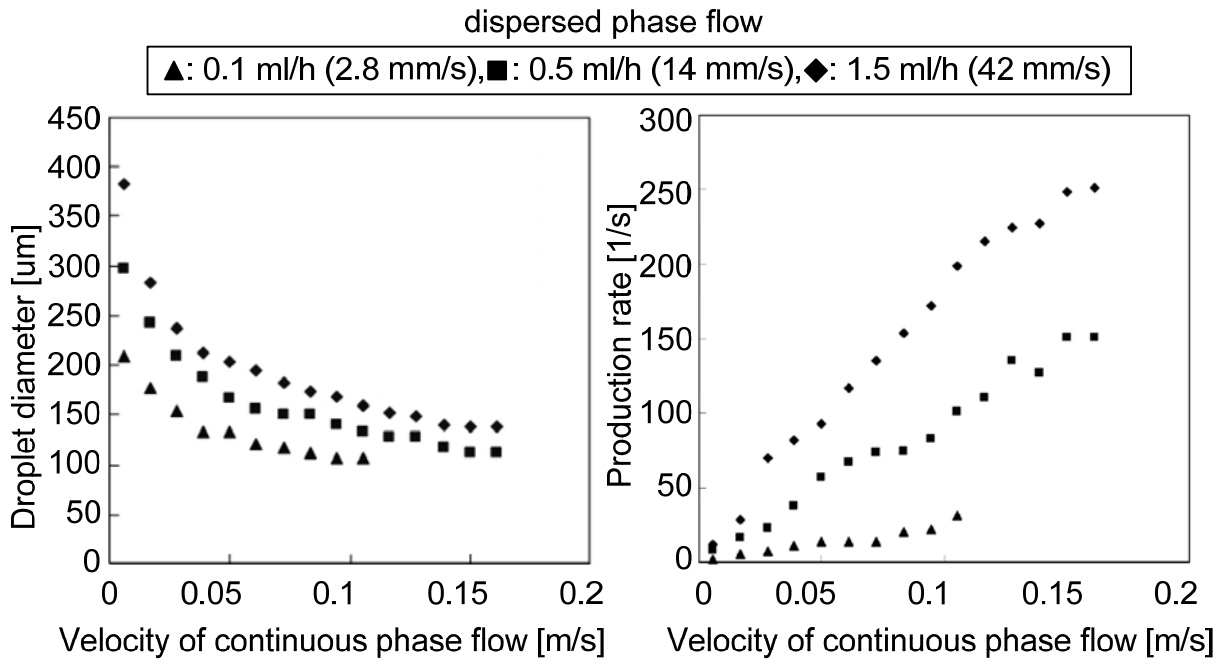

Figure 2.7 Effect of velocity of continuous phase flow on size and production of microspheres [49].

With a constant flow rate of the dispersed phase flow Q_d, the size of microspheres decreases as the velocity of the continuous phase flow increases, and the production of microspheres increases as the velocity of the continuous phase flow increases as shown in Figure 2.7.

Dendukuri et al. [41] proposed a controlled synthesis of nonspherical microspheres using a T-junction structure in a microchannel as illustrated in Figure 2.8. The microchannel was fabricated by the soft lithography technique [87] pouring poly-dimethyl siloxane (PDMS) on a patterned silicon wafer. A UV-curable polymer, Norland Optical Adhesive 60 (NOA 60), was used for microsphere material. The microspheres were formed at a T-junction by shearing the dispersed polymer phase by the continuous aqueous phase with a surfactant. The break-off of the microspheres is governed by competition between viscous stress and interfacial tension.

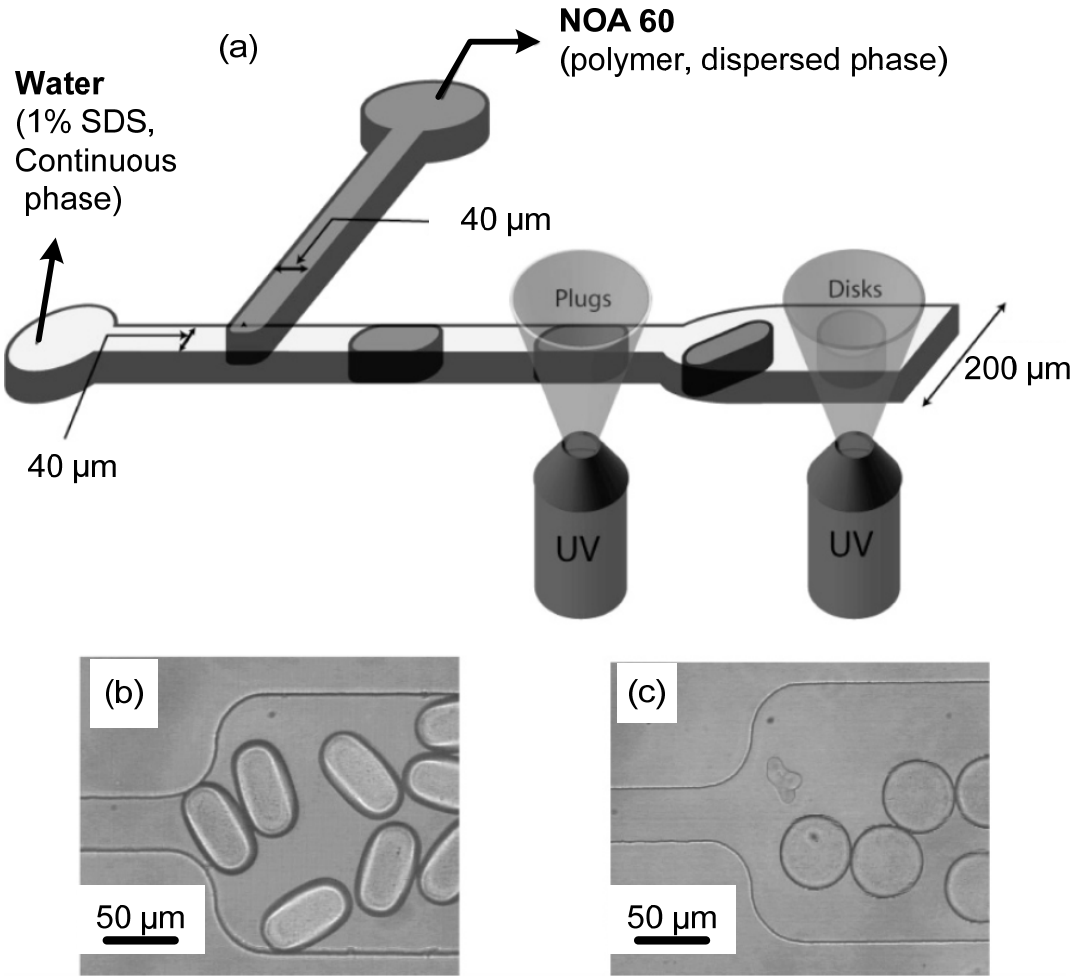

Figure 2.8 Microchannel geometry used to create plugs and disks: (a) schematic of channel with plug and disk creation zones marked; (b) polymerized plugs in the 200 µm section of the channel, 38 µm height; and (c) polymerized disks in the 200 µm section of the channel, 16 µm height [41].

The relative importance of the viscous stress and the interfacial tension can be characterized by the Capillary number as

$$Ca = \frac{\mu v_c}{\gamma} \tag{2.2}$$

where μ is the viscosity of continuous phase, v_c is the superficial velocity of continuous phase, and γ is the interfacial tension between the continuous and the dispersed phases [88]. By modifying Ca, the size of microspheres can be tuned [72], and the flow rate of the continuous

phase flow Q_c changes Ca. As Ca increases, the shear forces increase, yielding formation of smaller microspheres. Additionally, with constant Ca, the size of microspheres becomes larger with an increasing flow rate of dispersed phase flow Q_d. According to the experiments of Dendukuri et al. [41], researchers classified the microfluidic system into three phases: (I) wetting phase, (II) plug phase and (III) droplet phase. At the wetting phase, one phase of fluid flows through the microchannel at a very low Ca, yielding insufficient shear forces to pinch off at the T-junction. As Ca increases gradually at a constant flow rate of dispersed phase flow Q_d, plugs of polymer initiate to pinch off at the T-junction, reaching a critical Ca, Ca_{w-p}, at the transition of the wetting phase and the plug phase. When $Ca > Ca_{w-p}$, the dispersed phase starts breaking off at the T-junction. At low Ca, the size of microspheres is larger than the width of the microchannel, leading to plugs. As Ca increases, the length of the plugs decrease, leading eventually to spherical microspheres in the droplet phase. A UV light exposed for a short time (<1μs) to the polymer plugs for hardening. The size of nonspherical microspheres was uniform but larger than 10 μm.

Tice et al. [89, 90] investigated the three regimes of multiphase flow behavior by Ca in the formation of plugs in a microchannel (see Figure 2.9). (I) At low velocities and Ca, plugs immediately separated from the dispersed phase (aqueous) stream at the T-junction. The dimensions of the plugs were reproducible. (II) At a threshold of velocity and Ca, the dispersed phase flow formed a short laminar segment beyond the T-junction before plugs separated from the stream. (III) At higher flow velocities and Ca, the laminar segment elongated further downstream and its length varied with smaller size of microspheres.

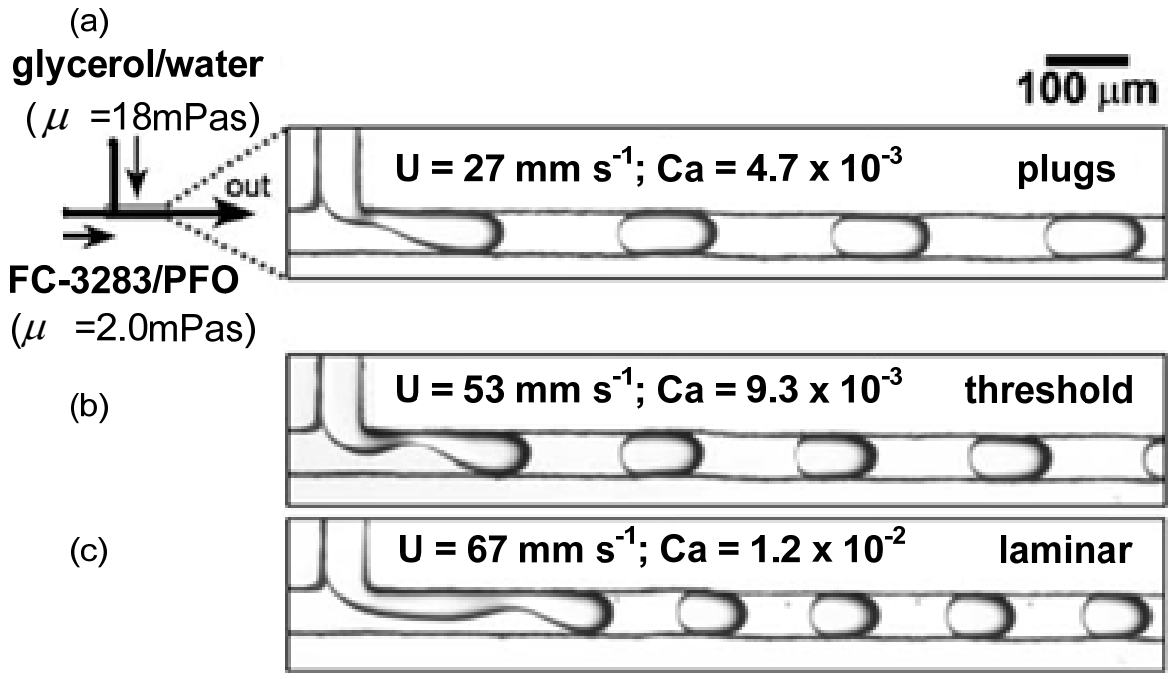

Figure 2.9 Visualization of the three regimes of behavior observed in two-phase flows of viscous fluids [89].

Guillot et al. [50] studied the flowing of immiscible flows after T-junctions in a microchannel in order to determine the shape of the parallel flows and to analyze the microsphere formation mechanism. In their study, a non-intuitive microsphere formation was realized by the blocking-pinching mechanism because of the parallel flows without involving the competition of viscous forces and interfacial tension (see Figure 2.10). Two inlet arms meet at a T-junction with a funnel design in a PDMS microchannel. The microspheres were generated after the T-junction with higher velocities of immiscible continuous (oil) phase and dispersed (aqueous) phase fluids. When the two phase fluids flow into the microchannel in parallel, the tip of the dispersed phase jet expands the size and moves ahead in the microchannel until it meets the channel walls. Since the dispersed phase blocks the continuous phase, the continuous phase starts to pinch the dispersed phase leading the formation of microspheres. The blocking-pinch

phenomenon was modeled, and it proved that low aqueous phase flow rates with a constant oil phase flow rate cause the instability of the parallel flows, yielding the formation of plugs.

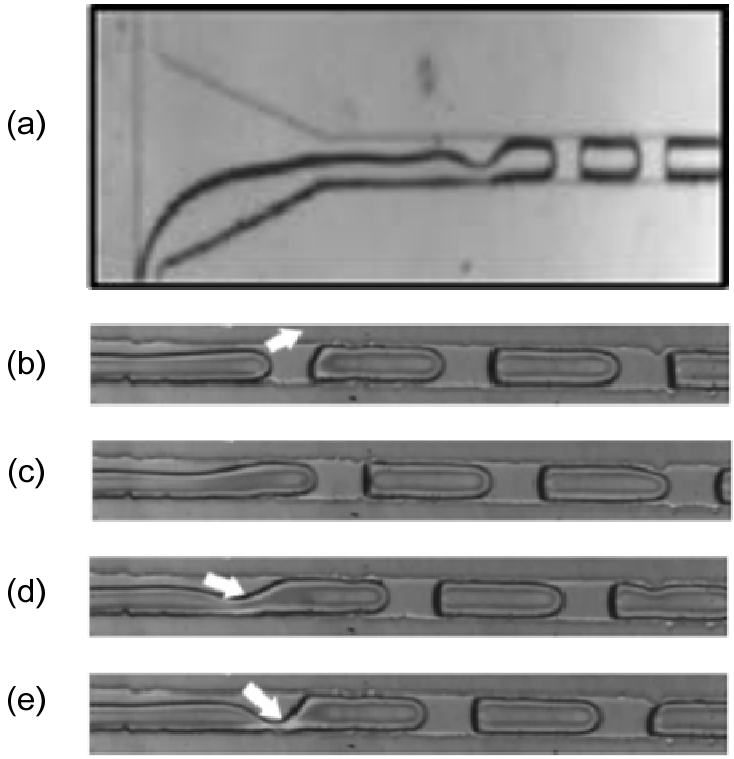

Figure 2.10 Microsphere formation mechanism in a channel. (a) T-junction with a funnel design, (b) the tip of the jet begins to expand in the channel, (c) the tip clogs the channel, (d) oil phase starts pinching the water jet, and (e) just before the microsphere formation. Time period is 3.1 ms [50].

Van der Graaf et al. [91] studied the influence of aqueous phase properties on the process of O/W microsphere formation in glass microchannels. As well, the detachment process and shape of the microsphere were studied in detail. The microsphere formation of oil phase in aqueous phase starts at the T-junction. After growing, the microsphere is deformed in the direction of the aqueous phase flow, and a neck is formed as the aqueous phase flow penetrates into the oil phase channel leading detachment as shown in Figure 2.11.

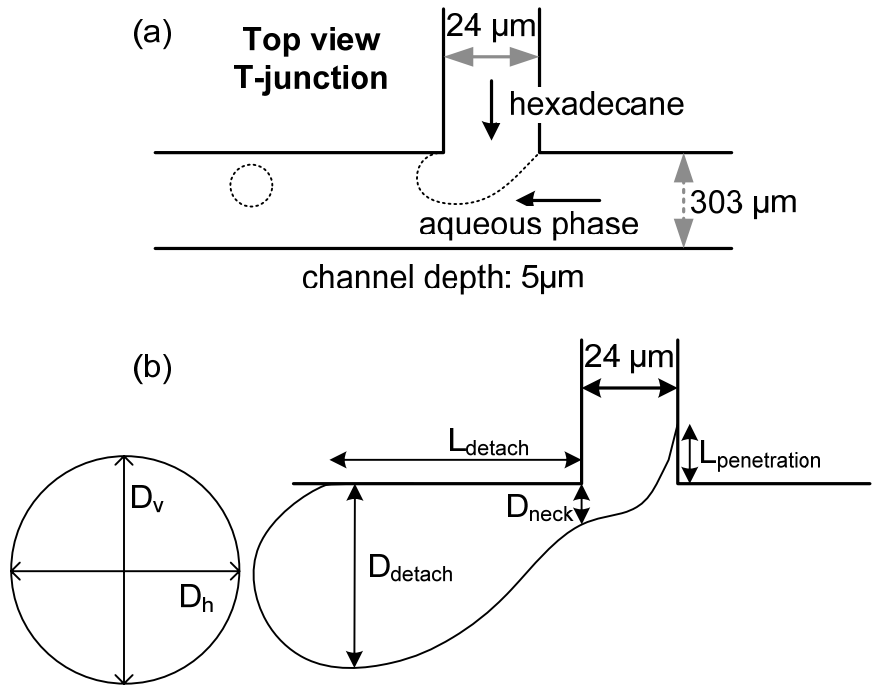

Figure 2.11 Schematic view of a T-junction: (a) top view of a T-junction and (b) schematic drawing of a microsphere with the definition of the horizontal (D_h) and vertical (D_v) diameters, as well as just before detachment with the definition of the neck diameter (D_{neck}), penetration length ($L_{penetration}$), detachment length (L_{detach}), and the microsphere diameter of the attached drop ($D_{detatach}$) [91].

By changing surfactants with the aqueous phase fluid, different break-up locations of the microsphere were observed. Around the critical dispersed (oil) phase velocity, a transition regime was observed where the jet and/or the microspheres are formed. For detachment of the microsphere, two characteristics were studied: the neck diameter (D_{neck}) and the penetration length ($L_{penetration}$). In membrane emulsification, the neck diameter is important for the detachment because the interfacial tension force, which is the main force to hold the droplet connection, is dependent on the neck diameter [80]. It was found that by the analysis of the Laplace pressure in the small part of the neck, detachment of the microspheres occurs when the neck diameter becomes smaller than the microchannel depth. As well, they observed that aqueous phase always penetrates into the oil phase channel, and the oil phase flow rate

contributes to both the detachment and size of microspheres. The radius of the neck before the detachment is calculated as

$$\frac{1}{R_{neck}} \approx \left(\frac{1}{R_c} + \frac{1}{R_{ms}}\right) \tag{2.3}$$

where R_c is half of the channel depth and R_{ms} is the radius of detached microspheres.

Later, van der Graaf et al. [13] investigated and simulated the microsphere formation in a rectangular microchannel with the lattice Boltzmann method [92, 93]. The computational fluid dynamics (CFD) with lattice Boltzmann code agreed well with the experimental results as illustrated in Figure 2.12. From the simulation studies, it follows that the volume of microspheres decreases as a function of the Capillary number and increases with increasing dispersed phase flow rate Q_d, yielding the following volume equation

$$V = V_{crit,ref} Ca^m + t_{neck,ref} Ca^n Q_d \tag{2.4}$$

where $V_{crit,ref}$ is the critical volume at $Ca = 1$, and $t_{neck,ref}$ is the necking time at $Ca = 1$.

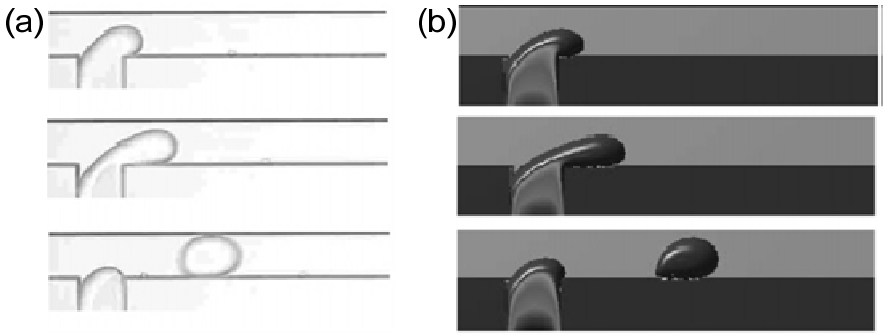

Figure 2.12 Snapshots of experiments (a) and simulations (b) of droplet detachment at a T-junction. The flow rate of the continuous phase Q_c is 2 mLh^{-1}, and that of the to-be-dispersed phase is 0.2 mLh^{-1} [13].

To obtain a certain size of microspheres, a combination of the Capillary number and the dispersed phase flow rate Q_d should be chosen. For a higher Ca and a higher Q_d, V_{neck} dominates for the size of microspheres, while for a lower Ca and a lower Q_d, V_{neck} is negligible.

The process of break-up and detailed quantitative analysis of the size of the microspheres in a T-junction structure were not examined before Garstecki et al. [94]. They studied the process, scaling characteristics, and mechanism of break-up of liquid and gas streams at T-junction in a rectangular cross-section of a microchannel altering the viscosities and flow rates of the fluids. They discovered that at low values of the Capillary number Ca, the dynamics of break-up are dominated by the pressure drop across the microsphere, and this process is called the squeezing regime. In this regime where $Ca < 0.01$, microsphere size is determined mainly by the ratio of the flow rates, leading to a simple scale law introduced as

$$\frac{L}{w} = 1 + \alpha \frac{Q_d}{Q_c} \tag{2.5}$$

where L is the length of the immiscible plug, w is the width of the channel, $Q_{d/c}$ are the flow rates of dispersed phase and continuous phase, respectively, and α is a constant of order one, whose particular value depends on the geometry of the T-junction. This simple scaling law can predict the size of the microspheres produced in a T-junction. In the squeezing regime, the shear stresses are not sufficient to deform the microsphere, so that the entire cross-section of the channel is almost blocked by the microsphere, yielding an increase of pressure drop and squeezing effect on the neck of the immiscible thread (see Figure 2.13). The squeezing mechanism occurs if the width of the main channel is greater than its height, and the width of the inlet channel is at least half the width of the main channel. This mechanism implies two important experimental predictions: (I) when $Ca \ll 1$, emulsions can be formed at small length scales, and (II) regardless of the surfactants, liquid microspheres and gas bubbles can be generated.

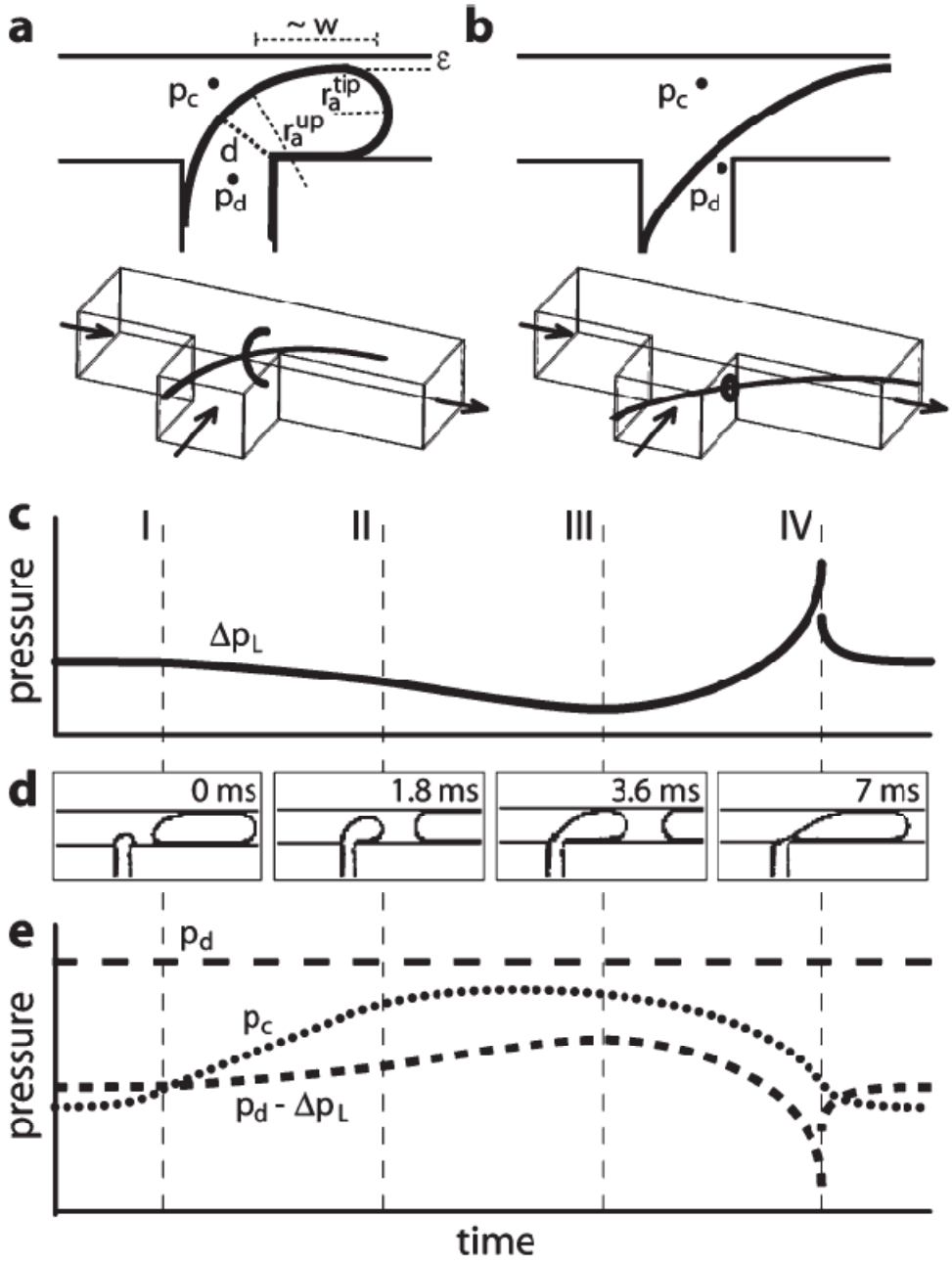

Figure 2.13 (a) and (b) A schematic illustration (top view) of the shape of the tip of the immiscible thread at an intermediate stage of break-up. (ε: the separation between walls and liquid-liquid interface, p_d: hydrostatic pressure in the dispersed phase, p_c: hydrostatic pressure in the continuous phase, d: thickness of the neck). (c) Evolution of the Laplace pressure jump across the interface Δp_L. (d) Micrograph of the reference stream (h = 33 μm, $w = 100$ μm, $w_{in} = 50$ μm) for $Q_{water} = 0.14$ μL s^{-1} and $Q_{oil} = 0.083$ μL s^{-1}. (e) Schematic illustration of the evolution of the hydrostatic pressures [94].

Liu et al. [95] studied the influence of Capillary number Ca, flow rate ratio, viscosity ratio, and contact angle for microsphere generation at a T-junction by 2D numerical simulations. From the experiments [49, 95, 96], it was noted that as Ca increases the size of the microspheres decreases with a constant flow rate of the dispersed phase Q_d (see Figure 2.14). When Ca increases from 0.032, the detachment point moves downstream of the T-junction by increasing the flow rate ratio $Q(= Q_d/Q_c)$ until a stable jet is formed, as observed in references ([97, 98]). The simulation results showed that in the squeezing regime, the effect of the flow rate ratio on the size of the microsphere agrees well with the scaling law (Eqn.(2.5)) by Garstecki et al. [94]. Similar to the simulation results from the flow rate ratio, as viscosity ratio $\lambda(= \eta_d/\eta_c)$ increases, the detachment point moves downstream. Moreover, in the squeezing regime, the viscosity ratio does not affect the size of the microspheres; the viscosity ratio plays an important role in determining the size in the dripping regime wherein the size of the microsphere decreases as the viscosity ratio increases. The contact angle was studied to examine the influence of wetting properties on microsphere formation as well. The contact angle affects the shape of microspheres, generation frequency, distance between neighboring microspheres, and detachment point. For smaller microsphere generation, more hydrophobicity of the channel walls is necessary. With a constant contact angle, bigger microspheres are generated with a greater viscosity ratio in the squeezing regime, while smaller microspheres are produced with a greater viscosity in the dripping regime. It was also found that at small Ca, the wetting property affects markedly the size of microspheres, but at high Ca, the wetting effect is negligible. From the simulation studies, a critical $Ca = 0.018$ was found, demonstrating that the transition from the squeezing regime to the dripping regime occurs regardless of the flow rate ratio, viscosity ratio, and contact angle.

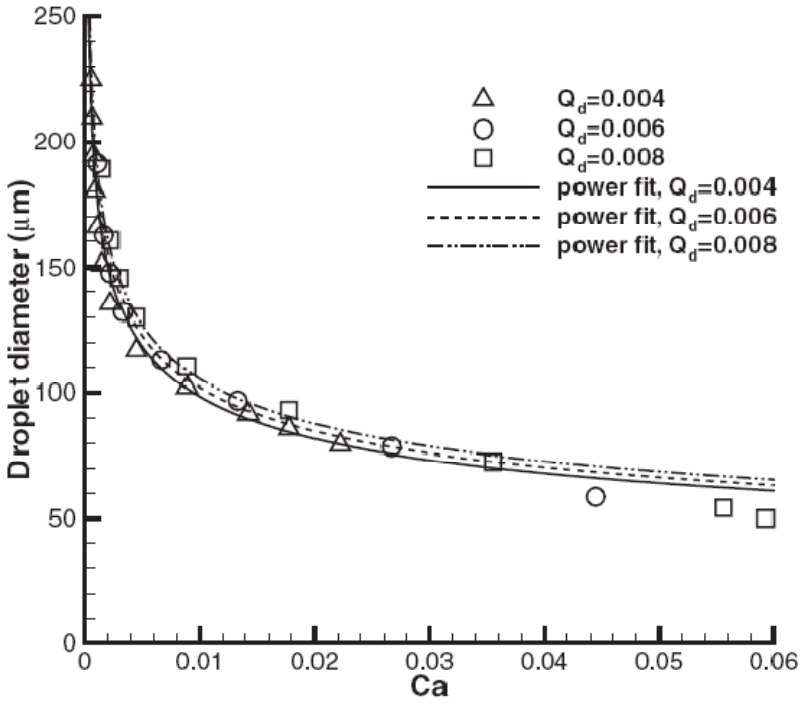

Figure 2.14 The effect of Capillary number on the droplet diameter at the dispersed phase flow rate Q_d of 4×10^{-3}, 6×10^{-3}, and 8×10^{-3}, respectively. The lines represent the power fitting of the simulation results [95].

In the squeezing regime, the Capillary number and the flow rate ratio play important roles to determine the size of microspheres without the effect of the viscosity ratio under completely hydrophobic wetting conditions. Additionally, with less hydrophobic wetting conditions, the size of microspheres is dependent on the viscosity ratio. In the dripping regime, the viscosity ratio mainly affects the size of the microspheres with the pressure drop through a microsphere.

2.3.3. Hydrodynamic flow focusing

Hydrodynamic flow focusing or flow focusing technique has been introduced for microsphere generation in order to overcome the limitations of other techniques, such as polydispersity, controllability, and microsphere size dependency on the channel size [99]. The flow focusing technique is adapted from the multistream laminar flow systems. The side-by-side parallel laminar streams are able to adjust the size of each stream by altering the flow rate of the

multistream [100]. Knight et al. [101] reported on a multistream laminar flow system in a microfluidic device to narrow or focus the center stream (i.e., flow focusing) by increasing the two outer neighbor streams for advanced mixing efficiency.

Anna et al. [102] integrated a flow focusing geometry to produce mono-dispersed and polydispersed microspheres in a microfluidic device as shown in Figure 2.15.

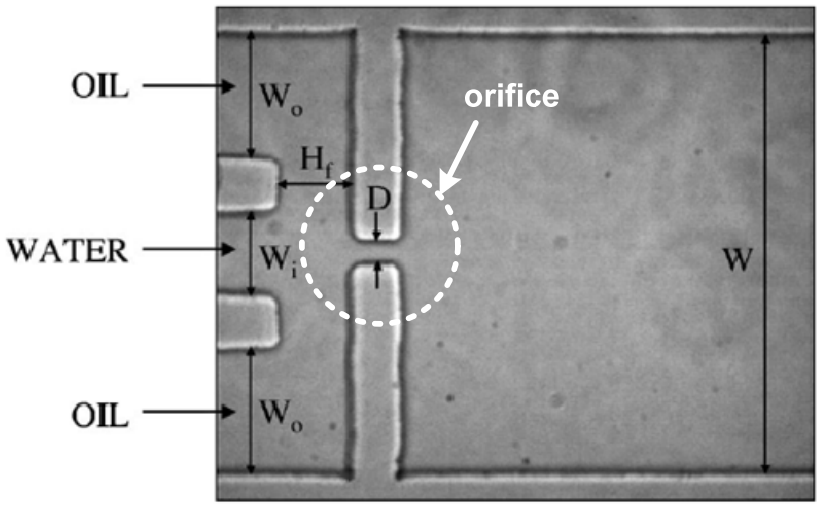

Figure 2.15 Flow focusing geometry implemented in a PDMS microfluidic device (W = 963 μm, W_i = 197 μm, W_o = 278 μm, H_f = 161 μm and D = 43.5 μm) [102].

The flow focusing technique was previously used by Ganan-Calvo et al. [103, 104] to form microthreads and micron-sized mono-dispersed spray in gas streams. The mechanism of the flow focusing is characterized by the formation of a steady focused flow (dispersed phase) in the middle (for 2D stream) or core (for 3D stream) of the highly accelerating sheath flow (continuous phase) at the small orifice geometry. As shown in Figure 2.15, the immiscible streams flow downstream in three separated channels, and the dispersed phase (water in this case) in the middle channel is focused by the continuous phases (oil in this case) in two outside channels. The two liquid phases are pressured to flow through a small orifice which is placed downstream of the three channels. The inner fluid (focused flow) is focused and interrupted by

the pressure and viscosity of the outer fluid (sheath flow), becoming a narrow thread. The narrow thread is to be broken into microspheres inside or downstream of the orifice.

By altering the flow rate ratio $Q(=Q_d/Q_c)$, researchers see that the size of the microspheres varies (see Figure 2.16). Over a range of the flow rates, the size of mono-dispersed microspheres is approximately the size of the orifice (43.5 μm). At low flow rates, collisions occur downstream of the orifice. At higher dispersed flow rate and lower flow rate ratio, bidispersed and polydispersed microsphere distributions can be observed. The sizes of microspheres from the other methods discussed in previous sections are based on the pore width and channel width. However, the sizes of microspheres from this flow focusing technique can be more various and even much smaller than the channel (i.e., orifice) width.

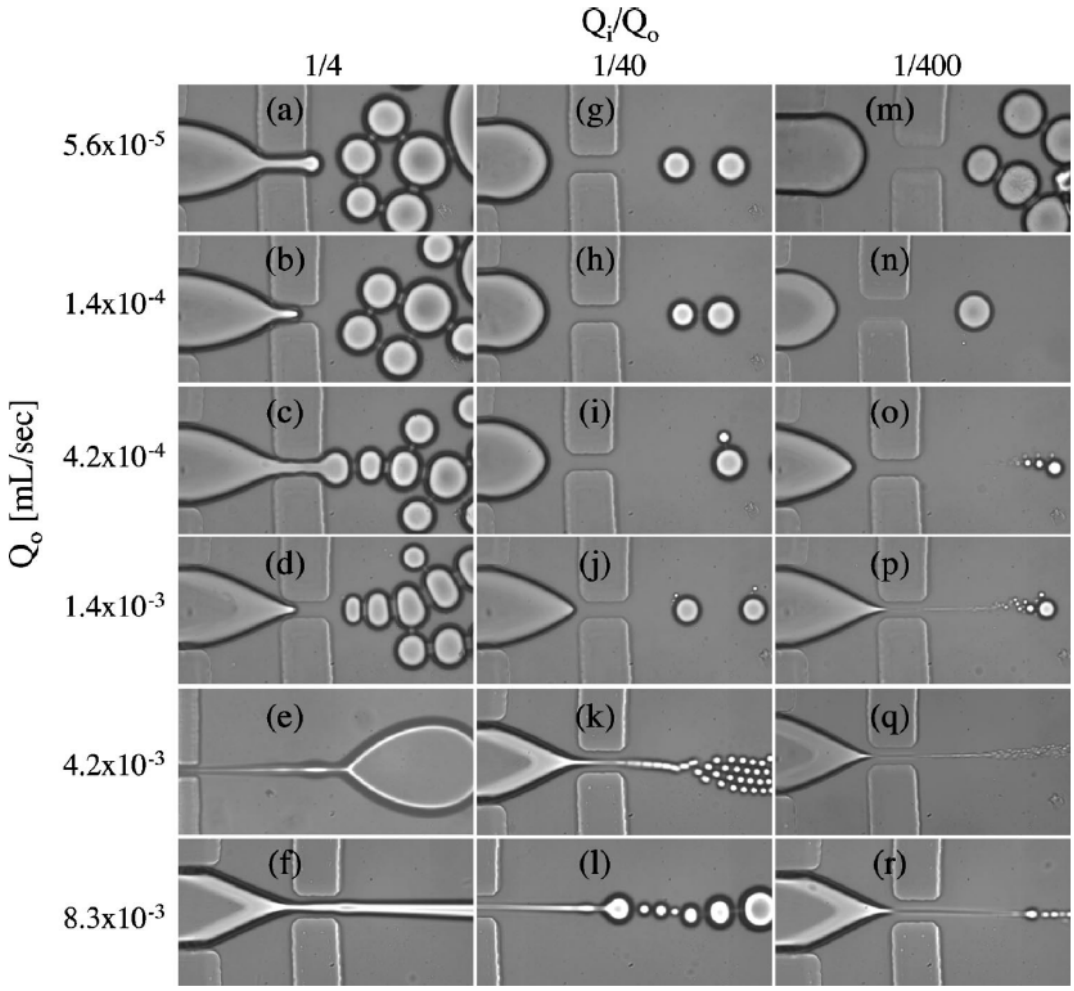

Figure 2.16 Phase diagram for microsphere formation in flow focusing. (Q_o: flow rate of outer fluid (continuous phase) (= Q_c), Q_i: flow rate of inner fluid (dispersed phase)(=Q_d)) [102].

Xu et al. [99] studied the critical breakup width of the central focused flow for highly mono-dispersed microsphere generation with the flow focusing technique. The microchannel was fabricated by micromachining on silicon plate with a dry etching process. The side flows (continuous phases) meet the central flow (dispersed phase) at the junction of a 60° angle as illustrated in Figure 2.17.

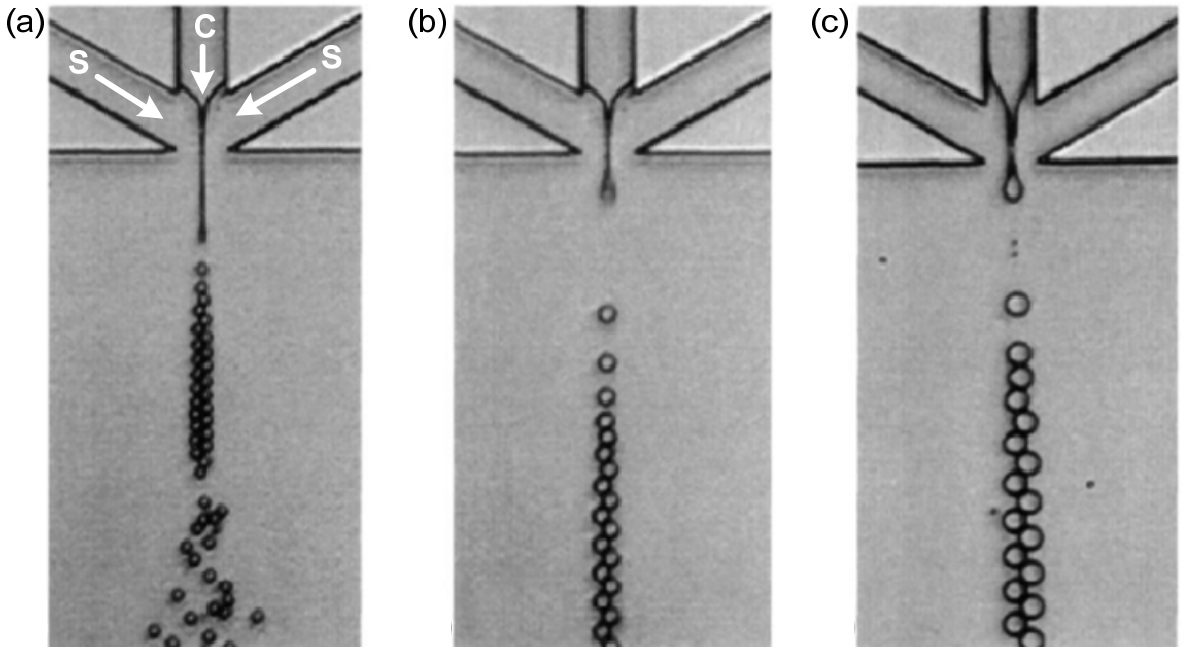

Figure 2.17 Precise control of size of microspheres in the microfluidic system through control of the operating flow condition. (a) d = 9μm, Q_c = 0.45 ml/h, Q_d = 0.002 ml/h. (b) d = 12μm, Q_c = 0.49 ml/h, Q_d = 0.002 ml/h. (c) d = 16μm, Q_c = 0.15 ml/h, Q_d = 0.001 ml/h. (C: central flow, S: side flow, d: diameter of microspheres, Q_c: side flow (continuous phase) rate, Q_d: central flow (dispersed phase) rate). The arrows indicate the directions of flows [99].

The central flow (C) is narrowed by the side flows (S) to a critical width, causing the Rayleigh instability and is broken up from the central flow (C) stream by altering the flow rate ratio $Q(= Q_d/Q_c\,, Q_c\ is\ constant)$ with a constant continuous phase flow rate. The critical breakup width is dependent on various parameters, such as viscosity, interfacial tension, and the geometric characteristics of the microchannel. From the experiments, it was found that 3.5 μm is the critical breakup width, and below the critical width, the central focused stream breaks up. Also, it was confirmed that the dispersed phase flow rate Q_d itself plays an important role on the narrowing and breakup. Slightly below the critical flow rate ratio, mono-dispersed microspheres are generated periodically after a transition from irregular microspheres to polydispersed microspheres, and the size of the microspheres is precisely controllable by altering the flow rate

ratio.

Anna et al. [105] studied the thread formation for smaller sizes of microspheres in the range of a few micrometers or smaller, considering a dimensionless number Ca as depicted in Figure 2.18. In the regime of the thread formation, a central focused stream (dispersed phase) becomes a thin thread downstream, and the width is much smaller than the minimum device feature size. With surfactants, the thread formation behavior is observed to depend strongly on the flow parameters and surfactant bulk concentration. The thread formation of the central flow occurs in the range of $0.4 \leq Ca \leq 1.0$ downstream of the flow focusing orifice. As the speed of side flows becomes faster than the speed of the central flow, the thread formation length increases until $Ca \approx 0.5$. At very small flow rate ratio $Q(= Q_d/Q_c)$, micrometer-scale microspheres are generated from the thread formation. At low Capillary number Ca, the geometry of the flow focusing orifice controls the pinchoff of the central focused (dispersed phase) stream into microspheres. As Ca increases, the viscous stresses from the side flows (continuous phase) narrow the central flow causing smaller size of microspheres than the orifice size. At high Ca, the central flow is elongated into a long jet downstream of the orifice where the size of the microspheres are larger and less controllable.

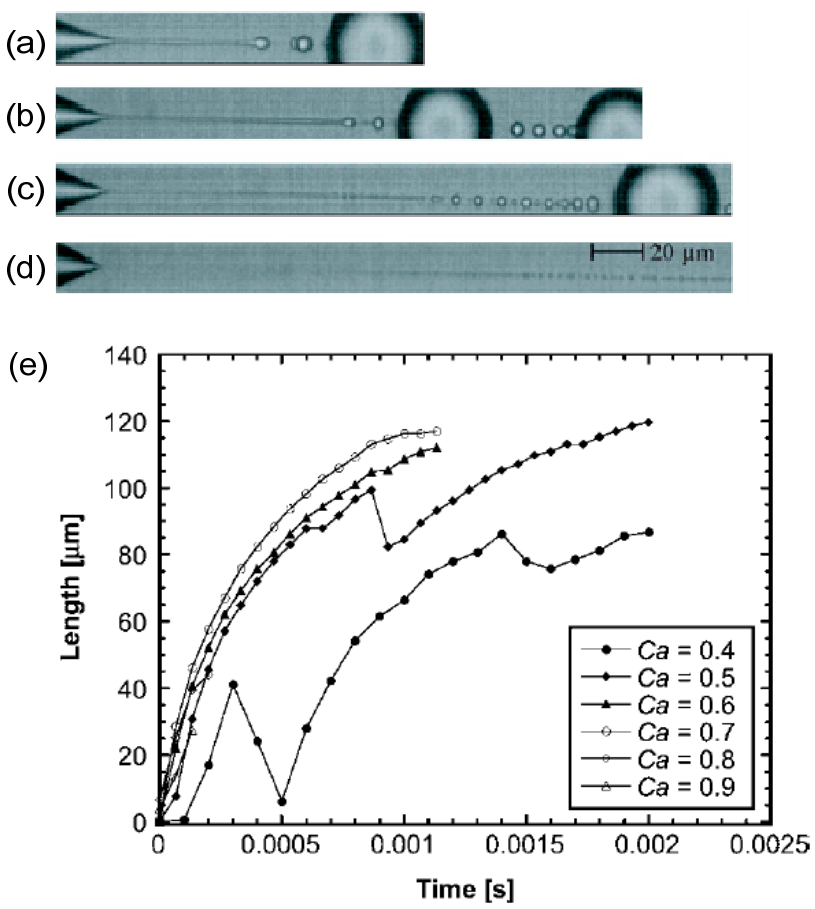

Figure 2.18 Representative images of thread formation ((a) $Q = 1/40$, (b) $Q = 1/80$, (c) $Q = 1/160$, (d) $Q = 1/320$), and (e) growth of the thread length with time for a fixed flow rate ratio $Q = 1/80$ [105].

Kim et al. [106] studied the electrospray using an electric field and flow focusing geometry to generate microspheres in microchannels. The electrodes were embedded in the PDMS microchannels in order to contact the slightly conducting immiscible fluids (see Figure 2.19). An electric field is generated between the electrodes to form a Taylor cone for fine microsphere generation [107, 108]. When the electric field is applied, the interface between aqueous phase and oil phase at the tip of the Taylor cone is charged to behave as a capacitor. With increasing voltages, the tip is elongated, becoming a thin filament downstream that is broken into microspheres by the Rayleigh instability [109]. The size of microspheres can be

controlled by the electric field at high voltages, while the flow focusing dominates the size at low voltages in the microchannels.

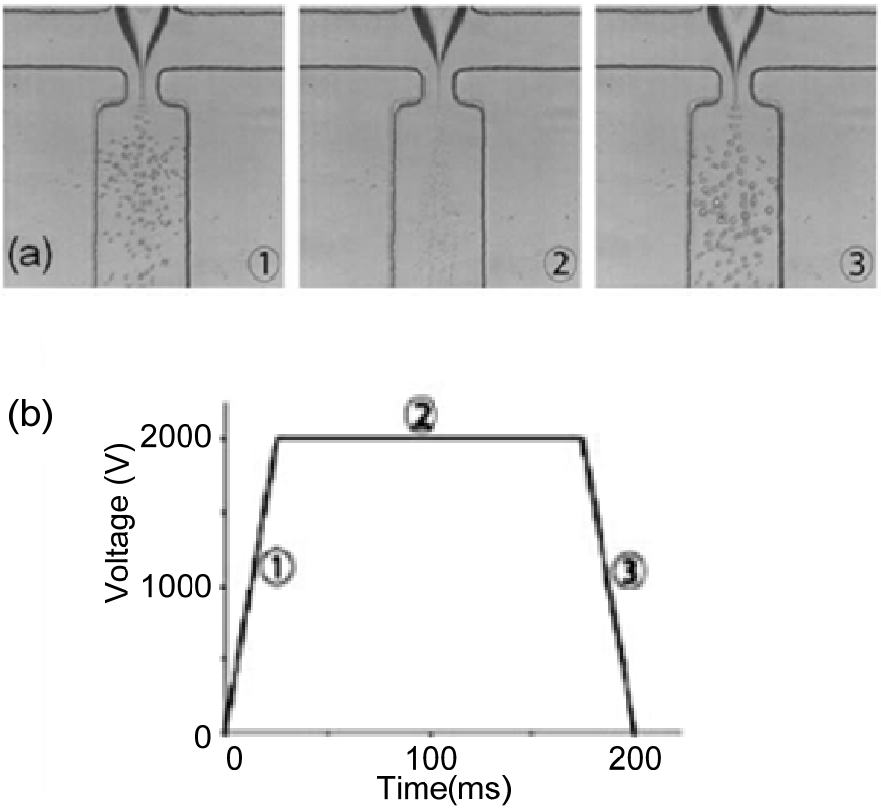

Figure 2.19 Periodic formation of a Taylor cone under an AC electric field. (a) Micrograph showing microsphere formation at the ramp and peak of a rectangular waveform. (b) Rectangular waveform. Flow-rate ratio ($Q = Q_d/Q_c$),5/350 and voltage, 2000 V [106].

Lee et al. [110] studied the impact of viscosity ratio λ which is the viscosity of the dispersed phase compared to viscosity of the continuous phase (μ_d/μ_c) on the microsphere breakup dynamics in a flow focusing device. The viscosity ratio affects the interfacial velocity, tangential stress along the fluid interface, and the surfactant distribution along the interface. The experiments reveal that the viscosity ratio does not affect microsphere formation time in the thread formation regime because the conservation of mass of the dispersed phase dominates to decide the size and formation of microspheres. As well, the deformation which determines the

final size of microspheres remains uninfluenced by a change of the viscosity ratio. However, the thread length increases considerably as the viscosity ratio decreases. As the viscosity ratio decreases, the high extensional strain rate on the thread overcomes the mass transfer along the interface by the interface tension gradient (Marangoni effect); thus, the interface is immobilized. The thread therefore becomes stretched, thin, and broken into microspheres.

Nie et al. [111] studied the effect of viscosity of the dispersed phase on the dynamics of microsphere generation from a flow focusing device (FFD) in a microfluidic system. For the experiments, the flow rate of continuous phase was constant, varying the viscosities. The low viscosity fluids follow the rate-of-flow-controlled break-up law [$V_d \propto (Q_d/Q_c)$] by Garstecki et al. [112], while the high viscosity fluids do not follow the law, yielding a conclusion that the smaller the viscosity, the larger the effect on microsphere volume. The dispersed phase (inner stream) with high viscosity is elongated to become a thread. The thread blocks most of the orifice to create pressure drop, and the continuous phase (outer stream) squeezes the thread by pressure to break the stream into microspheres slowly because the surface tension-driven collapse is slow. Thus, it takes a longer time for the break-up, and the size of microspheres becomes larger than in the case of lower viscosity fluids for the inner stream (dispersed phase).

Li et al. [113] studied the use of the quadruple-microfluidic droplet generator (QDG) consisting of four parallel flow focusing devices (FFDs) with different orifice geometries in PDMS microchannels as shown in Figure 2.20. The QDG in different dimensions yields broaden size distribution of microspheres and can be employed in various applications, such as simultaneous production of colloid particles with different sizes, high throughput screening of the effect of droplet volume on chemical reactions, and diffusion-controlled processes [114-117]. At a low dispersed phase flow rate Q_d ($Q < 6$), the FFDs with wider orifices generate a single

population of large microspheres. However, the FFDs with narrower orifices produce different ratios of microsphere numbers in each population as the flow rate ratio Q $(= Q_d/Q_c)$ varies. It was also found that the flow rates to the different sized orifices affect the size of microspheres.

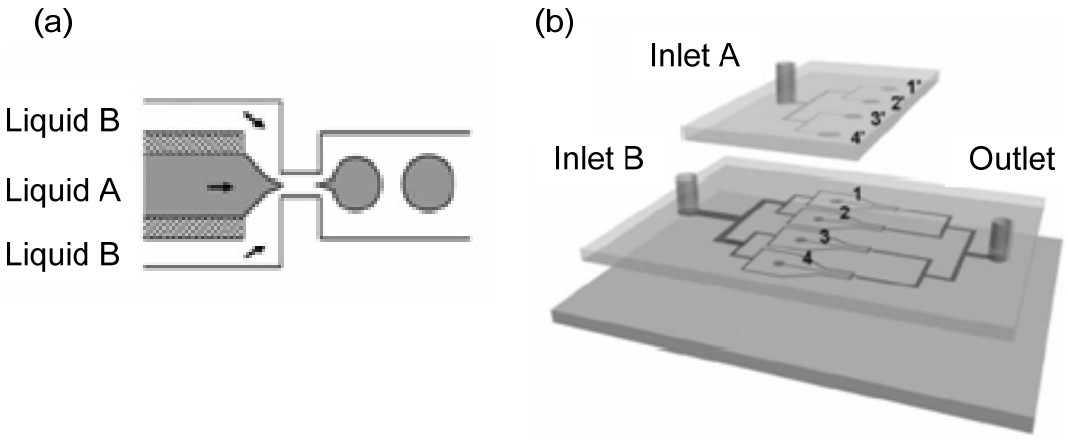

Figure 2.20 Design of the microfluidic QDG. (a) Schematic of the individual flow focusing device. (b) 3D illustration of QDG with three layers: a planar non-patterned bottom sheet; an intermediate sheet with an Inlet B for continuous phase; a top sheet with an inlet A for dispersed phase. The holes at 1-4 and 1'-4' are superimposed [113].

As the continuous phase flow rate Q_c increases, the size of the microspheres decreases at the narrowest FFD, while the size of the microspheres increases at the widest FFD as shown in Figure 2.21.

Tan et al. [118] studied the effect of temperature on microsphere formation in a flow focusing microchannel. A flow focusing device was fabricated using PDMS with integrated microheater and temperature sensor as illustrated in Figure 2.22. From the experiments, three different microsphere formation regimes were observed in a temperature range from 25 to 45°C. From 25 to 30°C, a dripping mode was observed. In the dripping regime, the inner stream (aqueous phase, distilled water or nanofluid) becomes narrower and longer to be broken by localized oscillation at a fixed point. At around 35°C, a squeezing mode was observed.

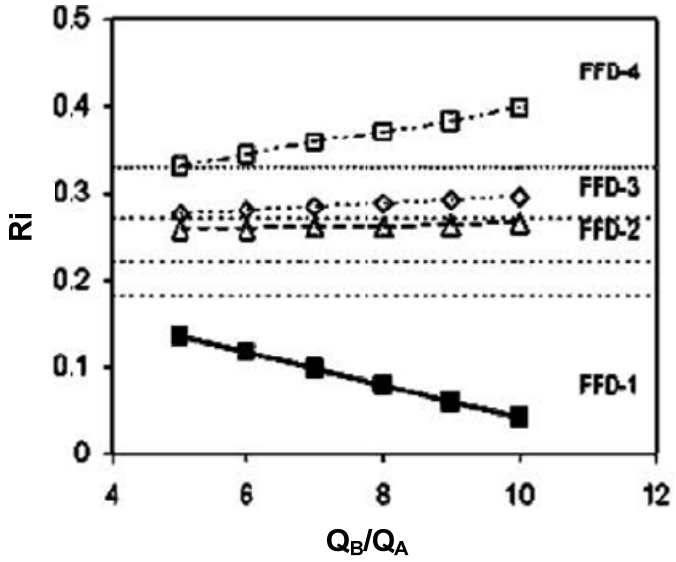

Figure 2.21 Variation in calculated volume fraction R_i of stream A (dispersed phase) in different FFDs as a function of the flow rate ratio (Q_B: flow rate of dispersed phase, Q_A: flow rate of continuous phase). $R_i = V_i/V_{tot}$ where V_i is the total volume of microspheres produced per unit time in individual FFDs, and V_{tot} is the total volume of microspheres obtained in the QDG. The mean orifice width of FFD-1 to FFD-4 are $41 \pm 1\mu m$, $50 \pm 1\mu m$, $61 \pm 1\mu m$, $75 \pm 1\mu m$ [113].

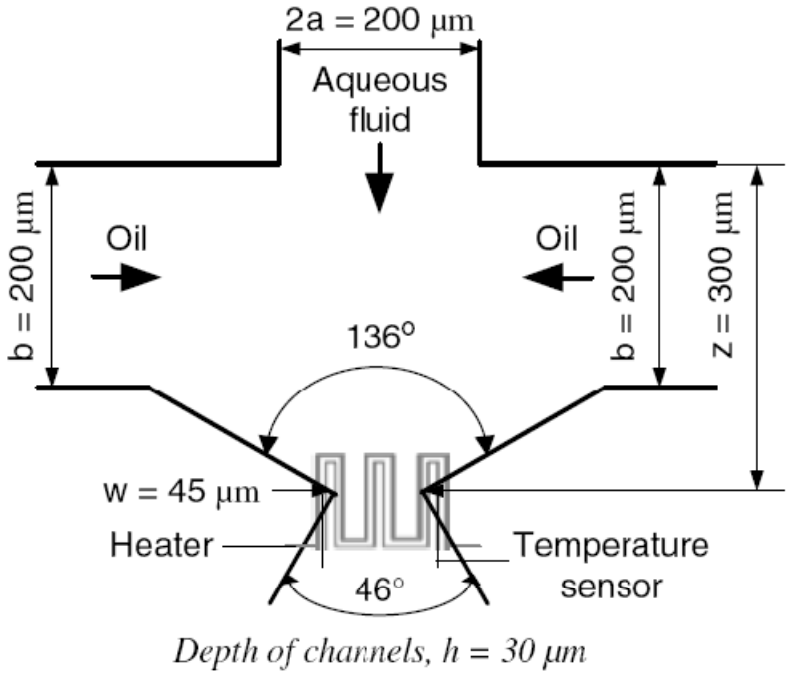

Figure 2.22 Schematic concept of the flow focusing device with an integrated microheater and a temperature sensor for microsphere formation [118].

In the squeezing regime A, the inner stream is squeezed and gradually narrowed down as it enters the orifice. Then, the stream grows to form a bulb to become a microsphere after break-up, yielding larger microspheres than those produced at the dripping regime. At around 45°C, another squeezing mode was observed. In this squeezing regime B, bigger bulbs are formed by the squeezing at the orifice. The Capillary number Ca is used to represent the three regimes as shown in Figure 2.23(a). The increase of temperature causes the change of the Capillary number through the interfacial tension and the viscosity of the outer stream (oil phase), influencing the size of the microspheres (see Figure 2.23(b)). Thus, microsphere size can be controlled by altering the temperature of the microheater with a constant flow rate of the inner fluid. In quasi-two-dimensional (2D) planar microfluidic devices, the wettability of the microchannel walls plays an important role in generating mono-dispersed microspheres. Hydrophobic walls are suitable for water-in-oil (W/O) microsphere generation, while hydrophilic walls are better for oil-in-water (O/W) microsphere generation. Thus, the choice of a material from which to fabricate microchannels is essential for hydrophobicity and hydrophilicity. In order to avoid the effect of the wettability on microchannel walls, three-dimensional (3D) axisymmetric flow focusing is promising since the inner stream is surrounded by the outer stream without contacting the walls. Several methods with capillary tubes [119-122] have been studied to fabricate the 3D axisymmetric flow focusing device; however, it is not easy to embed and align the capillary tubes in the microchannel.

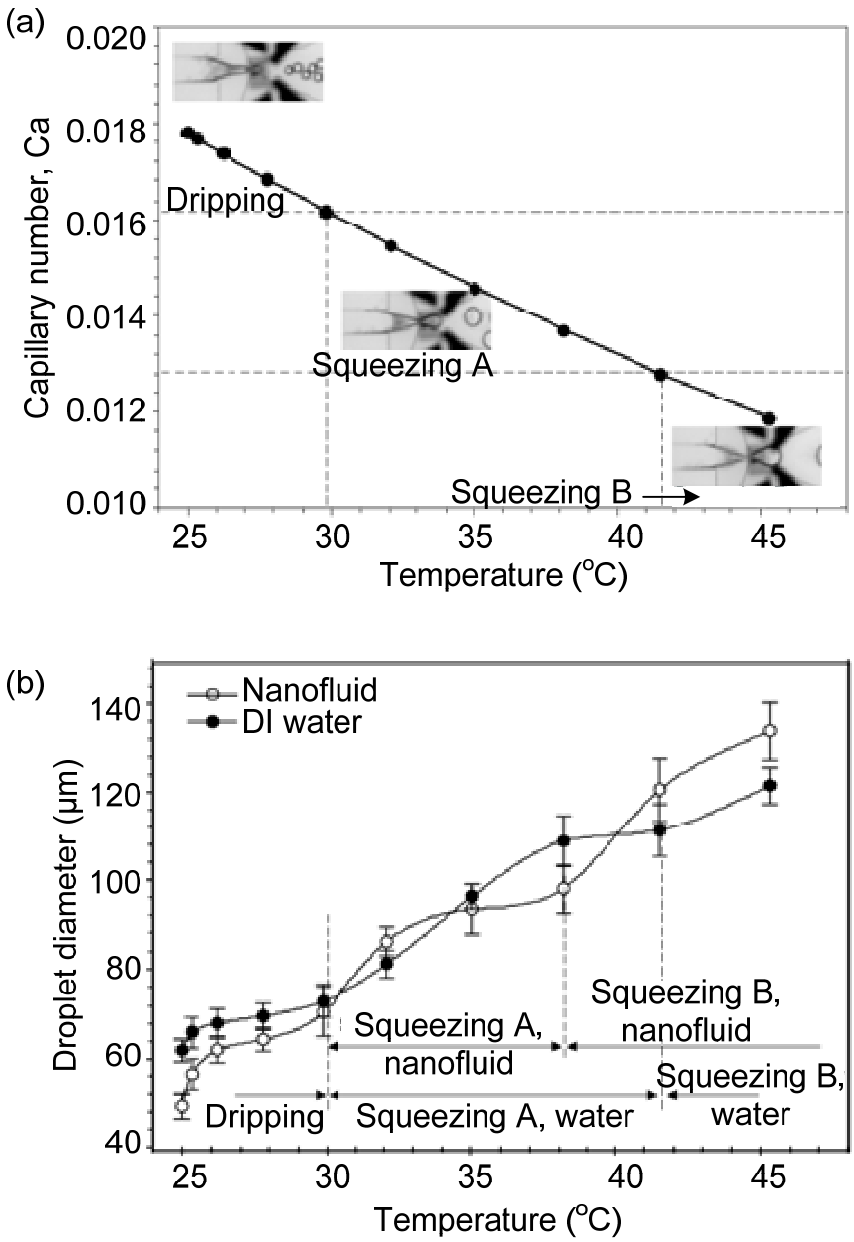

Figure 2.23 (a) Capillary number and microsphere formation regimes at flow rate ratios of 30:5:30 (oil:DI water:oil) (μl h^{-1}). (b) Microsphere size of nanofluid and DI water formed at the same flow rate ratio as (a) [118].

Huang et al. [123] proposed a design concept to fabricate a planar 3D microfluidic flow focusing device (MFFD) by using three layers of SU-8 resist structures to form embedded coaxial orifices as shown in Figure 2.24. Since the inner stream (dispersed phase) is not in contact with the surrounding walls, microspheres in both W/O and O/W are generated without changing the characteristic of the channel walls. Also, double emulsions such as water-in-oil-in-water (W/O/W) or oil-in-water-in-oil (O/W/O) microspheres can be generated with proper interfacial tension and viscosity ratio of the fluids by this technique.

Yobas et al. [124, 125] integrated a circular constriction directly into the 3D flow focusing device with 2D mask layouts yielding two channels: a T-channel for flow focusing and a pipette-channel for collecting the microspheres. A circular orifice is located between the two channels under the surfaces. The fabrication of the circular orifice is simple, engaging a single-step lithography and two-step etching processes: deep reactive ion etching (RIE) and isotropic etching using Sulfur hexafluoride (SF_6) (see Figure 2.25). The size of the orifice is determined by the minimum separation between the two channels and by the total isotropic etching. The circular constriction squeezes the inner stream (dispersed phase) in the channel in all directions, differing from a planar constriction which compresses in two directions (see Figure 2.26) resulting in mono-dispersed microsphere generation. Further, the production of microsphere is extremely spontaneous and reproducible at steady and high frequency.

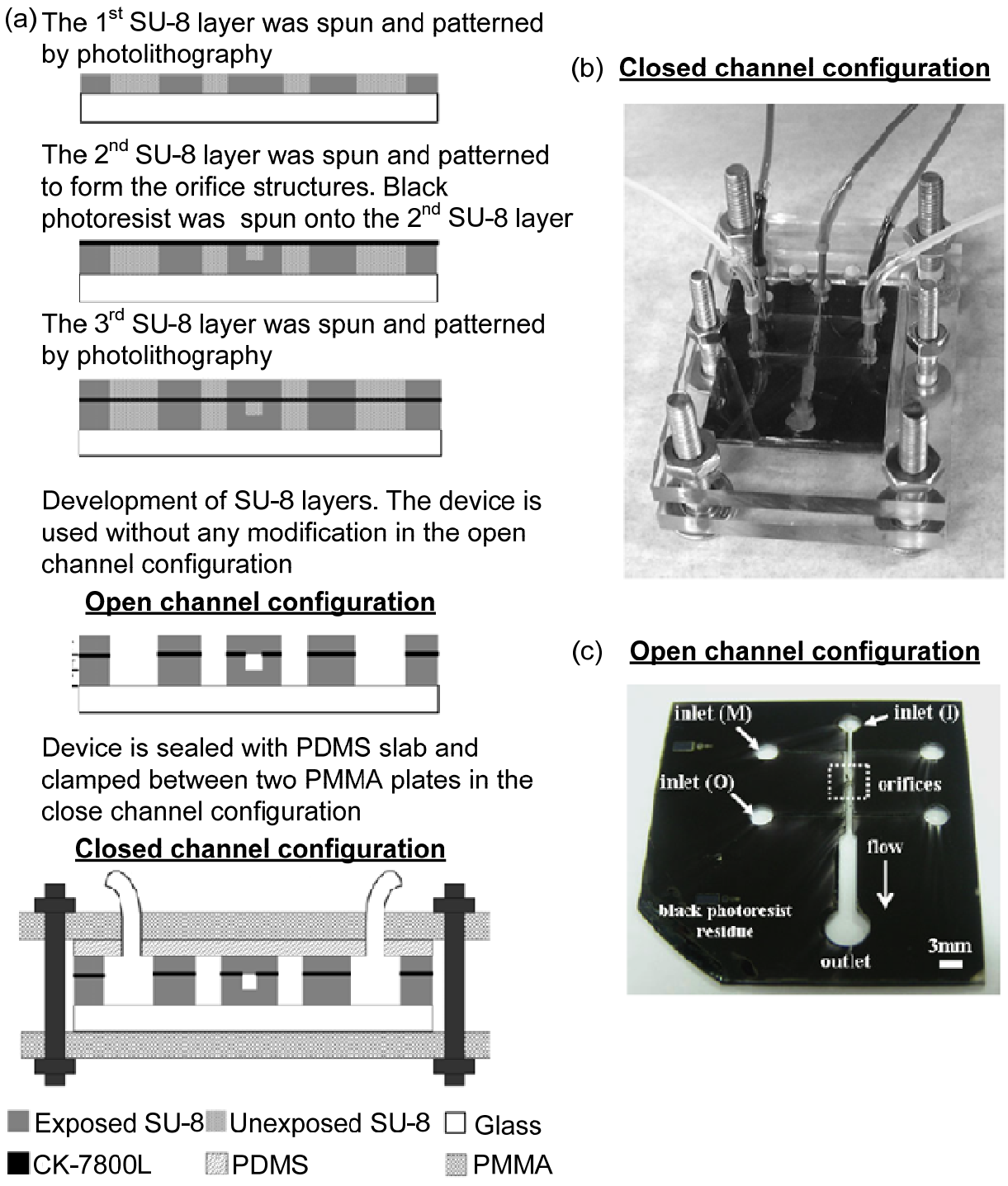

Figure 2.24 (a) Fabrication process of 3D MFFD. (b)-(c) Photographs of the 3D MFFD [123].

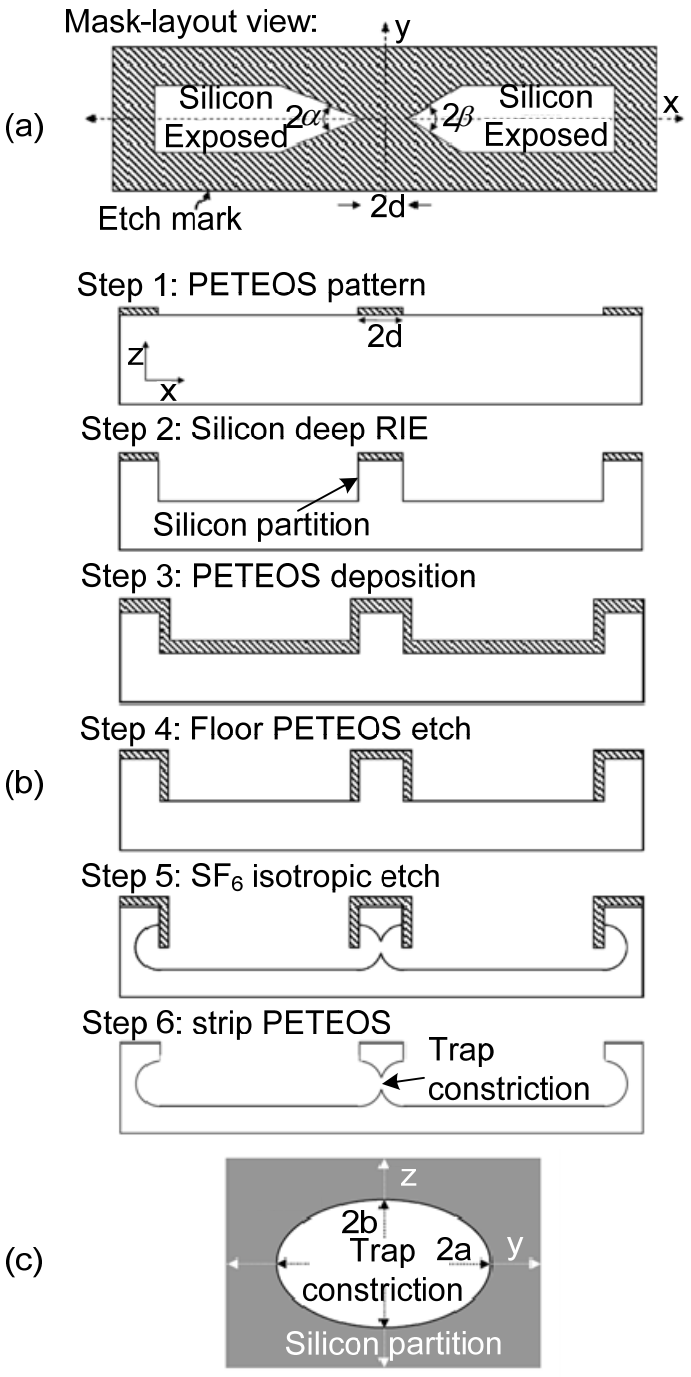

Figure 2.25 Schematic diagrams of the microfluidic device fabrication steps. (a) mask layout view (xy-plane), (b) substrate cross-section profile cut (xz-plane), (c) profile of the circular constriction (yz-plane) [125].

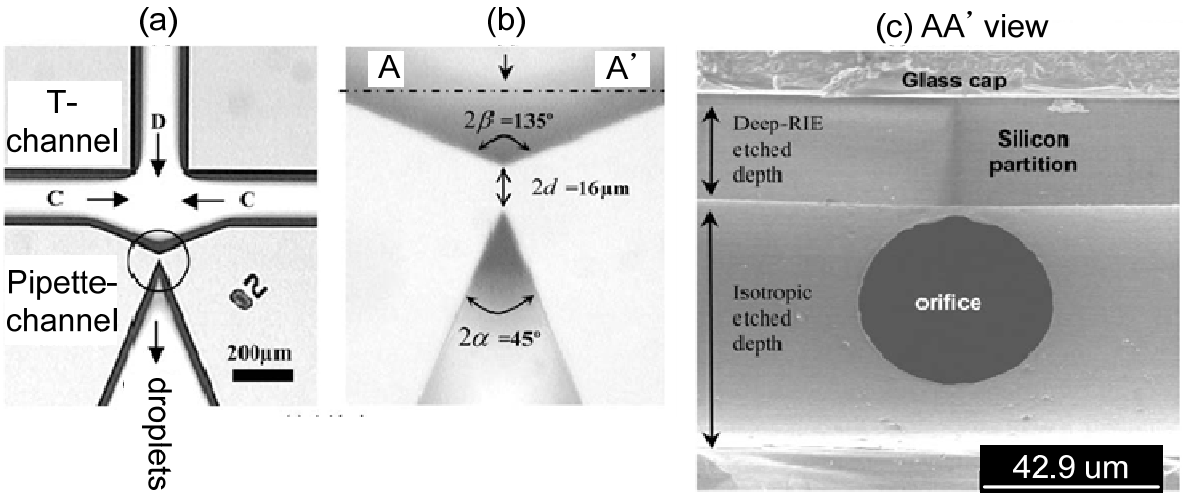

Figure 2.26 (a) planar view. (b) close-up view of the enclosed area from (a). (c) SEM image of the circular orifice taken from a cross-section along AA' [124].

2.3.4. Chopper

A new microfluidic system has been developed with the combination of the flow focusing geometry and liquid-chopping technique by pneumatic liquid-cutting choppers or moving walls of microchannels. These microfluidic devices can actively control the size of the microspheres by altering both the frequency and pressure of choppers and moving walls.

Chen et al. [44], Lin et al. [126], Lao et al. [127], and Lai et al. [128] introduced pneumatic liquid-choppers to generate microspheres in a microfluidic device. The inner stream (dispersed phase) is focused to form a narrow stream by the outer stream (continuous phase) at flow focusing geometry. The microfluidic device is fabricated by the MEMS fabrication process with multiple PDMS layers after the SU-8 molding process. Air chambers are located in the top layer to maintain a high air pressure (pneumatic micro-chopper). A flow focusing device is constructed in the second layer. The prefocused stream in the flow focusing device is driven downstream and cut into microspheres with sizes well-controlled by the active choppers. The pneumatic chopper is a membrane structure and moves vertically to block the fluid streams in the

other membrane when the air is fed to the choppers (see Figure 2.27). The active chopper is controlled by an electromagnetic valve switch (EMV). The size of microspheres can be regulated by either the flow rate ratio of dispersed and continuous phases or the chopping frequency of the pneumatic choppers. Various types of choppers are shown in Figure 2.28.

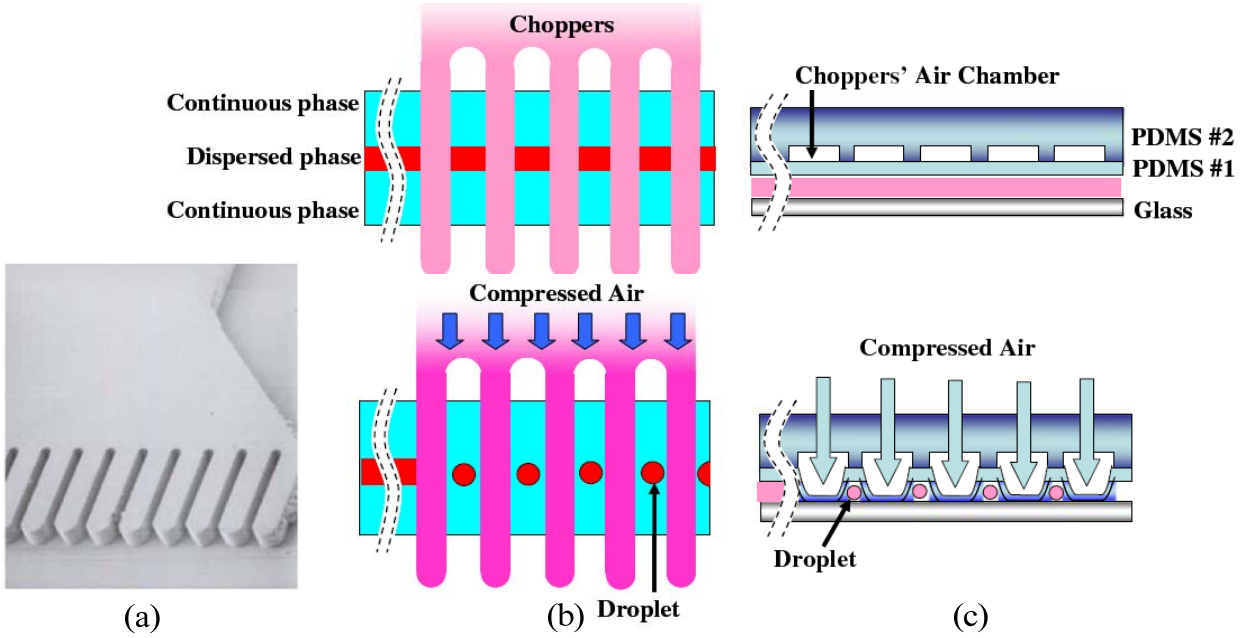

Figure 2.27 SEM image of SU-8 micro-chopper mold (a) and schematic illustrations of the working principle of the micro-choppers: (b) top view and (c) cross-section view [128].

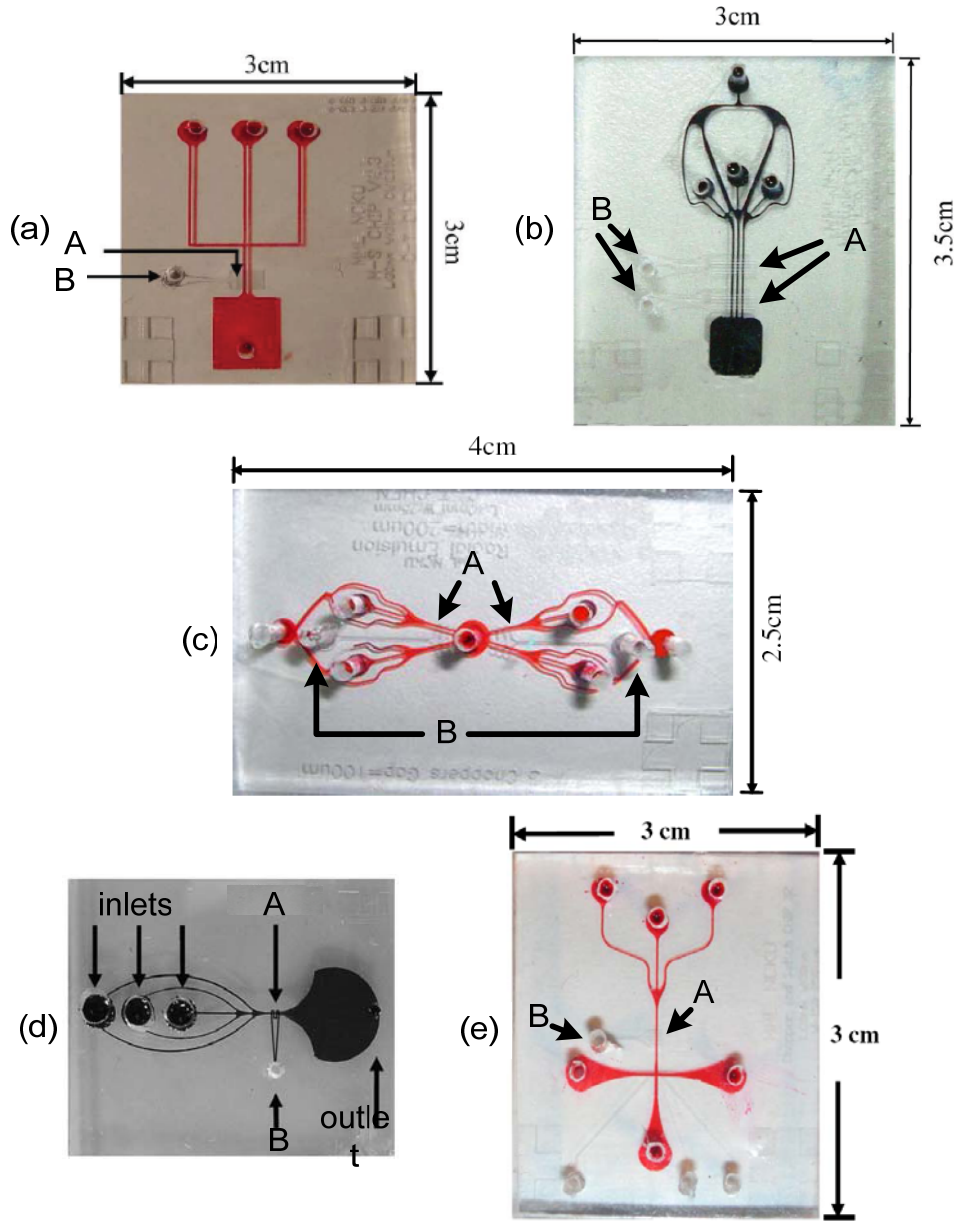

Figure 2.28 Photographs of pneumatic choppers: (a) single flow focusing chip [44], (b) multiple flow focusing chip [44], (c) single flow focusing chip for biotechnology applications [126], (d) flow focusing chip for double emulsion [127] and (e) flow focusing chip for formation and collection of microspheres (A: choppers, B: compressed air inlet) [128].

Hsiung et al. [129], Lee et al. [130], and Lin et al. [131] introduced a combination of flow focusing device and controllable pneumatic moving wall structure to generate microspheres. The microfluidic devices are fabricated by standard MEMS lithography technique with PDMS after

the SU-8 molding process. The focused inner stream (dispersed phase) at the flow focusing geometry is driven downstream, and the moving wall can block and chop the focused inner stream (dispersed phase) horizontally (see Figure 2.29). Controllable pneumatic moving walls are located between the side chamber and the sample flow channel. These pneumatic side chambers are well controlled by electromagnetic valves. Adjusting the flow rate ratio of dispersed and continuous phases, the frequency of the valve and pressure of the compressed air results in well controlled microsphere size. Multiple emulsion can also be achieved by this method.

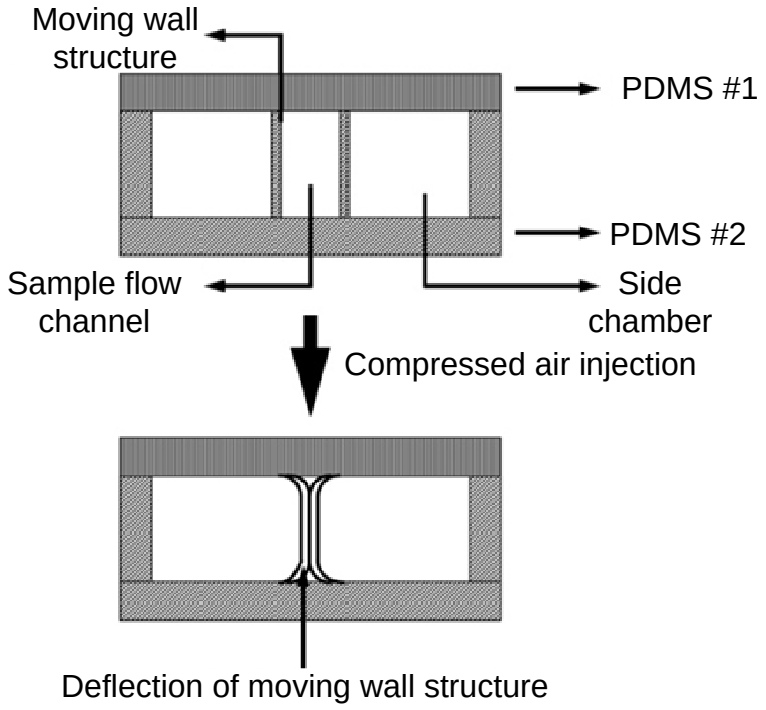

Figure 2.29 Cross-section view of the working principle of the microsphere formation area [129].

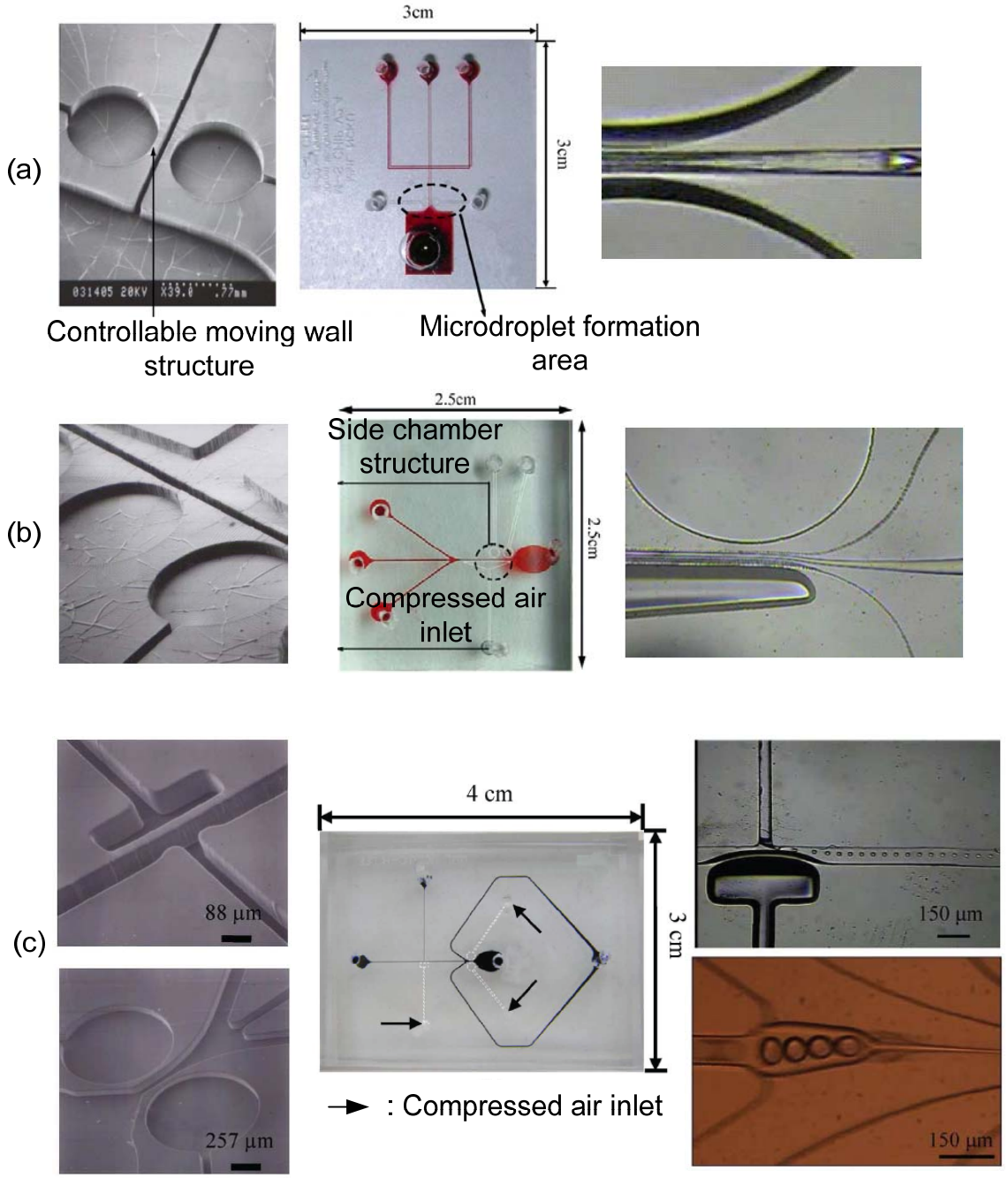

Figure 2.30 Photographs of pneumatic moving walls: (a) the PDMS moving wall structure and the device. A microsphere is generated after a chopping process by the wall [129], (b) the PDMS replica and the device. The inner stream is made narrower by moving the channel walls [132] and (c) the PDMS replicas for double emulsion and the device. After the first emulsion at T-junction utilizing the first moving wall, the second emulsion is achieved at flow focusing geometry by the second moving wall [131].

2.4. Hydrodynamics principle behind the formation of microspheres

The important properties of microsphere generation are the size and the size distribution of microspheres. However, the formation of microspheres during the emulsion is poorly understood [12, 13]. Many numerical analysis methods of microsphere formation have been studied for a better understanding of the formation. Abrahamse et al. [133] used computational fluid dynamics (CFD) software package CFX with the volume of fluids (VOF) method to simulate the break-up process of a droplet on a crossflow membrane. Ohta et al. [134] applied a VOF method to study the formation of a microsphere at an orifice. Kobayashi et al. [85] and Rayner et al. [135] used a CFD software package (CFD-ACE+) with the so-called piecewise linear interface construction (PLIC) method and the Surface Evolver to simulate microsphere formation from straight-through microchannels. However, these CFD packages have not explained all phenomena on a solid physical basis yielding ambiguous results, as is the case for modeling contact line dynamics [136]. Lately, lattice Boltzmann method (LBM) has developed for simulating fluid flows and modeling physics in fluids. The method of LBM is based on microscopic models and mesoscopic kinetic equations which deal with dynamics of particles (molecules) in a system. It is specifically successful in fluid flow applications with interfacial dynamics and complex boundaries [137]. Additionally, LBM can be extended to a multiphase model with two colors for two phases, and the perturbation process is applied to realize the interfacial tension effect. Applying LBM, it is not necessary to follow the trace of the interface explicitly. The interface dynamics are naturally produced as a result of simplified kinetic models resulting in an accurate sharp interface and the position of the interface [13, 138, 139]. Thus, LBM is certainly suitable for mobile contact interfaces in small channels such as microsphere formation in a microchannel where a correct description of all interfaces (including wetting) is

important [140].

2.4.1. Lattice Boltzmann scheme

In LBM, the space is divided into a simple cubic lattice in 3D. At each lattice site, a particle is located with state i (direction) which is defined by velocity vector e_i of a particle as described in Figure 2.31.

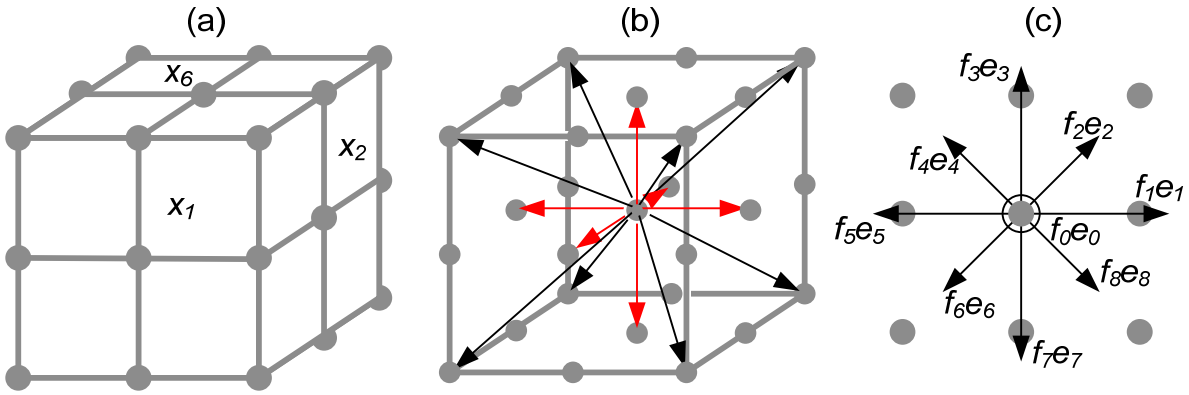

Figure 2.31 Schematic diagram of a cubic lattice: (a) lattice site $\boldsymbol{x}$, (b) the velocity vectors in directions of a particle. Six arrows (in red) point to nearest-neighbor site, and eight arrows (in black) point apices along body diagonals, and (c) the momentum in direction of motion at a site in 2D. The net momentum becomes zero in this example [141].

The sphere in the center of the cubic signifies zero velocity, $e_0 = 0$. During the discrete iteration time, particles move to the nearest lattice site along their direction of motion. Then, the particles collide with some other particles at the same site. The new particle distribution at that site after the collision is determined by the kinetic equation calculating the momentum of the interacting particles as

$$Total\ momentum\ at\ a\ lattice\ site = \sum_{i=1}^{n} f_i(x,t)e_i \tag{2.6}$$

where n is the number of directions, $f_i(x,t)$ is velocity distribution functions at lattice site x and time t, and $e_i(=\frac{\Delta x_i}{\Delta t})$ is velocity vectors of a particle [141].

By assuming that the colliding particles will be rearranged at some constant rate toward an equilibrium distribution of f_i^{eq}, the outcome of the collision is simply approximated by a single-time-relaxation approximation as

$$f_i(\boldsymbol{x}+\boldsymbol{e_i}, t+1) = f_i(\boldsymbol{x}, t) - \frac{1}{\tau}[f_i(\boldsymbol{x}, t) - f_i^{eq}(\boldsymbol{x}, t)] \tag{2.7}$$

where $i = 0,1,\cdots,14$ in a simple 3D lattice, and τ is a relaxation parameter and chosen by the fluid viscosity. The velocity distribution function $f_i(x,t)$ models the total density ρ. For a multiphase-flow system, another velocity distribution function $g_i(x,t)$ is added to model the order parameter ϕ to describe the dynamics of interfaces between different phases as

$$g_i(\boldsymbol{x}+\boldsymbol{e_i}, t+1) = g_i(\boldsymbol{x}, t) - \frac{1}{\tau_\phi}[g_i(\boldsymbol{x}, t) - g_i^{eq}(\boldsymbol{x}, t)] \tag{2.8}$$

where $g_i^{eq}(\boldsymbol{x}, t)$ is local equilibrium distribution, and τ_ϕ is a relaxation parameter.

The collision and relaxation rules lead to the following macroscopic mass and momentum equations [139, 142] as

$$\partial_t \rho + \nabla \cdot (\rho \boldsymbol{u}) = 0 \tag{2.9}$$

$$\partial_t \boldsymbol{u} + \boldsymbol{u} \cdot \nabla \boldsymbol{u} = -\frac{1}{\rho}\nabla p + \nu \nabla^2 \boldsymbol{u} \tag{2.10}$$

where ν is the kinematic viscosity. The total density ρ, the mean fluid velocity u, and the order parameter ϕ which expresses the normalized difference in density of the two fluids can be calculated by the distribution functions as

$$\rho = \sum_i f_i \quad \rho u = \sum_i f_i e_i \quad \phi = \sum_i g_i \tag{2.11}$$

Those quantities are locally conserved in any collision process [13].

Two kinds of models with LBM have been developed to explain multiphase systems.

These models are based on interparticle potentials [143-145] and free energy [93, 138, 146-148]. In this thesis, LBM based on the free-energy function developed by Swift et al. [93] is applied for modeling microsphere generation. Using the free-energy approach, the equilibrium distribution can be defined consistently based on thermodynamics. Accordingly, conservation of the total energy - surface, kinetic, and internal- can be appropriately satisfied [149]. Laudau free-energy function [95, 150] commonly used in a system is defined as

$$F(\phi, \nabla\phi) = \int \left\{ \psi(\phi) + \frac{1}{2}\kappa|\nabla\phi|^2 + \rho c_s^2 ln\rho \right\} dV \tag{2.12}$$

where ρ_A and ρ_B are the densities of fluid A and fluid B, $\rho = \rho_A + \rho_B$ is the total density, ϕ is the order parameter, $\psi(\phi) = \frac{1}{4}a(\phi^2 - 1)^2$ is the bulk free-energy density, $\frac{1}{2}\kappa|\nabla\phi|^2$ represents the interfacial energy density with interface curvature κ, and c_s is speed of sound. The derivative of this free-energy function with respect to the order parameter gives the chemical potential difference between the two fluids, i.e.,

$$\frac{\delta F}{\delta \phi} = \Delta\mu = \psi'(\phi) - \kappa\nabla^2\phi = a\phi(\phi^2 - 1) - \kappa\nabla^2\phi = -A\phi + B\phi^3 - \kappa\nabla^2\phi \tag{2.13}$$

where $a(= A, B)$ is coefficient of fluid A and fluid B for interface thickness. The full pressure tensor in a nonuniform fluid is defined as

$$P_{\alpha\beta} = p_0\delta_{\alpha\beta} + \kappa\partial_\alpha\phi\,\partial_\beta\phi \tag{2.14}$$

where $p_0 = c_s^2\rho - \frac{A}{2}\phi^2 + \frac{3B}{4}\phi^4 - \kappa\phi(\nabla^2\phi) - \frac{\kappa}{2}(\nabla\phi)^2$ is the scalar part of the pressure tensor. The interface thickness is determined by the dimensionless grid Cahn number (Ch) as

$$Ch = \frac{\zeta}{\Delta x} \tag{2.15}$$

where $\zeta = \sqrt{(2\kappa/A)}$ and Δx is the lattice spacing. Also, the profile of the order parameter at interface of inactive two-phase fluids is calculated as [151]

$$\phi(x) = \phi_0 \tanh\left(\frac{x}{\zeta}\right) \tag{2.16}$$

where $\phi_0 = \pm(A/B)^{1/2}$ setting $\nabla\phi = 0$. The interfacial tension of the interface is given by

$$\sigma = \int_{-\infty}^{+\infty} \kappa(\partial_x \phi)^2 dx = \frac{4\kappa\phi_0^2}{3\zeta} \tag{2.17}$$

After introducing the interfacial tension force, the momentum equation becomes

$$\partial_t \boldsymbol{u} + \boldsymbol{u} \cdot \nabla \boldsymbol{u} = -\frac{1}{\rho}\nabla p + \nu\nabla^2 \boldsymbol{u} + \boldsymbol{F} \tag{2.18}$$

where $\boldsymbol{F} = \sigma\kappa\, \nabla C/|\nabla C|$, and the color field $C(\boldsymbol{x}, t)$ and the interface curvature κ are given as

$$C(\boldsymbol{x}, t) = \rho_A(\boldsymbol{x}, t) - \rho_B(\boldsymbol{x}, t) \tag{2.19}$$

$$\kappa = -(\nabla \cdot \hat{\boldsymbol{n}}) = \frac{1}{|\boldsymbol{n}|}\left[\left(\frac{\boldsymbol{n}}{|\boldsymbol{n}|} \cdot \nabla\right)|\boldsymbol{n}| - (\nabla \cdot \boldsymbol{n})\right] \tag{2.20}$$

where $\hat{\boldsymbol{n}}(x)(= \boldsymbol{n}(x)/|\boldsymbol{n}(x)|)$ is the unit normal to the interface and $\boldsymbol{n}(x)(= \nabla C(\boldsymbol{x}))$ is the normal vector [139].

The local viscosity for the two phase fluids is calculated by a harmonic mean [152] as

$$\frac{\phi_0}{\nu(\phi)} = \frac{\phi_0 - \phi}{2\nu_A} + \frac{\phi_0 + \phi}{2\nu_B} \tag{2.21}$$

where $\nu_{A,B}$ is the viscosity of fluid A and fluid B, and the local relaxation parameter $\tau(\phi)$ can be estimated as [13]

$$\tau(\phi) = \frac{\nu(\phi)}{c_s^2 \Delta t} \tag{2.22}$$

2.4.2. Flow in a rectangular channel

In a long channel with a rectangular cross section, a fully developed flow has a specific flow profile as

$$v_y(x,z) = v_0\left[1 - \left(\frac{z}{w}\right)^2 + 4\sum_{k=1}^{\infty}\frac{(-1)^k}{\alpha_k^3}\frac{\cosh\left(\frac{\alpha_k x}{w}\right)}{\cosh\left(\frac{\alpha_k h}{w}\right)}\cos\left(\frac{\alpha_k z}{w}\right)\right] \tag{2.23}$$

with

$$v_0 = \frac{(2h)^2\Delta P}{8\eta L} \qquad \alpha_k = (2k-1)\frac{\pi}{2} \qquad k = 1,2,\ldots \tag{2.24}$$

where $2w$ is the width of a channel, $2h$ is the height of a channel ($-w \le x \le w \; and \; -h \le z \le h$), L is the length of the channel, η is the dynamic viscosity, and ΔP is the pressure drop over the channel [153, 154].

2.4.3. Taylor deformation

The deformation behavior of a droplet between two shearing plates in low Reynolds number Re can be explained with Taylor deformation [13]. The deformation occurs as a function of the shear rate which can be described as Capillary number Ca at a constant Peclet number Pe [155] as illustrated in Figure 2.32.

The definitions of Re, Ca and Pe are given, respectively, as

$$Re = \frac{\dot{\gamma} r^2 \rho}{\eta} \qquad Ca = \frac{\dot{\gamma} r \eta}{\sigma} \qquad Pe = \frac{\dot{\gamma} r \zeta}{MA} \tag{2.25}$$

where $\dot{\gamma}$ is the shear rate which is the velocity of the moving upper wall divided by the channel height, r is the radius of the droplet, ρ is the density, η is the dynamic viscosity, σ is the interfacial tension, ζ is the width of the interface, A is the parameter from the free-energy functional (Eqn.(2.13)), and $M\left(=\Gamma\left(\tau_\phi - 1/2\right)\right)$ is the mobility with a coefficient of mobility Γ. These dimensionless numbers express the importance of physical phenomena in a fluidic system: Re, relating inertial forces to viscous forces; Ca, relating viscous forces to interfacial tension; and Pe, relating convection to diffusion [156].

In the Stokes regime (low Re) and low Ca, a theoretical relation of an elliptically shaped droplet is known by the deformation parameter (D_f) [157, 158] as

$$D_f = \frac{19\lambda + 16}{16\lambda + 16} Ca \tag{2.26}$$

where $\lambda (= \eta_A / \eta_B)$ is the viscosity ratio of fluid A and fluid B.

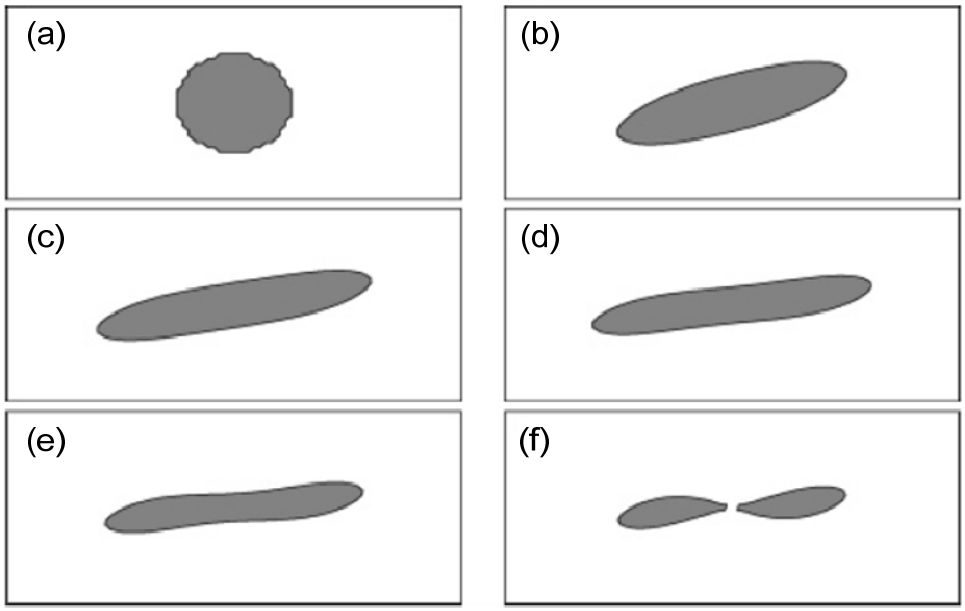

Figure 2.32 Deformation and break-up of a droplet. Droplet in a shear field at $Ca = 0.4$ is broken in two droplets at strains of 0(a), 5(b), 10(c), 15(d), 20(e), and 25(f) [13].

2.4.4. Contact angle

At liquid-liquid interfaces, the LBM also expresses the interactions between the fluids and the walls. Conventionally, the angle of the intersection, contact angle, between a fluid and a solid is fixed. By definition, the sum of the contact angles is equal to 180°. As the affinity (or wettability) of the fluid to the wall increases, the contact angle decreases. In other words, the contact angle decreases as the interfacial tension of the two surfaces decreases. The contact angle between a two-phase fluid (fluid A: red and fluid B: blue) interface and a solid surface is illustrated in Figure 2.33. As depicted in the figure, each fluid has its own contact angle to the

solid. The sum of the two must be 180°. The wetting fluid has a contact angle of less than 90°, and the nonwetting fluid has a contact angle of greater than 90° [137].

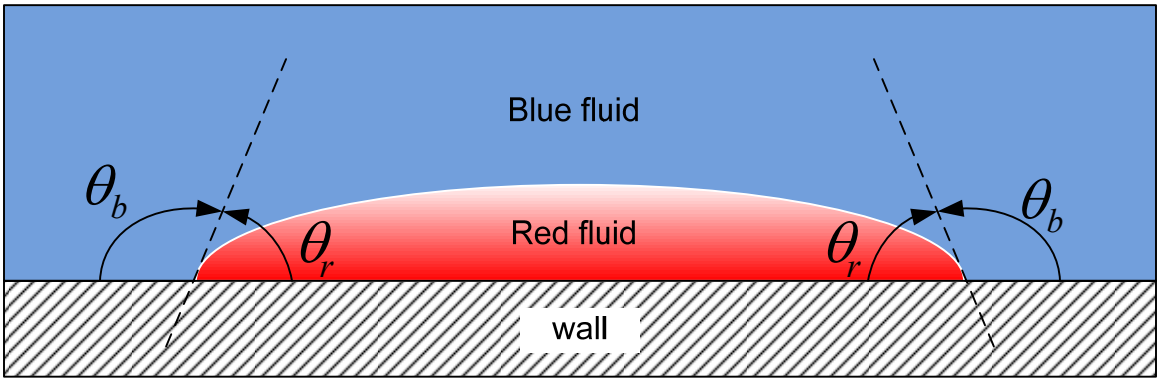

Figure 2.33 The definition of contact angle. ($\theta_r + \theta_b = 180°$).

Young's law expresses the relation between a contact angle and interfacial tension as

$$\cos(\theta) = \frac{\sigma_{r,wall} - \sigma_{b,wall}}{\sigma_{rb}} \tag{2.27}$$

where $\sigma_{r,wall}$ is the interfacial tension of red fluid with the surface, $\sigma_{b,wall}$ is the interfacial tension of blue fluid with the surface, and σ_{rb} is the interfacial tension of the red/blue surface. The surface tensions $\sigma_{r,wall}$, $\sigma_{b,wall}$, and σ_{rb} are defined as

$$\sigma_{r,wall} = \frac{4\kappa\phi_0^2}{\zeta}\left[\frac{2}{3} - \left\{\frac{\phi_{wall}}{\phi_0} - \frac{1}{3}\left(\frac{\phi_{wall}}{\phi_0}\right)^3\right\}\right] \tag{2.28}$$

$$\sigma_{b,wall} = \frac{4\kappa\phi_0^2}{\zeta}\left[\frac{2}{3} - \left\{-\frac{\phi_{wall}}{\phi_0} + \frac{1}{3}\left(\frac{\phi_{wall}}{\phi_0}\right)^3\right\}\right] \tag{2.29}$$

$$\sigma_{rb} = \frac{4\kappa\phi_0^2}{3\zeta} \tag{2.30}$$

Thus, Eqn.(2.27) is rewritten as

$$\cos(\theta) = \frac{3}{2}\bar{\phi}\left(1 - \frac{1}{3}\bar{\phi}^2\right) \tag{2.31}$$

where $\bar{\phi} = \phi_{wall}/\,\phi_0$ [13].

2.5. Discussion

In this chapter, four different microchannel methods to generate microspheres were discussed. Table 2.1 summarizes these methods by comparing the properties of each method.

In the membrane emulsification method, the fabrication of a perforated membrane is relatively more complicated than the other methods. Also, the fabrication cost is high because this method requires a specific perforation process such as dry etching. The size of microspheres generated by this method depends mainly on the size of perforation. Size uniformity by this method is satisfied; however, size controllability is limited. In the T-junction method and hydrodynamic flow focusing method, the fabrication of microchannels is relatively easy and cost-effective because of many underlying acting fabrication concepts such as molding technique (i.e., soft lithography). Various sizes of microspheres can be generated by adjusting flow rates of dispersed phase and continuous phase, and the uniformity of the microspheres in different sizes is acceptable according to the mono-dispersity (CV < 5%). The hydrodynamic flow focusing method generates much smaller sizes of microspheres. However, these methods create satellite drops during microsphere generation, which makes a high uniformity of microspheres by these methods difficult. In the chopper method, the fabrication process is extremely difficult since this method needs 3D microchannel structures. In order to fabricate the vertical structures, accurate alignment processes are necessary with many layers of microchannels. The sizes of generated microspheres are based on the frequency of choppers, which results in various sizes of microsphere generation with a small number of satellite drops. Sizes of microspheres generated by this method are much bigger than those made by other methods because the PDMS chopper limits applicable frequency by its elasticity. Additionally, some chopper methods cannot achieve uniformity of microspheres (CV > 5% [128, 130]).

Table 2.1 Comparison of different microchannel methods for generating microspheres

Properties	Membrane emulsification method	T-junction method	Hydrodynamic flow focusing method	Chopper method
Fabrication	Difficult	Easy	Easy	Difficult
Fabrication cost	High	Low	Low	Medium
Uniformity	High	Medium	Medium	High / Low
Satellite generation	Low	High	High	Low
Smaller size generation (< 5μm)	Low	Low	High	Low
Size control	Pore size, Flow rates	Flow rates	Flow rates	Frequency of choppers
Size controllability	Limited	Yes	Yes	Yes

2.6. Conclusion

Protein-based drugs have shown great potential in medical treatment for years, although proteins and peptides have limitations in some environments. Important studies have been performed in order to overcome the limitations, and microspheres by emulsion became one of the prospective solutions. However, typical methods for emulsion could not achieve the narrow size distribution (uniformity) of microspheres. Development of micro-electro-mechanical systems (MEMS) technology improved the possibility of defeating the disadvantages of the typical methods by introducing microfluidic devices to generate microspheres. The fundamental principle of modeling formation of microspheres assists in understanding of emulsions in a microchannel. Although various methods have been introduced by MEMS techniques, the uniformity of microspheres is still problematic. It has been shown that as the microsphere size from microchannels reduces, the uniformity of the microspheres decreases as well.

In this thesis, various types of microfluidic devices with the emulsion mechanism will be analyzed in order to improve the uniformity and the controllability of microsphere sizes by a systematic design process, Axiomatic Design Theory (ADT). Uniformity or mono-dispersity of microspheres is desirable for the constant and predictable responses of the microspheres to external fields [41]. Hence, the reliability of using these microspheres in various applications can be increased. Also, the controllability of microsphere sizes is demanded. By producing different sizes of microspheres with one microchannel, the cost of microsphere production in various sizes will be reduced. In order to achieve these major requirements (i.e., uniformity and controllability), from microfluidic systems, the ADT will be employed to guide the process to improve the existing designs. It is interesting to observe, through this review, that no general design theory and methodology seems to be applied to microfluidic systems in the current literature. This situation has been hypothesized in this thesis as responsible for the current state of arts of microfluidic systems for microspheres generation.

3. AXIOMATIC DESIGN THEORY INTO DESIGN OF MICROFLUDIC SYSTEMS FOR MICROSPHERE GENERATION

3.1. Introduction

In this chapter, a study to apply a systematic design theory, Axiomatic Design Theory (ADT), to analyze two conventional microfluidic system designs and to propose new conceptual microfluidic system designs will be described. The ADT approach has been applied to various fields with as yet few to MEMS applications such as pressure sensor [159], micro-actuator [160], micro-photonic beam steering system [161], and gyroscope [162]. Hence, this study may also contribute to the formulation of a systematic design approach to general MEMS products.

The ADT is briefly introduced in Section 3.2. In Section 3.3, the current microfluidic systems for microsphere generation are analyzed by the ADT, and novel microfluidic system designs are subsequently proposed. A conclusion is given in Section 3.4.

3.2. Axiomatic design theory (ADT)

Design is the interplay between ‘what we want to achieve’ and ‘how we want to achieve it’. Design has been defined in a variety of ways, depending on the specific context and/or the field of interest. The customers’ needs are filtered to define function requirements ($\boldsymbol{FRs}$), and an $\boldsymbol{FR}$ describes ”what we want to achieve.” Some of the customer’s needs may not be defined precisely, and thus they are translated into constraints. These constraints are required to be satisfied as well, so the term ”constraint requirements” ($\boldsymbol{CRs}$) emerges [163]. The descriptor of ”how to achieve it” is defined as design parameters ($\boldsymbol{DPs}$). To be efficient and to generate the design that meets the perceived needs, the designer must specifically state the design goals in

terms of ”what we want to achieve” and begin the design process. Iterations between ”what” and ”how” are necessary, but each iteration loop must redefine the ”what” clearly. There are many proposed approaches in the field of design theory and methodology in addition to the general design process as outlined above. Among them, Axiomatic Design Theory (ADT) is one of the most effective approaches. In this thesis, the ADT is tailored to microfluidic system design. The ADT can guide innovative microfluidic system designs to overcome the problems from conventional system design practice which is still conducted in often ad hoc circumstances, causing unnecessarily high costs and lowered robust behaviors during the system development. [164-168].

Design is separated into three phases: conceptual design, embodiment design, and detailed design. The purpose of the conceptual design is to generate a solution principle. At the conceptual design phase, ADT as a systematical design process has been applied in various research fields since ADT is the only design theory to assist to find the best design at the conceptual design phase. The details and applications of ADT are explained in Appendix A. The applications and developments of ADT support that ADT is an excellent means to study current microfluidic system designs systematically, and to realize a new design methodology of microfluidic systems to achieve more reliable and robust systems by avoiding possible failures during operations.

3.3. The ADT analysis of two Conventional Microfluidic Devices

3.3.1. Analysis of design

A typical microfluidic device consists of two parts which are shown in Figure 3.1: a substrate and a top plate. For easy observation during an experiment, either a substrate or a top wafer should be transparent. Microchannels including inlets and outlets are patterned and

fabricated on a top plate for easy fabrication.

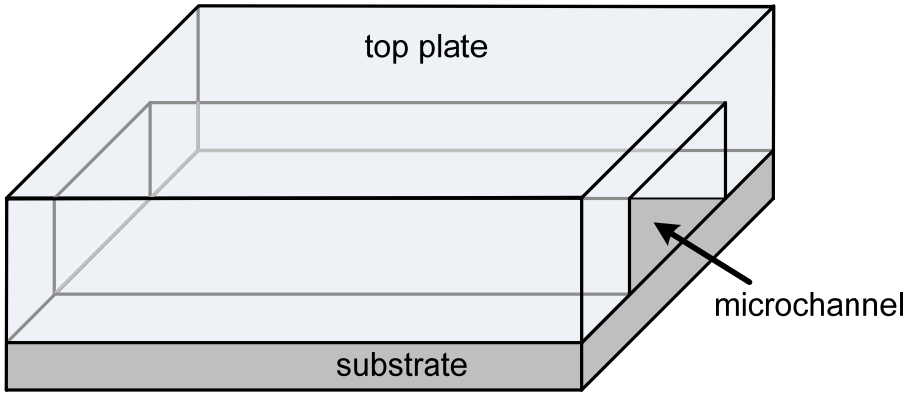

Figure 3.1 A typical microfluidic device with a microchannel.

In order to produce microspheres in microchannels, emulsion plays an important role. Emulsion of two immiscible fluids in micro scales has attracted great attention for generating microspheres to serve various applications, yielding a continuous phase to wrap up microspheres and a dispersed phase to be microspheres. Interaction between two immiscible fluids is governed by interfacial tension and inertial forces. The two forces play competing roles. When the interfacial tension force dominates, the interfacing area of the two fluids decreases, and when inertial force dominates, the interfacing area increases. The Weber number We describes the relative importance of interfacial tension and inertial force between the immiscible fluids [169]. The dimensionless Weber number is defined as

$$We = \frac{\rho V^2 l}{\sigma} \tag{3.1}$$

where ρ is the density of a dispersed phase, V is the relative velocity, l is the characteristic length which is the width of a dispersed phase and σ is the interfacial tension. Thus, the smaller characteristic length of the flow stream yields a higher proportion of the interfacial tension in the two-phase flow.

Functional requirements ($\boldsymbol{FRs}$) of a microchannel system to generate uniform and size-

controllable microspheres are size consistency (uniformity) and size controllability. Size consistency is important to regular and predictable responses, and it is apparently related to how uniform a continuous phase stream is. Then, breakage is regarded as a major functional requirement. At the same time, size controllability is necessary to a controlled release of drugs - for example, controlled release of active agents (i.e. antigens) from the polymeric microsphere [24, 45, 46, 48]. The size of microspheres is apparently relevant to the width of the dispersed phase stream. Hence, we define $\boldsymbol{FRs}$ as

- $\boldsymbol{FR_1}$: Size consistency (uniformity).
- $\boldsymbol{FR_2}$: Breakage of the flow stream.
- $\boldsymbol{FR_3}$: Size controllability.

According to the Axiomatic Design Theory (ADT), the next step is to define or conceive $\boldsymbol{DPs}$ to achieve $\boldsymbol{FRs}$. To conceive $\boldsymbol{DP_1}$ for $\boldsymbol{FR_1}$, continuous flow streams with consistent flow rates are necessary. A pneumatic pump can generate continuous and constant air pressures to feed fluids to microchannels. Altering the pressures cuts dispersed phase streams to form microspheres. The $\boldsymbol{DP}$ for each $\boldsymbol{FR}$ is as follows:

- $\boldsymbol{DP_1}$: Continuous and consistent pressures at inlets of microchannels.
- $\boldsymbol{DP_2}$: Alternation of air pressures on the both streams to create a high shear stress.
- $\boldsymbol{DP_3}$: Alternation of air pressures on dispersed phase streams.

3.3.2. Evaluation of designs

Typical designs of microchannels for microsphere generation are crossflow at T-junction and hydrodynamic flow focusing at intersection, as illustrated in Figure 3.2.

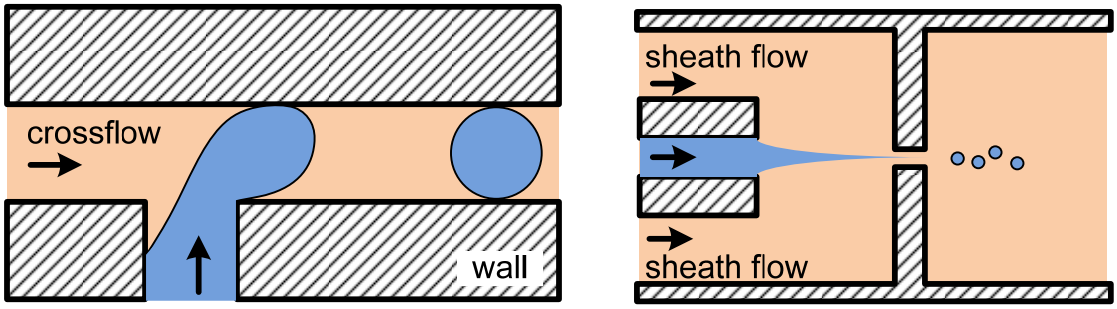

(a) crossflow at T-junction (b) hydrodynamic flow focusing

Figure 3.2 Schematic top views of typical methods to generate microspheres in microchannels. In the microchannels, different colors of fluids signify two immiscible flows which are continuous phase and dispersed phase, and the arrows represent directions of flows.

In the T-junction design, the flow rate of the continuous phase (crossflow) cuts the dispersed phase into droplets to form microspheres. A high velocity of the crossflow reduces the size of the width of the dispersed phase to break it into microspheres. In the intersection design, the sheath flow (continuous phase) breaks the focused flow (dispersed phase) to form microspheres. Similar to the T-junction design, the high flow rates of sheath flow reduce the width of dispersed phase.

The two conventional designs, as described above, are highly coupled. First, $\boldsymbol{DP}_1$, $\boldsymbol{DP}_2$ and $\boldsymbol{DP}_3$ are together to achieve $\boldsymbol{FR}_2$ and $\boldsymbol{FR}_3$. In other words, any change on $\boldsymbol{DP}_1$, $\boldsymbol{DP}_2$ and $\boldsymbol{DP}_3$ would cause same change on $\boldsymbol{FR}_2$ and $\boldsymbol{FR}_3$. Second, a change on $\boldsymbol{DP}_1$ can affect $\boldsymbol{FR}_1$, $\boldsymbol{FR}_2$ and $\boldsymbol{FR}_3$. In fact, according to the ADT, the design equation for the two designs can be represented by

$$\begin{Bmatrix} \boldsymbol{FR}_1 \\ \boldsymbol{FR}_2 \\ \boldsymbol{FR}_3 \end{Bmatrix} = \begin{bmatrix} \times & 0 & 0 \\ \times & \times & \times \\ \times & \times & \times \end{bmatrix} \begin{Bmatrix} \boldsymbol{DP}_1 \\ \boldsymbol{DP}_2 \\ \boldsymbol{DP}_3 \end{Bmatrix} \tag{3.2}$$

3.3.3. Proposed conceptual designs

As discussed in the previous section, a decoupled design is pursued in this thesis. The

semantics of decoupling process is as follows. First, inlet pressures to change the width of the dispersed phase stream and to break it must be separate. This can be in principle realized such that the width of the dispersed phase is narrowed by the continuous phase, and the dispersed phase is cut to form microspheres by a means which is independent of the continuous phase. Further, according to the ADT, coupled designs can lead systems to be sensitive to disturbances which are known to be significant in fluid systems. For fluid systems, they should better be designed into decoupled designs, if not uncoupled designs which are the best. The design equation for a decoupled design related to the microchannel system for microsphere generation is shown in the following equation.

$$\begin{Bmatrix} \boldsymbol{FR}_1 \\ \boldsymbol{FR}_2 \\ \boldsymbol{FR}_3 \end{Bmatrix} = \begin{bmatrix} \times & 0 & 0 \\ \times & \times & 0 \\ \times & \times & \times \end{bmatrix} \begin{Bmatrix} \boldsymbol{DP}_1 \\ \boldsymbol{DP}_2 \\ \boldsymbol{DP}_3 \end{Bmatrix} \tag{3.3}$$

Also, the design equation for the lower level must be uncoupled or decoupled as

$$\{\boldsymbol{FR}_{i_1 \dots i_k}\} = \begin{bmatrix} \times & 0 & \cdots & 0 \\ 0 & \times & \cdots & 0 \\ \vdots & \vdots & \ddots & 0 \\ 0 & 0 & \cdots & \times \end{bmatrix} \{\boldsymbol{DP}_{i_1 \dots i_k}\}, \quad \begin{cases} i_1 = \{1,2,3\} \\ i_2 = \{1,2,\dots,s_1\} \\ i_3 = \{1,2,\dots,s_2\} \\ \quad \vdots \\ i_k = \{1,2,\dots,s_z\} \end{cases} (uncoupled\ design) \tag{3.4}$$

$$\{\boldsymbol{FR}_{i_1 \dots i_k}\} = \begin{bmatrix} \times & 0 & \cdots & 0 \\ \times & \times & \cdots & 0 \\ \vdots & \vdots & \ddots & 0 \\ \times & \times & \cdots & \times \end{bmatrix} \{\boldsymbol{DP}_{i_1 \dots i_k}\}, \quad \begin{cases} i_1 = \{1,2,3\} \\ i_2 = \{1,2,\dots,s_1\} \\ i_3 = \{1,2,\dots,s_2\} \\ \quad \vdots \\ i_k = \{1,2,\dots,s_z\} \end{cases} (decoupled\ design) \tag{3.5}$$

In the subsequent sections, several microfluidic system designs are proposed, named by: (i) perforated silicon membrane, (ii) integration of hydrodynamic flow focusing and crossflow, and (iii) liquid chopper utilizing a piezoelectric actuator. Further, decoupling processes are discussed for the cases of (i), (ii) and (iii).

3.3.3.1. **Perforated silicon membrane**

The general idea with this method is such that a dispersed phase containing the dissolved microsphere matrix material reaches a continuous phase after a silicon membrane with micron-sized perforations, through which microdroplets are formed. The microdroplets are detached from the silicon membrane by a crossflow generated by spinning an agitator. After the droplet is detached from the membrane, a solvent which is used for a dispersed phase diffuses out of the detached droplets, leading to the formation of solid microspheres [170]. The formation of microspheres is illustrated in Figure 3.3.

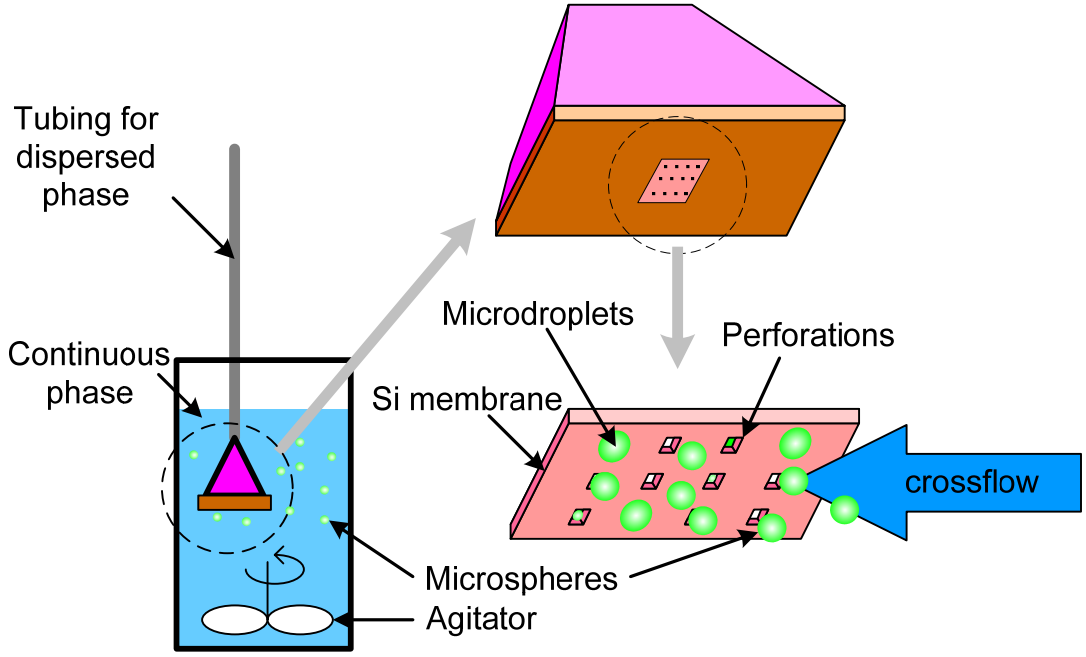

Figure 3.3 Schematic view of microsphere formation with a perforated silicon membrane. A dispersed phase is injected and passes through the perforations on the silicon membrane to form microspheres by a crossflow.

With the perforated silicon membrane, $\boldsymbol{FRs}$ and $\boldsymbol{DPs}$ are further decomposed into lower levels, and they are as follows:

- $\boldsymbol{FR_1}$: Size consistency (uniformity).
  - $\boldsymbol{FR_{11}}$: Keep constant flow rate of the dispersed phase.

- $\boldsymbol{DP}_1$: Continuous and consistent pressures.
    - $\boldsymbol{DP}_{11}$: Keep constant pressure for the dispersed phase.

$$\{\boldsymbol{FR}_{11}\} = [\times]\{\boldsymbol{DP}_{11}\} \tag{3.6}$$

- $\boldsymbol{FR}_2$: Break the dispersed phase from the main dispersed phase stream.
    - $\boldsymbol{FR}_{21}$: Change the flow rate of the crossflow.
- $\boldsymbol{DP}_2$: Detach microdroplets from the membrane.
    - $\boldsymbol{DP}_{21}$: Increase the speed of the agitator.

$$\{\boldsymbol{FR}_{21}\} = [\times]\{\boldsymbol{DP}_{21}\} \tag{3.7}$$

- $\boldsymbol{FR}_3$: Size controllability.
    - $\boldsymbol{FR}_{31}$: Change the pore size on the membrane.
- $\boldsymbol{DP}_3$: Change the size of the neck of microdroplet on the membrane.
    - $\boldsymbol{DP}_{31}$: NOT AVAILABLE (constant).

$$\{\boldsymbol{FR}_{31}\} = [\times]\{\quad\} \tag{3.8}$$

From the observation, the design of perforated silicon membrane results in an uncoupled design without satisfying $\boldsymbol{FR}_3$ because of the uncontrollable (constant) pore size on the membrane. The design equation of this conceptual design is

$$\begin{Bmatrix}\boldsymbol{FR}_1\\ \boldsymbol{FR}_2\end{Bmatrix} = \begin{bmatrix}\times & 0\\ 0 & \times\end{bmatrix}\begin{Bmatrix}\boldsymbol{DP}_1\\ \boldsymbol{DP}_2\end{Bmatrix} \tag{3.9}$$

This uncoupled design is the most demanded design, satisfying the independence axiom. The details of this microfluidic system will be discussed in Chapter 4.

3.3.3.2. **Integrating hydrodynamic flow focusing and crossflow**

A decoupled design is proposed by integrating hydrodynamic flow focusing and crossflow methods as shown in Figure 3.4. In this proposed design, the middle stream is focused hydrodynamically by the sheath flow from the intersection (A). After being focused, the velocity of a focused flow becomes higher since the width of the middle flow decreases. This

phenomenon is not avoidable in order to meet the flow rate of the middle flow, and it makes the focused flow stable with high inertial force. By integrating a crossflow mechanism and introducing an extra flow through the crossflow, the stable focused flow becomes "disturbed" and forms microspheres. A further decomposition of $\boldsymbol{FR_1}$ into lower levels is as follows.

- $\boldsymbol{FR_1}$: Size consistency (uniformity).
  - $\boldsymbol{FR_{11}}$: Keep constant flow rate of the sheath flow.
  - $\boldsymbol{FR_{12}}$: Keep constant flow rate of the middle flow.

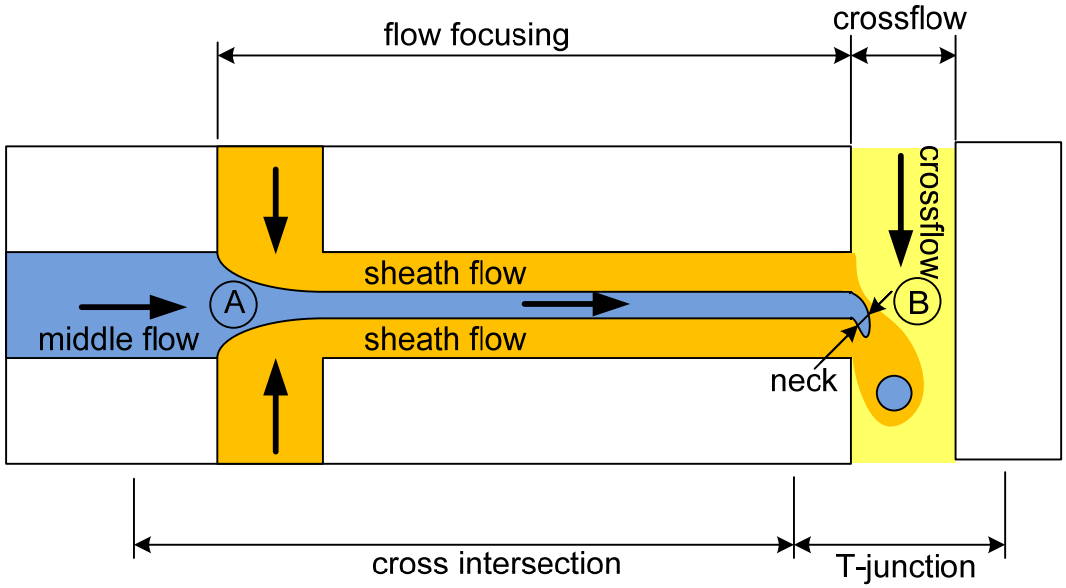

Figure 3.4 Schematic diagram of the proposed microchannel and the mechanism for microsphere generation. The sheath flow and crossflow are the same fluid as the continuous phase, and the middle flow is the dispersed phase. The thick arrows show the flow directions.

In order to satisfy the consistency of the microfluidic system, the most important design parameter is constant pressure. Thus, the $\boldsymbol{DP_1}$ required for $\boldsymbol{FR_1}$ are as follows.

- $\boldsymbol{DP_1}$: Continuous and consistent pressures for the inlets.
  - $\boldsymbol{DP_{11}}$: Keep constant pressure for the sheath flow.
  - $\boldsymbol{DP_{12}}$: Keep constant pressure for the middle flow.

The design equation for $\boldsymbol{FR_{1s}}$ and $\boldsymbol{DP_{1s}}$ ($s = \{1,2\}$) of the selected lower level then yields an

uncoupled design as

$$\begin{Bmatrix} \boldsymbol{FR}_{11} \\ \boldsymbol{FR}_{12} \end{Bmatrix} = \begin{bmatrix} \times & 0 \\ 0 & \times \end{bmatrix} \begin{Bmatrix} \boldsymbol{DP}_{11} \\ \boldsymbol{DP}_{12} \end{Bmatrix} \tag{3.10}$$

Decomposition of $\boldsymbol{FR}_2$ and $\boldsymbol{FR}_3$, and decomposition of $\boldsymbol{DP}_2$ and $\boldsymbol{DP}_3$ are as follows.

- $\boldsymbol{FR}_2$: Breakage of flow stream.
  - $\boldsymbol{FR}_{21}$: Keep high flow rate of the crossflow.
- $\boldsymbol{DP}_2$: High air pressure for breakage.
  - $\boldsymbol{DP}_{21}$: Keep high pressure for the crossflow.
- $\boldsymbol{FR}_3$: Size controllability.
  - $\boldsymbol{FR}_{31}$: Change the flow rate of the sheath flow.
  - $\boldsymbol{FR}_{32}$: Keep constant flow rate of the middle flow.
  - $\boldsymbol{FR}_{33}$: Change the flow rate of the crossflow.
- $\boldsymbol{DP}_3$: Change the air pressure to reduce the width of the dispersed phase.
  - $\boldsymbol{DP}_{31}$: Change the pressure for the sheath flow.
  - $\boldsymbol{DP}_{32}$: Keep constant pressure for the middle flow.
  - $\boldsymbol{DP}_{33}$: Change the pressure for the crossflow.

The design equations for $\boldsymbol{FR}_{2s}$ - $\boldsymbol{DP}_{2s}$ and for $\boldsymbol{FR}_{3s}$ - $\boldsymbol{DP}_{3s}$ ($s = \{1,2,3\}$) are as follows.

$$\{\boldsymbol{FR}_{21}\} = [\times]\{\boldsymbol{DP}_{21}\} \tag{3.11}$$

$$\begin{Bmatrix} \boldsymbol{FR}_{31} \\ \boldsymbol{FR}_{32} \\ \boldsymbol{FR}_{33} \end{Bmatrix} = \begin{bmatrix} \times & 0 & 0 \\ 0 & \times & 0 \\ 0 & 0 & \times \end{bmatrix} \begin{Bmatrix} \boldsymbol{DP}_{31} \\ \boldsymbol{DP}_{32} \\ \boldsymbol{DP}_{33} \end{Bmatrix} \tag{3.12}$$

The overall design equation of this decoupled design is

$$\begin{Bmatrix} \boldsymbol{FR}_1 \\ \boldsymbol{FR}_2 \\ \boldsymbol{FR}_3 \end{Bmatrix} = \begin{bmatrix} \times & 0 & 0 \\ \times & \times & 0 \\ \times & \times & \times \end{bmatrix} \begin{Bmatrix} \boldsymbol{DP}_1 \\ \boldsymbol{DP}_2 \\ \boldsymbol{DP}_3 \end{Bmatrix} \tag{3.13}$$

The details of this microfluidic system will be discussed in Chapter 5.

3.3.3.3. **Liquid chopper utilizing a piezoelectric actuator**

In this proposed design, an embedded liquid chopper is introduced by utilizing a

piezoelectric actuator as shown in Figure 3.5. A continuous phase (which is forming sheath flow) and a dispersed phase (middle stream) are driven by continuous air pressures. The middle stream is focused hydrodynamically by the sheath flow at the intersection (A). Then, a high fluctuating flow generated by a piezoelectric actuator is fed to the focused stream at the intersection structuring liquid chopper. The fluctuating flow pinches the focused flow, and the flow is disconnected to form droplets which are further emulsified to form microspheres [171, 172].

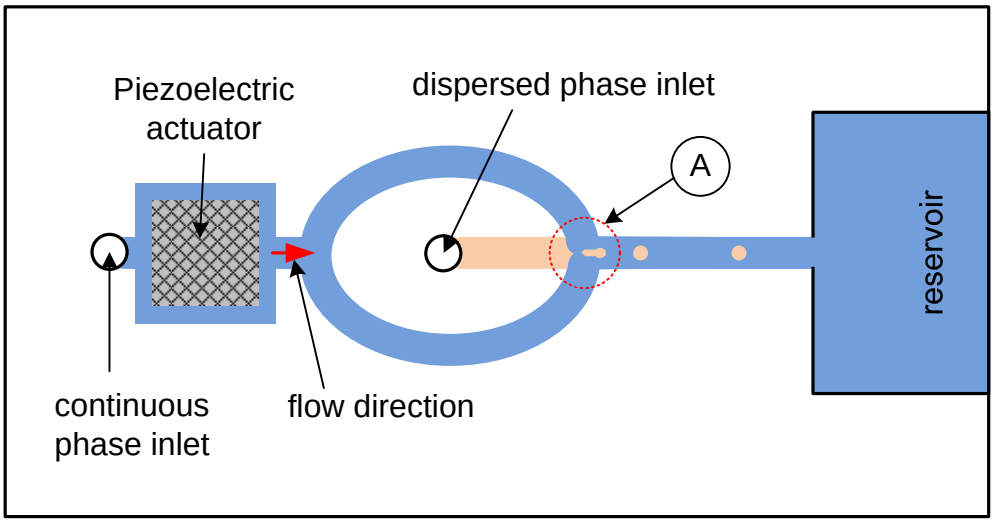

Figure 3.5 Schematic diagram of proposed microchannel design and microsphere generation.

The design equation of this design is as follows. $\boldsymbol{FR_1}$ is decomposed as

- $\boldsymbol{FR_1}$: Size consistency (uniformity).
  - $\boldsymbol{FR_{11}}$: Keep constant flow rate of the sheath flow.
  - $\boldsymbol{FR_{12}}$: Keep constant flow rate of the middle flow.

In order to satisfy the consistency of the microfluidic system, the most important design parameter is the constant pressure. Thus, decomposition of $\boldsymbol{DP_1}$ is as follows.

- $\boldsymbol{DP_1}$: Continuous and consistent pressures for inlets.
  - $\boldsymbol{DP_{11}}$: Keep constant pressure for the sheath flow.
  - $\boldsymbol{DP_{12}}$: Keep constant pressure for the middle flow.

The design equation for $\boldsymbol{FR_{1s}}$ and $\boldsymbol{DP_{1s}}$ $(s = \{1,2\})$ of the selected lower level is yielding an

uncoupled design as

$$\begin{Bmatrix} \boldsymbol{FR}_{11} \\ \boldsymbol{FR}_{12} \end{Bmatrix} = \begin{bmatrix} \times & 0 \\ 0 & \times \end{bmatrix} \begin{Bmatrix} \boldsymbol{DP}_{11} \\ \boldsymbol{DP}_{12} \end{Bmatrix} \tag{3.14}$$

Decomposition of $\boldsymbol{FR}_2$ and $\boldsymbol{FR}_3$, and decomposition of $\boldsymbol{DP}_2$ and $\boldsymbol{DP}_3$ are as follows.

- $\boldsymbol{FR}_2$: Breakage of flow stream.
    - $\boldsymbol{FR}_{21}$: Keep high flow rate of the sheath flow.
- $\boldsymbol{DP}_2$: Reduce the width of the dispersed phase to be cut.
    - $\boldsymbol{DP}_{21}$: Keep high pressure for the sheath flow.
- $\boldsymbol{FR}_3$: Size controllability.
    - $\boldsymbol{FR}_{31}$: Change the flow rate of the sheath flow.
    - $\boldsymbol{FR}_{32}$: Keep constant flow rate of the middle flow.
- $\boldsymbol{DP}_3$: Change the width of the dispersed phase.
    - $\boldsymbol{DP}_{31}$: Alter the frequency of the piezoelectric actuator.
    - $\boldsymbol{DP}_{32}$: Keep constant pressure for the middle flow.

The design equations for $\boldsymbol{FR}_{2s}$ - $\boldsymbol{DP}_{2s}$ and for $\boldsymbol{FR}_{3s}$ - $\boldsymbol{DP}_{3s}$ ($s \in \{1,2\}$) are as follows.

$$\{\boldsymbol{FR}_{21}\} = [\times]\{\boldsymbol{DP}_{21}\} \tag{3.15}$$

$$\begin{Bmatrix} \boldsymbol{FR}_{31} \\ \boldsymbol{FR}_{32} \end{Bmatrix} = \begin{bmatrix} \times & 0 \\ 0 & \times \end{bmatrix} \begin{Bmatrix} \boldsymbol{DP}_{31} \\ \boldsymbol{DP}_{32} \end{Bmatrix} \tag{3.16}$$

Thus, a decoupled design is achieved as

$$\begin{Bmatrix} \boldsymbol{FR}_1 \\ \boldsymbol{FR}_2 \\ \boldsymbol{FR}_3 \end{Bmatrix} = \begin{bmatrix} \times & 0 & 0 \\ \times & \times & 0 \\ \times & \times & \times \end{bmatrix} \begin{Bmatrix} \boldsymbol{DP}_1 \\ \boldsymbol{DP}_2 \\ \boldsymbol{DP}_3 \end{Bmatrix} \tag{3.17}$$

The details of this microfluidic system will be discussed in detail in Chapter 6.

3.4. Conclusion

In this chapter, the current microfluidic system designs for microsphere generation were analyzed by employing the ADT. It was found that the conventional designs are coupled designs indicating poor designs in particular sensitive behaviors of these systems. Three conceptual

microfluidic system designs were then proposed to make decoupled designs (better designs according to the ADT) in order to satisfy three functional requirements: size consistency (uniformity or mono-dispersity), breakage (forming microspheres), and size controllability. The proposed designs are: (i) perforated silicon membrane, (ii) integrating hydrodynamic flow focusing and crossflow, and (iii) liquid chopper utilizing a piezoelectric actuator. In the case of the perforated silicon membrane method, it is found that this design is an uncoupled design. However, this design satisfies two functional requirements without the requirement of size controllability. The other two designs are all decoupled designs satisfying the three functional requirements. Details of the proposed designs will be discussed in subsequent chapters to provide verification of the designs' promises through experiments.

4. FORMATION OF UNIFORM MICROSPHERES USING A PERFORATED SILICON MEMBRANE

4.1. Introduction

As discussed in previous chapters, the main three functional requirements for microsphere generation are: (i) consistency (uniformity or mono-dispersity), (ii) breakage (forming microspheres), and (iii) controllability (size control). One of the proposed designs to satisfy the requirements is the perforated silicon membrane by micro-electro-mechanical system (MEMS) technology. The general idea with this method is such that a dispersed phase containing the dissolved microsphere matrix material reaches a continuous phase after passing through $1.4 \times 1.4\ \mu m^2$ perforations on a silicon membrane, and microdroplets are formed on the membrane. The microdroplets are detached from the silicon membrane by a crossflow generated from an agitator, and form about 1.6 μm of oil-in-water (O/W) microspheres.

This perforated membrane method was evaluated in Chapter 3 by applying Axiomatic Design Theory (ADT), concluding that this design is an uncoupled design for two functional requirements: (i) consistency and (ii) breakage. These two functional requirements can be satisfied with independent design parameters such as constant flow rates and the agitation speed of an agitator. The size of microspheres depends mainly on the pore size of the membrane, which is constant and uncontrollable. It is expected that this method would achieve only the uniformity or mono-dispersity during microsphere generation.

4.2. Materials and Methods

4.2.1. Materials and preparation

In order to improve the robustness of microspheres in various applications, polymer

encapsulation of functional proteins has been proposed recently to form microspheres [9]. For this purpose, poly(lactic-co-glycolic acid) (PLGA) has been examined as one of the potential encapsulating polymers valued for its excellent biodegradable and biocompatible characteristics. The biodegradable encapsulated microspheres can deliver a therapeutic at a constant rate for a longer period of time with minimal toxicity [18, 173, 174].

For the experiments to generate microspheres from a perforated silicon membrane, PLGA with an internal viscosity of 0.61 and a polyanhydride-lactide ratio of 85:15 was purchased from Durect Corporation (USA). The PLGA was dissolved in methylene chloride to prepare 5% of PLGA solution as a dispersed phase (oil phase). Poly(vinyl alcohol) (PVA) with a molecular weight of 13,000~23,000 and an 87~89% hydrolyzed degree was purchased from Sigma (USA). The PVA was dissolved in distilled water to prepare 1% of PVA solution as a continuous phase (aqueous phase) which was functionalized as an emulsifier and stabilizer. The instruments in contact with the solutions were carefully cleaned to avoid any contamination.

4.2.2. Perforated silicon membrane fabrication by MEMS technology

A silicon on insulator (SOI) substrate was prepared for fabrication with a focused ion beam (FIB) and a chemical wet etchant. The SOI substrate has implanted an 1 μm silicon dioxide (SiO_2) layer between 2 μm and about 400 μm silicon (Si) layers. For decades, silicon has been widely used for ICs as well as miniature mechanical devices and components, such as sensors, since it has excellent mechanical and electrical properties [175]. Typically, silicon micromachining is fit to both bulk micromachining and surface micromachining, depending on what region of the wafer is used. Bulk micromachining falls into four categories: (1) wet isotropic, (2) wet anisotropic, (3) dry isotropic, and (4) dry anisotropic etching methods. Isotropic methods refer to equal etching rates in all directions, whereas anisotropic methods

result in different etching rates which are significantly faster in particular directions [176]. The crystal of a silicon substrate causes the isotropic and anisotropic etching. Silicon crystallizes in two ways. First, all the silicon atoms are aligned in the same crystal lattice arrangement, monocrystalline. Second, a silicon substrate is made up of many smaller crystals of silicon, polycrystalline. In MEMS and microfabrication, silicon wafers and substrates are almost in the monocrystalline form, leading to a constant etching rate. Also, different crystal planes of a silicon lattice have different densities of chemical bonds between silicon atoms, which results in different etching rates in different crystal planes leaving specific angles between the crystal planes. Crystal planes and orientations (directions) are identified using the Miller Indices based on the intercepts of a plane with the three crystal axes [177] as illustrated in Figure 4.1.

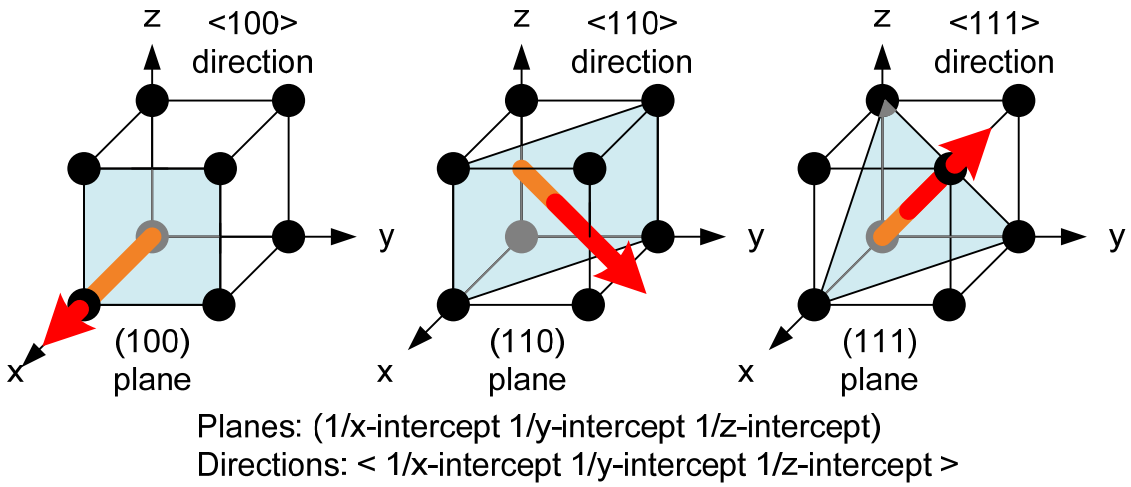

Figure 4.1 Different representations by Miller Indices. The <XXX> direction is perpendicular to the (XXX) plane.

The column structure of FIB is similar to that of a scanning electron microscope (SEM) except for a light beam (i.e., ion beam). Since the 1980s, FIB was adopted for a wide array of material science applications from circuit editing and transmission electron microscopy (TEM) sample preparation to micro-structural analysis and prototype micro- / nano-machining such as sharp scanning probe microscope tips and diamond indenters for hardness testing [178-180].

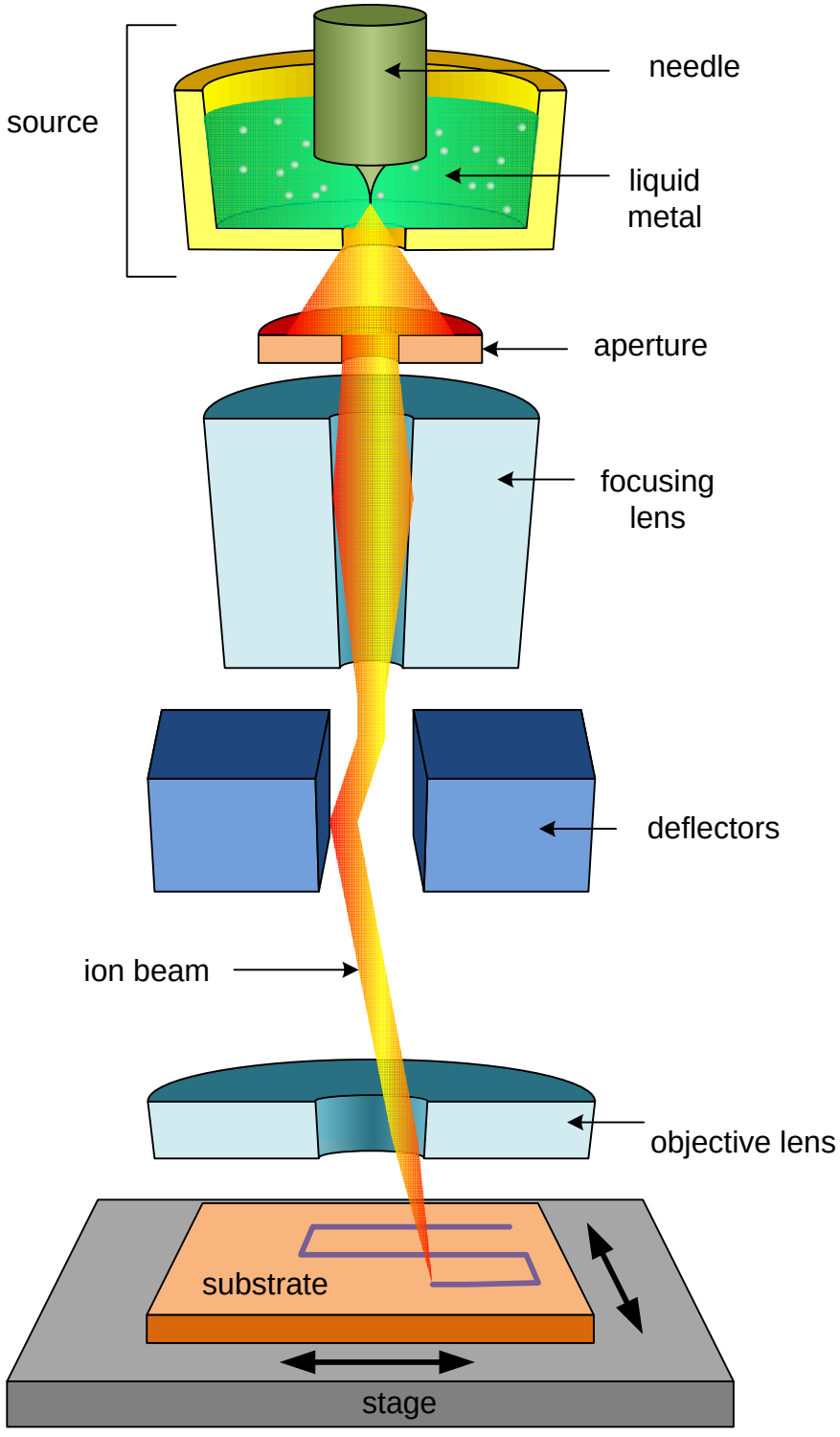

Figure 4.2 Schematic principle of focused ion beam (FIB).

FIB has received great attention as liquid metal ion sources (LMIS) developed from the brightness of LMIS with a current density of the order of 1 Acm^{-2} to sub-micron meters [181-183]. The most commonly used LMIS for FIB is Gallium, Ga. Liquid Ga metal contacts with a metal needle having a high surface tension (e.g., tungsten) with heat, which generates a huge electric field (10^{10} V/m) causing ionization and field emission (~ 2 μA) of the Ga atoms in the formation of a single Taylor cone with a tip radius of approximately 5 nm [180, 184, 185]. The schematic structure of FIB is shown in Figure 4.2. The versatility of FIB lies in sputtering and deposition leading to micro- / nano-machining and lithography. It can sputter and implant lines down to 10 nm, as well as deposit metals and insulators as narrow as 30 nm [186]. The larger and heavier ions (than electrons) break off chemical bonds of substrate atoms, allowing various substrate materials for lithography with better beam controllability. However, in order to pattern large areas, longer time consumption cannot be avoided.

Hydrofluoric acid (HF) is a common etchant for isotropic etching for oxides, nitrides, gold and silicon. However, HNO_3-free HF etchant does not attack silicon. A stronger concentration strips materials more rapidly. As an anisotropic etchant, potassium hydroxide (KOH) and tetramethylammonium hydroxide (TMAH) are popular. By altering the composition rate of an etchant, the etching rate can be varied.

Table 4.1 shows common wet etchants of silicon. As a rule of thumb, a slower etching rate gives smoother surfaces during etching. Figure 4.3 shows the most common silicon crystal orientation (100) using isotropic and anisotropic etchants.

Table 4.1 Common wet etchants of silicon [187-190]

Etchant (Diluent)	Composition	Temp. (°C)	(100) Etching Rate (μm/min)	(100):(111) Etching rate ratio	I/A*
HF HNO3 (water, CH3COOH)	10 ml 30 ml 80 ml	22	0.7-0.3	1:1	I
	25 ml 50 ml 25 ml	22	40	1:1	I
	9 ml 75 ml 30 ml	22	7.0	1:1	I
Ethylene diamine Pyrocatechol (EDP) (water)	750 ml 120 gr 100 ml	115	0.75	35:1	A
	750 ml 120 gr 240 ml	115	1.25	35:1	A
KOH (water)	20% 80%	80	1.4	400:1	A
	30 % 70 %	80	1.3	400:1	A
	44 % 56 %	120	5.8	290:1	A

Table 4.1 (continued)

Etchant (Diluent)	Composition	Temp. (°C)	(100) Etching Rate (μm/min)	(100):(111) Etching rate ratio	I/A*
TMAH (water)	5 % 95 %	90	1.4	20:1	A
	10 % 90 %	80	0.57	40:1	A
	22 % TMAH in H2O	90	0.9	50:1	A

* I: isotropic; A: anisotropic

The fabrication process of the perforated silicon membrane is illustrated in Figure 4.4. These steps, along with the rationale for them, are described in detail below. The fabrication process was performed at the cleanroom (AMPEL) in the University of British Columbia (UBC) and at Nano-Imaging Facility in Simon Fraser University (SFU).

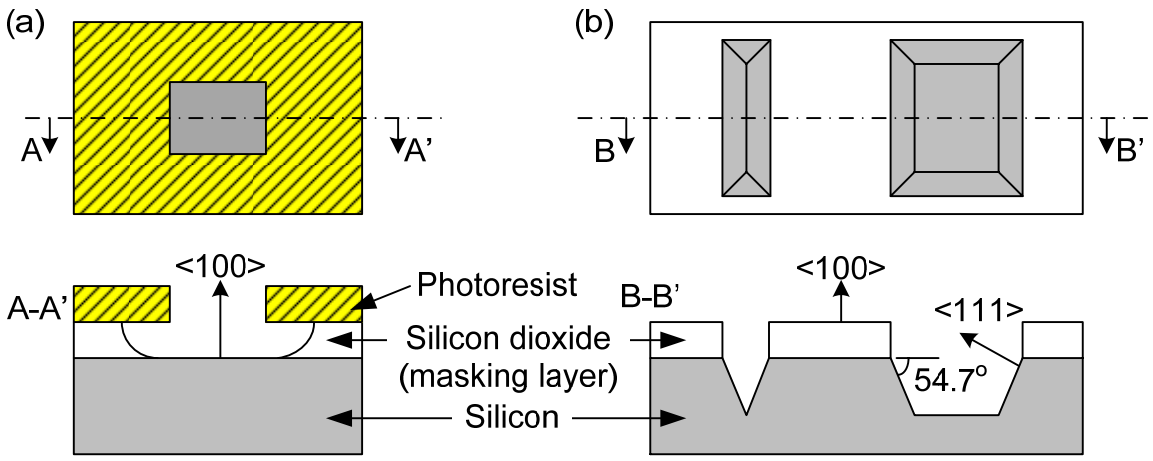

Figure 4.3 Schematic diagram of isotropic etching of silicon dioxide (a) and anisotropic etching of silicon (b) on (100) silicon plane (not to scale). This diagram shows top views and cross-section views of each etching method.

A 400 μm silicon on insulator (SOI) substrate with 2 μm silicon (Si) layer on top of 1 μm silicon dioxide (SiO_2) layer was prepared [Figure 4.4(a)]. After that, 1 μm SiO_2 layer was deposited on top of the SOI substrate using a plasma-enhanced chemical vapor deposition (PECVD) machine introducing silane (SiH_4) and nitrous oxide (N_2O, laughing gas) with a relatively lower temperature (about 250°C) than the temperatures of other SiO_2 deposition processes such as thermal deposition and physical vapor deposition [Figure 4.4(b)]. Then, flip the substrate upside down, deposit about 1 μm of positive photoresist layer on top of the bottom Si layer, and soft bake and hard bake the photoresist to make it harden. UV light was exposed onto the photoresist through a mask where desired shapes were patterned (photolithography process) [Figure 4.4(c)]. Only the photoresist area exposed by UV light was removed by a wet photoresist remover (developing process) because of the property of positive photoresist [Figure 4.4(d)]. A wet etching process with Tetramethylammonium hydroxide (TMAH) solution was followed at 80°C to remove silicon and open a window on the bottom side. This wet etching is anisotropic, leaving 54.7° of a slope on the (100) plane due to the crystal orientation of the

silicon substrate with about 0.9 μm/min etching ratio of silicon on the (100) plane. The embedded SiO_2 layer plays a role of protection against the TMAH solution. Hence, the etching process stops when the TMAH solution reaches the SiO_2 layer [191, 192] [Figure 4.4(e)]. After the implanted SiO_2 layer was exposed through the open window, a focused ion beam (FIB) was shot through the hidden SiO_2 layer, patterning $2.5 \times 2.5\ \mu m^2$ of square shapes until the top Si layer was exposed [Figure 4.4(f)]. Since the top Si layer was too thick (2 μm) for FIB to penetrate, another wet chemical etching with TMAH solution was applied, and the exposed Si was etched away [Figure 4.4(g)]. Extra photoresist was deposited on the bottom side before SiO_2 removal to cover and protect the Si and SiO_2 on the bottom side from an etchant, and a soft bake process was performed to make the photoresist harden [Figure 4.4(h)].

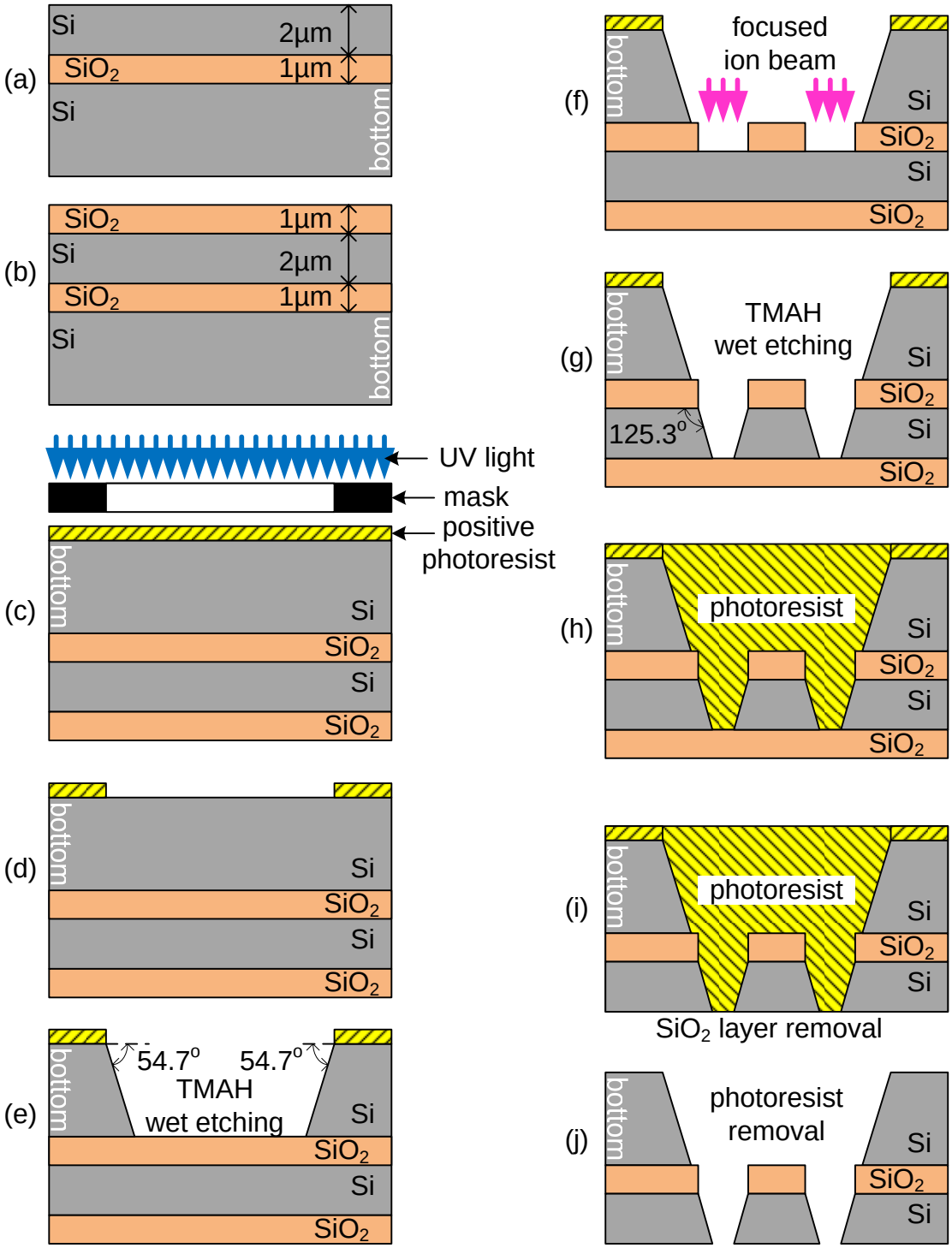

Figure 4.4 Schematic cross section view of the fabrication process (not drawn to scale).

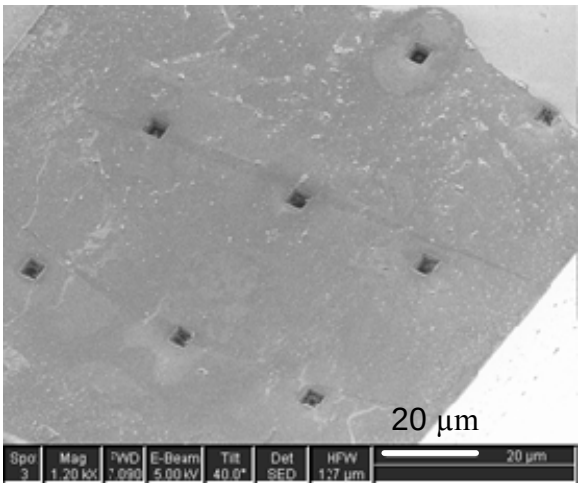

(a) 3 x 3 array of perforations

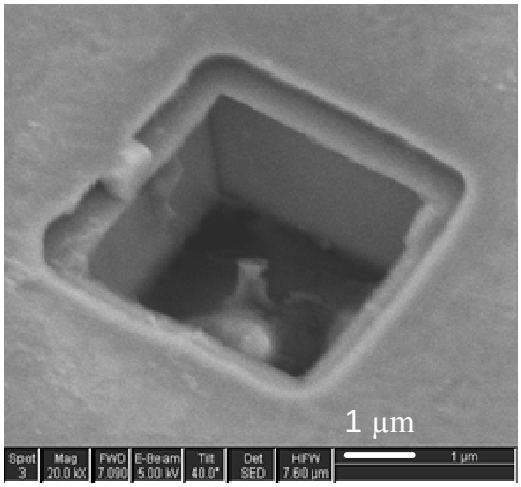

(b) close view of a perforation

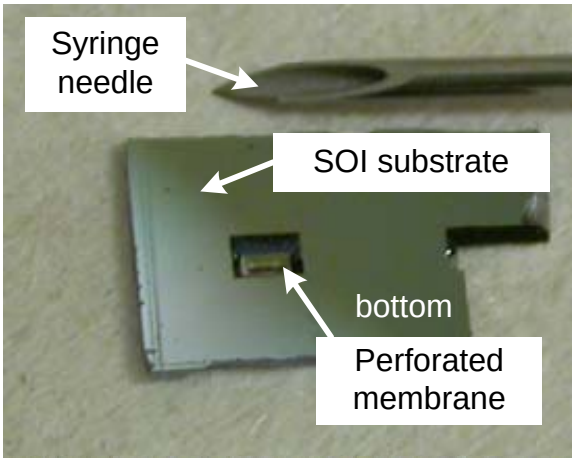

(c) 10 x 3 array of perforated Si membrane

(d) 3 x 3 array of perforated Si membrane on a lure of syringe needle

Figure 4.5 SEM images and photo images of the perforated Si membrane after the fabrication. The perforations were positioned far enough apart to avoid merging of the droplets during microsphere formation.

Buffered oxide etch (BOE), a wet etchant, consisting of a 10:1 ratio of hydrofluoric acid (HF) and ammonium bifluoride (NH_4HF) was used to remove the deposited SiO_2 layer [193, 194] [Figure 4.4(i)]. Finally, all the photoresist was removed by common organic solvents such as acetone, methyl acetate and ethyl acetate, and a perforated silicon membrane was achieved [Figure 4.4(j)]. The fabricated perforated silicon membrane is shown in Figure 4.5. On the

bottom side, the size of perforation was $2.5 \times 2.5\,\mu m^2$, but on the top side, the size of perforation became about $1.4 \times 1.4\,\mu m^2$ from the crystal orientation of silicon.

4.2.3. Microsphere generation

Oil-in-water (O/W) PLGA microspheres were generated using the perforated silicon membrane fabricated by the foregoing process. The membrane was then glued on a plastic luer of a syringe needle, and the PLGA solution was pumped by a syringe pump (New Era Pump Systems, Inc.) into the PVA solution. The experiment was setup as shown in Figure 4.6and performed at MEMS lab and the Hafeli lab in the UBC.

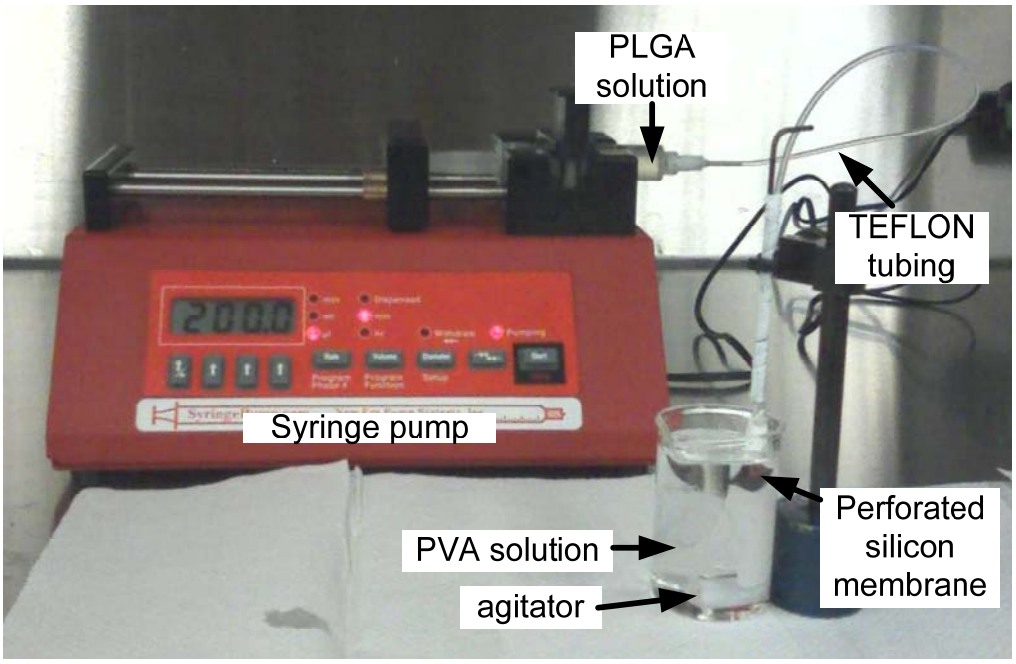

Figure 4.6 Experimental setup for microsphere generation. The PLGA is injected by a syringe pump and passes through perforations on the silicon membrane. The PLGA icrosphere is forming when the droplet on the membrane is detached off by the crossflow underneath the membrane. The speed of the agitator determines the speed of the crossflow.

The pumped PLGA flux formed a droplet on the silicon membrane under the four major forces caused by the action of the fluid: a drag force produced by the continuous phase flow, a

force caused by the interfacial tension, a buoyant force, and an inertial force caused by the dispersed phase flow. The buoyant force and the inertial force are relatively small and can be neglected. The major forces on the droplet are described as Figure 4.7. Thus, the droplet size can be estimated simply from a torque balance equation before detachment as follows:

$$F_1 = 10.2\pi\mu VR \tag{4.1}$$

$$F_2 = 2\sigma\pi R_p \tag{4.2}$$

$$F_1 R = F_2 R_p \tag{4.3}$$

where R is the radius of the droplet which eventually becomes a microsphere, and R_p is the radius of a perforation. Thus, the equation for the radius of a microsphere can be derived as

$$R = \sqrt{\left(\frac{\sigma R^2}{10.2\mu V}\right)} \tag{4.4}$$

where V is the tangential flow velocity of the continuous phase on the membrane, σ is the interfacial tension, and μ is the viscosity of the crossflow [82, 83].

The PLGA droplet on the membrane was detached by the continuous phase crossflow generated by the agitator at the bottom of the glassware. The formation of droplets on the perforated silicon membrane without applying the crossflow is shown in Figure 4.8. During the experiment, the velocity of the PLGA solution was 0.185 m/s, and a minimal pressure of 17.4 psi was applied through the pore. The speed of the agitator in the glassware was varied to optimize the capillary number, Ca. The desired microsphere diameter was reached at $Ca = 0.15$. The detached PLGA droplets from the membrane were stabilized by PVA, underwent solvent evaporation, and were transformed into microspheres. Microspheres were separated by centrifugation followed by a drying procedure.

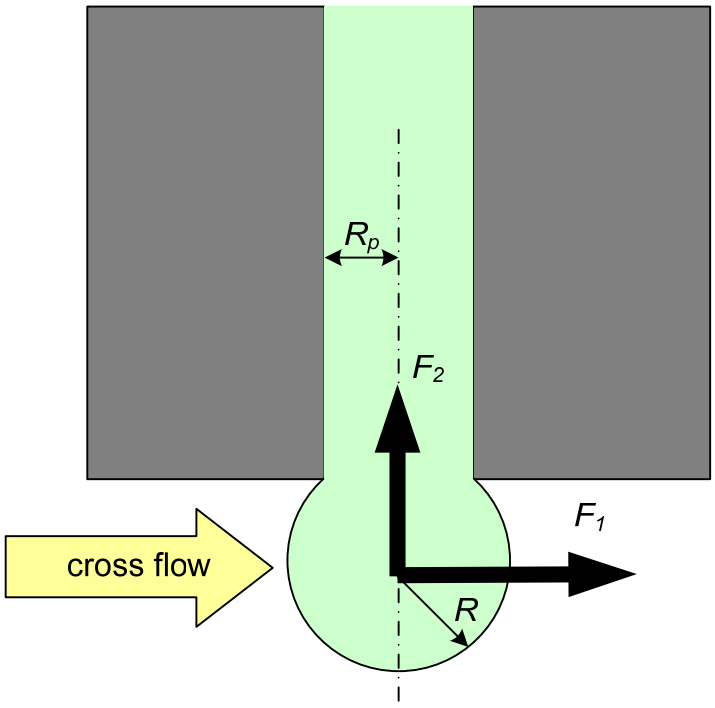

Figure 4.7 Simplified acting forces on a droplet formed at perforation

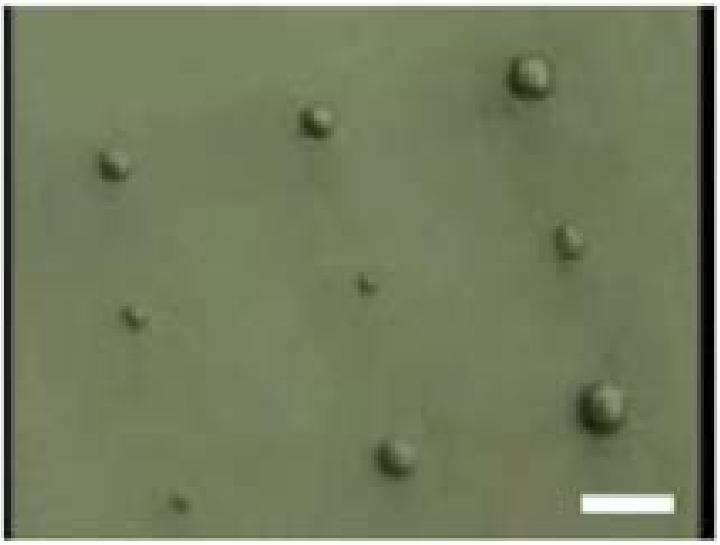

Figure 4.8 The optical image of the droplets on the perforated Si membrane without agitation. The white bar represents 25 μm.

Since the number of the collected microspheres at each experiment was not enough for size analysis using a machine, a computational image process was applied to measure the diameter of the spheres. Digital images of the microspheres were captured by a camera attached on an optical microscope. This experiment was performed three times, and at each experiment, 100 samples of microspheres were measured randomly.

4.3. Results and Discussion

The major concern of the experiment was to prove that a narrower distribution of microspheres can be achieved by using a silicon membrane with micro-sized perforations. The results of the experiment indicate a promising outcome. The size distribution of the microspheres is shown in Figure 4.9, showing results with different agitation speeds.

With this design, only slow stirring speeds were applied to the continuous phase to avoid damage of microspheres, which can occur with a vigorous stirring emulsion process such as a homogenizer. The results were achieved after three times of experimentation at each agitation speed. The size distribution gives an average size of 1.56 μm and a narrower size distribution with the definition of mono-dispersity, leading to a conclusion that over 90% of the generated microsphere is distributed between 1μm and 2μm (CV_{400rpm} = 6.7% and CV_{500rpm} = 9.1%). Table 4.2 shows the average diameter from the experiment and the model prediction (Eqn.(4.4) where $\mu = 1.7 \times 10^{-3}$ kg/m-s and $\sigma = 4.6 \times 10^{-3}$ N/m). The two are very close. As discussed in Chapter 3, the proposed design is an uncoupled design to achieve only two functional requirements: uniformity and breakage (formation of microspheres). The design parameters (constant flow rates and agitator speed) satisfy the functional requirements independently. The constant flow rate is responsible for an extremely narrow size distribution of the microspheres (i.e., achieving mono-dispersity). A certain agitation speed yields the detachment of microdroplets from the

silicon membrane to form microspheres.

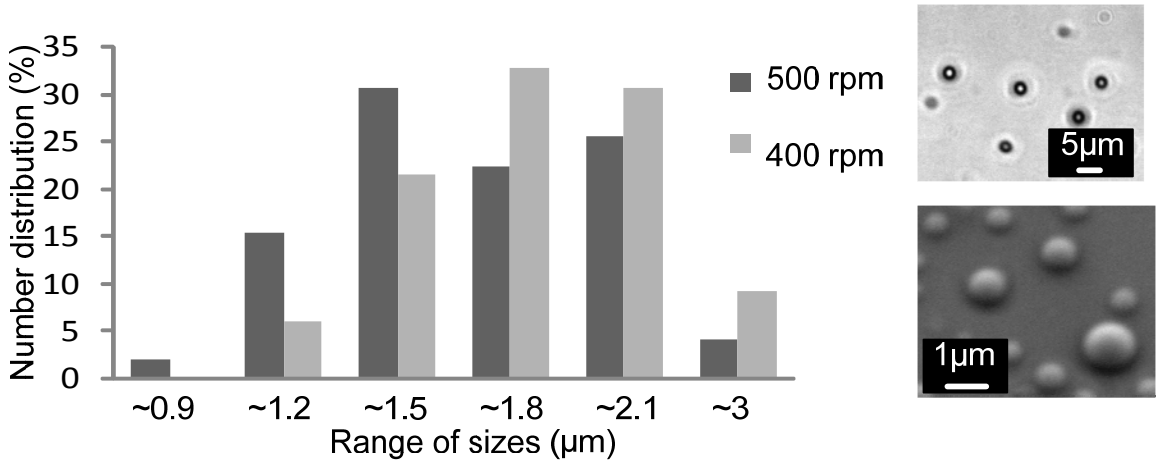

Figure 4.9 Size distribution of the microspheres by two different agitation speeds (400 rpm and 500 rpm). Optical (upper) and SEM (lower) images of microsphere are shown on the side.

Table 4.2 The average diameters from the experiments and model

	agitation speed	
	400 rpm	**500 rpm**
size measured	1.7 μm	1.56 μm
size predicted	1.4 μm	1.25 μm

When the agitation speed is lower, the microfluidic system can generate closely mono-dispersed microspheres. However, as the agitation speed increases, this system is malfunctional, leading to a performance failure. This happens because as the agitation speed increases, the flow rate or speed of crossflow becomes higher, increasing the pressure drop between the outside and inside of the membrane. Thus, the dispersed phase cannot come out of the pore to form microdroplets on the membrane. As the flow rate of the dispersed phase is increased, the pressure drop between outside and inside of the membrane is reduced, and the dispersed phase can then pass through the perforation to form microdroplets on the membrane. However, considering the

thickness of the membrane, the pressure applied to the dispersed phase should not exceed the maximum stress that the membrane can bear; otherwise, the membrane would be broken, leading to failure of the operation as shown in Figure 4.10. For successful results, the applied pressure for the dispersed phase has to be low, allowing a low flow rate, ($< 0.1\ \mu l/h$), which leads to a very small amount of microsphere production. Also, an extremely limited range of microsphere sizes is achievable.

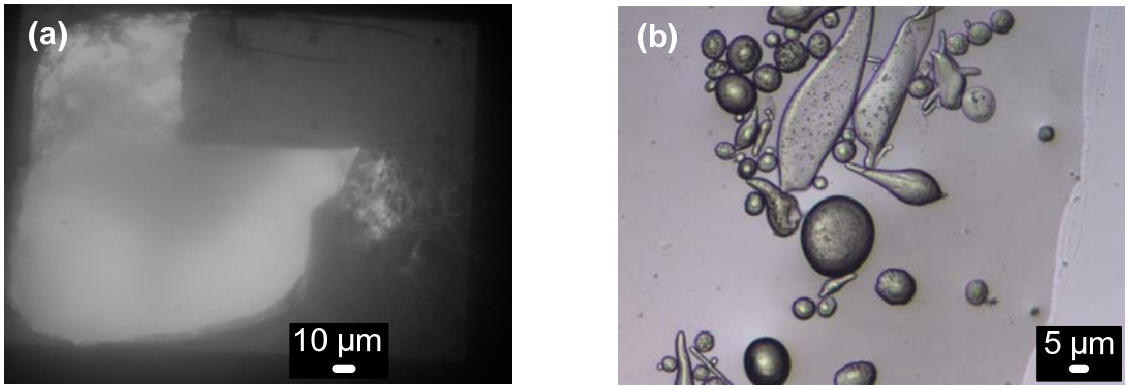

Figure 4.10 Failures with inappropriate agitation speed. (a) a broken membrane due to a high flow rate of dispersed phase, and (b) bigger sizes of microsphere from the broken membrane.

4.4. Conclusion

In this chapter, a perforated silicon membrane method was present to generate oil-in-water (O/W) microspheres. This method was discussed in Chapter 3, demonstrating that this design is an uncoupled design since each functional requirement is satisfied with a different design parameter independently.

A new MEMS fabrication method was applied to realize this perforated silicon membrane using an SOI substrate, and photolithography and wet etching processes with FIB. This fabrication method could achieve pores about $1.4 \times 1.4\ \mu m^2$ in size. The experiment with PLGA solution and PVA solution as dispersed phase and continuous phase, respectively, resulted

in closely mono-dispersed microspheres of about 1.6 μm in diameter with 7.9% CV in average.

Although the proposed perforated silicon membrane method satisfies consistency and breakage as expected, it is not fully suitable for the three functional requirements for microsphere generation. Furthermore, rupturing of the membrane may occur as the flow rate increases. It becomes clear that this kind of design (membrane emulsification) should be applied for the mono-dispersed microsphere generation in a single size. As a part of future work, one suggestion may be to design a microfluidic device which allows changing the stream size of the dispersed phase in order to achieve controllability.

5. INTEGRATING HYDRODYNAMIC FLOW FOCUSING AND CROSSFLOW FOR UNIFORM AND SIZE-CONTROLLABLE MICROSPHERE GENERATION

5.1. Introduction

In this chapter, a new conceptual design resulting from the application of Axiomatic Design Theory (ADT), named integration of hydrodynamic flow focusing and crossflow based on the phase separation principle, will be discussed in detail. The new design was evaluated as a decoupled design for which the independence of functional requirements can be assured if design parameters are determined in an appropriate sequence.

The fundamental idea of this method is that a dispersed phase is focused hydrodynamically at a cross intersection, and this focused flow then meets a crossflow to form microspheres at the T-junction. By introducing immiscible fluids to a microfluidic device and varying flow parameters, microspheres can be successfully produced in various sizes. With a constant flow rate of the focused flow, the size of microspheres decreases as the velocity of the crossflow increases, which indicates that this method overcomes some limitations seen with the perforated silicon membrane method. Thus, all three functional requirements (consistency, breakage, and controllability) for the microsphere generation can be satisfied by this method.

Paraffin oil and water are used for a continuous phase (oil phase) and a dispersed phase (aqueous phase), respectively, to form water-in-oil (W/O) microspheres. A simulation study is presented to verify the proposed microchannel design for generating uniform and size-controllable W/O microspheres. Additionally, the experimental results verify the simulation. By varying an applied pressure on the crossflow, the size of the W/O microspheres can be

successfully controlled from 16 μm to 35 μm in diameter with about 5% CV (coefficient of variation). The new method has advantages such as good sphericity, few satellite droplets, active control of the microsphere diameter, and high throughput with a simple and low cost process.

5.2. Microfluidic device

As discussed in Chapter 3, the proposed decoupled design was introduced to make breakage of the dispersed phase from a jet ($\boldsymbol{FR}_2$) independent of the size-controllability ($\boldsymbol{FR}_3$). The inlet pressures for the immiscible flows must be independently controlled to change the width of a dispersed phase stream and to break it. The width of a dispersed phase stream is narrowed by a sheath flow (continuous phase) hydrodynamically, and the focused flow is then cut to form microspheres by a crossflow downstream, as illustrated in Figure 5.1.

The proposed microchannel device consists of two geometrical structures, a cross intersection for hydrodynamic flow focusing and a T- junction for crossflow. The middle stream is focused by the sheath flow hydrodynamically from the intersection to downstream. The width of the focused stream does not depend on the magnitude of applied pressures, but rather on the ratio of side pressure from the sheath flow to inlet pressure of the middle flow, which is proportional to the flow velocities. After being focused, the velocity of the focused flow increases, which yields a high value of the Weber number, We, and makes the focused flow stable. Adding an extra force disturbs the stability of the focused flow to form droplets. A crossflow is introduced to enhance the instability of the focused stream. Once the focused stream reaches the T-junction, it meets the crossflow and experiences a high shear stress. The crossflow breaks the focused flow droplets, which are further emulsified to microspheres. The feasibility study of this integration method has been done through simulation, and the details are described in Appendix B.1.

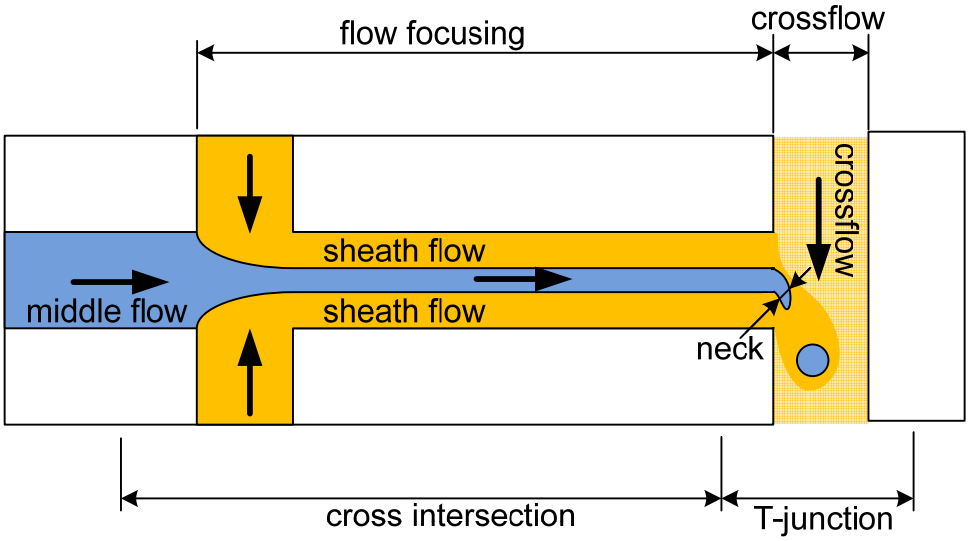

Figure 5.1 Schematic diagram of a proposed microchannel and the mechanism of microsphere generation. The sheath flow and crossflow are oil phase, and the focused middle flow is aqueous phase. The arrows indicate the flow directions.

5.3. Experiments

5.3.1. Materials and methods

5.3.1.1. Materials and preparation

Span 80, a non-ionic oil surfactant, was purchased from Fluka, and Paraffin oil with a 98.5% purity grade was supplied from Sigma-Aldrich. The 1% of Span 80 was mixed in the paraffin oil by stirring for 15 minutes at room temperature and was prepared as an oil phase solution. As an aqueous phase solution, distilled water was used. The instruments in contact with the solutions were carefully cleaned to avoid any contamination.

5.3.1.2. Fabrication process of the microfluidic device

The microchannel was fabricated by the soft lithography technique using poly-dimethyl siloxane (PDMS) at the cleanroom in the UBC. Soft lithography was first introduced by Whitesides et al. [195-198]. This technique refers to a family of techniques using a patterned

elastomer as the stamp, mold, or mask to generate micropatterns and microstructures. The term ”soft” comes from the usage of the flexible organic molecules and materials for a replica such as PDMS [197]. Several characteristics make this material useful in micro-fluidic systems: easy fabrication, transparency in the UV-visible regions, high gas permeability, high compressibility, chemical inertness, low polarity, low electrical conductivity, and elasticity [199-201]. PDMS is composed of two components, base polymer (silicone elastomer) and a curing agent. The most widely used PDMS is Sylgard 184 from Dow Corning Corporation [202]. The base polymer is composed of dimethylsiloxane oligomers ($[SiO(CH_3)_2]_n$) with vinyl-terminated end groups ($-CH=CH_2$), platinum (Pt) catalyst, and silica filler (dimethylvinylated and trimethylated silica). The curing agent contains a cross-linking agent (dimethylmethylhydrogen siloxane) and an inhibitor (tetramethyltetravinyl cyclotretrasiloxane) [203, 204]. Mixing the vinyl and the silicon hydride groups causes the cross-linking in the presence of the catalyst to form a Si-C bond building ($-CH_2-CH_2-$) linkage between PDMS chains. The cross-linking reaction is accelerated as the temperature increases [205, 206]. Figure 5.2 illustrates the cross-linking of PDMS.

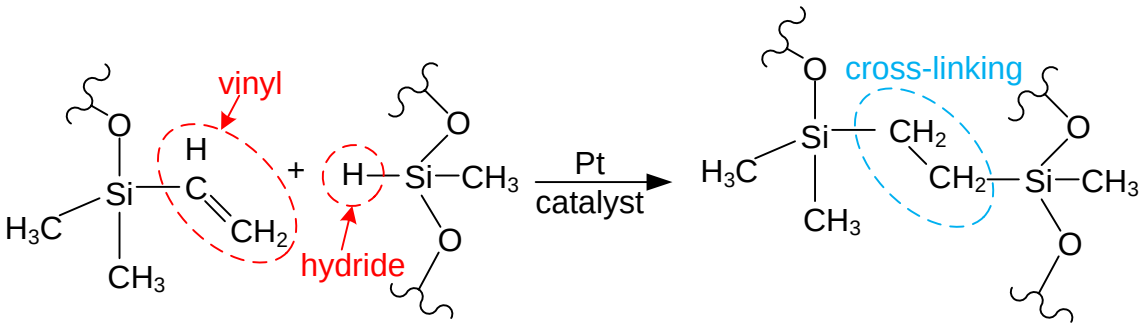

Figure 5.2 Schematic diagram of PDMS cross-linking.

Conventionally, a mixture of 10:1 (base polymer : curing agent) composition of PDMS is broadly used. However, 4:1 PDMS gives a higher ($-CH_2-CH_2-$) cross-linking since the ratio

contains a higher fraction of curing agent [206].

In order to fabricate a micro-fluidic system by soft lithography, a master (mold) with a desired pattern is a prerequisite. The master can be prepared by various methods such as UV photolithography and x-ray lithography. A schematic process of a PDMS micro-device is illustrated in Figure 5.3. As long as the patterned master is not damaged after a peeling off process, the entire process can be repeatable. The soft lithography method has the advantages of low cost, easy of learning, straightforward applying, and accessibility to a wide range of users [197]. Soft lithography includes various microfabrication methods using a patterned master: micro-contact printing (μCP) [207], replica molding (REM) [208], micro-transfer molding (μTM) [209], micro-molding in capillaries (MIMIC) [210], solvent-assisted micro-molding (SAMIN) [211], cast molding [212, 213], embossing [214, 215], and injection molding [216, 217].

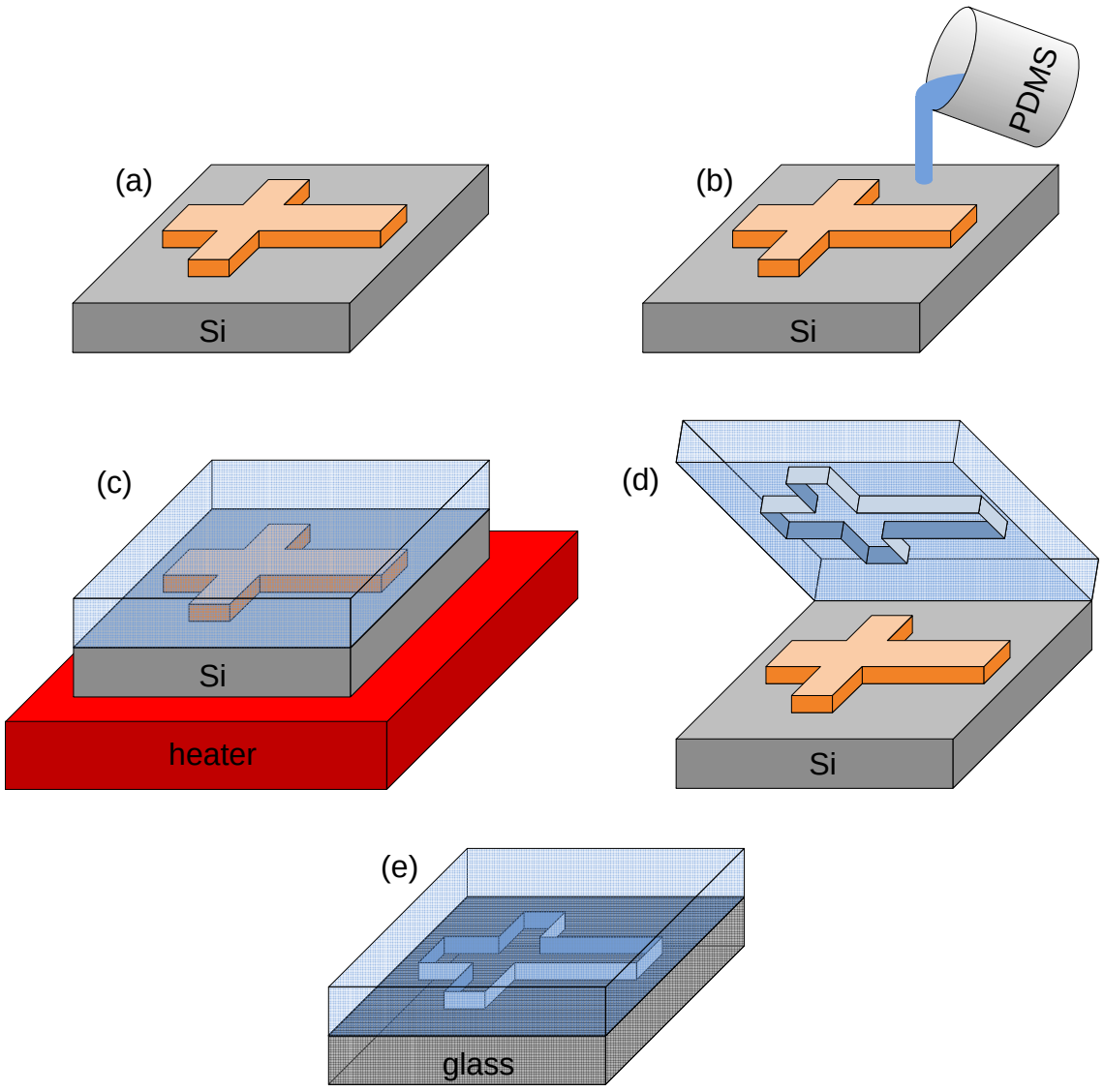

Figure 5.3 Schematic diagram of a PDMS micro-device process: (a) a master with desired pattern, (b) pouring PDMS, (c) curing PDMS at high temperature. The PDMS was baked in a furnace with 100°C or on a hotplate with 130°C, (d) peeling off PDMS replica, and (e) bonding (sealing) with glass substrate after surface treatment for adhesion. For better adhesion, O_2 plasma (commonly used for organic material removal) was applied on the patterned PDMS, then firmly attached on a new glass substrate for better examination of the operation during the experiments.

Good adhesion requires strong interfacial forces via chemical compatibility and/or chemical bonding. Oxygen plasma surface treatment can assist the creation of a chemically active functional group, hydroxyl (-OH), to improve interfacial adhesion between PDMS and

glass. This chemical reaction yields Si-O-Si bonds after loss of a water molecule [218-220], as illustrated in Figure 5.4. This oxygen plasma process was performed at the plasma lab in the University of Saskatchewan (UofS).

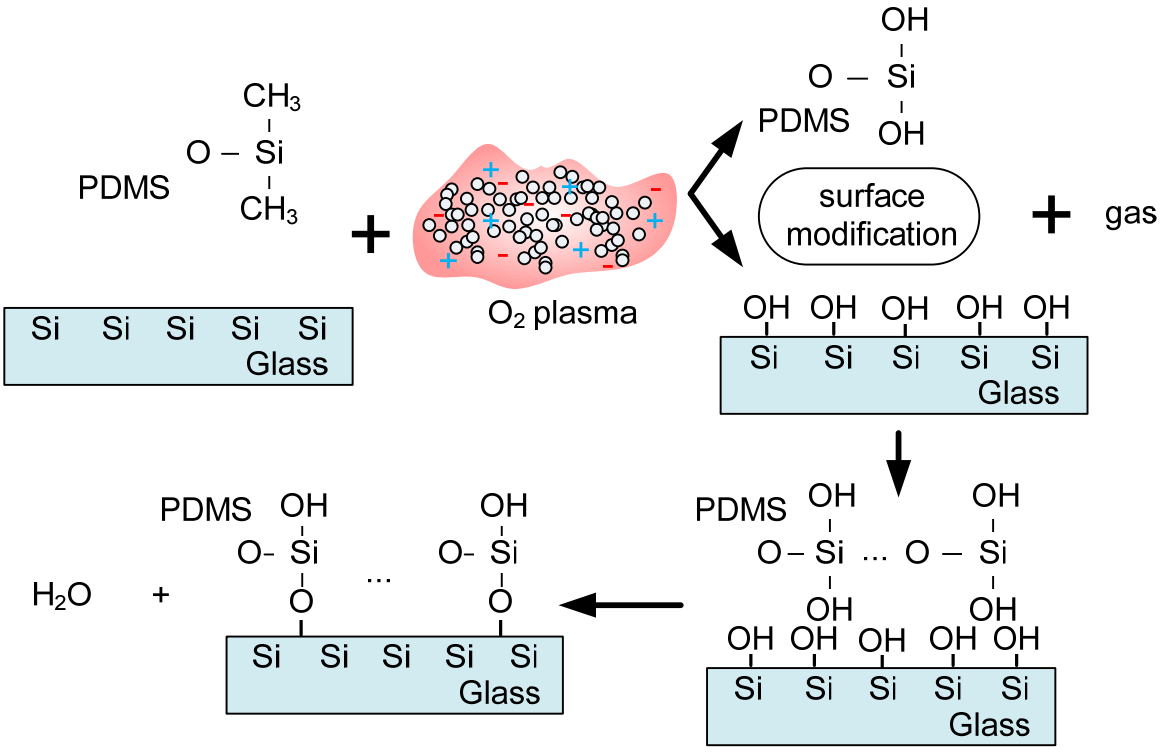

Figure 5.4 Schematic view of the surface modification of PDMS and glass by O_2 plasma and their bonding.

5.3.2. Experiment

The microchannel consists of two structures, a cross intersection for flow focusing and a T- junction for crossflow. The overall size of the microfluidic device is $15mm \times 20mm \times 5mm$ with $38\mu m$ of width (D) and $5\mu m$ of height (h) for both the flow focusing and the T-junction structures. Typically, the flow focusing method has been used for a flow cytometry technique with miscible fluids [221]. The width of the focused stream does not depend on the magnitude of applied pressures but rather on the ratio of side pressure to inlet pressure of the middle flow, which is further proportional to the flow velocity [101]. Once the focused stream reaches the T-

junction, it meets the crossflow and experiences high shear stress. The crossflow breaks the focused flow droplets which are emulsified to microspheres.

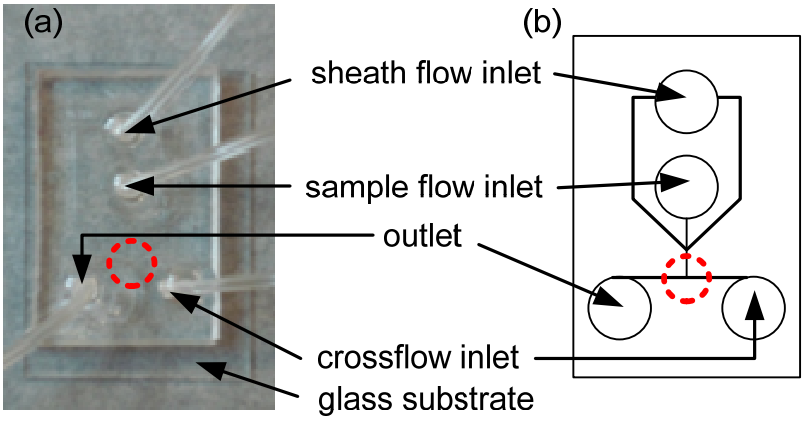

Figure 5.5 Photograph of the PDMS microfluidic device (a) and its schematic diagram (b). This device is connected to a dispensing machine for pressure through Teflon tubes. Microspheres are generated in the encircled area.

5.3.2.1. **Apparatus and analysis**

As shown in Figure 5.6, the microfluidic device was setup, and the experiment was performed at Tissue Engineering Research Lab in UofS. The device was placed on the optical microscope (Olympus) which is connected to a computer system from a CCD camera (TK-1270U, JVC) on the microscope for capturing images and videos of microsphere formation. Images with resolution of 1024×768 pixels were taken during the experiment. A dispensing machine (C0720M, Asymtek) for controllable continuous air pressures was connected to the microfluidic device by Teflon tubes containing the immiscible solutions for sheath flow, crossflow, and middle flow. The tubes were sealed with PDMS at the opening of the channel. The aqueous phase was used as a middle flow to be focused, and the oil phase was used as a sheath flow and a crossflow. The flow rates of the solutions were manipulated by altering the air pressure; thus, the width of the focused middle flow and the flow rate of the crossflow were changed, controlling the size of microspheres. After changing a flow parameter, at least one

minute of equilibrium time was taken to capture the microsphere images. The diameter of microspheres was measured from the optical microscope images. The average size of microspheres was verified by measuring the size of 40 microspheres from the captured images using an image processing software (ImageJ, National Institutes of Health). The coefficient of variation ($CV = \delta/dm_{av} \times 100\%$) [51, 52, 81] was calculated for the size distribution of microspheres, where δ is the standard deviation, and dm_{av} is the average diameter of microspheres.

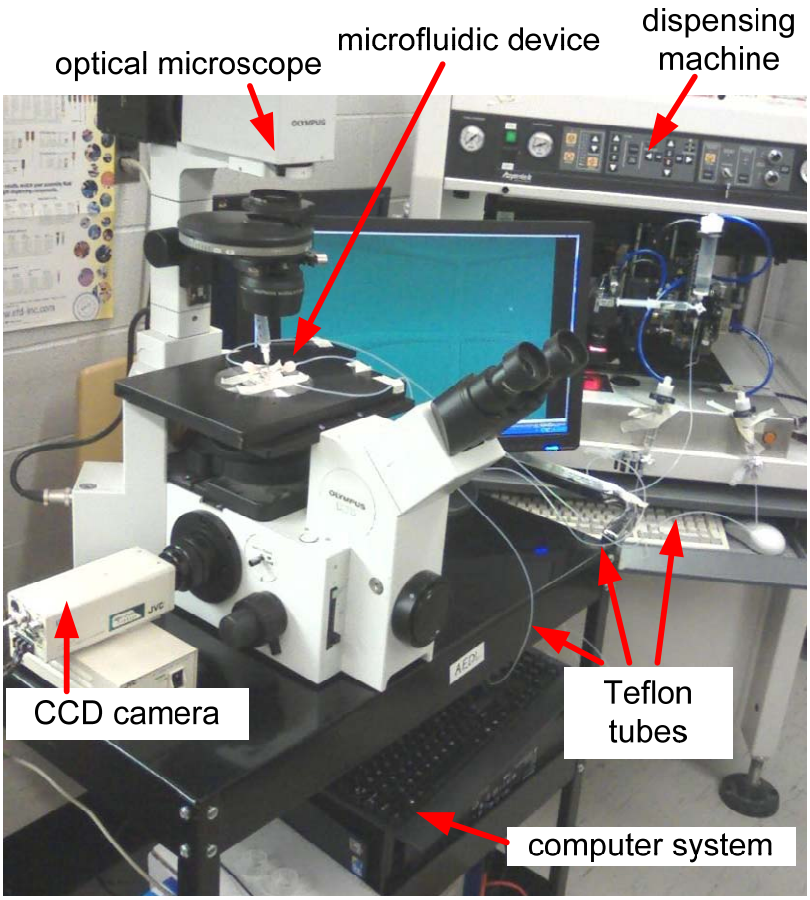

Figure 5.6 Experiment setup.

5.3.2.2. **Results and Discussion**

For the W/O microsphere generation, Paraffin oil with 1% of Span 80 solution was fed to

the sheath flow inlet and crossflow inlet, and distilled water was fed to the middle flow inlet by the continuous air pressure from the dispensing machine. First, the width of the focused flow was determined by adjusting the pressures to the sheath flow and the middle flow independently. The width of the focused flow was reduced by increasing the sheath flow rate. Then, the pressure to the crossflow was applied to realize the microsphere generation once the width of the focused flow became stable with certain pressures, as shown in Figure 5.7. At the T-junction, the induced instability from the crossflow interrupts the stable focused flow under a very high pressure.

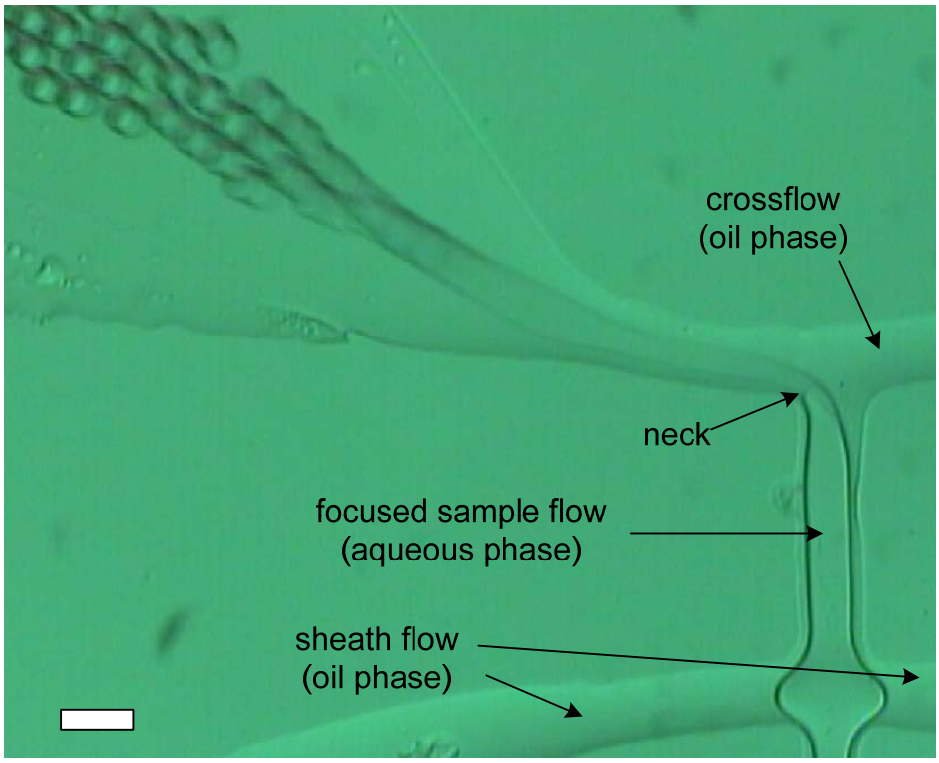

Figure 5.7 The microscope image of the break-up from the focused middle flow jet by the crossflow. The applied pressures are 10.5 psi, 13 psi, and 27 psi for sheath flow, middle flow, and crossflow, respectively. The bar in the image represents 40 μm.

With the constant pressures to the sheath flow and middle flow, respectively, as the flow rate of the crossflow increased, the neck width of focused flow jet decreased, although the width of the focused flow slightly increased. Thus, the size of microspheres became smaller with

higher pressure to the crossflow. However, when the applied pressure to the crossflow was over a limit, a counterflow of the middle flow appeared to the sheath flow stream. Thus, the experiments were conducted by varying the pressure prior to the one which induces a counterflow. By varying the pressure, different sizes of microspheres were generated as shown in Figure 5.8. The results of the experiment have promising outcomes. After the middle flow was focused to a stable state, W/O microspheres started to form from a certain pressure to the crossflow. As the pressure to the crossflow increased, the size of microspheres decreased. As well, as the applied pressure to the sheath flow and middle flow increased, the size of microspheres decreased. The size of microspheres fills the range of 16μm ~ 35μm in diameter with about 5% coefficient of variation (CV) on average, which suggests that the proposed method achieves controllability and uniformity in the generation of microspheres.

The microscopic image and the microsphere size distribution are shown in Figure 5.9 with different pressures. As it can be seen from the figure, when the applied pressure increases, the size of microspheres reduces and the size distribution becomes narrower. Table 5.1 shows the standard deviations of the microsphere sizes with different applied pressures. In the literature reviewed in Chapter 2, it is a common observation that satellite droplets occur during microsphere formation by the hydrodynamic flow focusing method and the T-junction method. However, the proposed method produced very few satellite droplets. Additionally, as the applied pressure increased, no satellite droplet was observed.

In some cases, coalescence occurs when microspheres flow downstream of the T-junction, although the flow rates of focused flow, sheath flow, and crossflow are not low. This may be because acting forces from the collision overcomes interfacial tension to disturb the stabilization, and/or surfactants may not be evenly distributed on microspheres.

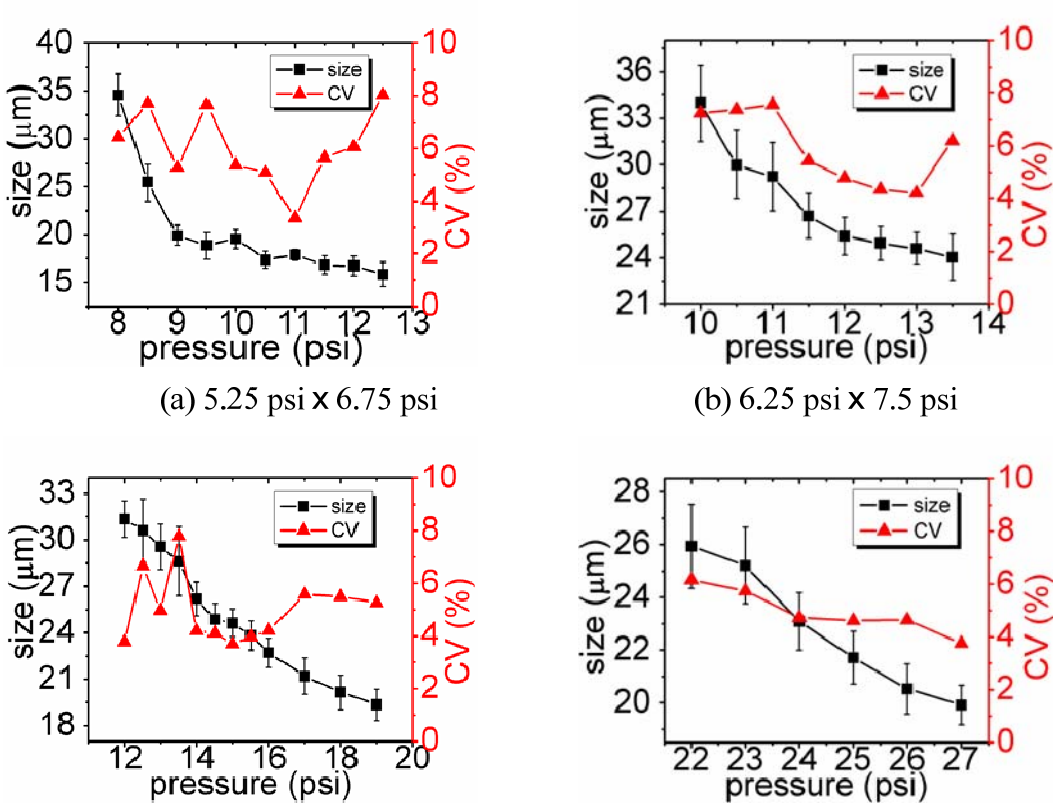

(a) 5.25 psi x 6.75 psi

(b) 6.25 psi x 7.5 psi

(c) 7.25 psi x 8.5 psi

(d) 10.5 psi x 13 psi

Figure 5.8 Size of microspheres with the error bar (standard deviation) and coefficient of variance (CV) by varying the applied pressure to the crossflow. The title at each graph indicates the applied pressure to the sheath flow and middle flow, respectively.

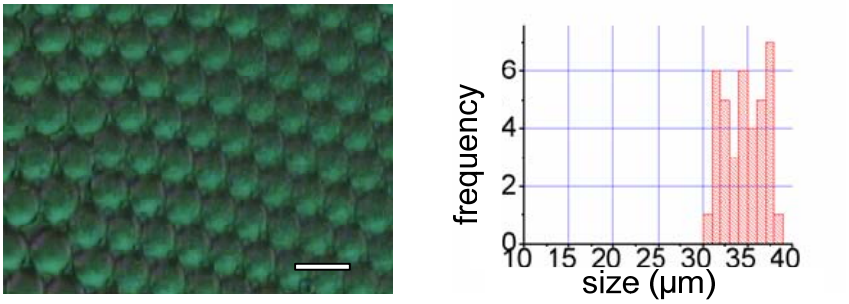

(a) 5.25 psi x 6.75 psi x 8 psi

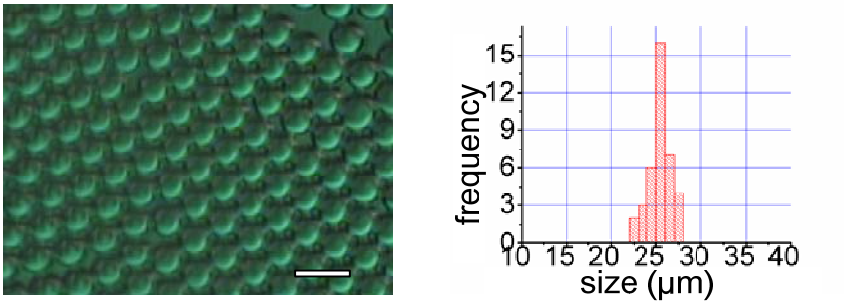

(b) 6.25 psi x 7.5 psi x 12 psi

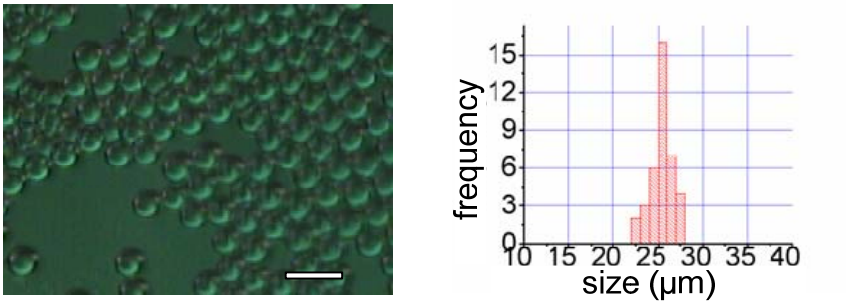

(c) 7.25 psi x 8.5 psi x 16.5 psi

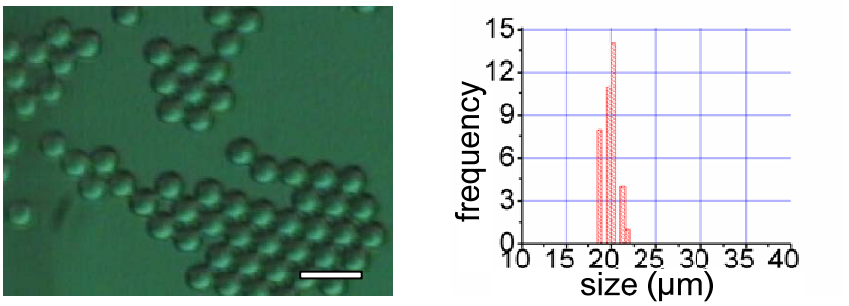

(d) 10.5 psi x 13 psi x 27 psi

Figure 5.9 Microscope images of W/O microspheres with resolution of 1024×768 pixels, and the size distribution with different pressures to sheath flow, middle flow, and crossflow, respectively. The bar in the images represents 40 μm.

Table 5.1 The standard deviation (SD) of microsphere sizes with different pressures

Applied pressure (psi) (sheath flow × middle flow)	Applied pressure (psi) (crossflow)	SD (μm)
5.25 × 6.75	8	2.22
	8.5	1.96
	9	1.05
	9.5	1.44
	10	1.05
	10.5	0.88
	11	0.6
	11.5	0.95
	12	1.0
	12.5	1.27
6.25 × 7.5	10	2.46
	10.5	2.21
	11	2.21
	11.5	1.45
	12	1.21
	12.5	1.09
	13	1.04
	13.5	1.49
7.25 × 8.5	12	1.18
	12.5	2.04
	13	1.47
	13.5	2.23
	14	1.1
	14.5	1.02
	15	0.91

Table 5.1 (continued)

Applied pressure (psi) (sheath flow × middle flow)	Applied pressure (psi) (crossflow)	SD (μm)
7.25 × 8.5	15.5	0.95
	16	0.95
	17	1.18
	18	1.11
	19	1.02
10.5 × 13	22	1.6
	23	1.45
	24	1.09
	25	1.0
	26	0.95
	27	0.75

5.4. Conclusion

In this chapter, a microfluidic device based on integration of hydrodynamic flow focusing and crossflow methods was described, which generates water-in-oil (W/O) microspheres using paraffin oil and distilled water. As discussed in Chapter 3, this method is a decoupled design in that the design realizes the breakage of the dispersed phase from a jet ($\boldsymbol{FR}_2$) and the size-controllability ($\boldsymbol{FR}_3$); these points are independently satisfied.

Two immiscible fluids were fed to the microfluidic device, and varying the flow rates was made by changing air pressures acting on the fluids. At the cross-intersection area of the microchannel, the dispersed phase (middle flow) was focused, and the focused flow met the crossflow at T-junction for break-up. The simulation study verified that this proposed method can

achieve uniformity and controllability in the production of microspheres. Furthermore, the experimental results confirmed that with the proposed method, uniform W/O microspheres with various sizes (16 μm to 35 μm) were produced, and the CV of microsphere sizes was about 5%. By increasing the inlet pressure for the crossflow, the size of microspheres can be controlled.

In short, the proposed method has the advantages of fine sphericity, few satellite drops, active control of the microsphere diameter, and high throughput with a simple and low cost process.

6. SIZE-CONTROLLABLE MONO-DISPERSED MICROSPHERE GENERATION BY LIQUID CHOPPER UTILIZING PZT ACTUATOR

6.1. Introduction

This chapter discusses in detail the design of a microchannel system applying Axiomatic Design Theory (ADT) to create a liquid chopper utilizing a piezoelectric actuator. The main goal of this microchannel system is to generate microspheres by satisfying the three functional requirements: (i) consistency (uniformity or mono-dispersity), (ii) breakage (forming microspheres) and (iii) controllability (size control). As discussed in Chapter 3, conventional microfluidic devices to generate microspheres are coupled in that the size of microspheres and the formation of microspheres are achieved by one design parameter (i.e., flow rate), which can cause a failure during operation. By applying a decoupling process based on ADT, a decoupled design, a liquid chopper in particular, is born.

The principle of this method is as follows: A stable continuous phase (oil phase) stream previously sheathes a dispersed phase (aqueous phase) flow in the microchannel to control the width of the dispersed phase (i.e., hydrodynamically focused). A piezoelectric actuator is embedded in the microchannel of the continuous phase and connected to an electric power system. As the piezoelectric actuator is activated periodically, a fluctuating flow is generated, and the focused flow is pinched off, readily forming water-in-oil (W/O) microspheres. The size of microspheres is uniform and controllable by altering the frequencies of the piezoelectric actuator.

Paraffin oil and water are used for a continuous phase (oil phase) and a dispersed phase (aqueous phase), respectively, to form water-in-oil (W/O) microspheres. A simulation study will

be first presented to verify the proposed microchannel design for generating uniform and size-controllable W/O microspheres. Additionally, experimental results with a lead-zirconate-titanate (PZT) actuator as a piezoelectric actuator and with continuous air pressure confirm the simulation. By changing the frequencies of the PZT actuator, the size of the W/O microspheres can be successfully controlled in various sizes with very good uniformity (i.e., CV < 5%).

6.2. Microfluidic device

As discussed in Chapter 3, this proposed decoupled design was introduced by applying a decoupling process which makes the requirement of the breakage of the dispersed phase from a jet ($\boldsymbol{FR}_2$) independent of that of the size-controllability ($\boldsymbol{FR}_3$). This point means that independent design parameters need to be defined with one to change the width of the dispersed phase stream and the other to break it. The width of the dispersed phase is narrowed by the sheath flow (continuous phase) hydrodynamically, and the focused flow is then cut to form microspheres by the fluctuated flow induced by the PZT actuator. Hydrodynamic flow focusing is widely used in order to squeeze and keep the width of the focused flow for cytometry applications [221]. The width of the focused stream does not depend on the magnitude of applied pressures, but rather on the ratio of side pressure from the sheath flow to inlet pressure of the middle flow (which is proportional to the flow velocity). After being focused, a higher velocity of the focused flow is not avoidable, which makes the focused flow stable, yielding a higher value of the Weber number. Hence, an extra force is needed to increase interfacial tension surrounding a potential microsphere. A fluctuating flow is introduced to the focused stream by an embedded PZT actuator. By structuring a liquid chopper, the fluctuating flow pinches the stable focused flow, and the focused flow is disconnected to form droplets which are emulsified into microspheres. The schematic diagram of the proposed microchannel design is illustrated in Figure 6.1. The

feasibility study of this chopper method has been done through simulation, and the details are described in Appendix B.2.

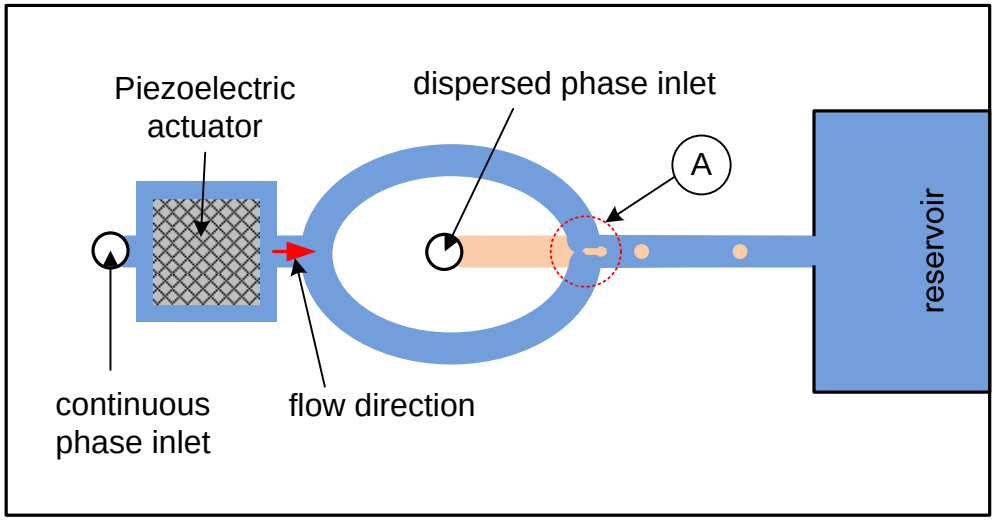

Figure 6.1 Schematic diagram of the proposed microchannel design and microsphere generation. The hydrodynamic flow focusing and the liquid chopper form at the intersection (A).

PZT is widely applied for actuators to convert a strain into a force and one of the commonly used materials, as the interests in manufacturing and assembly for small parts with sizes ranging from few millimeters down to nanometers increases [222, 223]. A PZT actuator is a well-known device for managing very small displacements in the range of 10 pm (1 pm $= 10^{-12}$ m) to 100 μm [224]. The displacement is proportional to the applied external voltage. The dimension changes can be adjusted with extremely high resolution for millions of cycles without wear or deterioration. The advantages of the PZT actuator are sub-nanometer resolution, large force generation, sub-millisecond response, no magnetic fields, extremely low steady state power consumption, no wear and tear, and vacuum and clean room compatibility [223].

Commonly used PZT actuators have two piezoelectric modes (d_{31} and d_{33}) as shown in Figure 6.2. The induced strain direction of the PZT plate is either perpendicular (d_{31}) or parallel (d_{33}) to the electric field direction [225]. The characteristic of the PZT actuator is suitable to the

proposed method for microsphere generation.

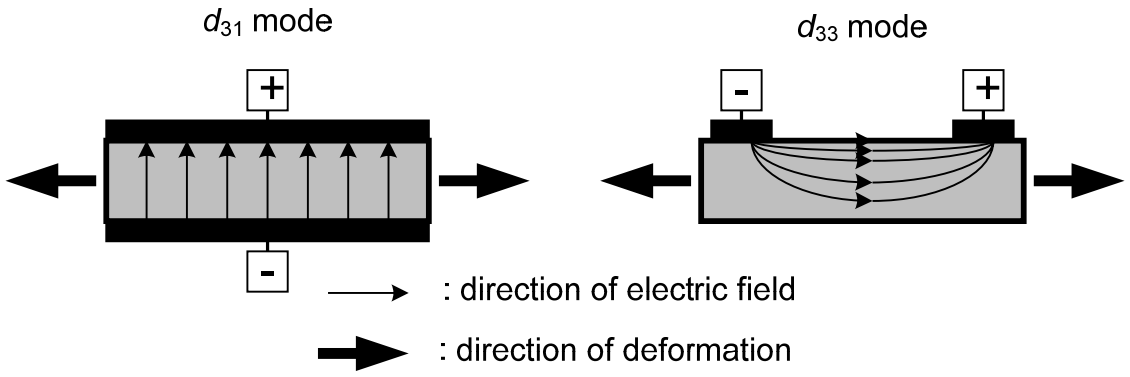

Figure 6.2 Schematic cross-sectional view of the two piezoelectric modes by electric field. When the electric field is applied through the PZT plates, the PZT plates deform in perpendicular (d_{31}) or parallel (d_{33}) to the electric field. Once the electric field is off, the PZT plate returns to its original shape.

6.3. Experiment

6.3.1. Materials and methods

6.3.1.1. **Materials and preparation**

The same materials used for the method described in Chapter 5 were used for this experiment. A solution with paraffin oil (98.5% purity grade) and 1% Span 80 (a non-ionic oil surfactant) was prepared as oil phase by stirring for 15 minutes at room temperature. As an aqueous phase solution, distilled water was used. The instruments in contact with the solutions were carefully cleaned to avoid any contamination.

6.3.1.2. **Fabrication process of the microfluidic device**

The microchannel for the experiment was fabricated by xurography and soft lithography methods at the Advanced Engineering Design Lab (AEDL) and Saskatchewan Structural Science Center (SSSC) in UofS. Xurography was introduced by Bartholomeusz et al. [226]. The term ”xurography” is made of ”xuron” and ”graphe” in Greek meaning ”razor” and ”writing,”

respectively. This method is rapid and inexpensive, using a commercial cutting plotter which is a plotter containing a knife blade. Polymer films in various thicknesses are used as substrates. The schematic diagram of the xurography is illustrated in Figure 6.3.

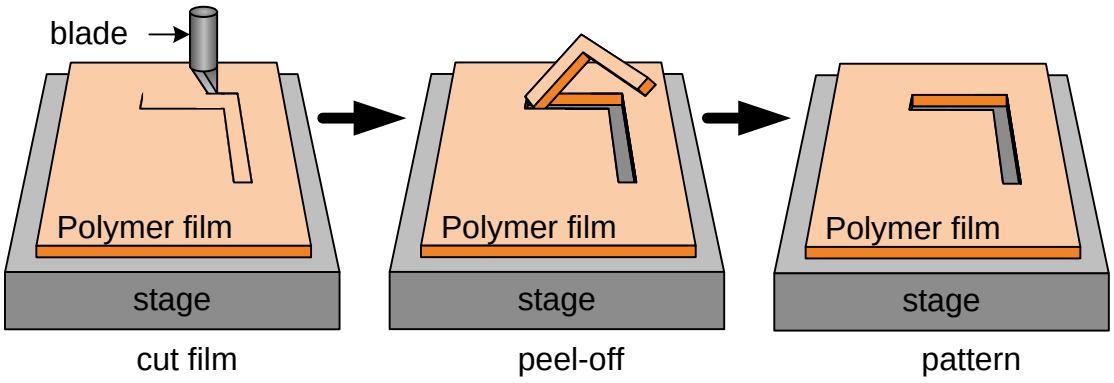

Figure 6.3 Schematic diagram of xurography (positive structure).

After cutting with desired patterns, unnecessary parts are peeled off, leaving the desired patterns. Currently, a commercial cutting plotter can cut a feature in a resolution of 10 μm. Overall, this method can achieve a clean cut for 100 μm width on 50 μm thick pressure sensitive adhesive (PSA) film [227]. The major factors to determine the size of cutting (scratches) are tension of substrate, blade sharpness, cutting speed and material property of substrate (e.g., Young's modulus and Poisson's ratio). The width of a scratch increases linearly as applied force on the blade increases. As well, the depth of a scratch and the applied force have a linear relationship [228].

A commercial cutter (Craft Robo Pro) was purchased from Graphtec America, Inc. with a variable cutting force between 0.2 N and 2.9 N, 5 μm of mechanical resolution, and a 0.9 mm of 45^{o} vinyl cutting blade as shown in Figure 6.4.

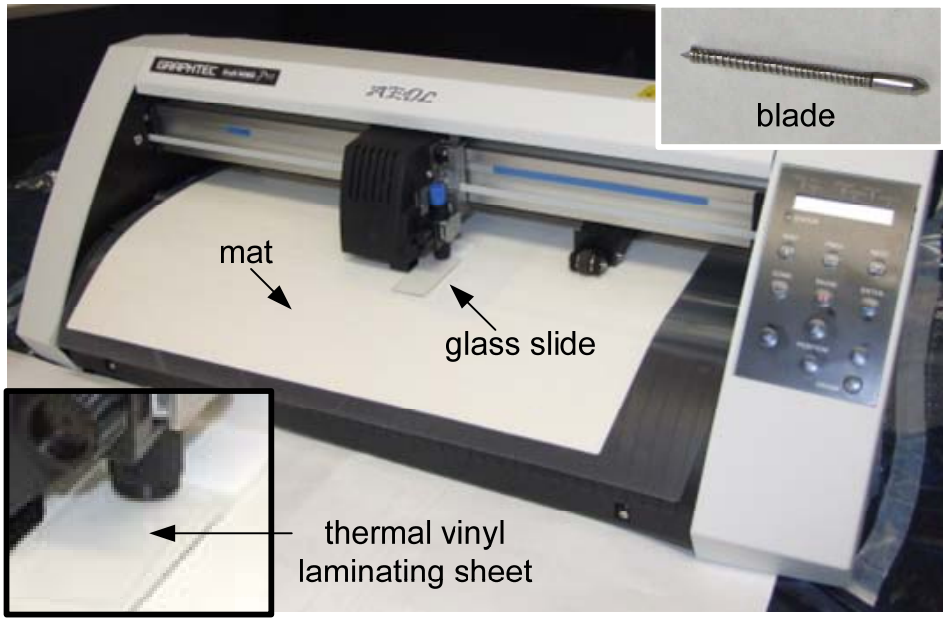

Figure 6.4 Xurography with Craft Robo pro from Graphtec America, Inc. and vinyl cutting blade.

A desired microchannel pattern was prepared by AutoCAD, and the pattern was transmitted to the cutter by a computer system through a USB connection. Activating the software of the cutter, the pattern of microchannel was transferred on to a 3M thermal vinyl laminating sheet in about 200 μm of thickness. After laminating the vinyl sheet on a glass slide with a thermal laminator, the soft lithography process was operated to achieve PDMS replicas. The surfaces of PDMS replicas were treated with oxygen plasma for better bonding on a glass substrate. For fluctuating flow, a $2\ cm\ (H) \times 0.5\ cm\ (L) \times 0.5\ cm\ (W)$ PZT actuator was used in order to achieve a large deformation of a PZT actuator. This PZT actuator deformed about 1 μm in the direction of height (H) when 120 V was used for the experiment.

6.3.2. Experiment

6.3.2.1. Apparatus and analysis

The overall size of the PDMS microchannel was $2.5\ cm \times 3.5\ cm$ with 200 μm of

height and 130 μm of channel width at the intersection. The mold and replica by xurography and soft lithography methods are shown in Figure 6.5.

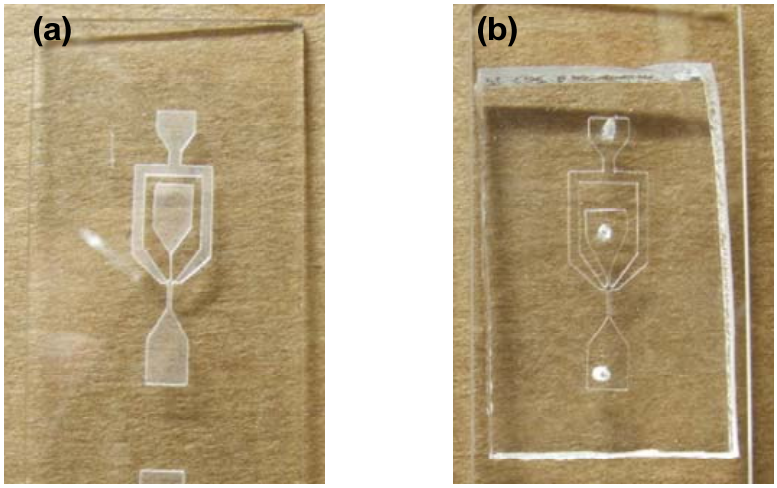

Figure 6.5 (a) Master with microchannel patterns by xurography and (b) PDMS replica of the microchannels by soft lithography process.

The microchannel was placed on the optical microscope connected to a computer system for capturing images and videos of microsphere formation. Images with resolution of 1024×768 pixels were taken during the observation. Instead of being embedded in the microchannel because of the size, the PZT actuator was glued on a glass slide in a small container which was connected to the oil phase (paraffin oil) inlet. The PZT actuator was connected to an amplifier which amplified the voltage from a signal generator to 120 V. The signal generator generated a sinusoidal wave in various frequencies from 1 Hz to 5000 Hz. An oscilloscope was connected through the electric connection to observe the voltage and frequency applied to the PZT actuator. Oil phase flow was fed to the inlet by continuous air pressure through the PZT container, and the container was completely sealed with PDMS and epoxy glue. The oil phase was used as both the sheath flow and the oscillating flow. Aqueous phase (distilled water) flow was also fed by a continuous air pressure to the inlet. The aqueous phase was used as a middle flow to be focused

by the oil phase. No leakage was found through the Teflon tubing connections between pressure sources and the microchannel. The experiment was setup as illustrated in Figure 6.6 and performed at SSSC in UofS.

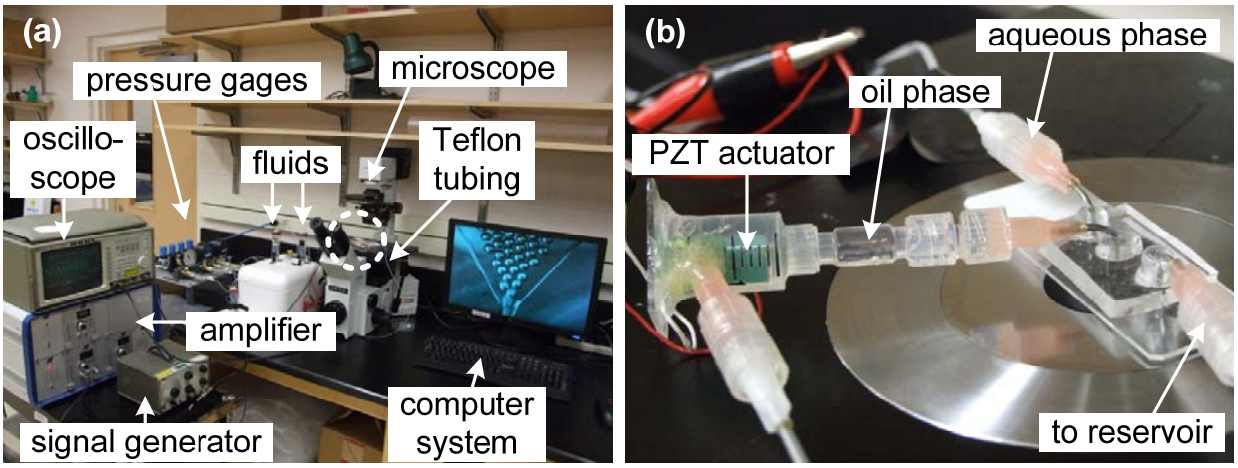

Figure 6.6 Experiment setup: (a) apparatuses and their connections, and (b) a close view of the part encircled in (a).

The flow rates of the solutions were manipulated by altering the air pressure to achieve a steady state of the focused flow. Once the focused flow became stable, the PZT was activated by turning on the signal generator with various frequencies. At each frequency, at least one minute of equilibrium time was taken to capture the images of microspheres. The diameters of microspheres were measured from the optical microscope images. The average size of microspheres was verified by measuring the size of 40 microspheres from the captured images using an image processing software (ImageJ, National Institutes of Health). The coefficient of variation ($CV = \delta/dm_{av} \times 100\%$) [51, 53, 81] is calculated for the size distribution of the microspheres, where δ is the standard deviation, and dm_{av} is the average diameter of microspheres.

6.3.2.2. **Results and discussion**

For the W/O microsphere generation, paraffin oil with 1% of Span 80 solution was fed as

the sheath flow and fluctuating flow, and distilled water was fed as the middle flow. First, the width of the focused flow was determined by adjusting the continuous air pressures to the sheath flow and the middle flow, respectively. The width of the focused flow was reduced by increasing the sheath flow rates. Once the focused flow was stable, the PZT actuator was activated to generate the fluctuating flow that would realize the microsphere generation. However, the fluctuating flow was not able to pinch off the focused flow completely.

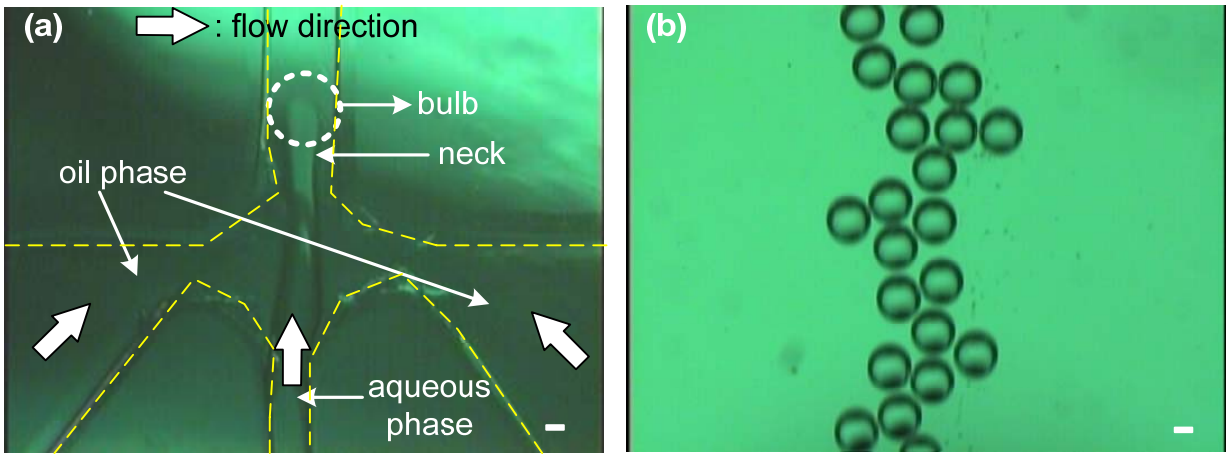

Figure 6.7 The microscope images: (a) Bulb forms and the neck is pinched before the break-up of the focused flow, and (b) the microspheres after the breakage. The applied pressures are 0.6 psi and 1 psi for aqueous phase and oil phase, respectively, with 100 Hz of frequency of the PZT actuator. The bar in the images represents 50 μm.

The focused flow became unstable, but no microsphere was formed. This occurred because the deformation of the PZT actuator was inadequate to generate enough oscillation to break the focused flow in such a large size channel. Thus, the applied pressures were increased to reach breakup point of the focused flow. As microspheres started to form from the focused flow, the PZT actuator was activated, and the size of the microsphere decreased as the frequency increased. The PZT actuator created high impact forces with vibrations and generated oscillating flows served as liquid chopper on the focused flow generating high shear forces. Optical images of microsphere generation are shown in Figure 6.7. The applied air pressures were altered to

change the width of the focused flow: (i) 0.6 psi (w) × 0.8 psi (o), (ii) 0.6 psi (w) × 1 psi (o), and (iii) 0.85 psi (w) × 1.35 psi (o), where w and o represent aqueous phase and oil phase, respectively. At 0.6 psi (w) × 0.8 psi (o), the average initial size of microspheres was 196.5 μm with 2.8 % CV, at 0.6 psi (w) × 1 psi (o), the average initial size of microspheres was 118.1 μm with 1.6 % CV, and at 0.85 psi (w) × 1.35 psi (o), the average initial size of microspheres was 87.8 μm with 3.1 % CV. For different cases, the CV values were lower than 5%, indicating that the system reached a steady and stable state. With the constant pressures to the sheath flow and the middle flow, the applied frequencies of the PZT actuator were varied from 1 Hz to 5000 Hz. The experimental results are illustrated in Figure 6.8 and Figure 6.9 for case (i), Figure 6.10 and Figure 6.11 for case (ii) and Figure 6.12 and Figure 6.13 for case (iii). In all the cases, as the frequency increased, the size of microspheres generated became smaller (i.e., the controllability was achieved). The higher pressure generated from the PZT actuator interrupted the steady state to increase instability and form microspheres. However, the uniformity was not satisfied with lower frequencies (< 10 Hz). In some cases, CV values at lower frequencies reached over 20 %, and the sizes of microspheres were distributed widely, forming two separated peaks. This phenomenon indicated that by slow fluctuation, the instability on the focused flow caused two microsphere size groups.

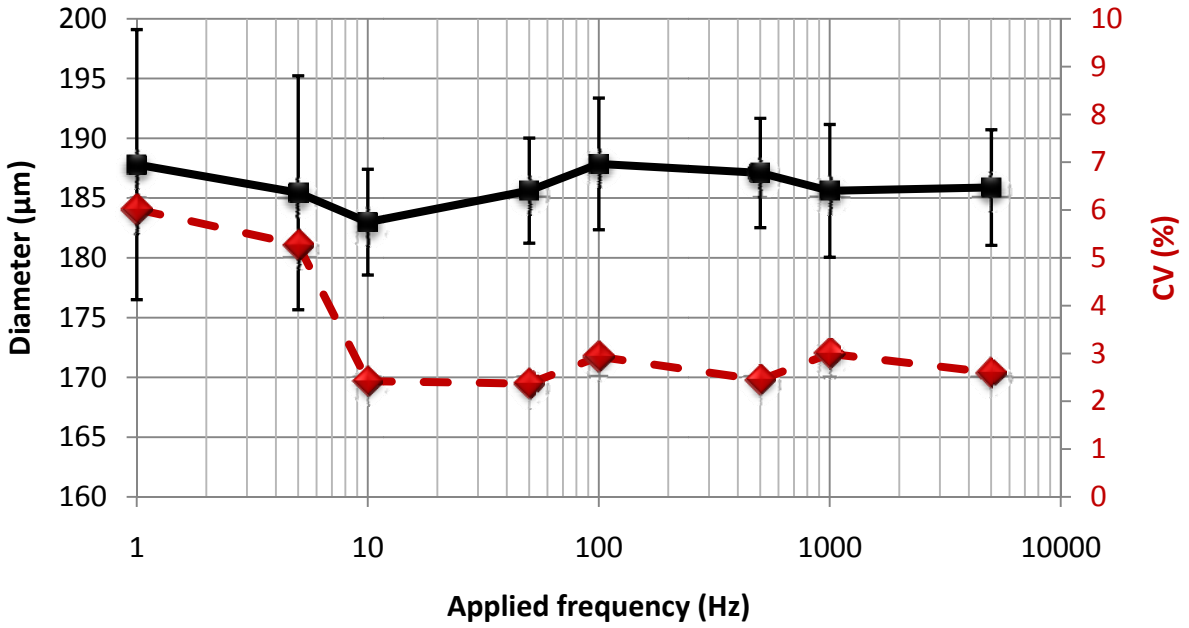

(a) The size of microspheres with error bar (, standard deviation) and coefficient of variation (, CV) at different frequency

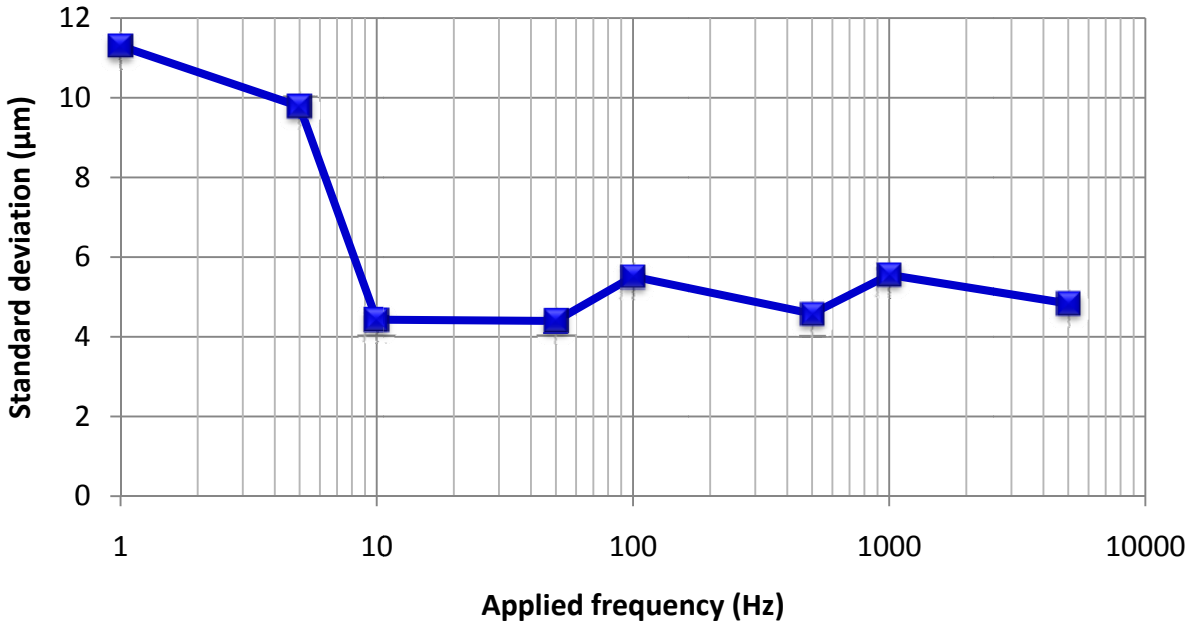

(b) The standard deviation at different frequency

Figure 6.8 Size of microspheres by varying the applied frequency of the PZT actuator at 0.6 psi and 0.8 psi for aqueous phase and oil phase, respectively.

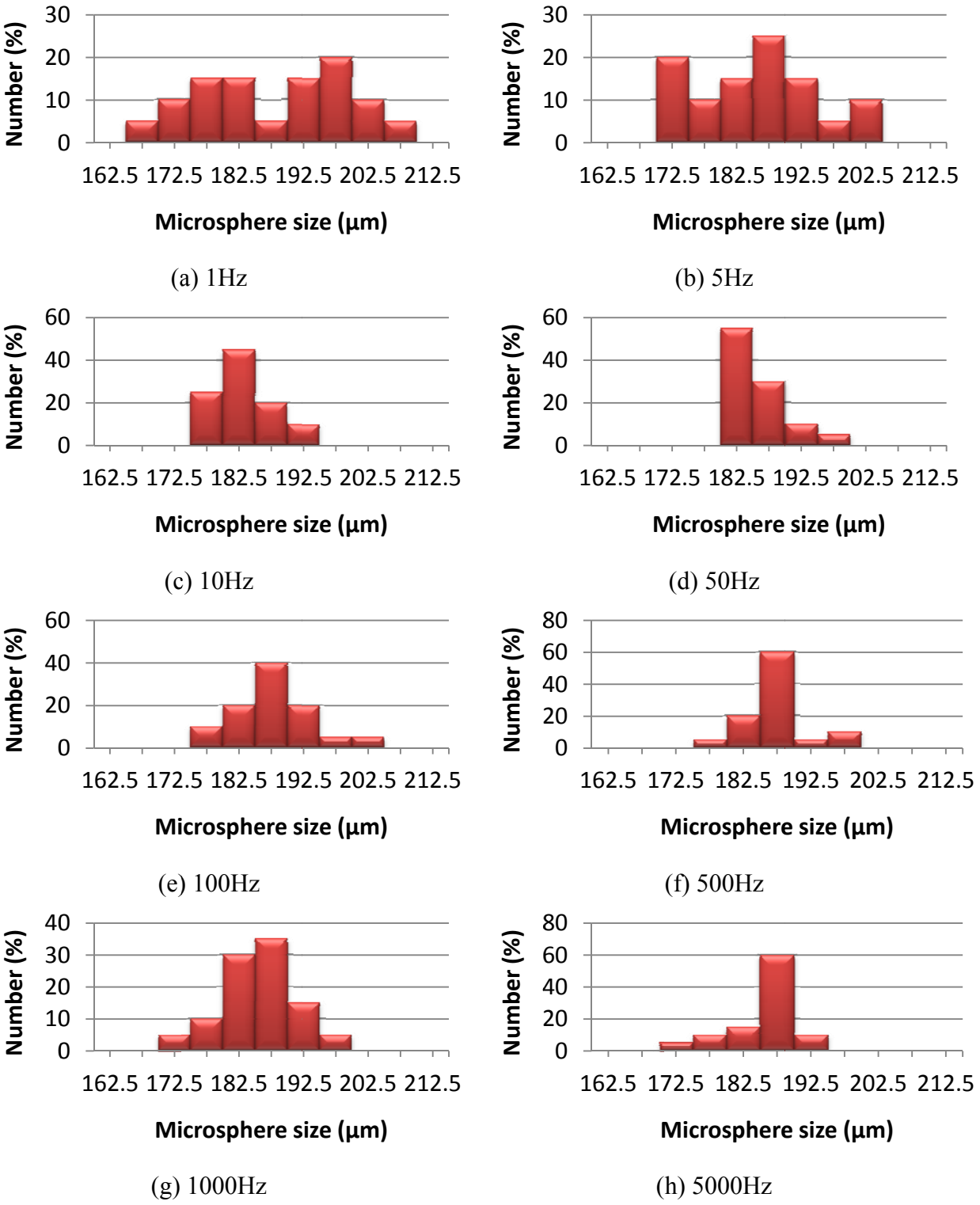

Figure 6.9 Size distribution of microspheres with different applied frequencies of the PZT actuator at 0.6 psi and 0.8 psi for aqueous phase and oil phase, respectively.

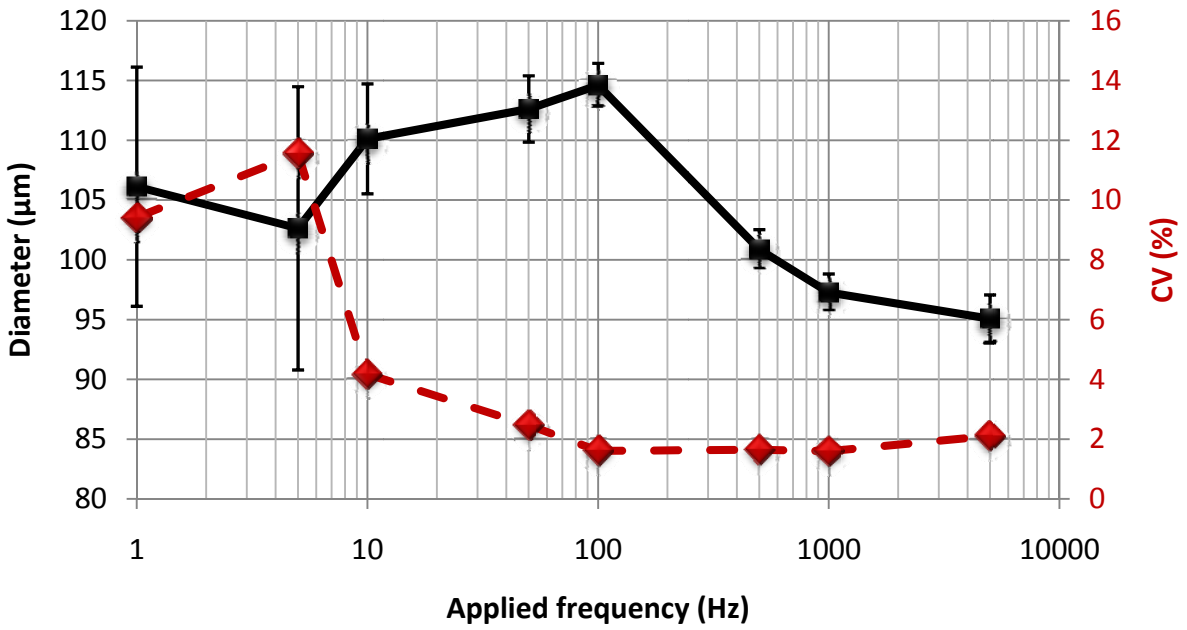

(a) The size of microspheres with error bar (, standard deviation) and coefficient of variation (, CV) at different frequency

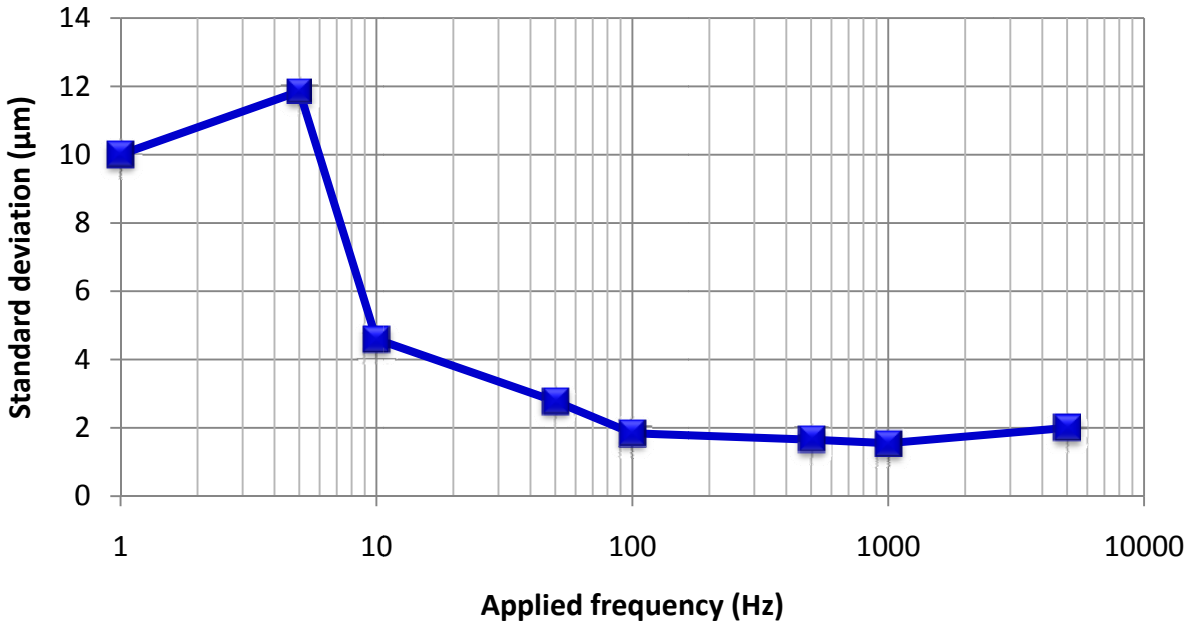

(b) The standard deviation at different frequency

Figure 6.10 Size of microspheres by varying the applied frequency of the PZT actuator at 0.6 psi and 1 psi for aqueous phase and oil phase, respectively.

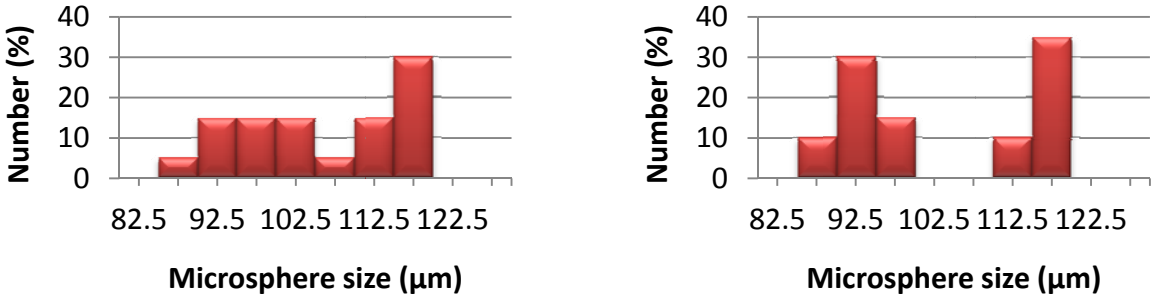

(a) 1Hz

(b) 5Hz

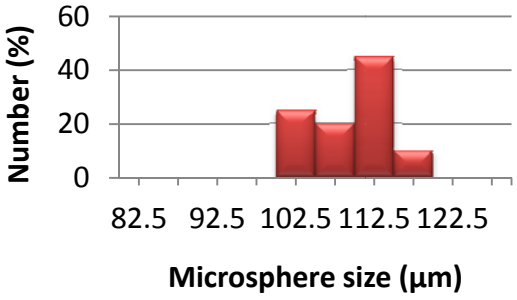

(c) 10Hz

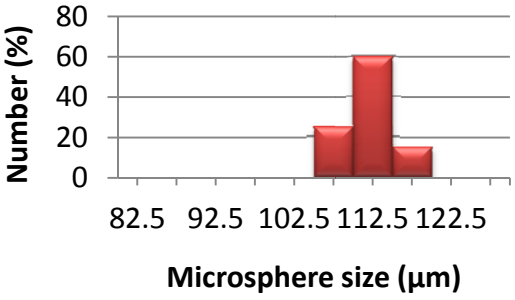

(d) 50Hz

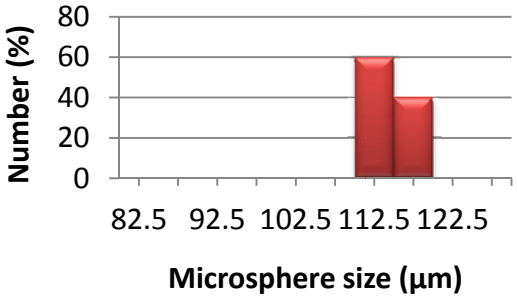

(e) 100Hz

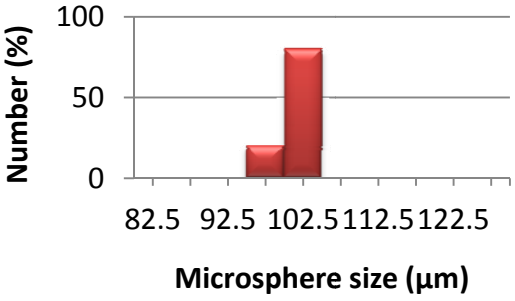

(f) 500Hz

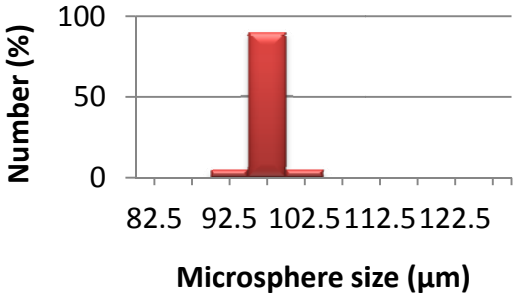

(g) 1000Hz

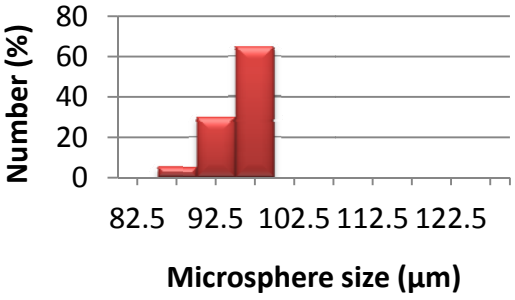

(h) 5000Hz

Figure 6.11 Size distribution of microspheres with different applied frequencies of the PZT actuator at 0.6 psi and 1 psi for aqueous phase and oil phase, respectively.

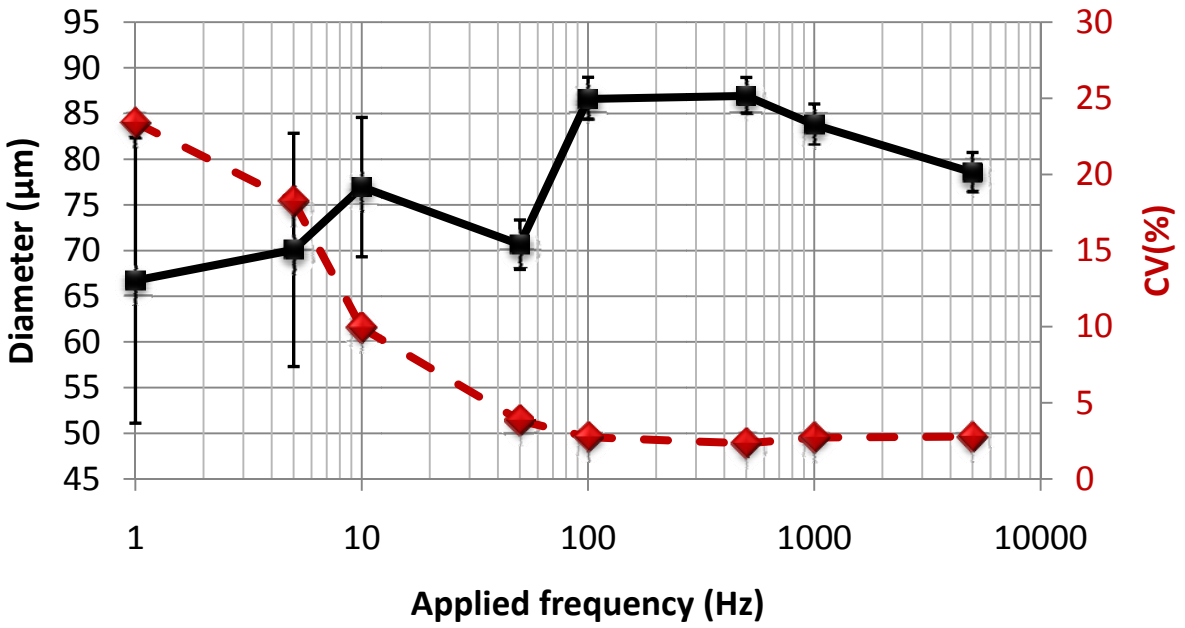

(a) The size of microspheres with error bar (, standard deviation) and coefficient of variation (, CV) at different frequency

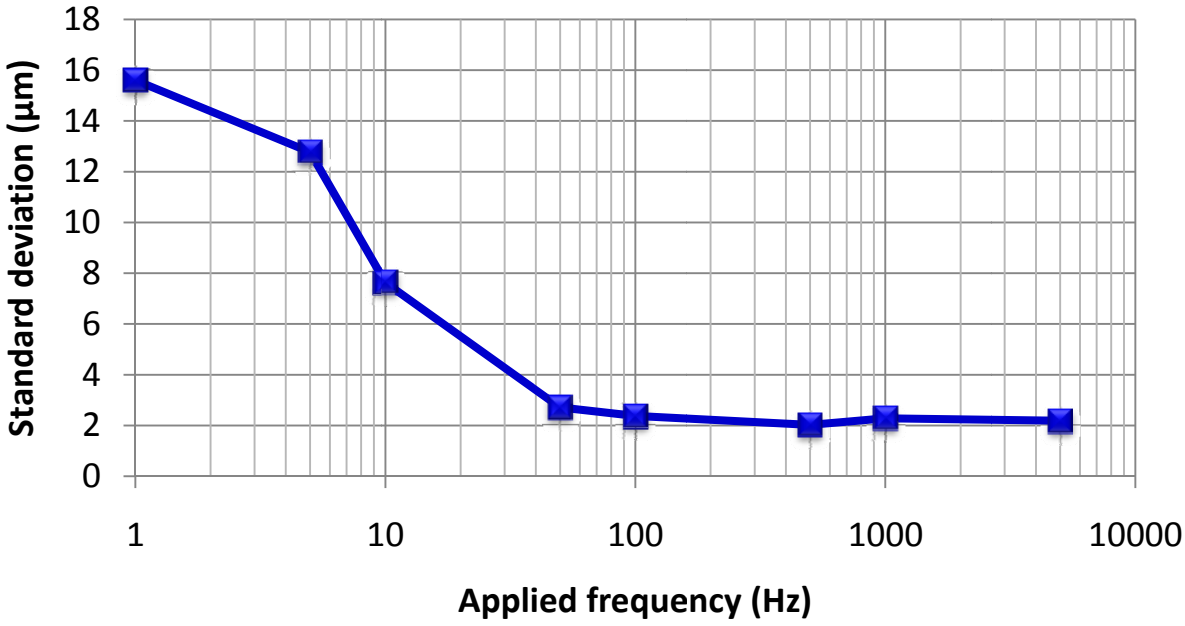

(b) The standard deviation at different frequency

Figure 6.12 Size of microspheres by varying the applied frequency of the PZT actuator at 0.85 psi and 1.35 psi for aqueous phase and oil phase, respectively.

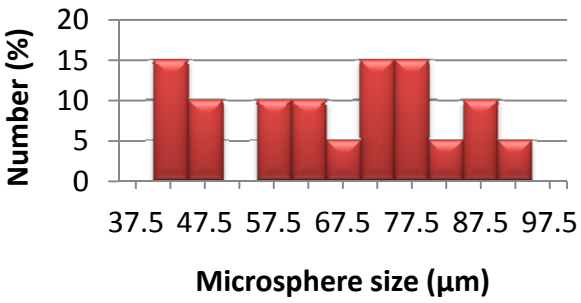

(a) 1Hz

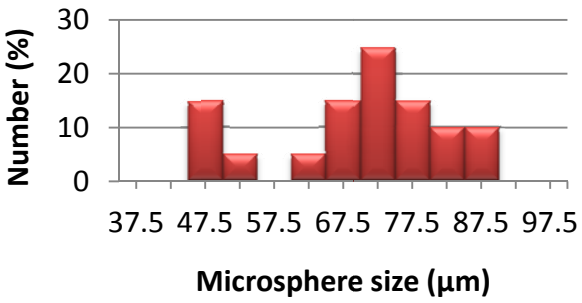

(b) 5Hz

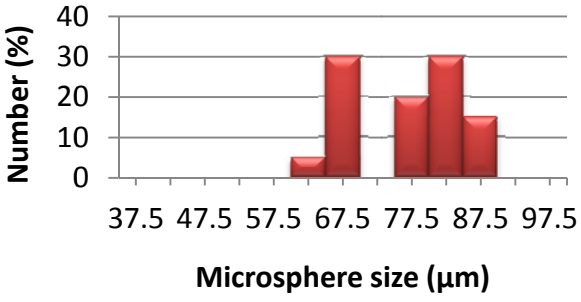

(c) 10Hz

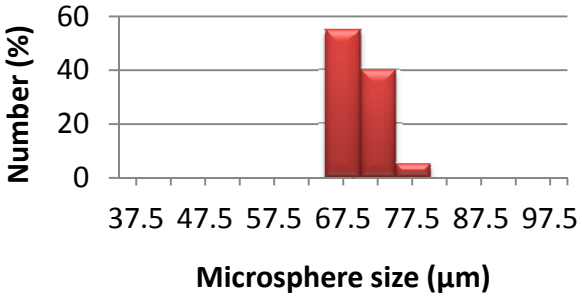

(d) 50Hz

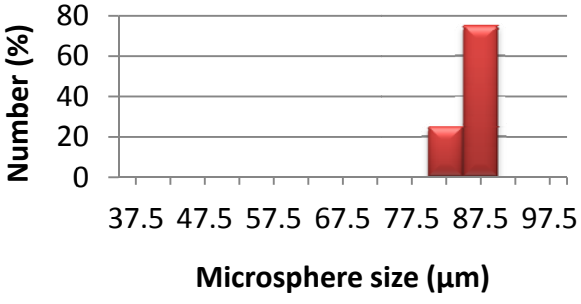

(e) 100Hz

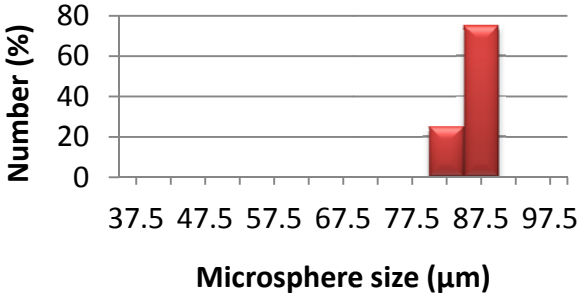

(f) 500Hz

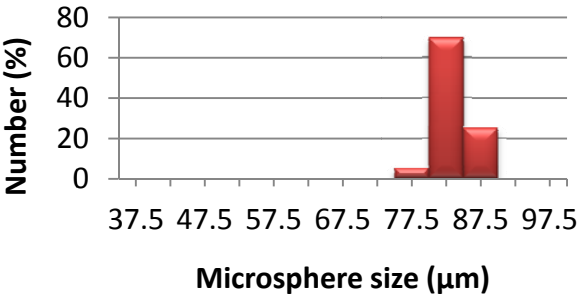

(g) 1000Hz

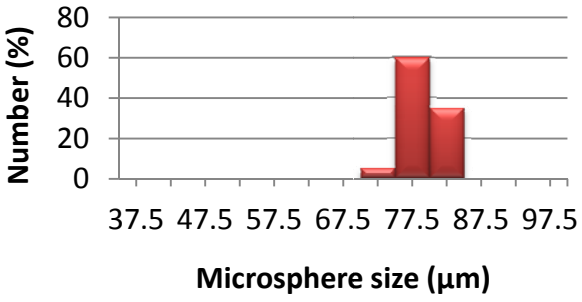

(h) 5000Hz

Figure 6.13 Size distribution of microspheres with different applied frequencies of the PZT actuator at 0.85 psi and 1.35 psi for aqueous phase and oil phase, respectively.

However, at higher frequencies (>10 Hz), the CV values became lower than 5 % in smaller sizes, yielding both excellent uniformity and controllability. At higher frequencies, the sizes of microspheres changed through varying the applied frequencies of the PZT actuator. As shown in the figures for the size distribution, the widely distributed sizes at lower frequencies became closer at higher frequencies, satisfying uniformity. The average size of microspheres started to increase slightly at the frequencies between 10 Hz and 100 Hz, but the average size decreased at over 100 Hz. This result suggested that interfacing forces of two-phase flows were completely overcome by the oscillating flow to form microspheres. In every case, the average size at different frequencies (>100 Hz) was smaller than the initial average size, indicating that the oscillating flow affected the formation of microspheres, thereby achieving controllability. However, the sizes of microspheres did not change significantly after an extremely high frequency (>5000 Hz).

6.4. Conclusion

In this chapter, a liquid chopper method utilizing a PZT actuator was studied to generate water-in-oil (W/O) microspheres. As discussed in Chapter 3, this method is a decoupled design because size-controllability is independently satisfied from the breakage of the dispersed phase flow. A decoupling process was proposed to develop this method.

A stable hydrodynamically focused flow is interrupted by the fluctuating flow generated by a PZT actuator in the microchannel. The high pressure of the oscillating flow overcomes interfacing forces of two-phase flows, and the focused flow is pinched off, which is characterized as a liquid chopper. The simulation study verified that the proposed liquid chopper method can achieve uniformity and controllability in the production of microspheres. Furthermore, experimental results confirmed the simulation results. The liquid chopper was activated in

various frequencies by changing the frequency of the PZT actuator in different initial pressures, and microspheres of different sizes under 5 % of the coefficient of variation were generated.

This microchannel design can achieve tunable microspheres with uniform size, and it reveals a high potential for the emulsification process. In this study, the size of microchannel was relatively bigger to analyze the effect of the oscillating flow on the focused flow in a direct way due to the limitation in deformation of the PZT actuator. Smaller sizes of microchannels are recommended with this method in order to examine the direct effect of the oscillating flow on a stable stream.

7. CONCLUSION AND FUTURE WORK

7.1. Overview and conclusions

This study was intended to develop theories and methodologies for microfluidic systems to generate microspheres in uniform and different sizes by applying Axiomatic Design Theory (ADT). Specifically, three microfluidic systems with new principles were studied in this thesis, and they are: (1) perforated silicon membrane, (2) integration of hydrodynamic flow focusing and crossflow methods, and (3) liquid chopper using a piezoelectric actuator.

This study began with two extensive reviews of the state-of-the-art of the microfluidic systems and ADT. The former discussed microfluidic systems of microsphere generation based on micro-electro-mechanical system (MEMS) technology, in particular including MEMS fabrication processes for microchannel systems. The review focuses on principles for microchannel systems, such as membrane emulsification, hydrodynamic flow focusing, crossflow, and pneumatic chopper. The latter set of reviews discussed ADT, which is extremely effective for a more systematic design process, especially through its function independence axiom and information axiom. The limitations of current microfluidic systems for microsphere generation were then identified, namely uniformity and size-controllability of microspheres. It is noted that rational design practice in microfluidc systems was surprisingly missing.

Next, systematic design methodologies and analysis of the current microfluidic methods for microsphere generation were discussed by applying ADT. The current microfluidic systems for microsphere generation were evaluated as ”coupled designs” in terms of management of microsphere generation which further derived the required functions: (i) size consistency (uniformity), (ii) breakage of the flow stream to form microdroplets, and (iii) size controllability.

In particular, the size-controllability and breakage were satisfied by one design parameter.

A design process, named the decoupling process and based on ADT, was applied to lead to uncoupled and decoupled microfluidic systems for microsphere generation, resulting in three new methods: (1) perforated silicon membrane, (2) integration of hydrodynamic flow focusing and crossflow methods, and (3) liquid chopper using a piezoelectric actuator. In these new designs, the coupled functional requirements (size-controllability and breakage) were independently satisfied by different design parameters such as agitator (breakage) in the case of (1), hydrodynamic flow focusing (size-controllability) and crossflow (breakage) in the case of (2), and hydrodynamic flow focusing (size-controllability) and a PZT actuator (breakage) in the case of (3). Validation of the proposed methods was performed through both simulation and experiments. In particular, models and simulations were developed for methods (2) and (3), while experiments were performed for all the three methods. Three microfluidic systems based on the three methods were designed and fabricated with technologies such as photolithography, wet etching and soft lithography.

The general conclusion of the study reported in this thesis is that the application of the systemic design process, ADT in this case, to design a microfluidic system for microsphere generation is successful. Such an ADT-based rational design of microfluidic systems may likely be promising for other applications as well.

Some specific conclusions are :

(1) The current microfluidic systems for microsphere generation found in the literature are considerably inadequate for satisfying both uniformity and size-controllability or have rooms to be improved.

(2) Through the ADT analysis, the current microfluidic system designs for microsphere generation are defined as coupled designs, which are prone to operational failures.

(3) A decoupling process based on ADT can assist in changing coupled designs to uncoupled or decoupled designs, which can better fulfill functions such as uniformity and size-controllability for microsphere generation.

(4) The proposed microfluidic system designs based on ADT are very promising in terms of their capability for mono-dispersed microsphere generation in various sizes. With method (1) (i.e., perforated silicon membrane), about 90% of the microspheres were in the range from 1 to 2 μm (CV = 7.9%). With method (2) (i.e., integration of hydrodynamic flow focusing and crossflow), the nominal size of microspheres varies from 16 to 37 μm in diameter with about 5% of CV. With method (3) (i.e., liquid chopper), the nominal size of microspheres varies from 78 μm to 186 μm in diameter with less than 5% of CV.

7.2. Future research work

There are a few limitations in the present study, from which we come to the following recommendations for future research work.

First, in the study of perforated silicon membrane discussed in Chapter 4, uniformity was achieved; however, size-controllability was not realized because of the constant pore size. A further study on changeable pore size should be valuable in order to accomplish the size-controllability with the membrane method. Furthermore, the silicon membrane fabricated in this thesis was extremely thin (< 2 μm) and therefore brittle, causing membrane fracture. In order to avoid the fracture, low flow rates were applied during the operation, yielding low productivity of microspheres from this method. It is recommended to develop a fabrication technique to make pores with a high aspect ratio (i.e., the ratio of the height to the width) to overcome this

limitation. Additionally, for more accurate measurement, the flow speeds on the membrane should be measured instead of agitation speeds.

Second, in the device which implements the liquid chopper concept discussed in Chapter 6, the size of the microchannel was relatively big, which caused the deformation of the PZT actuator and subsequently caused a higher force requirement to pinch off the focused stream. Also, the oscillating flow generated by the PZT actuator may not be fully converted to the focused stream due to the external connection of the PZT actuator to the PDMS microchannel device. A new method to embed a PZT actuator with a high deformation rate in a microchannel device is recommended to overcome this limitation. Furthermore, a study of the liquid chopper with smaller size microchannels should be interesting, as it is expected that this may generate more disturbances coming from the external connection between the PZT actuator and PDMS microchannel.

Third, through the study reported in this thesis, two types of microsphere were generated, oil-in-water (O/W) and water-in-oil (W/O) microspheres, without including functional agents (e.g., proteins or antigens) in these microspheres. In order to complete functionalized microspheres for the applications such as drug delivery and cosmetics, functional agents are necessary to be included in microspheres and confirm the feasibility of the proposed methods in this thesis. Furthermore, perspective applications with the functionalized microspheres are recommended, such as drug delivery for medical application.

Last, it is suggested to insert magnet particles in microspheres to realize magnetic microspheres as a future work. Magnetic microspheres (or mimetic particles) have been widely utilized biomedical applications such as cell separation [229-231] and isolation [232], immunoprecipitation [233, 234], immunoassays [235, 236], biosensors [237, 238], and

biopanning [239, 240] by providing numerous benefits including easiness and automation [241]. The proposed principles for microsphere generation in this thesis may be able to enhance the quality and production of magnetic microspheres.

REFERENCES

[1] Wikipedia, "Online Encyclopedia: Drug," 2007, <http://en.wikipedia.org/wiki/Drug>.

[2] E. D. Rosen, "Protein-Based Drugs: A Look Through The Crystal Ball," 2002, <http://www.diabetesincontrol.com/modules.php?name=News&file=article&sid=599>.

[3] Government of Canada, "Protein-Based Drugs," 2006, <http://www.biostrategy.gc.ca/english/view.asp?x=782>.

[4] R. Bailey, "Protein Function," 2010, <http://biology.about.com/od/molecularbiology/a/aa101904a.htm>.

[5] K. J. Morrow, "Developing Sophisticated Protein-Based Drugs - Engineering and Expressing Novel Protein Therapeutics," *Genetic Engineering News,* vol. 25, pp. 85-85, Aug 2005.

[6] G. J. Moore, "Designing Peptide Mimetics," *Trends in Pharmacological Sciences,* vol. 15, pp. 124-129, 1994.

[7] Chinese Medical & Biological Information, "Phage Display and Its Application," 2002, <http://cmbi.bjmu.edu.cn/www-learn/labmeeting/labmeeting_006.pdf>.

[8] V. P. Torchilin and A. N. Lukyanov, "Peptide and Protein Drug Delivery to and into Tumors: Challenges and Solutions," *Drug Discovery Today,* vol. 8, pp. 259-266, 2003.

[9] R. Liu, G. Ma, F.-T. Meng, and Z.-G. Su, "Preparation of Uniform-sized PLA Microcapsules by Combining Shirasu Porous Glass Membrane Emulsification Technique Multiple Emulsion-Solvent Evaporation Method," *Journal of Controlled Release,* vol. 103, pp. 31-43, 2005.

[10] C. Charcosset, I. Limayem, and H. Fessi, "The Membrane Emulsification Process: A Review," *Journal of Chemical Technology & Biotechnology,* vol. 79, pp. 209-218, 2004.

[11] S. M. Joscelyne and G. Tragardh, "Membrane Emulsification - A Literature Review," *Journal of Membrane Science,* vol. 169, pp. 107-117, 2000.

[12] D. J. McClements and R. Chanamai, "Physicochemical Properties of Monodisperse Oil-in-Water Emulsions," *Journal of Dispersion Science and Technology,* vol. 23, pp. 125-134, 2002.

[13] S. van der Graaf, T. Nisisako, C. G. P. H. Schroen, R. G. M. van der Sman, and R. M. Boom, "Lattice Boltzmann Simulations of Droplet Formation in a T-shaped Microchannel," *Langmuir,* vol. 22, pp. 4144-4152, Apr 25 2006.

[14] J. Akbuga, "Effect of Microsphere Size and Formulation Factors on Drug Release from Controlled-release Furosemide Microspheres," *Drug Development and Industrial Pharmacy,* vol. 17, pp. 593-607, 1991.

[15] E. Dickinson, *Emulsions and Droplet Size Control*. Oxford: Butterworth-Heinemann, 1994.

[16] K. Kandori, "Applications of Microporous Glass Membranes: Membrane Emulsification," in *Food Processing: Recent Developments*, Gaonkar, Ed.: Elsevier Science B.V., 1995.

[17] R. Katoh, Y. Asano, A. Furuya, K. Sotoyama, and M. Tomita, "Preparation of Food Emulsions using Membrane Emulsification System," in *the 7th International Symposium on Synthetic Membranes in Science*, Tübingen, Germany, 1994, p. 407.

[18] R. Narayani and K. P. Rao, "Gelatin Microsphere Cocktails of Different Sizes for the Controlled Release of Anticancer Drugs," *International Journal of Pharmaceutics,* vol.

143, pp. 255-258, 1996.
[19] X. S. Wu, "Synthesis and Properties of Biodegradable Lactic/Glycolic Acid Polymers," in *Encyclopedic Handbook of Biomaterials and Bioengineering, Part A: Materials*, D.L. Wise, D.J. Trantolo, D.E. Altobelli, M.J. Yaszemski, J.D. Gresser, and E. R. Schwartz, Eds. New York: Marcel Dekker, 1995.
[20] D. Bodmer, T. Kissel, and E. Traechslin, "Factors Influencing the Release of Peptides and Proteins from Biodegradable Parenteral Depot Systems," *Journal of Controlled Release,* vol. 21, pp. 129-137, 1992.
[21] F. G. Hutchinson and B. J. A. Furr, "Biodegradable Polymer Systems for the Sustained-Release of Polypeptides," *Journal of Controlled Release,* vol. 13, pp. 279-294, 1990.
[22] I. Soriano, A. Delgado, R. V. Diaz, and C. Evora, "Use of Surfactants in Polylactic Acid Protein Microspheres," *Drug Development and Industrial Pharmacy,* vol. 21, pp. 549-558, 1995.
[23] H. V. Maulding, "Prolonged Delivery of Peptides by Microcapsules," *Journal of Controlled Release,* vol. 6, pp. 167-176, 1987.
[24] D. T. O'Hagan, H. Jeffery, and S. S. Davis, "The Preparation and Characterization of Poly(Lactide-Co-Glycolide) Microparticles .3. Microparticle/Polymer Degradation Rates and the in-Vitro Release of a Model Protein," *International Journal of Pharmaceutics,* vol. 103, pp. 37-45, 1994.
[25] Wikipedia, "Online encyclopedia: PLGA," 2007, <http://en.wikipedia.org/wiki/PLGA>.
[26] A. M. Reed and D. K. Gilding, "Biodegradable Polymers for Use in Surgery - Poly(Ethylene Oxide)-Poly(Ethylene Terephthalate) (Peo-Pet) Co-Polymers .2. Invitro Degradation," *Polymer,* vol. 22, pp. 499-504, 1981.
[27] D. L. Wise, T. D. Fellman, J. E. Sanderson, and R. L. Wentworth, "Lactic/Glycolic Acid Polymers," in *Drug Carriers in Biology and Medicine*, G. Gregoriadis, Ed. London: Academic Press, 1979, pp. 237-270.
[28] A. K. Schneider, "Polylactide Sutures," in *US Patent*, 1972.
[29] S. Cohen, T. Yoshioka, M. Lucarelli, L. H. Hwang, and R. Langer, "Controlled Delivery Systems for Proteins based on Poly(Lactic glycolic acid) Microspheres," *Pharmaceutical Research,* vol. 8, pp. 713-720, 1991.
[30] S. Freitas, H. P. Merkle, and B. Gander, "Microencapsulation by Solvent Extraction/Evaporation: Reviewing the State of the Art of Microsphere Preparation Process Technology," *Journal of Controlled Release,* vol. 102, pp. 313-332, 2005.
[31] H. Marchais, F. Boury, C. Damge, J. E. Proust, and J. P. Benoit, "Formulation of Bovine Serum Albumin loaded PLGA microspheres - Influence of the Process Variables on the Loading and in vitro Release," *STP Pharma Sciences,* vol. 6, pp. 417-423, 1996.
[32] M. J. B. Prieto, F. Delie, E. Fattal, A. Tartar, F. Puisieux, A. Gulik, and P. Couvreur, "Characterization of V3 Bru Peptide-loaded Small PLGA Microspheres Prepared by a (W(1)/O)W(2) Emulsion Solvent Evaporation Method," *International Journal of Pharmaceutics,* vol. 111, pp. 137-145, 1994.
[33] H. Rafati, A. G. A. Coombes, J. Adler, J. Holland, and S. S. Davis, "Protein-loaded Poly(DL-lactide-co-glycolide) Microparticles for Oral Administration: Formulation, Structural and Release Characteristics," *Journal of Controlled Release,* vol. 43, pp. 89-102, 1997.
[34] Y. Y. Yang, T. S. Chung, and N. P. Ng, "Morphology, Drug Distribution, and In Vitro

Release Profiles of Biodegradable Polymeric Microspheres Containing Protein Fabricated by Double-Emulsion Solvent Extraction / Evaporation Method," *Biomaterials,* vol. 22, pp. 231-241, 2001.

[35] L. R. Beck, D. R. Cowsar, D. H. Lewis, R. J. Cosgrove, C. T. Riddle, S. L. Lowry, and T. Epperly, "New Long-Acting Injectable Microcapsule System for the Administration of Progesterone," *Fertility and Sterility,* vol. 31, pp. 545-551, 1979.

[36] R. R. M. Bos, F. R. Rozema, G. Boering, A. J. Nijenhuis, A. J. Pennings, A. B. Verwey, P. Nieuwenhuis, and H. W. B. Jansen, "Degradation of and Tissue Reaction to Biodegradable Poly(L-Lactide) for Use as Internal-Fixation of Fractures: A Study in Rats," *Biomaterials,* vol. 12, pp. 32-36, 1991.

[37] S. J. Holland, M. Yasin, and B. J. Tighe, "Polymers for Biodegradable Medical Devices .7. Hydroxybutyrate-Hydroxyvalerate Copolymers - Degradation of Copolymers and Their Blends with Polysaccharides under Invitro Physiological Conditions," *Biomaterials,* vol. 11, pp. 206-215, 1990.

[38] H. Jeffery, S. S. Davis, and D. T. Ohagan, "The Preparation and Characterization of Poly(Lactide-co-glycolide) Microparticles .1. Oil-in-Water Emulsion Solvent Evaporation," *International Journal of Pharmaceutics,* vol. 77, pp. 169-175, 1991.

[39] H. Jeffery, S. S. Davis, and D. T. Ohagan, "The Preparation and Characterization of Poly(Lactide-Co-Glycolide) Microparticles .2. The Entrapment of a Model Protein Using a (Water-in-Oil)-in-Water Emulsion Solvent Evaporation Technique," *Pharmaceutical Research,* vol. 10, pp. 362-368, 1993.

[40] A. J. Abrahamse, R. van Lierop, R. G. M. van der Sman, A. van der Padt, and R. M. Boom, "Analysis of Droplet Formation and Interactions during Cross-Flow Membrane Emulsification," *Journal of Membrane Science,* vol. 204, pp. 125-137, 2002.

[41] D. Dendukuri, K. Tsoi, T. A. Hatton, and P. S. Doyle, "Controlled Synthesis of Nonspherical Microparticles using Microfluidics," *Langmuir,* vol. 21, pp. 2113-2116, Mar 15 2005.

[42] C. Wibowo and K. M. Ng, "Product-Oriented Process Synthesis and Development: Creams and Pastes," *AIChE Journal,* vol. 47, pp. 2746-2767, 2001.

[43] R. A. Williams, S. J. Peng, D. A. Wheeler, N. C. Morley, D. Taylor, M. Whalley, and D. W. Houldsworth, "Controlled Production of Emulsions Using a Crossflow Membrane Part II: Industrial Scale Manufacture," *Journal of Chemical Engineering,* vol. 76, pp. 902-910, 1998.

[44] C. T. Chen and G. B. Lee, "Formation of Microdroplets in Liquids Utilizing Active Pneumatic Choppers on a Microfluidic Chip," *Journal of Microelectromechanical Systems,* vol. 15, pp. 1492-1498, 2006.

[45] J. H. Eldridge, C. J. Hammond, J. A. Meulbroek, J. K. Staas, R. M. Gilley, and T. R. Tice, "Controlled Vaccine Release in the Gut-Associated Lymphoid Tissues. I. Orally Administered Biodegradable Microspheres Target the Peyer's Patches," *Journal of Controlled Release,* vol. 11, pp. 205-214, 1990.

[46] J. H. Eldridge, J. K. Staas, J. A. Meulbroek, T. R. Tice, and R. M. Gilley, "Biodegradable and Biocompatible Poly(DL-lactide-co-glycolide) Microspheres as an Adjuvant for Staphylococcal Enterotoxin B Toxoid which Enhances the Level of Toxin-Neutralizing Antibodies," *Infection and Immunity,* vol. 59, pp. 2978-2986, 1991.

[47] P. Jani, G. W. Halbert, J. Langridge, and A. T. Florence, "The Uptake and Translocation

of Latex Nanospheres and Microspheres after Oral-Administration to Rats," *Journal of Pharmacy and Pharmacology,* vol. 41, pp. 809-12, 1989.
[48] D. T. O'Hagan, H. Jeffery, and S. S. Davis, "Long-term Antibody Responses in Mice Following Subcutaneous Immunization with Ovalbumin Entrapped in Biodegradable Microparticles," *Vaccine,* vol. 11, pp. 965-969, 1993.
[49] T. Nisisako, T. Torii, and T. Higuchi, "Droplet Formation in a Microchannel Network," *Lab on a Chip,* vol. 2, pp. 24-26, 2002.
[50] P. Guillot and A. Colin, "Stability of Parallel Flows in a Microchannel after a T junction," *Physical Review E,* vol. 72, pp. 066301-4, Dec 2005.
[51] I. Kobayashi, M. Nakajima, and S. Mukataka, "Preparation Characteristics of Oil-in-Water Emulsions using Differently Charged Surfactants in Straight-Through Microchannel Emulsification," *Colloids and Surfaces A-Physicochemical and Engineering Aspects,* vol. 229, pp. 33-41, Nov 24 2003.
[52] I. Kobayashi and M. Nakajima, "Effect of Emulsifiers on the Preparation of Food-grade Oil-in-Water Emulsions using a Straight-Through Extrusion Filter," *European Journal of Lipid Science and Technology,* vol. 104, pp. 720-727, Nov 2002.
[53] I. Kobayashi, M. Yasuno, S. Iwamoto, A. Shono, K. Satoh, and M. Nakajima, "Microscopic Observation of Emulsion Droplet Formation from a Polycarbonate Membrane," *Colloids and Surfaces A-Physicochemical and Engineering Aspects,* vol. 207, pp. 185-196, Jul 30 2002.
[54] R. Arshady, "Preparation of Biodegradable Microspheres and Microcapsules .2. Polyactides and Related Polyesters," *Journal of Controlled Release,* vol. 17, pp. 1-21, 1991.
[55] R. Jalil and J. R. Nixon, "Biodegradable Poly(Lactic acid) and Poly(Lactide-co-glycolide) Microcapsules - Problems Associated with Preparative Techniques and Release Properties," *Journal of Microencapsulation,* vol. 7, pp. 297-325, 1990.
[56] Y. Ogawa, M. Yamamoto, H. Okada, T. Yashiki, and T. Shimamoto, "A New Technique to Efficiently Entrap Leuprolide Acetate into Microcapsules of Polylactic Acid or Copoly(lactic glycolic) Acid," *Chemical & Pharmaceutical Bulletin,* vol. 36, pp. 1095-1103, 1988.
[57] Y. F. Maa and C. C. Hsu, "Effect of Primary Emulsions on Microsphere Size and Protein-Loading in the Double Emulsion Process," *Journal of Microencapsulation,* vol. 14, pp. 225-241, 1997.
[58] N. Nihant, C. Schugens, C. Grandfils, R. Jerome, and P. Teyssie, "Polylactide Microparticles Prepared by Double Emulsion/Evaporation Technique .1. Effect of Primary Emulsion Stability," *Pharmaceutical Research,* vol. 11, pp. 1479-1484, 1994.
[59] T. Uchida, K. Yoshida, A. Ninomiya, and S. Goto, "Optimization of Preparative Conditions for Polylactide (Pla) Microspheres Containing Ovalbumin," *Chemical & Pharmaceutical Bulletin,* vol. 43, pp. 1569-1573, 1995.
[60] R. Arshady, "Microspheres and Microcapsules, a Survey of Manufacturing Techniques .3. Solvent Evaporation," *Polymer Engineering and Science,* vol. 30, pp. 915-924, Aug 1990.
[61] T. Kawakatsu, Y. Kikuchi, and M. Nakajima, "Regular-sized Cell Creation in Microchannel Emulsification by Visual Microprocessing Method," *Journal of the American Oil Chemists Society,* vol. 74, pp. 317-321, 1997.
[62] T. Nakashima and M. Shimizu, "Preparation of Monodispersed O/W Emulsion by

Porous-Glass Membrane," *Kagaku Kogaku Ronbunshu,* vol. 19, pp. 984-990, Nov 1993.
[63] T. Nakashima, M. Shimizu, and M. Kukizaki, "Effect of Surfactant on Production of Monodispersed O/W Emulsion in Membrane Emulsification," *Kagaku Kogaku Ronbunshu,* vol. 19, pp. 991-997, Nov 1993.
[64] F. Olson, C. A. Hunt, F. C. Szoka, W. J. Vail, and D. Papahadjopoulos, "Preparation of Liposomes of Defined Size Distribution by Extrusion through Polycarbonate Membranes," *Biochimica Et Biophysica Acta,* vol. 557, pp. 9-23, 1979.
[65] T. Thorsen, S. J. Maerkl, and S. R. Quake, "Microfluidic Large-Scale Integration," *Science,* vol. 298, pp. 580-584, Oct 18 2002.
[66] T. Kawakatsu, Y. Kikuchi, and M. Nakajima, "Visualization of Microfiltration Phoenomena using Microscope Video System and Silicon Microchannels," *Journal of Chemical Engineering of Japan,* vol. 29, pp. 399-401, Apr 1996.
[67] Y. Kikuchi, K. Sato, and Y. Mizuguchi, "Modified Cell-Flow Microchannels in a Single-Crystal Silicon Substrate and Flow Behavior of Blood-Cells," *Microvascular Research,* vol. 47, pp. 126-139, Jan 1994.
[68] Y. Kikuchi, K. Sato, H. Ohki, and T. Kaneko, "Optically Accessible Microchannels formed in a Single-Crystal Silicon Substrate for Studies of Blood Rheology," *Microvascular Research,* vol. 44, pp. 226-240, Sep 1992.
[69] T. McCreedy, "Fabrication Techniques and Materials Commonly used for the Production of Microreactors and Micro Total Analytical Systems," *TrAC-Trends in Analytical Chemistry,* vol. 19, pp. 396-401, Jun 2000.
[70] MEMS and Nanotechnology Exchange, "The Beginner's Guide to MEMS Processing," <http://www.mems-exchange.org/MEMS/processes/>.
[71] D. Bokenkamp, A. Desai, X. Yang, Y. C. Tai, E. M. Marzluff, and S. L. Mayo, "Microfabricated Silicon Mixers for Submillisecond Quench-Flow Analysis," *Analytical Chemistry,* vol. 70, pp. 232-236, Jan 15 1998.
[72] T. Thorsen, R. W. Roberts, F. H. Arnold, and S. R. Quake, "Dynamic Pattern Formation in a Vesicle-generating Microfluidic Device," *Physical Review Letters,* vol. 86, pp. 4163-4166, Apr 30 2001.
[73] T. Kawakatsu, R. M. Boom, H. Nabetani, Y. Kikuchi, and M. Nakajima, "Emulsion Breakdown: Mechanisms and Development of Multilayer Membrane," *AIChE Journal,* vol. 45, pp. 967-975, May 1999.
[74] T. Kawakatsu, G. Tragardh, Y. Kikuchi, M. Nakajima, H. Komori, and T. Yonemoto, "Effect of Microchannel Structure on Droplet Size during Crossflow Microchannel Emulsification," *Journal of Surfactants and Detergents,* vol. 3, pp. 295-302, Jul 2000.
[75] J. H. Tong, M. Nakajima, H. Nabetani, and Y. Kikuchi, "Surfactant Effect on Production of Monodispersed Microspheres by Microchannel Emulsification Method," *Journal of Surfactants and Detergents,* vol. 3, pp. 285-293, Jul 2000.
[76] P. Walstra, *Dispersed Systems: Basic Consideration, in Food Chemistry 3rd edn*. New York: Marcel Dekker, Inc., 1996.
[77] R. Katoh, Y. Asano, A. Furuya, K. Sotoyama, and M. Tomita, "Preparation of Food Emulsions using Membrane Emulsification System," *Journal of Membrane Science,* vol. 113, pp. 131-135 1996.
[78] T. Nakashima, M. Shimizu, and M. Kukizaki, "Membrane Emulsification by Microporous Glass," *Key Engineering Materials,* vol. 61-62, pp. 513-516, 1992.

[79] K. Suzuki, I. Shuto, and Y. Hagura, "Characteristics of the Membrane Emulsification Method Combined with Preliminary Emulsification for Preparing Corn Oil-in-Water Emulsions," *Food Science and Technology International,* vol. 2, pp. 43-47, 1996.
[80] V. Schröder, O. Behrend, and H. Schubert, "Effect of Dynamic Interfacial Tension on the Emulsification Process using Microporous, Ceramic Membranes," *Journal of Colloid and Interface Science,* vol. 202, pp. 334-340, Jun 15 1998.
[81] I. Kobayashi, M. Nakajima, K. Chun, Y. Kikuchi, and H. Fukita, "Silicon Array of Elongated Through-Holes for Monodisperse Emulsion Droplets," *AIChE Journal,* vol. 48, pp. 1639-1644, Aug 2002.
[82] S. J. Peng and R. A. Williams, "Controlled Production of Emulsions using a Crossflow Membrane Part I: Droplet Formation from a Single Pore," *Chemical Engineering Research & Design,* vol. 76, pp. 894-901, Nov 1998.
[83] S. J. Peng and R. A. Williams, "Controlled Production of Emulsions using a Crossflow Membrane," *Particle & Particle Systems Characterization,* vol. 15, pp. 21-25, Feb 1998.
[84] I. Kobayashi, S. Mukataka, and M. Nakajima, "Effect of Slot Aspect Ratio on Droplet Formation from Silicon Straight-Through Microchannels," *Journal of Colloid and Interface Science,* vol. 279, pp. 277-280, Nov 1 2004.
[85] I. Kobayashi, S. Mukataka, and M. Nakajima, "CFD Simulation and Analysis of Emulsion Droplet Formation from Straight-Through Microchannels," *Langmuir,* vol. 20, pp. 9868-9877, Oct 26 2004.
[86] I. Kobayashi, S. Mukataka, and M. Nakajima, "Effects of Type and Physical Properties of Oil Phase on Oil-in-Water Emulsion Droplet Formation in Straight-Through Microchannel Emulsification, Experimental and CFD Studies," *Langmuir,* vol. 21, pp. 5722-5730, Jun 21 2005.
[87] D. C. Duffy, J. C. McDonald, O. J. A. Schueller, and G. M. Whitesides, "Rapid Prototyping of Microfluidic Systems in Poly(dimethylsiloxane)," *Analytical Chemistry,* vol. 70, pp. 4974-4984, Dec 1 1998.
[88] H. A. Stone, "Dynamics of Drop Deformation and Breakup in Viscous Fluids," *Annual Review of Fluid Mechanics,* vol. 26, pp. 65-102, 1994.
[89] J. D. Tice, A. D. Lyon, and R. F. Ismagilov, "Effects of Viscosity on Droplet Formation and Mixing in Microfluidic Channels," *Analytica Chimica Acta,* vol. 507, pp. 73-77, Apr 1 2004.
[90] J. D. Tice, H. Song, A. D. Lyon, and R. F. Ismagilov, "Formation of Droplets and Mixing in Multiphase Microfluidics at Low Values of the Reynolds and the Capillary Numbers," *Langmuir,* vol. 19, pp. 9127-9133, Oct 28 2003.
[91] S. van der Graaf, M. L. J. Steegmans, R. G. M. van der Sman, C. G. P. H. Schroen, and R. M. Boom, "Droplet Formation in a T-shaped Microchannel Junction: A Model System for Membrane Emulsification," *Colloids and Surfaces A-Physicochemical and Engineering Aspects,* vol. 266, pp. 106-116, Sep 15 2005.
[92] X. W. Shan and H. D. Chen, "Lattice Boltzmann Model for Simulating Flows with Multiple Phases and Components," *Physical Review E,* vol. 47, pp. 1815-1819, Mar 1993.
[93] M. R. Swift, E. Orlandini, W. R. Osborn, and J. M. Yeomans, "Lattice Boltzmann Simulations of Liquid-Gas and Binary Fluid Systems," *Physical Review E,* vol. 54, pp. 5041-5052, Nov 1996.
[94] P. Garstecki, M. J. Fuerstman, H. A. Stone, and G. M. Whitesides, "Formation of

Droplets and Bubbles in a Microfluidic T-junction - Scaling and Mechanism of Break-up," *Lab on a Chip,* vol. 6, pp. 437-446, Mar 2006.
[95] H. H. Liu and Y. H. Zhang, "Droplet Formation in a T-shaped Microfluidic Junction," *Journal of Applied Physics,* vol. 106, p. 8, Aug 1 2009.
[96] T. Nisisako, T. Torii, and T. Higuchi, "Novel Microreactors for Functional Polymer Beads," *Chemical Engineering Journal,* vol. 101, pp. 23-29, Aug 1 2004.
[97] G. F. Christopher, N. N. Noharuddin, J. A. Taylor, and S. L. Anna, "Experimental Observations of the Squeezing-to-Dripping Transition in T-shaped Microfluidic Junctions," *Physical Review E,* vol. 78, pp. -, Sep 2008.
[98] M. De Menech, P. Garstecki, F. Jousse, and H. A. Stone, "Transition from Squeezing to Dripping in a Microfluidic T-shaped Junction," *Journal of Fluid Mechanics,* vol. 595, pp. 141-161, Jan 25 2008.
[99] Q. Y. Xu and M. Nakajima, "The Generation of Highly Monodisperse Droplets through the Breakup of Hydrodynamically Focused Microthread in a Microfluidic Device," *Applied Physics Letters,* vol. 85, pp. 3726-3728, Oct 25 2004.
[100] P. J. A. Kenis, R. F. Ismagilov, and G. M. Whitesides, "Microfabrication inside Capillaries using Multiphase Laminar Flow Patterning," *Science,* vol. 285, pp. 83-85, Jul 2 1999.
[101] J. B. Knight, A. Vishwanath, J. P. Brody, and R. H. Austin, "Hydrodynamic Focusing on a Silicon Chip: Mixing Nanoliters in Microseconds," *Physical Review Letters,* vol. 80, pp. 3863-3866, Apr 27 1998.
[102] S. L. Anna, N. Bontoux, and H. A. Stone, "Formation of Dispersions using "Flow Focusing" in Microchannels," *Applied Physics Letters,* vol. 82, pp. 364-366, Jan 20 2003.
[103] A. M. Ganan-Calvo, "Generation of Steady Liquid Microthreads and Micron-sized Monodisperse Sprays in Gas Streams," *Physical Review Letters,* vol. 80, pp. 285-288, Jan 12 1998.
[104] A. M. Ganan-Calvo and A. Barrero, "A Novel Pneumatic Technique to Generate Steady Capillary Microjets," *Journal of Aerosol Science,* vol. 30, pp. 117-125, Jan 1999.
[105] S. L. Anna and H. C. Mayer, "Microscale Tipstreaming in a Microfluidic Flow Focusing Device," *Physics of Fluids,* vol. 18, pp. -, Dec 2006.
[106] H. Kim, D. W. Luo, D. Link, D. A. Weitz, M. Marquez, and Z. D. Cheng, "Controlled Production of Emulsion Drops using an Electric Field in a Flow-Focusing Microfluidic Device," *Applied Physics Letters,* vol. 91, pp. -, Sep 24 2007.
[107] I. Hayati, A. I. Bailey, and T. F. Tadros, "Mechanism of Stable Jet Formation in Electrohydrodynamic Atomization," *Nature,* vol. 319, pp. 41-43, Jan 2 1986.
[108] G. Taylor, "Disintegration of Water Drops in Electric Field," *Proceedings of the Royal Society of London Series A,* vol. 280, pp. 383-+, 1964.
[109] Rayleigh, "Investigation of the Character of the Equilibrium of an Incompressible Heavy Fluid of Variable Density," *Proceedings London Mathematical Society,* vol. s1-14, pp. 170-177, November 1, 1882 1882.
[110] W. Lee, L. M. Walker, and S. L. Anna, "Impact of Viscosity Ratio on the Dynamics of Droplet Breakup in a Microfluidic Flow Focusing Device," *XVth International Congress on Rheology - the Society of Rheology 80th Annual Meeting, Pts 1 and 2,* vol. 1027, pp. 994-996, 1473, 2008.
[111] Z. H. Nie, M. S. Seo, S. Q. Xu, P. C. Lewis, M. Mok, E. Kumacheva, G. M. Whitesides, P.

Garstecki, and H. A. Stone, "Emulsification in a Microfluidic Flow-Focusing Device: Effect of the Viscosities of the Liquids," *Microfluidics and Nanofluidics,* vol. 5, pp. 585-594, Nov 2008.
[112] P. Garstecki, M. J. Fuerstman, and G. M. Whitesides, "Nonlinear Dynamics of a Flow-Focusing Bubble Generator: An Inverted Dripping Faucet," *Physical Review Letters,* vol. 94, pp. -, Jun 17 2005.
[113] W. Li, E. W. K. Young, M. Seo, Z. Nie, P. Garstecki, C. A. Simmons, and E. Kumacheva, "Simultaneous Generation of Droplets with Different Dimensions in Parallel Integrated Microfluidic Droplet Generators," *Soft Matter,* vol. 4, pp. 258-262, 2008.
[114] J. A. Davidson and D. E. Witenhafer, "Particle Structure of Suspension Poly(Vinyl-chloride) and Its Origin in the Polymerization Process," *Journal of Polymer Science Part B-Polymer Physics,* vol. 18, pp. 51-69, 1980.
[115] Q. Lu, Z. X. Weng, G. R. Shan, G. Q. Lai, and Z. R. Pan, "Effect of Acrylonitrile Water Solubility on the Suspension Copolymerization of Acrylonitrile and Styrene," *Journal of Applied Polymer Science,* vol. 101, pp. 4270-4274, Sep 15 2006.
[116] M. Okubo, Y. Konishi, T. Inohara, and H. Minami, "Size Effect of Monomer Droplets on the Production of Hollow Polymer Particles by Suspension Polymerization," *Colloid and Polymer Science,* vol. 281, pp. 302-307, Apr 2003.
[117] T. A. Shedd, "General Model for Estimating Bubble Dissolution and Droplet Evaporation Times," *Journal of Microlithography Microfabrication and Microsystems,* vol. 4, pp. -, Jul-Sep 2005.
[118] S. H. Tan, S. M. S. Murshed, N. T. Nguyen, T. N. Wong, and L. Yobas, "Thermally Controlled Droplet Formation in Flow Focusing Geometry: Formation Regimes and Effect of Nanoparticle Suspension," *Journal of Physics D-Applied Physics,* vol. 41, pp. -, Aug 21 2008.
[119] W. J. Jeong, J. Y. Kim, J. Choo, E. K. Lee, C. S. Han, D. J. Beebe, G. H. Seong, and S. H. Lee, "Continuous Fabrication of Biocatalyst Immobilized Microparticles using Photopolymerization and Immiscible Liquids in Microfluidic Systems," *Langmuir,* vol. 21, pp. 3738-3741, Apr 26 2005.
[120] H. J. Oh, S. H. Kim, J. Y. Baek, G. H. Seong, and S. H. Lee, "Hydrodynamic Micro-encapsulation of Aqueous Fluids and Cells via 'on the Fly' Photopolymerization," *Journal of Micromechanics and Microengineering,* vol. 16, pp. 285-291, Feb 2006.
[121] S. Takeuchi, P. Garstecki, D. B. Weibel, and G. M. Whitesides, "An Axisymmetric Flow-Focusing Microfluidic Device," *Advanced Materials,* vol. 17, pp. 1067-+, Apr 18 2005.
[122] A. S. Utada, E. Lorenceau, D. R. Link, P. D. Kaplan, H. A. Stone, and D. A. Weitz, "Monodisperse Double Emulsions generated from a Microcapillary Device," *Science,* vol. 308, pp. 537-541, Apr 22 2005.
[123] S. H. Huang, W. H. Tan, F. G. Tseng, and S. Takeuchi, "A Monolithically Three-Dimensional Flow-Focusing Device for Formation of Single/Double Emulsions in Closed/Open Microfluidic Systems," *Journal of Micromechanics and Microengineering,* vol. 16, pp. 2336-2344, Nov 2006.
[124] L. Yobas, S. Martens, W. L. Ong, and N. Ranganathan, "High-Performance Flow-Focusing Geometry for Spontaneous Generation of Monodispersed Droplets," *Lab on a Chip,* vol. 6, pp. 1073-1079, 2006.
[125] L. Yobas, R. K. Sharma, R. Nagarajan, V. D. Samper, and P. S. R. Naidu, "Precise Profile

Control of 3D Lateral Junction Traps by 2D Mask Layout and Isotropic Etching," *Journal of Micromechanics and Microengineering,* vol. 15, pp. 386-393, Feb 2005.
[126] Y. H. Lin, C. T. Chen, L. L. H. Huang, and G. B. Lee, "Multiple-Channel Emulsion Chips utilizing Pneumatic Choppers for Biotechnology Applications," *Biomedical Microdevices,* vol. 9, pp. 833-843, Dec 2007.
[127] K. L. Lao and G. B. Lee, "Monodisperse Double Emulsions Generated by Microfluidic Chips utilizing Flow Focusing and Pneumatic Chopping Devices," *Transducers '07 & Eurosensors Xxi, Digest of Technical Papers, Vols 1 and 2,* pp. U136-U137; 2616, 2007.
[128] C. W. Lai, Y. H. Lin, and G. B. Lee, "A Microfluidic Chip for Formation and Collection of Emulsion Droplets utilizing Active Pneumatic Micro-Choppers and Micro-Switches," *Biomedical Microdevices,* vol. 10, pp. 749-756, Oct 2008.
[129] S. K. Hsiung, C. T. Chen, and G. B. Lee, "Micro-droplet Formation utilizing Microfluidic Flow Focusing and Controllable Moving-Wall Chopping Techniques," *Journal of Micromechanics and Microengineering,* vol. 16, pp. 2403-2410, Nov 2006.
[130] C. H. Lee, S. K. Hsiung, and G. B. Lee, "A Tunable Microflow Focusing Device utilizing Controllable Moving Walls and its Applications for Formation of Micro-droplets in Liquids," *Journal of Micromechanics and Microengineering,* vol. 17, pp. 1121-1129, Jun 2007.
[131] Y. H. Lin, C. H. Lee, and G. B. Lee, "Droplet Formation utilizing Controllable Moving-Wall Structures for Double-Emulsion Applications," *Journal of Microelectromechanical Systems,* vol. 17, pp. 573-581, Jun 2008.
[132] K. S. Lee, S. W. Cha, and S. M. Koo, "Applying Axiomatic Design to Improve Thermoforming Multilayered Plastic Container," *Polymer-Plastics Technology and Engineering,* vol. 46, pp. 781-788, 2007.
[133] A. J. Abrahamse, A. van der Padt, R. M. Boom, and W. B. C. de Heij, "Process Fundamentals of Membrane Emulsification: Simulation with CFD," *AIChE Journal,* vol. 47, pp. 1285-1291, Jun 2001.
[134] M. Ohta, M. Yamamoto, and M. Suzuki, "Numerical-Analysis of a Single Drop Formation Process under Pressure Pulse Condition," *Chemical Engineering Science,* vol. 50, pp. 2923-2931, Sep 1995.
[135] M. Rayner, G. Trägårdh, C. Trägårdh, and P. Dejmek, "Using the Surface Evolver to Model Droplet Formation Processes in Membrane Emulsification," *Journal of Colloid and Interface Science,* vol. 279, pp. 175-185, 2004.
[136] D. Jacqmin, "Calculation of Two-Phase Navier-Stokes Flows using Phase-Field Modeling," *Journal of Computational Physics,* vol. 155, pp. 96-127, 1999.
[137] S. Chen and G. D. Doolen, "Lattice Boltzmann Method for Fluid Flows," *Annual Review of Fluid Mechanics,* vol. 30, pp. 329-364, 1998.
[138] A. Lamura and et al., "A Lattice Boltzmann Model of Ternary Fluid Mixtures," *EPL (Europhysics Letters),* vol. 45, p. 314, 1999.
[139] L. Wu, M. Tsutahara, L. S. Kim, and M. Ha, "Three-Dimensional Lattice Boltzmann Simulations of Droplet Formation in a Cross-Junction Microchannel," *International Journal of Multiphase Flow,* vol. 34, pp. 852-864, 2008.
[140] A. C. Balazs, R. Verberg, C. M. Pooley, and O. Kuksenok, "Modeling the Flow of Complex Fluids through Heterogeneous Channels," *Soft Matter,* vol. 1, pp. 44-54, Jun 14 2005.

[141] S. Chen, G. D. Doolen, and K. G. Eggert, "Lattice-Boltzmann Fluid dynamics: A Versatile Tool for Multiphase and Other Complicated Flows," *Los Alamos Science,* vol. 22, pp. 98-111, 1994.
[142] D. H. Rothman and S. Zaleski, *Lattice-Gas Cellular Automata: Simple Models of Complex Hydrodynamics*: Cambridge University Press, 1997.
[143] Q. Kang, D. Zhang, and S. Chen, "Displacement of a Two-Dimensional Immiscible Droplet in a Channel," in *Physics of Fluids*. vol. 14: American Institute of Physics, 2002, p. 3203.
[144] B. R. Sehgal, R. R. Nourgaliev, and T. N. Dinh, "Numerical Simulation of Droplet Deformation and Break-up by Lattice-Boltzmann Method," *Progress in Nuclear Energy,* vol. 34, pp. 471-488, 1999.
[145] X. Shan and H. Chen, "Simulation of Nonideal Gases and Liquid-Gas Phase Transitions by the Lattice Boltzmann Equation," *Physical Review E,* vol. 49, p. 2941, 1994.
[146] J.-C. Desplat, I. Pagonabarraga, and P. Bladon, "LUDWIG: A Parallel Lattice-Boltzmann Code for Complex Fluids," *Computer Physics Communications,* vol. 134, pp. 273-290, 2001.
[147] M. R. Swift, W. R. Osborn, and J. M. Yeomans, "Lattice Boltzmann Simulation of Nonideal Fluids," *Physical Review Letters,* vol. 75, p. 830, 1995.
[148] O. Theissen and G. Gompper, "Lattice-Boltzmann Study of Spontaneous Emulsification," *The European Physical Journal B - Condensed Matter and Complex Systems,* vol. 11, pp. 91-100, 1999.
[149] B. T. Nadiga and S. Zaleski, "Investigations of a Two-Phase Fluid Model," *European Journal of Mechanics B-Fluids,* vol. 15, pp. 885-896, 1996.
[150] V. M. Kendon, M. E. Cates, I. Pagonabarraga, J.-C. Desplat, and P. Bladon, "Inertial Effects in Three-Dimensional Spinodal Decomposition of a Symmetric Binary Fluid Mixture: A Lattice Boltzmann Study," *Journal of Fluid Mechanics,* vol. 440, pp. 147-203, 2001.
[151] P. Yue, J. J. Feng, C. Liu, and J. Shen, "A Diffuse-Interface Method for Simulating Two-Phase Flows of Complex Fluids," *Journal of Fluid Mechanics,* vol. 515, pp. 293-317, 2004.
[152] C. Liu and J. Shen, "A Phase Field Model for the Mixture of Two Incompressible Fluids and its Approximation by a Fourier-Spectral Method," *Physica D: Nonlinear Phenomena,* vol. 179, pp. 211-228, 2003.
[153] J. F. L. Duval, H. P. van Leeuwen, J. Cecilia, and J. Galceran, "Rigorous Analysis of Reversible Faradaic Depolarization Processes in the Electrokinetics of the Metal/electrolyte Solution Interface," *The Journal of Physical Chemistry B,* vol. 107, pp. 6782-6800, 2003.
[154] F. M. White, *Fluid Mechanics*, 6th ed. Boston: McGraw-Hill Higher Education, 2008.
[155] R. Chella and J. Viñals, "Mixing of a Two-Phase Fluid by Cavity Flow," *Physical Review E,* vol. 53, p. 3832, 1996.
[156] T. M. Squires and S. R. Quake, "Microfluidics: Fluid Physics at the Nanoliter Scale," *Reviews of Modern Physics,* vol. 77, p. 977, 2005.
[157] G. I. Taylor, "The Viscosity of a Fluid Containing Small Drops of Another Fluid," *Proceedings of the Royal Society of London. Series A,* vol. 138, pp. 41-48, October 1, 1932 1932.

[158] G. I. Taylor, "The Formation of Emulsions in Definable Fields of Flow," *Proceedings of the Royal Society of London. Series A,* vol. 146, pp. 501-523, October 1, 1934 1934.
[159] S. M. Kannapan and D. L. Taylor, "The Interplay of Context, Process, and Conflict in Concurrent Engineering," *Concurrent Engineering-Research and Applications,* vol. 2, pp. 183-196, Sep 1994.
[160] S. G. Kim and M. K. Koo, "Design of a Microactuator Array against the Coupled Nature of Microelectromechanical systems (MEMS) Processes," *CIRP Annals 2000: Manufacturing Technology,* pp. 101-104;450, 2000.
[161] S. G. Kim, Y. Shi, and Y. Jeon, "Design of Micro-photonic Beam Steering Systems," *CIRP Annals-Manufacturing Technology,* vol. 51, pp. 335-338, 2002.
[162] K. H. Hwang, K. H. Lee, G. J. Park, B. L. Lee, Y. C. Cho, and S. H. Lee, "Robust Design of a Vibratory Gyroscope with an Unbalanced Inner Torsion Gimbal using Axiomatic Design," *Journal of Micromechanics and Microengineering,* vol. 13, pp. 8-17, Jan 2003.
[163] W. Zhang, "Can Design be More Creative?," *invited lecture, NJUST, China,* 2010.
[164] F. Engelhardt, "Improving Systems by Combining Axiomatic Design, Quality Control Tools and Designed Experiments," *Research in Engineering Design-Theory Applications and Concurrent Engineering,* vol. 12, pp. 204-219, 2000.
[165] S. D. Eppinger, D. E. Whitney, R. P. Smith, and D. A. Gebala, "A Model-Based Method for Organizing Tasks in Product Development," *Research in Engineering Design-Theory Applications and Concurrent Engineering,* vol. 6, pp. 1-13, 1994.
[166] E. Rechtin, "The Art of Systems Architecting," *IEEE Spectrum,* vol. 29, pp. 66-69, Oct 1992.
[167] N. P. Suh, "Design of Systems," *CIRP Annals - Manufacturing Technology,* vol. 46, pp. 75-80, 1997.
[168] N. P. Suh, "Axiomatic Design Theory for Systems," *Research in Engineering Design-Theory Applications and Concurrent Engineering,* vol. 10, pp. 189-209, 1998.
[169] Y. Zhao, G. Chen, and Q. Yuan, "Liquid-liquid Two-Phase Flow Patterns in a Rectangular Microchannel," *AIChE Journal,* vol. 52, pp. 4052-4060, 2006.
[170] K.-Y. Song, M. Chiao, B. Stoeber, U. Hafeli, M. M. Gupta, and W. J. Zhang, "Formation of Uniform Microspheres Using a Perforated Silicon Membrane: A Preliminary Study," *Journal of Medical Devices,* vol. 3, pp. 034503-3, 2009.
[171] K.-Y. Song, W. J. Zhang, and M. M. Gupta, "Uniform Microsphere Formation by Liquid Choppers Utilizing PZT Actuator: Theoretical and Simulation Study," in *3rd International Conference on Bioinformatics and Biomedical Engineering (ICBBE 2009)*, 2009, pp. 1-4.
[172] K.-Y. Song, W. J. Zhang, and M. M. Gupta, "A Conceptual Microchannel System Design Methodology incorporating Axiomatic Design Theory for Size-controllable Monodispersed Microsphere Generation by Liquid Chopper utilizing PZT Actuator," *Journal of Engineering Manufacture (accepted, April, 2011)*.
[173] C. Berkland, K. Kim, and D. W. Pack, "PLG Microsphere Size Controls Drug Release Rate through Several Competing Factors," *Pharmaceutical Research,* vol. 20, pp. 1055-1062 2003.
[174] J. M. Bezemer, R. Radersma, D. W. Grijpma, P. J. Dijkstra, C. A. V. Blitterswijk, and J. Feijen, "Microspheres for Protein Delivery Prepared from Amphiphilic Multiblock Copolymers 2. Modulation of Release Rate," *Journal of Controlled Release,* vol. 67, pp.

249-260, 2000.
[175] K. E. Petersen, "Silicon as a Mechanical Material," *Proceedings of the IEEE,* vol. 70, pp. 420-457, 1982.
[176] E. Verpoorte and N. F. De Rooij, "Microfluidics Meets MEMS," *Proceedings of the IEEE,* vol. 91, pp. 930-953, 2003.
[177] C. Barrett, *Structure of Metals*: Lightning Source Inc, 2007.
[178] M. J. Vasile, Z. Niu, R. Nassar, W. Zhang, and S. Liu, "Focused Ion Beam Milling: Depth Control for Three-Dimensional Microfabrication," *Journal of Vacuum Science & Technology B,* vol. 15, pp. 2350-2354, Nov-Dec 1997.
[179] M. J. Vasile, J. S. Xie, and R. Nassar, "Depth Control of Focused Ion-Beam Milling from a Numerical Model of the Sputter Process," *Journal of Vacuum Science & Technology B,* vol. 17, pp. 3085-3090, Nov-Dec 1999.
[180] C. A. Volkert and A. M. Minor, "Focused Ion Beam Microscopy and Micromachining," *MRS Bulletin,* vol. 32, pp. 389-395, 2007.
[181] R. Clampitt, K. L. Aitken, and D. K. Jefferies, "Intense Field-Emission-Source of Liquid-Metals," *Journal of Vacuum Science & Technology,* vol. 12, pp. 1208-1208, 1975.
[182] A. Wagner, "Applications of Focused Ion-Beams," *Nuclear Instruments & Methods in Physics Research,* vol. 218, pp. 355-362, 1983.
[183] A. Wagner and T. M. Hall, "Liquid Gold Ion-Source," *Journal of Vacuum Science & Technology,* vol. 16, pp. 1871-1874, 1979.
[184] P. D. Prewett, G. L. R. Mair, and S. P. Thompson, "Some Comments on the Mechanism of Emission from Liquid-Metal Ion Sources," *Journal of Physics D-Applied Physics,* vol. 15, pp. 1339-1348, 1982.
[185] L. W. Swanson, "Liquid-Metal Ion Sources - Mechanism and Applications," *Nuclear Instruments & Methods in Physics Research,* vol. 218, pp. 347-353, 1983.
[186] R. M. Langford, P. M. Nellen, J. Gierak, and Y. Q. Fu, "Focused Ion Beam Micro- and Nanoengineering," *MRS Bulletin,* vol. 32, pp. 417-423, 2007.
[187] D. Banks, *Microengineering, MEMS, and Interfacing: A Practical Guide*. Boca Raton, FL: Dekker/CRC Press, 2006.
[188] U. Schnakenberg, W. Benecke, B. L?hel, S. Ullerich, and P. Lange, "NH4OH-based Etchants for Silicon Micromachining: Influence of Additives and Stability of Passivation Layers," *Sensors and Actuators A: Physical,* vol. 25, pp. 1-7, 1990.
[189] H. Seidel, L. Csepregi, A. Heuberger, and H. Baumgartel, "Anisotropic Etching of Crystalline Silicon in Alkaline-Solutions .1. Orientation Dependence and Behavior of Passivation Layers," *Journal of the Electrochemical Society,* vol. 137, pp. 3612-3626, Nov 1990.
[190] O. Tabata, R. Asahi, H. Funabashi, K. Shimaoka, and S. Sugiyama, "Anisotropic Etching of Silicon in Tmah Solutions," *Sensors and Actuators A: Physical,* vol. 34, pp. 51-57, Jul 1992.
[191] G. S. Chung, "Anisotropic Etching and Electrochemical Etch-stop Properties of Silicon in TMAH : IPA : Pyrazine Solutions," *Metals and Materials International,* vol. 7, pp. 643-649, Dec 2001.
[192] O. Tabata, "Anisotropic Etching of Silicon in TMAH Solutions," *Sensors and Materials,* vol. 13, pp. 271-283, 2001.
[193] D. T. Liang and D. W. Readey, "Dissolution Kinetics of Crystalline and Amorphous Silica

in Hydrofluoric-Hydrochloric Acid Mixtures," *Journal of the American Ceramic Society,* vol. 70, pp. 570-577, 1987.
[194] D. J. Monk, D. S. Soane, and R. T. Howe, "Determination of the Etching Kinetics for the Hydrofluoric-Acid Silicon Dioxide System," *Journal of the Electrochemical Society,* vol. 140, pp. 2339-2346, Aug 1993.
[195] G. M. Whitesides, "Soft Lithography," *Abstracts of Papers of the American Chemical Society,* vol. 212, pp. 31-INOR, 1996.
[196] Y. N. Xia and G. M. Whitesides, "Soft Lithography," *Abstracts of Papers of the American Chemical Society,* vol. 214, pp. 348-PMSE, 1997.
[197] Y. N. Xia and G. M. Whitesides, "Soft Lithography," *Angewandte Chemie-International Edition,* vol. 37, pp. 551-575, 1998.
[198] X. M. Zhao, Y. N. Xia, and G. M. Whitesides, "Soft Lithographic Methods for Nano-Fabrication," *Journal of Materials Chemistry,* vol. 7, pp. 1069-1074, 1997.
[199] J. N. Lee, C. Park, and G. M. Whitesides, "Solvent Compatibility of Poly(dimethylsiloxane)-based Microfluidic Devices," *Analytical Chemistry,* vol. 75, pp. 6544-6554, 2003.
[200] J. C. McDonald and G. M. Whitesides, "Poly(dimethylsiloxane) as a Material for Fabricating Microfluidic Devices," *Accounts of Chemical Research,* vol. 35, pp. 491-499, 2002.
[201] J. M. K. Ng, I. Gitlin, A. D. Stroock, and G. M. Whitesides, "Components for Integrated Poly(dimethylsiloxane) Microfluidic Systems," *Electrophoresis,* vol. 23, pp. 3461-3473, 2002.
[202] K. M. Choi and J. A. Rogers, "A Photocurable Poly(dimethylsiloxane) Chemistry Designed for Soft Lithographic Molding and Printing in the Nanometer Regime," *Journal of the American Chemical Society,* vol. 125, pp. 4060-4061, 2003.
[203] Dow Corninig Corporation, "MSDS: Sylgard(R) 184 Silicone Elastomer Kit," 2010.
[204] J. N. Lee, X. Jiang, D. Ryan, and G. M. Whitesides, "Compatibility of Mammalian Cells on Surfaces of Poly(dimethylsiloxane)," *Langmuir,* vol. 20, pp. 11684-11691, 2004.
[205] G. C. Lisensky, D. J. Campbell, K. J. Beckman, C. E. Calderon, P. W. Doolan, M. O. Rebecca, and A. B. Ellis, "Replication and Compression of Surface Structures with Polydimethylsiloxane Elastomer," *Journal of Chemical Education,* vol. 76, pp. 537-null, 1999.
[206] H. Ye, Z. Gu, and D. H. Gracias, "Kinetics of Ultraviolet and Plasma Surface Modification of Poly(dimethylsiloxane) Probed by Sum Frequency Vibrational Spectroscopy," *Langmuir,* vol. 22, pp. 1863-1868, 2006.
[207] A. Kumar and G. M. Whitesides, "Freaures of Gold having Micrometer to Centimeter Dimensions can be formed through a Combination of Stamping with an Elastomeric Stamp and an Alkanethiol Ink followed by Chemical Etching," *Applied Physics Letters,* vol. 63, pp. 2002-2004, 1993.
[208] Y. N. Xia, E. Kim, X. M. Zhao, J. A. Rogers, M. Prentiss, and G. M. Whitesides, "Complex Optical Surfaces formed by Replica Molding against Elastomeric Masters," *Science,* vol. 273, pp. 347-349, 1996.
[209] X. M. Zhao, Y. N. Xia, and G. M. Whitesides, "Fabrication of Three-Dimensional Micro-Structures: Microtransfer Molding," *Advanced Materials,* vol. 8, pp. 837-&, 1996.
[210] E. Kim, Y. N. Xia, and G. M. Whitesides, "Pollymer Microstructures formed by Molding

in Capillaries," *Nature,* vol. 376, pp. 581-584, 1995.
[211] E. Kim, Y. N. Xia, X. M. Zhao, and G. M. Whitesides, "Solvent-assisted Microcontact Molding: A Convenient Method for Fabricating Three-Dimensional Structures on Surfaces of Polymers," *Advanced Materials,* vol. 9, pp. 651-654, 1997.
[212] H. C. Haverkorn van Rijsewijk, P. E. J. Legierse, and G. E. Thomas, "Manufacture of Laser Vision Video Discs by a Photopolymerization Process," *Philips Technical Review,* vol. 40, pp. 287-297, 1982.
[213] B. D. Terris, H. J. Mamin, M. E. Best, J. A. Logan, D. Rugar, and S. A. Rishton, "Nanoscale Replication for Scanning Probe Data Storage," *Applied Physics Letters,* vol. 69, pp. 4262-4264, 1996.
[214] S. Y. Chou, P. R. Krauss, and P. J. Renstrom, "Imprint of Sub-25 nm Vias and Trenches in Polymers," *Applied Physics Letters,* vol. 67, pp. 3114-3116, 1995.
[215] H. W. Lehmann, R. Widmer, M. Ebnoether, A. Wokaun, M. Meier, and S. K. Miller, "Fabrication of Sub-micron crossed Square-wave Gratings by Dry Etching and Thermoplastic Replication Techniques," *Journal of Vacuum Science & Technology B,* vol. 1, pp. 1207-1210, 1983.
[216] P. Hoyer, "Semiconductor Nanotube Formation by a Two-Step Template Process," *Advanced Materials,* vol. 8, pp. 857-&, 1996.
[217] H. Masuda and K. Fukuda, "Ordered Metal Nanohole Arrays made by a 2-step Replication Honeycomb Structures of Anodic Alumina," *Science,* vol. 268, pp. 1466-1468, 1995.
[218] S. Bhattacharya, A. Datta, J. M. Berg, and S. Gangopadhyay, "Studies on Surface Wettability of Poly(dimethyl) Siloxane (PDMS) and Glass under Oxygen-Plasma Treatment and Correlation with Bond Strength," *Journal of Microelectromechanical Systems,* vol. 14, pp. 590-597, 2005.
[219] M. Karol and et al., "A PDMS/LTCC Bonding Technique for Microfluidic Application," *Journal of Micromechanics and Microengineering,* vol. 19, p. 105016, 2009.
[220] K. C. Tang and et al., "Evaluation of Bonding between Oxygen Plasma Treated Polydimethyl Siloxane and Passivated Silicon," *Journal of Physics: Conference Series,* vol. 34, p. 155, 2006.
[221] M. R. Melamed, T. Lindmo, and M. L. Mendelsohn, "Flow Cytometry and Sorting," New York: Wiley-Liss, 1994.
[222] K. D. Dessau and D. Arnone, "Novel Actuators Achieve Greater Stability and Precision," in *Laser Focus World*, 1999, pp. 189–195.
[223] P. R. Ouyang, R. C. Tjiptoprodjo, W. J. Zhang, and G. S. Yang, "Micro-motion Devices Technology: The State of Arts Review," *The International Journal of Advanced Manufacturing Technology,* 2007.
[224] H. J. M. T. S. Adriaens, W. L. De Koning, and R. Banning, "Modeling Piezoelectric Actuators," *IEEE/ASME Transactions on Mechatronics,* vol. 5, pp. 331-341, 2000.
[225] Y. B. Jeon, R. Sood, J. h. Jeong, and S. G. Kim, "MEMS Power Generator with Transverse Mode Thin Film PZT," *Sensors and Actuators A: Physical,* vol. 122, pp. 16-22, 2005.
[226] D. A. Bartholomeusz, R. W. Boutte, and J. D. Andrade, "Xurography: Rapid Prototyping of Microstructures using a Cutting Plotter," *Journal of Microelectromechanical Systems,* vol. 14, pp. 1364-1374, 2005.

[227] P. K. Yuen and V. N. Goral, "Low-cost Rapid Prototyping of Flexible Microfluidic Devices using a Desktop Digital Craft Cutter," *Lab on a Chip,* vol. 10, pp. 384-387, 2009.
[228] J. Do, J. Y. Zhang, and C. M. Klapperich, "Maskless Writing of Microfluidics: Rapid Prototyping of 3D Microfluidics using Scratch on a Polymer Substrate," *Robotics and Computer-Integrated Manufacturing,* vol. 27, pp. 245-248, 2010.
[229] J. M. Blander, I. Visintin, C. A. Janeway Jr., and R. Medzhitov, "α(1,3)-Fucosyltransferase VII and α(2,3)-Sialyltransferase IV are Up-Regulated in Activated CD4 T Cells and Maintained after their Differentiation into Th1 and Migration into Inflammatory Sites," *Journal of Immunology,* vol. 163, pp. 3746-3752, 1999.
[230] A. Boonstra, C. Asselin-Paturel, M. Gilliet, C. Crain, G. Trinchieri, Y.-J. Liu, and A. O'Garra, "Flexibility of Mouse Classical and Plasmacytoid-derived Dendritic Cells in Directing T Helper Type 1 and 2 Cell Development," *The Journal of Experimental Medicine,* vol. 197, pp. 101-109, 2003.
[231] S. A. Przyborski, "Isolation of Human Embryonal Carcinoma Stem Cells by Immunomagnetic Sorting," *Stem Cells,* vol. 19, pp. 500-504, 2001.
[232] P. A. Zuk and L. A. Elferink, "Rab15 Mediates an Early Endocytic Event in Chinese Hamster Ovary Cells," *Journal of Biological Chemistry,* vol. 274, pp. 22303-22312, 1999.
[233] Q. Sha, K. L. Lansbery, D. Distefano, R. W. Mercer, and C. G. Nichols, "Heterologous Expression of the Na+,K+-ATPase γ Subunit in Xenopus Oocytes induces an Endogenous, Voltage-gated Large Diameter Pore," *The Journal of Physiology,* vol. 535, pp. 407-417, 2001.
[234] D. R. Bolster, S. J. Crozier, S. R. Kimball, and L. S. Jefferson, "AMP-activated Protein Kinase Suppresses Protein Synthesis in Rat Skeletal Muscle through Down-regulated Mammalian Target of Rapamycin (mTOR) Signaling," *Journal of Biological Chemistry,* vol. 277, pp. 23977-23980, 2002.
[235] T. Alefantis, P. Grewal, J. Ashton, A. S. Khan, J. J. Valdes, and V. G. Del Vecchio, "A Rapid and Sensitive Magnetic Bead-based Immunoassay for the Detection of Staphylococcal Enterotoxin B for High-through Put Screening," *Molecular and Cellular Probes,* vol. 18, pp. 379-382, 2004.
[236] G. U. Lee, S. Metzger, M. Natesan, C. Yanavich, and Y. F. Dufrêne, "Implementation of Force Differentiation in the Immunoassay," *Analytical Biochemistry,* vol. 287, pp. 261-271, 2000.
[237] G.-H. Kim, A. G. Rand, and S. V. Letcher, "Impedance Characterization of a Piezoelectric Immunosensor Part II: Salmonella Typhimurium Detection using Magnetic Enhancement," *Biosensors and Bioelectronics,* vol. 18, pp. 91-99, 2003.
[238] D. R. Baselt, G. U. Lee, M. Natesan, S. W. Metzger, P. E. Sheehan, and R. J. Colton, "A Biosensor based on Magnetoresistance Technology," *Biosensors and Bioelectronics,* vol. 13, pp. 731-739, 1998.
[239] Y. A. Yeung and K. D. Wittrup, "Quantitative Screening of Yeast Surface-Displayed Polypeptide Libraries by Magnetic Bead Capture," *Biotechnology Progress,* vol. 18, pp. 212-220, 2002.
[240] M. J. Feldhaus, R. W. Siegel, L. K. Opresko, J. R. Coleman, J. M. W. Feldhaus, Y. A. Yeung, J. R. Cochran, P. Heinzelman, D. Colby, J. Swers, C. Graff, H. S. Wiley, and K. D. Wittrup, "Flow-cytometric Isolation of Human Antibodies from a Nonimmune Saccharomyces Cerevisiae Surface Display Library," *Nature Biotechnology,* vol. 21, pp.

163-170, 2003.
[241] B. Sinclair, "To Bead or Not To Bead: Applications of Magnetic Bead Technology," *The Scientist,* vol. 12, p. 17, 1998.
[242] N. P. Suh, *The Principles of Design*. New York: Oxford University Press, 1990.
[243] F. Kreith, *The CRC Handbook of Mechanical Engineering*. Boca Raton, FL.: CRC Press, 2004.
[244] N. P. Suh, "Design Axioms and Quality Control," *Robotics and Computer-Integrated Manufacturing,* vol. 9, pp. 369-376, 1992
[245] N. P. Suh, "Designing-in of Quality through Axiomatic Design," *IEEE Transactions on Reliability,* vol. 44, pp. 256-264, Jun 1995.
[246] N. P. Suh, *Axiomatic Design: Advances and Applications*. New York: Oxford University Press, 2001.
[247] D. G. Lee and N. P. Suh, *Axiomatic design and fabrication of composite structures: applications in robots, machine tools, and automobiles*: Oxford University Press, 2006.
[248] L. D. Albano and N. P. Suh, "Axiomatic Design and Concurrent Engineering," *Computer-Aided Design,* vol. 26, pp. 499-504, Jul 1994.
[249] A. M. Goncalves-Coelho, A. J. F. Mourao, and Z. L. Pereira, "Improving the Use of QFD with Axiomatic Design," *Concurrent Engineering-Research and Applications,* vol. 13, pp. 233-239, Sep 2005.
[250] S. J. Kim, N. P. Suh, and S. G. Kim, "Design of Software Systems Based on Axiomatic Design," *Robotics and Computer-Integrated Manufacturing,* vol. 8, pp. 243-255, 1991.
[251] N. P. Suh and S. H. Do, "Axiomatic Design of Software Systems," *CIRP Annals 2000: Manufacturing Technology,* pp. 95-100; 450, 2000.
[252] J. Y. Jung and S. B. Billatos, "An Expert-System for Assembly Based on Axiomatic Design Principles," *Journal of Intelligent & Robotic Systems,* vol. 8, pp. 245-265, Oct 1993.
[253] C. B. Park, D. F. Baldwin, and N. P. Suh, "Axiomatic Design of a Microcellular Filament Extrusion System," *Research in Engineering Design-Theory Applications and Concurrent Engineering,* vol. 8, pp. 166-177, 1996.
[254] B. Babic, "Axiomatic Design of Flexible Manufacturing Systems," *International Journal of Production Research,* vol. 37, pp. 1159-1173, Mar 20 1999.
[255] P. Gu, H. A. Rao, and M. M. Tseng, "Systematic Design of Manufacturing Systems based on Axiomatic Design Approach," *CIRP Annals-Manufacturing Technology,* vol. 50, pp. 299-304, 2001.
[256] E. Stiassnie and M. Shpitalni, "Incorporating Lifecycle Considerations in Axiomatic Design," *CIRP Annals-Manufacturing Technology,* vol. 56, pp. 1-4, 2007.
[257] B. J. Jeon, Y. H. Kim, K. S. Lee, S. W. Cha, G. J. Nam, C. Y. Park, and G. J. Lee, "Parameter Design of a Coaxial Cable Insulation Manufacturing Process using Axiomatic Design and the Taguchi Method," *Polymer-Plastics Technology and Engineering,* vol. 47, pp. 785-790, 2008.
[258] X. H. Tran, R. Tawie, and H. K. Lee, "A Systematic Approach for the Development of Porous Concrete based on Axiomatic Design Theory," *Computers and Concrete,* vol. 6, pp. 491-503, Dec 2009.
[259] H. N. Yu, S. S. Kim, J. Do Suh, and D. G. Lee, "Axiomatic Design of the Sandwich Composite Endplate for PEMFC in Fuel Cell Vehicles," *Composite Structures,* vol. 92, pp.

1504-1511, May 2010.
[260] Z. M. Bi, Y. Lin, and W. J. Zhang, "The General Architecture of Adaptive Robotic Systems for Manufacturing Applications," *Robotics and Computer-Integrated Manufacturing,* vol. 26, pp. 461-470, Oct 2010.
[261] O. Kulak and C. Kahraman, "Multi-Attribute Comparison of Advanced Manufacturing Systems using Fuzzy vs. Crisp Axiomatic Design Approach," *International Journal of Production Economics,* vol. 95, pp. 415-424, Mar 18 2005.
[262] K. D. Lee, N. P. Suh, and J. H. Oh, "Axiomatic Design of Machine Control System," *CIRP Annals-Manufacturing Technology,* vol. 50, pp. 109-114, 2001.
[263] M. K. Shin, S. W. Hong, and G. J. Park, "Axiomatic Design of the Motor-driven Tilt/Telescopic Steering System for Safety and Vibration," *Proceedings of the Institution of Mechanical Engineers Part D-Journal of Automobile Engineering,* vol. 215, pp. 179-187, 2001.
[264] A. A. Boxwala, Q. Zeng, D. Tate, R. A. Greenes, and D. G. Fairchild, "Applying Axiomatic Design Methodology to Create Guidelines that are Locally Adaptable," *Proceedings of AMIA 2002 Symposium,* pp. 980-980;1258, 2002.
[265] B. S. Jang, Y. S. Yang, Y. S. Song, Y. S. Yeun, and S. H. Do, "Axiomatic Design Approach for Marine Design Problems," *Marine Structures,* vol. 15, pp. 35-56, Jan-Feb 2002.
[266] Y. S. Pyun, Y. D. Jang, I. H. Cho, J. H. Park, A. Combs, and Y. C. Lee, "Evolutionary Design of No Spin Differential Models for Off-road Vehicles using the Axiomatic Approach," *International Journal of Automotive Technology,* vol. 7, pp. 795-801, Dec 2006.
[267] Y. S. Pyun, Y. D. Jang, I. H. Cho, J. H. Park, A. Combs, and Y. C. Lee, "Design Evaluation of No Spin Differential Models using the Axiomatic Approach," *International Journal of Automotive Technology,* vol. 7, pp. 595-601, Aug 2006.
[268] J. Thielman and P. Ge, "Applying Axiomatic Design Theory to the Evaluation and Optimization of Large-scale Engineering Systems," *Journal of Engineering Design,* vol. 17, pp. 1-16, Jan 2006.
[269] J. H. Kim, K. S. Kim, and Y. J. Kang, "Ride Comfort Evaluation and Suspension Design using Axiomatic Design," *Journal of Mechanical Science and Technology,* vol. 21, pp. 1066-1076, Jul 2007.
[270] M. K. Shin, B. S. Kang, Y. I. Kim, S. I. Yi, and G. J. Park, "Design of an Automobile Seat with Regulations using Axiomatic Design," *Proceedings of the ASME International Design Engineering Technical Conferences and Computers and Information in Engineering Conference,* vol. 2, pp. 627-636;1335, 2005.
[271] M. K. Shin, Y. I. Kim, B. S. Kang, and G. J. Park, "Design of an automobile seat with regulations using axiomatic design," *Proceedings of the Institution of Mechanical Engineers Part D-Journal of Automobile Engineering,* vol. 220, pp. 269-279, Mar 2006.
[272] S. Bae, J. M. Lee, and C. N. Chu, "Axiomatic Design of Automotive Suspension Systems," *Cirp Annals-Manufacturing Technology,* vol. 51, pp. 115-118, 2002.
[273] K. S. Lee, P. J. Jeong, H. Lee, S. J. Lee, and S. W. Cha, "Conceptual Design of Microcellular Plastics Bumper Parts Using Axiomatic Approach," *Polymer-Plastics Technology and Engineering,* vol. 48, pp. 1101-1106, 2009.
[274] J. W. Melvin and N. P. Suh, "Simulation within the Axiomatic Eesign Framework," *CIRP*

Annals-Manufacturing Technology, vol. 51, pp. 107-110, 2002.
[275] K. Z. Chen, X. A. Feng, and B. B. Zhang, "Development of Computer-Aided Quotation System for Manufacturing Enterprises using Axiomatic Design," *International Journal of Production Research,* vol. 41, pp. 171-191, 2003.
[276] W. S. Chin, J. W. Kwon, and D. G. Lee, "Trenchless Repairing of Underground Pipes using RTM based on the Axiomatic Design Method," *Journal of Composite Materials,* vol. 37, pp. 1109-1126, 2003.
[277] R. B. Xiao and X. F. Cheng, "An Analytic Approach to the Relationship of Axiomatic Design and Robust Design," *International Journal of Materials & Product Technology,* vol. 31, pp. 241-258, 2008.
[278] K. J. Park, B. S. Kang, K. N. Song, and G. J. Park, "Design of a Spacer Grid using Axiomatic Design," *Journal of Nuclear Science and Technology,* vol. 40, pp. 989-997, Dec 2003.
[279] J. H. Yang, K. Y. Lee, and C. Y. Dong, "Application of the Axiomatic Design Methodology to the Design of PBGA Package with Polyimide Coating Layer," *KSME International Journal,* vol. 18, pp. 1572-1581, Sep 2004.
[280] J. S. Choi, S. Hong, H. W. Kim, T. K. Yeu, and T. H. Lee, "Design Evaluation of a Deepsea Manganese Nodule Miner based on Axiomatic Design," *Proceedings of the Sixth (2005) ISOPE Ocean Mining Symposium,* pp. 163-167;256, 2005.
[281] A. M. Goncalves-Coelho and A. J. F. Mourao, "Selection of Rapid Prototyping Systems Based on the Axiomatic Design Theory," *Virtual Modeling and Rapid Manufacturing,* pp. 533-538;638, 2005.
[282] J. W. Yi and G. J. Park, "Development of a Design System for EPS Cushioning Package of a Monitor using Axiomatic Design," *Advances in Engineering Software,* vol. 36, pp. 273-284, Apr 2005.
[283] E. Eraslan, D. Akay, and M. Kurt, "Usability Ranking of Intercity Bus Passenger Seats using Fuzzy Axiomatic Design Theory," *Cooperative Design, Visualization, and Engineering, Proceedings,* vol. 4101, pp. 141-148, 2006.
[284] M. Celik, C. Kahraman, S. Cebi, and I. D. Er, "Fuzzy Axiomatic Design-based Performance Evaluation Model for Docking Facilities in Shipbuilding Industry: The case of Turkish Shipyards," *Expert Systems with Applications,* vol. 36, pp. 599-615, Jan 2009.
[285] G. Buyukozkan, J. Arsenyan, and G. Ertek, "Evaluation of E-Learning Web Sites Using Fuzzy Axiomatic Design Based Approach," *International Journal of Computational Intelligence Systems,* vol. 3, pp. 28-42, Apr 2010.
[286] S. Cebi, M. Celik, and C. Kahraman, "Structuring Ship Design Project Approval Mechanism towards Installation of Operator-System Interfaces via Fuzzy Axiomatic Design Principles," *Information Sciences,* vol. 180, pp. 886-895, Mar 15 2010.
[287] S. Cebi and C. Kahraman, "Indicator Design for Passenger Car using Fuzzy Axiomatic Design Principles," *Expert Systems with Applications,* vol. 37, pp. 6470-6481, Sep 2010.
[288] M. Celik and I. D. Er, "Fuzzy Axiomatic Design Extension for Managing Model Selection Paradigm in Decision Science," *Expert Systems with Applications,* vol. 36, pp. 6477-6484, Apr 2009.
[289] J. D. Jiang, F. Xu, X. R. Zhen, X. Zhang, Y. Y. Wang, and L. B. Zhang, "Axiomatic Design using Ontology Modeling for Interoperability in Small Agriculture Machinery Product Development," *Knowledge Enterprise: Intelligent Strategies in Product Design,*

Manufacturing, and Management, vol. 207, pp. 184-191;1046, 2006.
[290] X. B. Chen, J. Kai, and M. Hashemi, "Evaluation of Fluid Dispensing Systems using Axiomatic Design Principles," *Journal of Mechanical Design,* vol. 129, pp. 640-648, Jun 2007.
[291] A. M. Goncalves-Coelho and A. J. F. Mourao, "Axiomatic Design as Support for Decision-Making in a Design for Manufacturing Context: A Case Study," *International Journal of Production Economics,* vol. 109, pp. 81-89, Sep 2007.
[292] B. Bras and F. Mistree, "Concurrent Axiomatic and Robust Design Using Compromise Decision-Support Problems," *Concurrent Engineering-Research and Applications,* vol. 2, pp. 17-31, Mar 1994.
[293] G. Y. Heo and S. K. Lee, "Design Evaluation of Emergency Core Cooling Systems using Axiomatic Design," *Nuclear Engineering and Design,* vol. 237, pp. 38-46, Jan 2007.
[294] J. Thielman, P. Ge, Q. Wu, and L. Parme, "Evaluation and Optimization of General Atomics' GT-MHR Reactor Cavity Cooling System using an Axiomatic Design Approach," *Nuclear Engineering and Design,* vol. 235, pp. 1389-1402, Jun 2005.
[295] I. C. Bang and G. Heo, "An Axiomatic Design Approach in Development of Nanofluid Coolants," *Applied Thermal Engineering,* vol. 29, pp. 75-90, Jan 2009.
[296] I. C. Bang, G. Heo, Y. H. Jeong, and S. Heo, "An Axiomatic Design Approach of Nanofluid-Engineered Nuclear Safety Features for Generation III Plus Reactors," *Nuclear Engineering and Technology,* vol. 41, pp. 1157-1170, Nov 2009.
[297] M. B. Durmusoglu and O. Kulak, "A Methodology for the Design of Office Cells using Axiomatic Design Principles," *Omega-International Journal of Management Science,* vol. 36, pp. 633-652, Aug 2008.
[298] M. Cavique and A. M. Goncalves-Coelho, "Axiomatic Design and HVAC Systems: An Efficient Design Decision-Making Criterion," *Energy and Buildings,* vol. 41, pp. 146-153, Feb 2009.
[299] C. Kahraman, S. Cebi, and I. Kaya, "Selection among Renewable Energy Alternatives Using Fuzzy Axiomatic Design: The Case of Turkey," *Journal of Universal Computer Science,* vol. 16, pp. 82-102, 2010.
[300] L. J. Zhang, "Integrating Axiomatic Design and TRIZ to Solve Design Problems," *Proceedings of the International Conference on Mechanical Transmissions,* vol. 1 and 2, pp. 1567-1570;1703, 2006.
[301] M. Nakao, K. Tsuchiya, and K. Iino, "Three Typical Failure Scenarios of the Mind Process of Design from the Axiomatic Design Perspective," *CIRP Annals-Manufacturing Technology,* vol. 58, pp. 165-168, 2009.
[302] C. I. Hung, B. J. Ke, G. R. Huang, B. H. Hwei, H. F. Lai, and G. B. Lee, "Hydrodynamic Focusing for a Micromachined Flow Cytometer," *Journal of Fluids Engineering-Transactions of the Asme,* vol. 123, pp. 672-679, Sep 2001.
[303] COMSOL-Multiphysics, "Documentation," 2007.
[304] M. T. Kreutzera, F. Kapteijna, J. A. Moulijna, and J. J. Heiszwolf, "Multiphase Monolith Reactors: Chemical Reaction Engineering of Segmented Flow in Microchannels," *Chemical Engineering Science,* vol. 60, pp. 5895-5916, 2005.
[305] C. Zhou, P. Yue, and J. J. Feng, "Formation of Simple and Compound Drops in Microfluidic Devices," *Physics of Fluids,* vol. 18, pp. 092105-14, 2006.

APPENDIX

APPENDIX A. AXIOMATIC DESIGN THEORY

A.1. Axiomatic Design Theory

Axiomatic design theory (ADT) concept was introduced by Suh [242] to provide a basis for correct design decisions. ADT provides the scientific base to augment the designer's experience by providing the underlying principles, theories, and methodologies to fully enable the designer's creativity. ADT is a rational way of developing a complicated system that satisfies $\boldsymbol{FRs}$ and $\boldsymbol{CRs}$ at low cost and on time without mistakes [242, 243]. Design issues become easier to understand when they are analyzed using the framework of axiomatic design [242, 244, 245]. The world of axiomatic design has four domains: customer domain, functional domain, physical domain, and process domain [245]. The domain structure is shown in Figure A. 1.

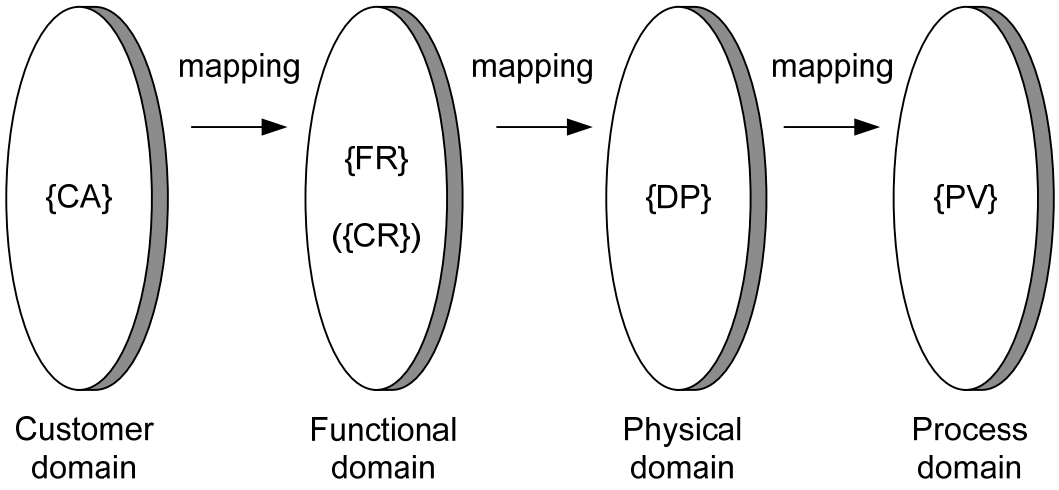

Figure A. 1 The four domains of the design world. {x} are the characteristic vectors of each domain. The domain on the left relative to the domain on the right represents, "what we want to achieve," while the domain on the right represents the design solution of "how we propose to satisfy the requirements in the left domain."

The customer domain is characterized from the customer's attributes (or needs) ($\boldsymbol{CAs}$) in a product, process, system, or materials. The customer's needs are specified in terms of functional requirements ($\boldsymbol{FRs}$) and constraints. Design parameters ($\boldsymbol{DPs}$) satisfy the specific

$\boldsymbol{FRs}$. Process variables ($\boldsymbol{PVs}$) characterize an optimal process in the process domain [243]. ADT is based on two design axioms: the Independence Axiom and the Information Axiom [245].

Axiom 1: The Independence Axiom - Maintain the independence of the $\boldsymbol{FRs}$.

The independence of $\boldsymbol{FRs}$ must always be maintained; i.e., design decisions must always be made without violating the independence of each functional requirement from other functional requirements. The $\boldsymbol{FRs}$ are defined as the minimum number of independent requirements that characterize the design goals. Once $\boldsymbol{FRs}$ are defined based on the $\boldsymbol{CAs}$, the $\boldsymbol{FRs}$ are mapped onto the physical domain by a suitable set of $\boldsymbol{DPs}$ as illustrated in Figure A. 2.

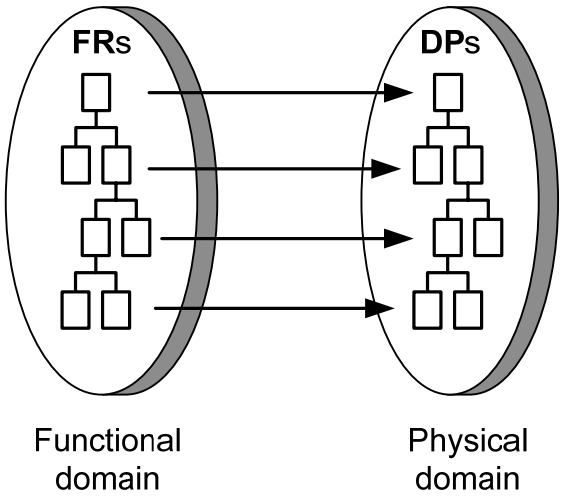

Figure A. 2 Mapping from the functional domain to the physical domain. The squares in domains represent elements of the domain.

If the design details are missing at the highest level of design, the highest level design must be decomposed to develop the design details. As the highest level design is decomposed, the decision of the lower level design must be consistent with the highest level design intent without a violation of the independence axiom. In order to decompose $\boldsymbol{FRs}$ and $\boldsymbol{DPs}$, the zigzag method is applied as illustrated in Figure A. 3. From an $\boldsymbol{FR}$ in the functional domain, a conceptualized design in the physical domain is determined corresponding $\boldsymbol{DP}$. $\boldsymbol{FR_1}$ and $\boldsymbol{FR_2}$ at

the next level are created satisfying the highest level $\boldsymbol{FR}$ for the highest level $\boldsymbol{DP}$. Then, $\boldsymbol{DP}_1$ and $\boldsymbol{DP}_2$ are found to satisfy $\boldsymbol{FR}_1$ and $\boldsymbol{FR}_2$, respectively, by conceptualizing a design at this level. This process is continued until the $\boldsymbol{FR}$ can be satisfied without further decomposition. The final states are indicated by thick-bordered boxes which is called "leaves" [243]. During the mapping process, all the possible different ways of satisfying the $\boldsymbol{FRs}$ need to be considered by identifying reasonable $\boldsymbol{DPs}$. This step is called conceptualization process; it encompasses considering all available methods, such as brainstorming, morphological techniques, analogy from other examples, extrapolation and interpolation, law of nature, order-of-magnitude analysis, and reverse engineering.

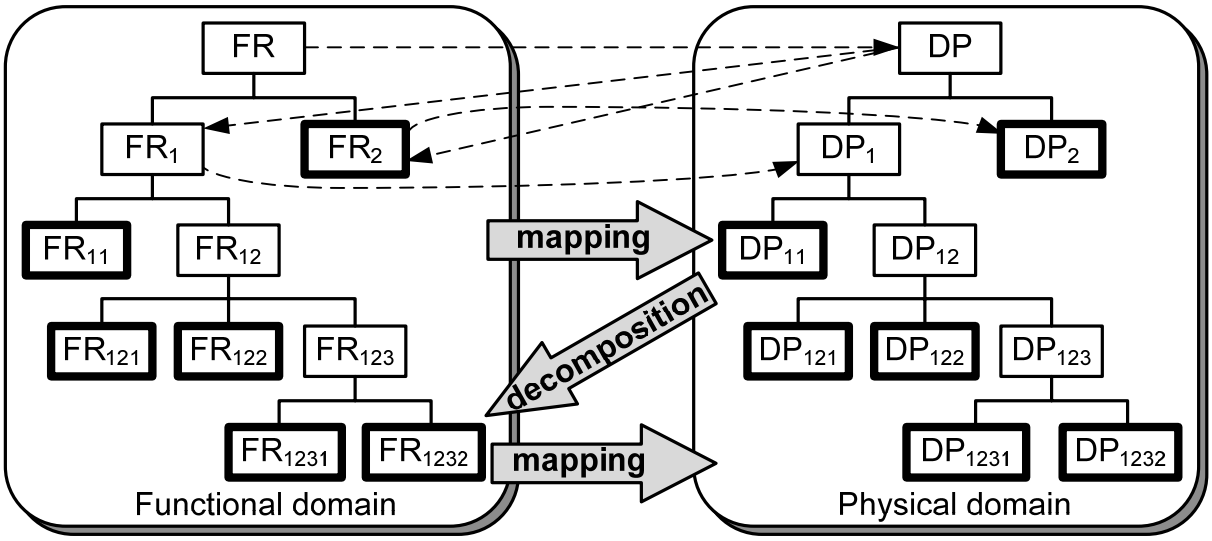

Figure A. 3 Zigzagging to decompose $\boldsymbol{FRs}$ and $\boldsymbol{DPs}$ in the functional and physical domains. Boxes with thick lines express "leaves" that do not require further decomposition [243].

At a given level of the design hierarchy, an $\boldsymbol{FR}$ vector is made up representing the set of $\boldsymbol{FRs}$ in the functional domain, and a $\boldsymbol{DP}$ vector in the physical domain is constituted corresponding to the $\boldsymbol{DPs}$ that satisfy the $\boldsymbol{FRs}$. A design equation that describes the relation between the two vectors can be expressed mathematically as

$$\{\boldsymbol{FR}\} = [A]\{\boldsymbol{DP}\} \tag{A. 1}$$

where $[A]$ is called a design matrix that characterizes the product design. A design matrix for a design that has n $\boldsymbol{FRs}$ and n $\boldsymbol{DPs}$ is expressed as

$$[A] = \begin{bmatrix} A_{11} & A_{12} & \cdots & A_{11} \\ A_{21} & A_{22} & \cdots & A_{2n} \\ \vdots & \vdots & \ddots & \vdots \\ A_{n1} & A_{n2} & \cdots & A_{nn} \end{bmatrix} \tag{A. 2}$$

In a differential form, Eqn.(A.1) can be rewritten as

$$\{d\boldsymbol{FR}\} = [A]\{d\boldsymbol{DP}\} \tag{A. 3}$$

and the elements of the design matrix are given by

$$A_{ij} = \partial \boldsymbol{FR}_i / \partial \boldsymbol{DP}_j \tag{A. 4}$$

In general, with n $\boldsymbol{FRs}$ and $\boldsymbol{DPs}$, Eqn.(A. 1) can be rewritten in terms of its elements as

$$\boldsymbol{FR}_i = \sum_{j=1}^{n} A_{ij}\boldsymbol{DP}_j \qquad (i = 1, 2, \ldots, n) \tag{A. 5}$$

or

$$\begin{aligned} FR_1 &= A_{11}DP_{11} + A_{12}DP_{12} + \cdots + A_{1n}DP_{1n} \\ FR_2 &= A_{21}DP_{21} + A_{22}DP_{22} + \cdots + A_{2n}DP_{2n} \\ &\vdots \\ FR_n &= A_{n1}DP_{n1} + A_{n2}DP_{n2} + \cdots + A_{nn}DP_{nn} \end{aligned} \tag{A. 6}$$

For a linear design, A_{ij} are constants, and for a nonlinear design, A_{ij} are functions of the $\boldsymbol{DPs}$. If a design matrix [A] is a full matrix which is neither diagonal nor triangular, a design cannot satisfy the independence axiom and is called a "coupled design." The matrix [A] must be either diagonal or triangular in order to satisfy the independence axiom. Each of the $\boldsymbol{FRs}$ can be satisfied independently with one $\boldsymbol{DP}$ if the design matrix [A] is diagonal, resulting in an "uncoupled design." If the design matrix is triangular, the independence of $\boldsymbol{FRs}$ can be assured if and only if the $\boldsymbol{DPs}$ are determined in an appropriate sequence; it is called a "decoupled design."

Axiom 2: The Information Axiom - Minimize the information content of the design.

Among the designs that satisfy the Independence Axiom, the design that has the smallest information content and the highest probability of success is the best design. The probability of success is defined as

$$P_s = \frac{Common\ range\ (CR)}{System\ range\ (SR)} \tag{A. 7}$$

P_s is governed by the intersection of the design range (DR) and the system range (SR). DR is defined by a given design specification of $\boldsymbol{FR}s$, and SR is a distribution of the performance of a designed product. The overlap between DR and SR is called the common range (CR) as illustrated in Figure A. 4. If an $\boldsymbol{FR}$ is a continuous random variable, P_s can be expressed as

$$P_s = \int_{\boldsymbol{FR}^*-\Delta}^{\boldsymbol{FR}^*+\Delta} \phi(\boldsymbol{FR}) d\boldsymbol{FR} \tag{A. 8}$$

where $\phi(\boldsymbol{FR})$ is a system probability density function (PDF), Δ is half of DR, and $\boldsymbol{FR}^*$ is the target value [162].

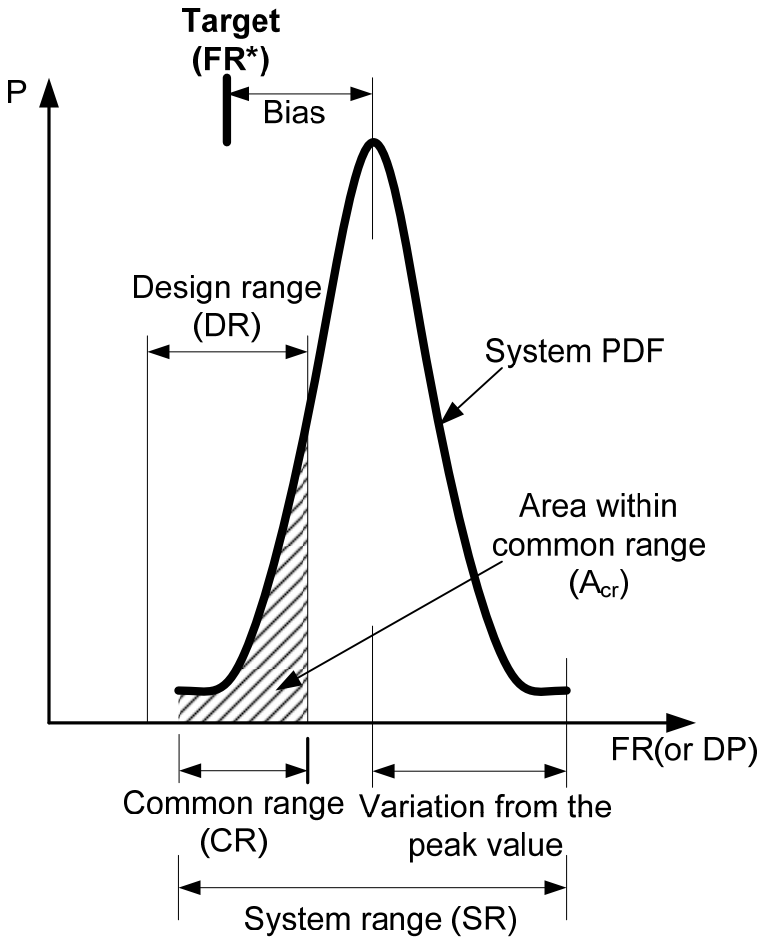

Figure A. 4 Design range, system range, common range, and system PDF for a function requirement [162].

The ordinate is the probability density and the abscissa is either the $\boldsymbol{FR}$ or $\boldsymbol{DP}$. The system PDF is plotted over the SR for a specified $\boldsymbol{FR}$. The distance between the target value and the mean of the system PDF is called bias, and the $\boldsymbol{FR}$ is satisfied only in CR which can be computed by Eqn.(A. 7) after P_s is known from Eqn.(A. 8). The area under the system PDF within CR, A_{cr}, is the design's probability of achieving the specified goal, and information content I can be calculated as [242, 243].

$$I = \log_2 \frac{1}{A_{cr}} \tag{A. 9}$$

Information content I_i for a given $\boldsymbol{FR_i}$ is defined in terms of the probability P_i satisfying $\boldsymbol{FR_i}$:

$$I_i = \log_2 \frac{1}{P_i} = -\log_2 P_i \tag{A. 10}$$

Either the logarithm based on 2 or the natural logarithm may be used. In case of multiple $\boldsymbol{FRs}$, $m\boldsymbol{FRs}$, the information content for the entire system I_{sys} is

$$I_{sys} = -\log_2 P_{\{m\}} \tag{A. 11}$$

where $P_{\{m\}}$ is the joint probability that all $m\boldsymbol{FRs}$ are satisfied. In case of an uncoupled design where all $\boldsymbol{FRs}$ are statistically independent,

$$P_{\{m\}} = \prod_{i=1}^{m} P_i \tag{A. 12}$$

I_{sys} is calculated as

$$I_{sys} = \sum_{i=1}^{m} I_i = -\sum_{i=1}^{m} \log_2 P_i \tag{A. 13}$$

In case of a decoupled design where all $\boldsymbol{FRs}$ are not statistically independent,

$$P_{\{m\}} = \prod_{i=1}^{m} P_{i|\{j\}} \qquad for\{j\} = \{1, 2, \dots, i-1\} \tag{A. 14}$$

where $P_{i|\{j\}}$ is the conditional probability of satisfying FR_i. I_{sys} can be calculated as [246]

$$I_{sys} = -\sum_{i=1}^{m} \log_2 P_{i|\{j\}} \qquad for\{j\} = \{1, 2, \dots, i-1\} \tag{A. 15}$$

Thus, it is found that the smallest information content *I* represents the best design, requiring the least information to achieve the design goals. Inversely, the highest probability represents the best design. If the probability is low, more information is required to satisfy $\boldsymbol{FRs}$.

A.1.1. **Functional design: Reduction of the information content, *I***

The ultimate goal of a design is to make a system function as designed by minimizing the information content *I* with large variations in design parameters ($\boldsymbol{DPs}$) and process variables ($\boldsymbol{PVs}$); a design must satisfy the $\boldsymbol{FRs}$, leading to a functional design. In order to realize a functional design, the variance of a system must be reduced and the bias must be eliminated, so that the system range (SR) can be positioned inside the design range (DR) reducing *I* to zero (see Figure A. 4). If the mean of the system PDF is close to the target value, the bias is very small. The bias can be eliminated by satisfying the independence axiom, yielding an uncoupled or decoupled design. Variability, which measures variance, is caused by numerous factors such as noise, coupling, environment, and random variations in $\boldsymbol{DPs}$. There are several ways to reduce the variance of a design if a design satisfies the independence axiom [247]:

a) Reduce the variance of a design through reduction of stiffness

   If one $\boldsymbol{FR}$ is related to its $\boldsymbol{DP}$, it can be expressed as

$$\boldsymbol{FR}_1 = (A_{11})\boldsymbol{DP}_1 \tag{A. 16}$$

$\boldsymbol{DP}_1$ depends on the magnitude of A_{11} in a particular DR for $\boldsymbol{FR}_1$. The coefficient A_{11} is the stiffness affecting the allowable variation of $\boldsymbol{DP}_1$ as shown in Figure A. 5.

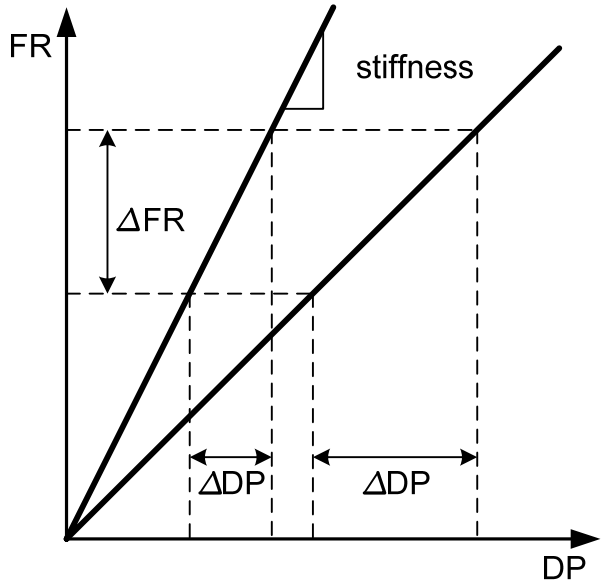

Figure A. 5 Schematic diagram of stiffness. For a particular $\Delta \boldsymbol{FR}$, the allowable variation $\Delta \boldsymbol{DP}$ increases with a decreasing stiffness A_{11}.

b) Reduce the variance of a design through the design of a system that is immune to variation

If a stiffness becomes zero in Eqn.(A. 16) a system is completely immune (insensitive) to variation in $\boldsymbol{DP}$. However, if the goal is to vary the $\boldsymbol{FR}$ by altering the $\boldsymbol{DP}$, the stiffness must be large enough to control the $\boldsymbol{FR}$. If many (suppose three) $\boldsymbol{DPs}$ affect one $\boldsymbol{FR}$, it can be expressed as

$$\boldsymbol{FR} = f(\boldsymbol{DP}_a, \boldsymbol{DP}_b, \boldsymbol{DP}_c) \tag{A. 17}$$

or

$$\boldsymbol{FR} = A_a \boldsymbol{DP}_a + A_b \boldsymbol{DP}_b + A_c \boldsymbol{DP}_c \tag{A. 18}$$

where A_a, A_b, and A_c are coefficients. Any uncontrolled variation of coefficients and $\boldsymbol{DPs}$ can alter the variation in $\boldsymbol{FR}$. If A_b and A_c are very small, or $\boldsymbol{DP}_b$ and $\boldsymbol{DP}_c$ are fixed, $\boldsymbol{FR}$ is immune to changes of $\boldsymbol{DP}_b$ and $\boldsymbol{DP}_c$. Thus, $\boldsymbol{FR}$ can be controlled by changing only $\boldsymbol{DP}_a$ with random variation A_a.

c) Reduce the variance of a design by fixing the values of extra $\boldsymbol{DPs}$

When a design is a redundant design such that the number of $\boldsymbol{DPs}$ are more than that of $\boldsymbol{FRs}$, it can be expressed, for example, as

$$\begin{bmatrix} \boldsymbol{FR}_1 \\ \boldsymbol{FR}_2 \\ \boldsymbol{FR}_3 \end{bmatrix} = \begin{bmatrix} A_{11} & 0 & 0 & A_{14} & A_{15} & 0 \\ 0 & A_{22} & 0 & 0 & A_{25} & A_{26} \\ 0 & 0 & A_{33} & A_{34} & 0 & A_{36} \end{bmatrix} \begin{bmatrix} \boldsymbol{DP}_1 \\ \boldsymbol{DP}_2 \\ \boldsymbol{DP}_3 \\ \boldsymbol{DP}_4 \\ \boldsymbol{DP}_5 \\ \boldsymbol{DP}_6 \end{bmatrix} \tag{A. 19}$$

In order to reduce the variance of this design, the values of extra $\boldsymbol{DPs}$ (i.e., $\boldsymbol{DP}_4$, $\boldsymbol{DP}_5$, and $\boldsymbol{DP}_6$) should be fixed, or the coefficients associated with the extra $\boldsymbol{DPs}$ (i.e., A_{14}, A_{15}, A_{25}, A_{26}, A_{34}, and A_{36}) should be zero.

d) Reduce the variance of a design by minimizing the random variation of $\boldsymbol{DPs}$ and $\boldsymbol{PVs}$

Random variation of input parameters redounds to the total random variation of the $\boldsymbol{FRs}$. The variance of the $\boldsymbol{FRs}$ is

$$\sigma_{FR_i}^2 = \sum_{j=1}^{n} A_{ij}^2 \sigma_{DP_j}^2 + 2 \sum_{j=1}^{n} \sum_{k=1}^{j-1} A_{ij} A_{ik} COV\left(\boldsymbol{DP}_j, \boldsymbol{DP}_k\right) \tag{A. 20}$$

where σ_{DP_j} is the variance of $\boldsymbol{DPs}$, and COV represents covariance. Contribution of the random variation of input parameters to the variance of $\boldsymbol{FR}_i$ can be decreased by reducing the variance of the $\boldsymbol{DP}_j$. Furthermore, independent $\boldsymbol{DPs}$ causes the relevant covariance term to desert the contribution to the variance of $\boldsymbol{FR}_i$.

e) Reduce the variance of a design by compensation

If extra $\boldsymbol{DPs}$ in a redundant design cannot be reduced, and a design cannot be immune to random variations of the extra $\boldsymbol{DPs}$, compensation can assist to lessen the effect of the extra $\boldsymbol{DPs}$. Suppose that A_a is much larger than other coefficients in Eqn.(A. 18). The main design

parameter becomes $\boldsymbol{DP}_a$, and the random variation such as noise can be represented as $\delta\boldsymbol{DP}_b$ and $\delta\boldsymbol{DP}_c$. Eqn.(A. 18) is rewritten as

$$\boldsymbol{FR} = A_a\boldsymbol{DP}_a + \sum_{i=extra\ terms} A_i\delta\boldsymbol{DP}_i \tag{A. 21}$$

The random variation term can be compensated by adjusting $\boldsymbol{DP}_a$. The necessary adjustment $\Delta\boldsymbol{DP}_a$ to compensate for the random variation is

$$\Delta\boldsymbol{DP}_a = \frac{1}{A_a}\left(\Delta\boldsymbol{FR} - \sum_{i=extra\ terms} A_i\delta\boldsymbol{DP}_i\right) \tag{A. 22}$$

where $\Delta\boldsymbol{FR}$ is the allowable random variation (i.e., the design range (DR) of $\boldsymbol{FR}$).

f) Reduce the variance of a design by increasing the design range (DR)

In some cases, design range (DR) can be enlarged, and system range (SR) may then fall within the range of DR without violating the design goals.

g) Reduce the variance of a design through integration of $\boldsymbol{DPs}$

All physical parts of a system are integrated in a single physical part without compromising the independence of $\boldsymbol{FRs}$. An example is a can and bottle opener wherein a can opener at one end and a bottle opener at the other end are integrated in the same steel sheet stock. This way leads to reduction of the error changes or simplification of the manufacturing operation [243].

A.1.2. **Applications of Axiomatic Design Thoery**

Applications	References
Concurrent engineering	[248, 249]
Software design	[250, 251]
Design for assembly (DFA)	[252]
Product quality and process productivity	[245]
Extrusion system of a microcellular polymer processing system	[253]
Manufacturing	[132, 254-261]
Chemical-Mechanical Polishing (CMP) machine	[262]
Motor-driven tilt/telescopic steering column	[263]
Clinical guideline representation	[264]
Vehicles	[265-273]
Simulating designs	[274]
Computer-aided quotation system	[275]
Rehabilitation process of underground pipes	[276]
Robust design process	[162, 277]
Spacer grid	[278]
Plastic ball grid array (PBGA) package	[279]
Deepsea manganese nodule miner (DSNM) system	[280]
Rapid prototyping (RP) system	[281]
Cushioning package of a monitor	[282]
Fuzzy axiomatic design theory (FADT)	[283-288]
Small agriculture machinery (SAM)	[289]
Fluid dispensing system	[290]
Decision-making	[291, 292]
Nuclear system	[293-296]
Office operation	[297]
Heat ventilation and air-conditioning (HVAC) system	[298]
Renewable energy selection	[299]
Conceptual design	[300]
Failure case analysis	[301]

APPENDIX B. SIMULATION STUDY

B.1. Modeling and simulation for integration method

B.1.1. Governing equation

Two immiscible fluids, oil phase and aqueous phase, are introduced to the microfluidic device by inlet pressures for middle flow and sheath flow. At the cross intersection, the immiscible fluids come into contact downstream, and the middle flow is squeezed by the sheath flow as shown in Figure B. 1.

The width of a focused flow is calculated by the mass conservation law as

$$\dot{m}_{in} = \dot{m}_{out} \tag{B. 1}$$

$$\rho_1 v_1 h D_1 + \rho_2 v_2 h D_2 + \rho_3 v_3 h D_3 = \rho_a v_a h D_a \tag{B. 2}$$

$$v_a = \frac{\rho_1 v_1 D_1 + \rho_2 v_2 D_2 + \rho_3 v_3 D_3}{\rho_a D_a} \tag{B. 3}$$

where $\dot{m}_{in}$ and $\dot{m}_{out}$ are mass flow rates of the inlet and outlet flows; ρ is the density of the flow; v is the velocity of the flow; D is the width of the microchannel; h is the height of the microchannel, which is perpendicular to the sheet plane; the subscripts, 1,2,3 and *a,* represent inlet 1, inlet 2, inlet 3, and the average property of the outlet, respectively. Likewise, mass conservation requires that the amount of middle flow at point A is equal to the amount of middle flow at point B as

$$\rho_1 v_1 h D_1 = \rho_1 v_f \left(\frac{\pi}{4}\right) d^2 \tag{B. 4}$$

$$d = \sqrt{\frac{4 v_1 h D_1}{\pi v_f}} \tag{B. 5}$$

where the cross section of the microchannel is circular, and v_f is the velocity of the focused

stream.

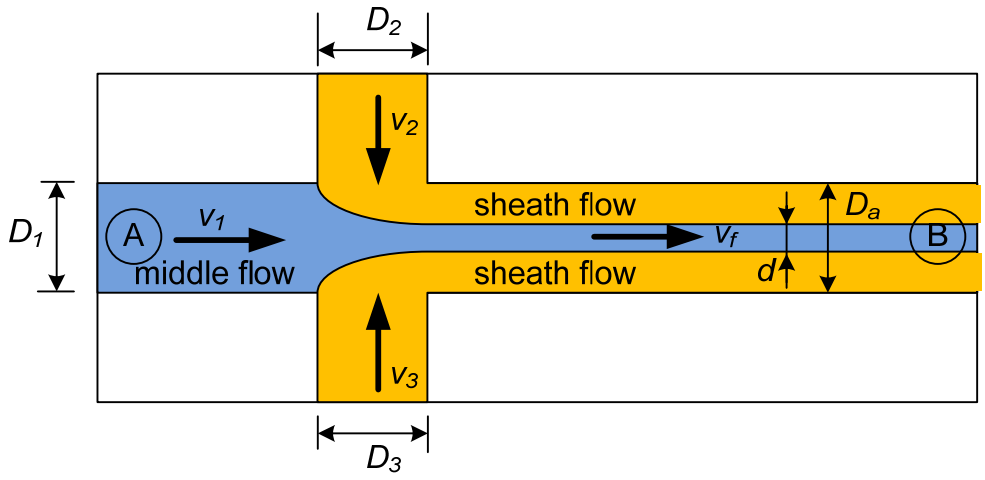

Figure B. 1 Schematic diagram of hydrodynamic flow focusing (D: width of the channel, v: velocity of the flow, d: width of the focused flow).

Assuming that the fluid stream is a fully developed laminar flow inside of the microchannel, the velocity profile inside section D_a is parabolic-distributed, i.e.,

$$v_f = v_{max} = 1.5v_a \tag{B. 6}$$

Thus, the width of the focused stream is represented as [302]

$$d = \sqrt{\frac{4v_1 h D_1}{\pi v_f}} = \sqrt{\frac{4v_1 h D_1 \rho_a D_a}{1.5\pi(\rho_1 v_1 D_1 + \rho_2 v_2 D_2 + \rho_3 v_3 D_3)}} \tag{B. 7}$$

A commercial computational fluid dynamics package, COMSOL MULTIPHYSICS, was used to perform the numerical simulation of the proposed microsphere formation method. This package applies lattice Boltzmann method (LBM) for calculation during the simulation. In the simulation, only the T-junction in the microchannel was simulated by varying the flow rates of the fluids. The simulation could be simplified by designing the model geometry in two dimensions as shown in Figure B. 2. The flows in the system during the simulation are laminar and immiscible. The aqueous middle flow is the dispersed phase (distilled water), and the oily

sheath flow and the crossflow are the continuous phase (paraffin oil) in this study. The T-junction is initially filled with the immiscible fluids, and the properties of the fluids are given in Table B. 1.

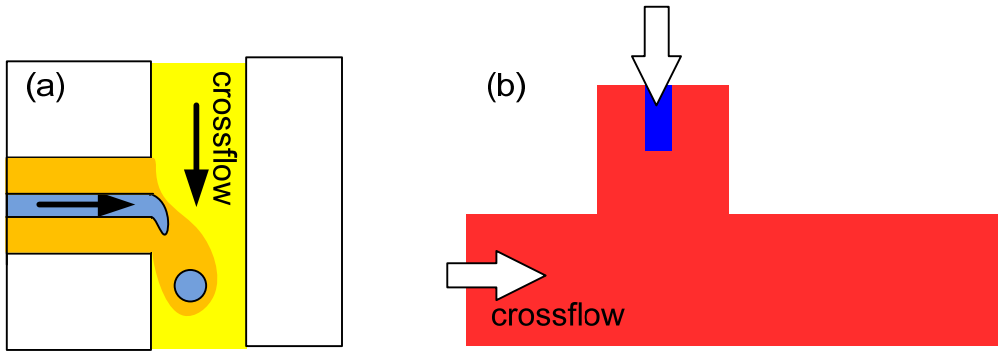

Figure B. 2 Schematic geometry of the simulation model: (a) T-junction in the microchannel, and (b) initial set up of the 2-D simulation model. Blue color represents aqueous dispersed phase and red color represents oily continuous phase. The arrows indicate the direction of the flows.

The dimensions of the microchannel were 20 μm of width and 10 μm of height and 80 μm of length of the crossflow channel. Initially, the aqueous dispersed phase flow was set to be 2 μm wide, and it is led to the crossflow channel. The channel was initially filled with immiscible flows which are continuous phase and dispersed phase.

Table B. 1 Properties of the fluids used for the simulation

Water (dispersed phase)	
Density	1000 kg/m^3
Viscosity	1.002 × 10^{-3} Pa-s
Paraffin Oil (continuous phase)	
Density	800 kg/m^3
Viscosity	0.19 Pa-s
Interfacial Tension	52 × 10^{-3} N/m

The focused flow was the dispersed phase, and the sheath and external flows were the continuous phase. The governing equation for this method is as follows [303].

$$continuity\ equation: \quad \nabla \cdot \boldsymbol{u} = 0 \tag{B. 8}$$

$$momentum\ equation: \quad \rho \frac{\partial \boldsymbol{u}}{\partial t} + \rho(\boldsymbol{u} \cdot \nabla)\boldsymbol{u} = \nabla \cdot [-p\boldsymbol{I} + \eta(\nabla \boldsymbol{u} + (\nabla \boldsymbol{u})^T)] + \boldsymbol{F_{st}} \tag{B. 9}$$

where ρ is density (kg/m^3), $\boldsymbol{u}$ is velocity (m/s), t is time (s), η is dynamic viscosity (Pa-s), p is pressure (Pa) and $\boldsymbol{F_{st}}$ is the interfacial tension force (N/m). Additionally, a level set equation for tracking the interfaces and shapes is defined as

$$level\ set\ equation: \frac{\partial \emptyset}{\partial t} + \boldsymbol{u} \cdot \nabla \emptyset = \gamma \nabla \cdot \left(-\emptyset(1-\emptyset)\frac{\nabla \emptyset}{|\nabla \emptyset|} + \epsilon \nabla \emptyset\right) \tag{B. 10}$$

where $\emptyset$ is the level set function, and γ and ϵ are numerical stabilization parameters. The density and viscosity are calculated from

$$\rho = \rho_1 + (\rho_2 - \rho_1)\emptyset \tag{B. 11}$$

$$\eta = \eta_1 + (\eta_2 - \eta_1)\emptyset \tag{B. 12}$$

where ρ_1, ρ_2, η_1 and η_2 are the densities and viscosities of the continuous phase and the dispersed phase [303]. Parabolic velocity profiles were specified at the inlet with zero pressure at the outlet. The wetted boundary condition applied to all solid boundaries. The contact angle between the fluid interface and solid wetted wall is specified as 135°.

B.1.2. **Simulation results and discussion**

In Figure B. 3, the sizes of generated microspheres are shown with different applied velocities. In this simulation study, three different velocities of the focused flow (v_f) were applied for the focused flow by varying the velocities of the sheath flow and the crossflow. As the velocity of the sheath flow (v_s) increased, the width of the focused flow reduced.

When the velocity of the crossflow (v_c) was zero, the focused flow kept the width and exited to the outlet of the crossflow channel. As v_c increased, the width of the focused flow decreased. At the T-junction, the induced instability from the crossflow interrupts the steadiness

of the focused flow under very high pressure. With the constant v_f and v_s, as the flow rate of crossflow increased, the neck width of the focused flow jet decreased. Thus, the size of microspheres became smaller with higher v_c yielding higher pressure on the focused flow. As the velocities became higher, the size trend indicates that the microsphere size reduced. By varying v_f from 0.06 m/s to 0.08 m/s, the generated microsphere sizes were between 2.9 μm and 8.3 μm in diameter with about 5% of coefficient of variation ($CV = \frac{standard\ deviation}{average\ diameter} \times 100\ (\%)$ [51]), which signifies that the proposed method can achieve both the controllability and the uniformity in the formation of microsphere generation. As well, it was pointed out that the pinch-off position of the focused flow was changed with different velocities of the fluids. At low velocities, the pinch-off position was close to the upstream of the T-junction. However, at high velocities, the position moved downstream of the microchannel. Figure B. 4 shows a case of the pinch-off position movement achieved by increasing v_c with constant v_f and v_s. The pinch-off position is correlated to the size of the microspheres. As the position is farther from the T-junction, the size of microsphere becomes smaller.

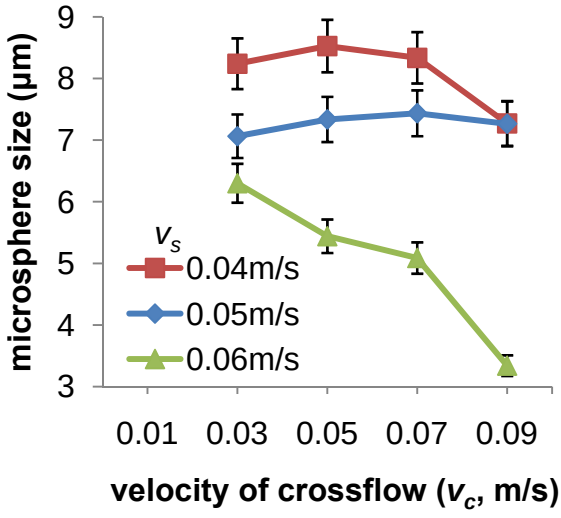

(a) v_f = 0.06 m/s

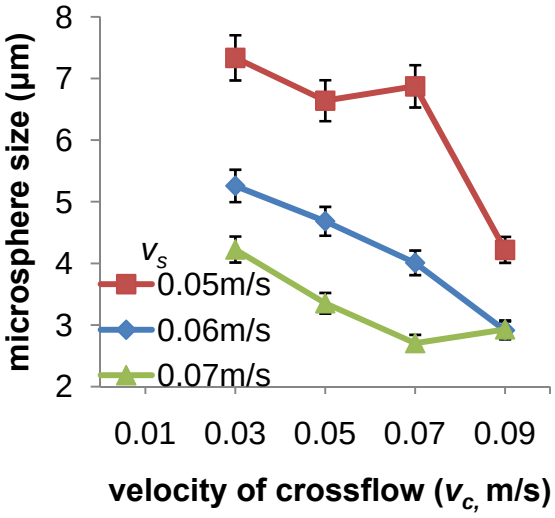

(b) v_f = 0.07 m/s

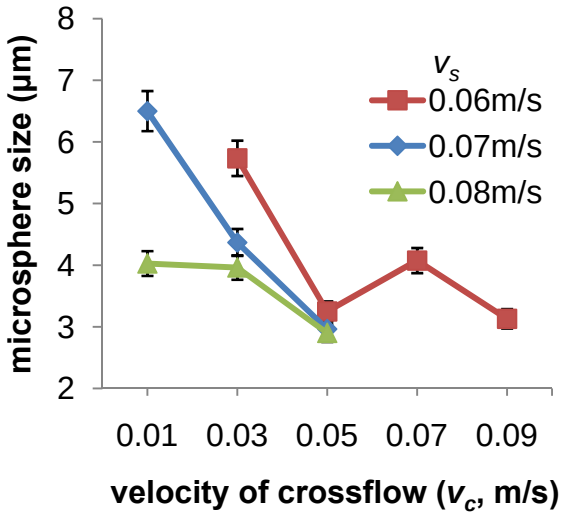

(c) v_f = 0.08 m/s

Figure B. 3 Sizes of the microspheres obtained by varying applied flow velocities, focused flow (v_f), sheath flow (v_s), and crossflow (v_c).

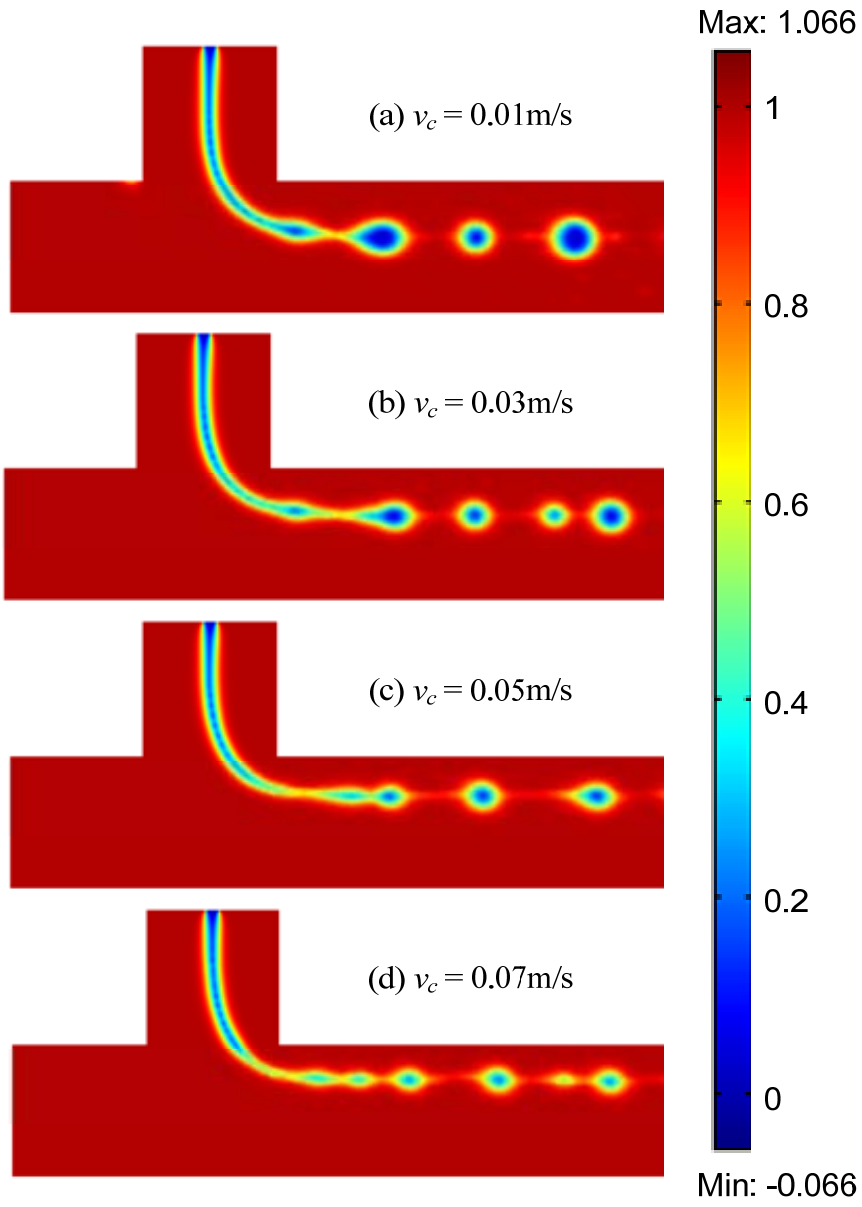

Figure B. 4 Frames of the simulation with $v_f = 0.08\,m/s$ and $v_s = 0.08\,m/s$ showing the generation of the microspheres with different v_c. The color legend indicates the phase of the fluids. (red: oil phase, blue: aqueous phase)

B.2. Modeling and simulation of liquid chopper

B.2.1. Governing equation

Similar to the method discussed in Chapter 5, two immiscible fluids (oil phase and aqueous phase) are introduced to the microfluidic device by inlet pressures for middle flow and sheath flow, respectively. This process will form hydrodynamic flow focusing as shown in Figure B. 5. The width of the focused flow is calculated the same way as Eqn.(B. 7). The focused flow keeps the width without any disturbance before the fluctuating flow is driven by a PZT actuator with a frequency f (Hz).

A commercial computational fluid dynamics package, COMSOL MULTIPHYSICS, was used to perform the numerical simulation for this proposed microsphere formation method, by taking the properties of paraffin oil and distilled water for the continuous oil phase and the dispersed aqueous phase, respectively. This simulation could be simplified by designing the model geometry in 3 dimensions as illustrated in Figure B. 5.

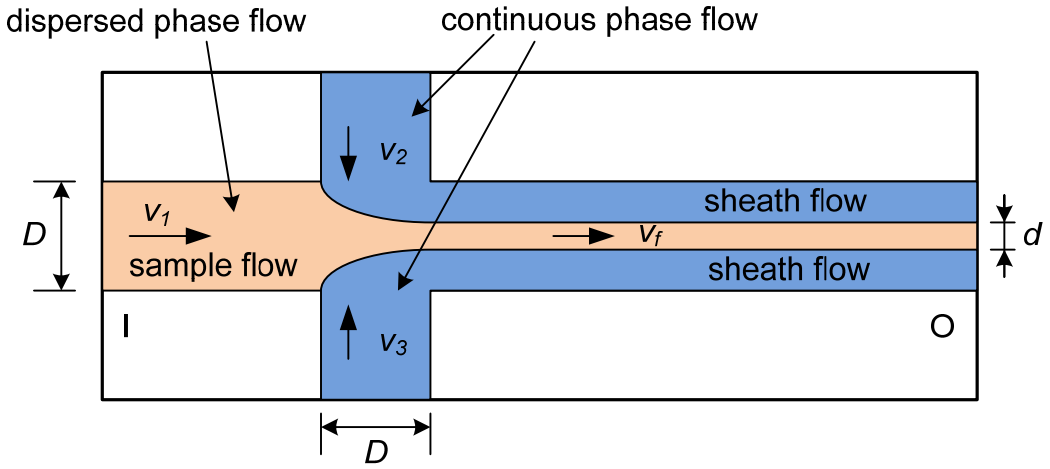

Figure B. 5 Schematic view of the microchannel for hydrodynamic flow focusing at the intersection (A) illustrated in Figure 6.1 (D: width of the channel, v: velocity of the flow, d: width of the focused flow).

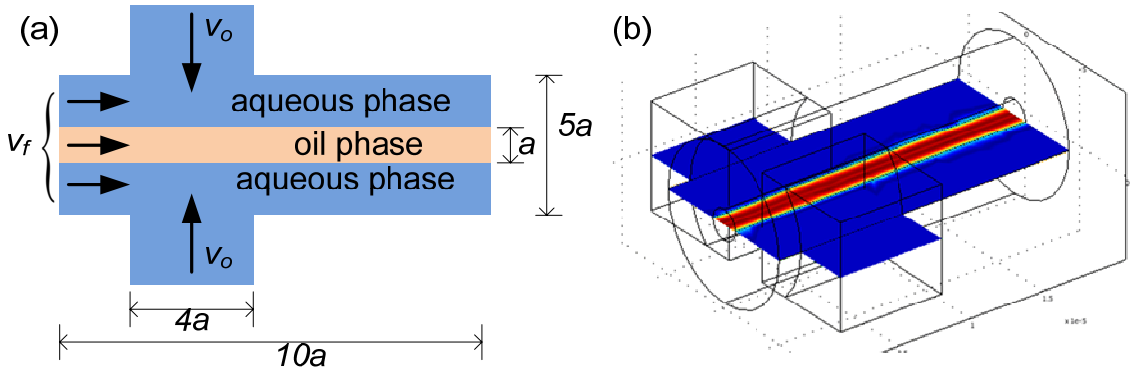

Figure B. 6 Design of microchannel for liquid chopper simulation study: (a) Simulation geometry for droplet formation by a liquid chopper based on a PZT actuator. (b) Cross section view of the 3-D model for simulation.

The flows in the system during the simulation are laminar and immiscible. The aqueous focused flow is the dispersed phase (distilled water), and the oily sheath flow as well as the oscillating flow are continuous phase (paraffin oil) in this study. The intersection area is initially filled with the immiscible fluids, and the properties of the fluids are given in Table B. 1. The governing equation for this method is the same as that presented for integration method. Parabolic velocity profiles were specified at inlets with zero pressure at the outlet. The wetted boundary condition applied to all solid boundaries. The contact angle between the fluid interface and the solid wetted wall is specified as 135°. In reality, it is considered that multiphase flow is one of the most difficult topics in CFD simulation, causing the results of theory and experiment to be not always correct [304]. In order to represent the oscillating flow by the PZT actuator, the velocity of the external flow is defined as

$$v_o = v_f(1 + |Asin(2\pi ft)|) \quad \text{(B. 13)}$$

where A is amplitude, f is frequency (Hz) and t is time (s). The external flow is continuous and propagates the fluctuation, generating instability in the main stream.

B.2.2. **Simulation results and discussion**

The channel was initially filled with immiscible flows which were continuous phase and dispersed phase. Parabolic velocity profiles were specified at inlets with zero pressure at the outlet of the intersection. For the simulation, the width of the focused flow, a, was set to 2 μm, and the velocity of the sheath flow, v_s, is considered as the same value of v_f. These parameters were satisfying $\boldsymbol{FR}_2$ (breakage of flow) by pinching the focused flow when an oscillating flow was fed in. The oscillating flow driven by the PZT actuator had the same property of the sheath flow, oil phase.

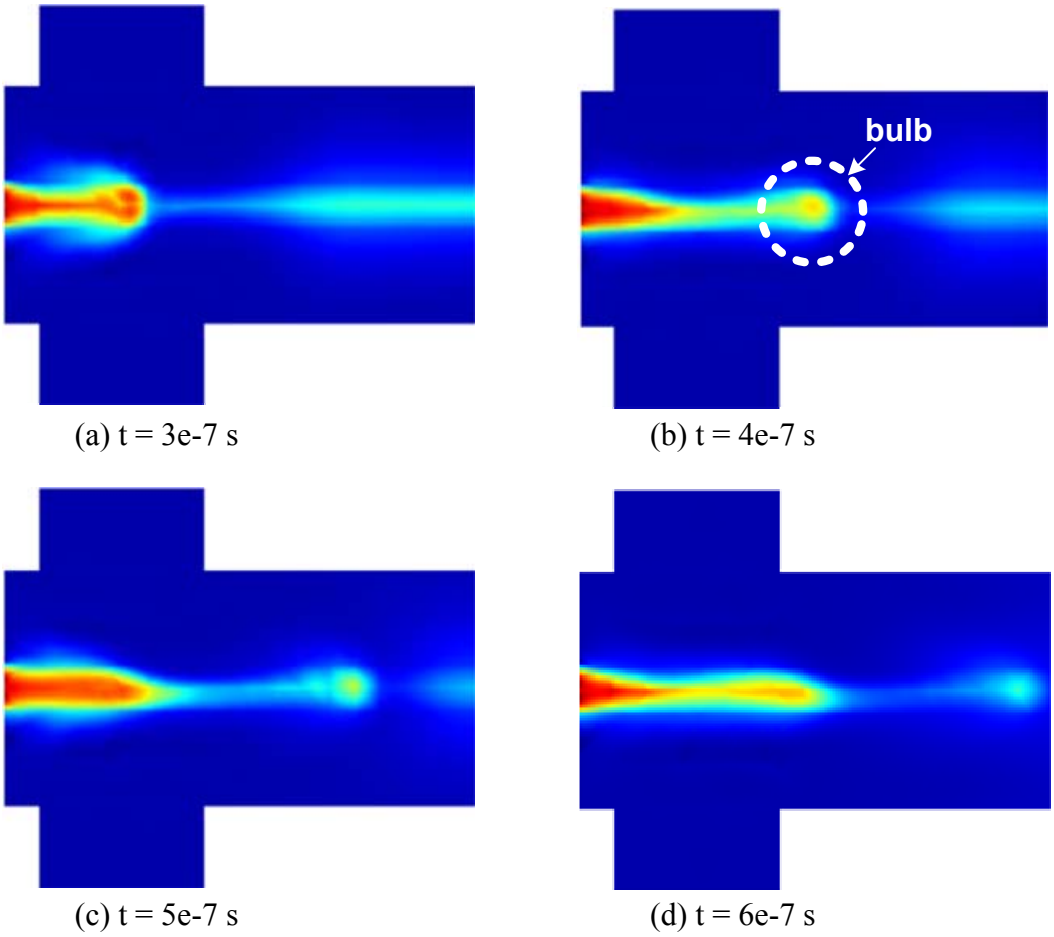

(a) t = 3e-7 s (b) t = 4e-7 s

(c) t = 5e-7 s (d) t = 6e-7 s

Figure B. 7 Snapshots of droplet formation at f = 1 MHz

In Figure B. 7, the formation of microspheres in the microchannel is illustrated at different simulation times. The simulation showed that the external flow was introduced with high pressure to the main stream, and the focused stream was interrupted [Figure B. 7(a)]. Shortly after, the focused flow was squeezed, and an oval shaped bulb produced [Figure B. 7(b)]. The neck of the bulb was pinched off, and the bulb was disconnected from the main focused stream, forming a droplet and traveling downstream [Figure B. 7(c) and Figure B. 7(d)]. This process occurred periodically with highly uniform sizes of droplets. During the periodic droplet formation process, the oscillation transmitted high pressure to the main stream, pinching the neck of the bulb. The formation of the microsphere occurred after the neck of a liquid bulb was pinched off (chopped).

The microsphere formation does not depend only on the applied external force to the flow, but also on the width of the focused flow as well as on the geometry change of the microchannel [305]. However, we only considered the applied fluctuating force generated by the PZT actuator because the width of the focused flow was fixed during the simulation. The size of microspheres by different frequencies of the PZT actuator is shown in Figure B. 8. By varying frequency f from 1MHz to 2.1 MHz, the microsphere sizes were in the range of 1.74 μm to 3.65 μm in diameter with about 2.4% of CV, which suggests that the proposed method achieves controllability and uniformity in the generation of microspheres.

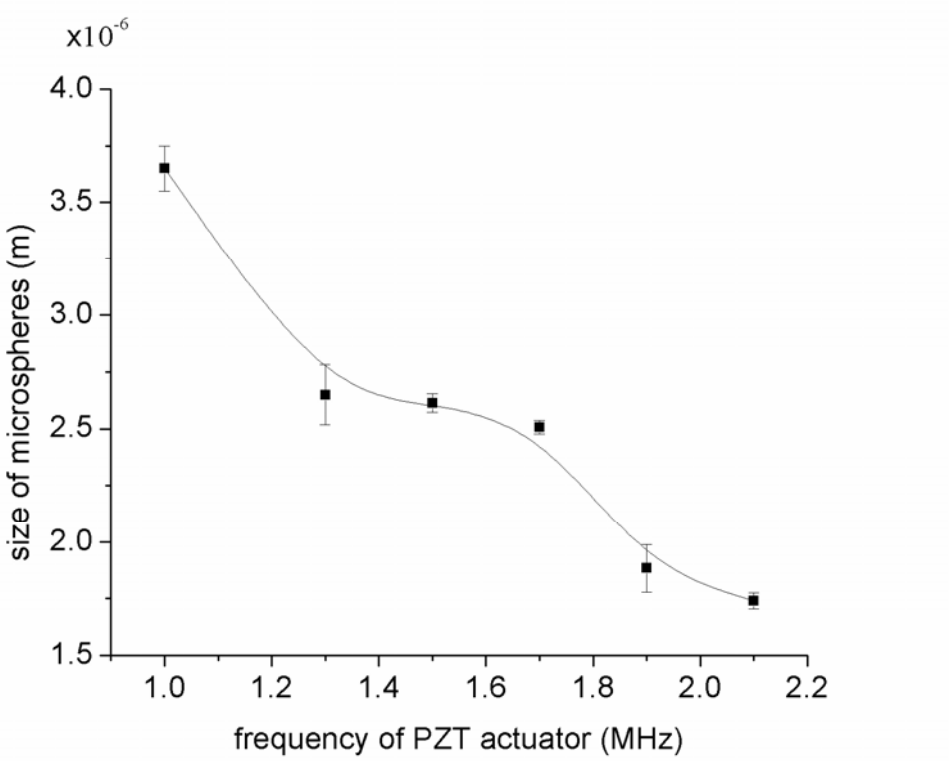

Figure B. 8 Size of microspheres versus the frequencies of the PZT actuator. The solid line is a polynomial fitting line of the sphere sizes indicating a trend of the size change.

APPENDIX C. DETAILED EXPERIMENT SETUP

C.1. ROBO-Pro setting up for Xurography

1. Connect ROBO-Pro to the computer system through a USB port, and turn it on.

2. Place the cutting mat in ROBO-Pro

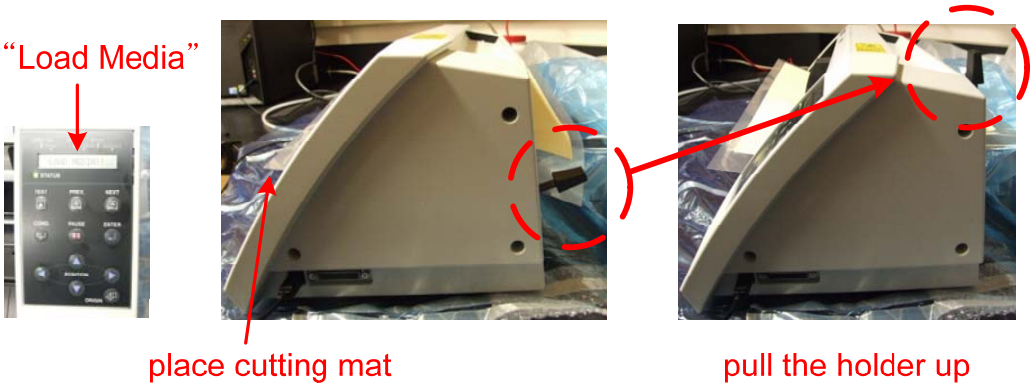

3. Stick a vinyl sheet on the mat and adjust the cutter position


Press 'ENTER' button to locate the cutter at initial origin


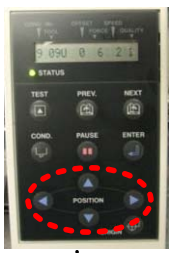


Adjust the cutter position by pressing 'POSITION' buttons,
and press 'ORIGIN' button for new origin

4. Adjust the blade appearance (about 1mm) by rotating the blue handle on the blade case

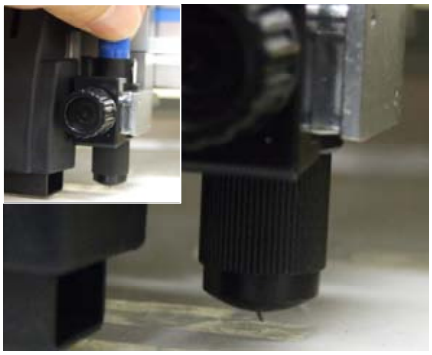

C.2. Xurography by ROBO-Pro

1. Prepare design with AutoCAD: ‘pline’ commend is recommended to draw the designs

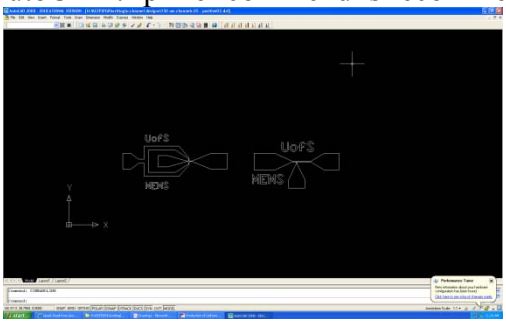

2. Save the design in .DXF format

3. Run ROBO Master-Pro program

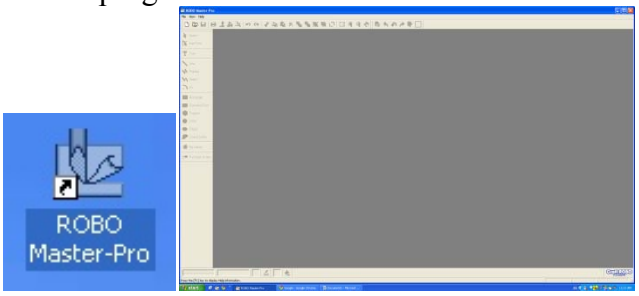

4. Load DXF file (design) and adjust the position

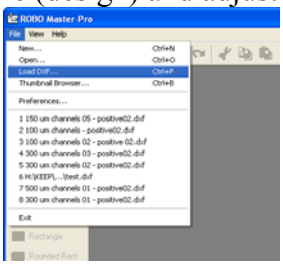

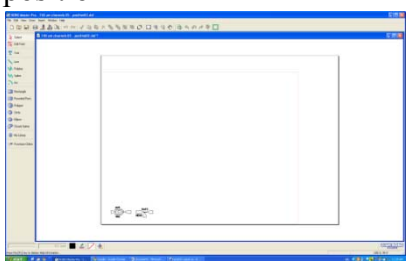

5. Press  (cut) button

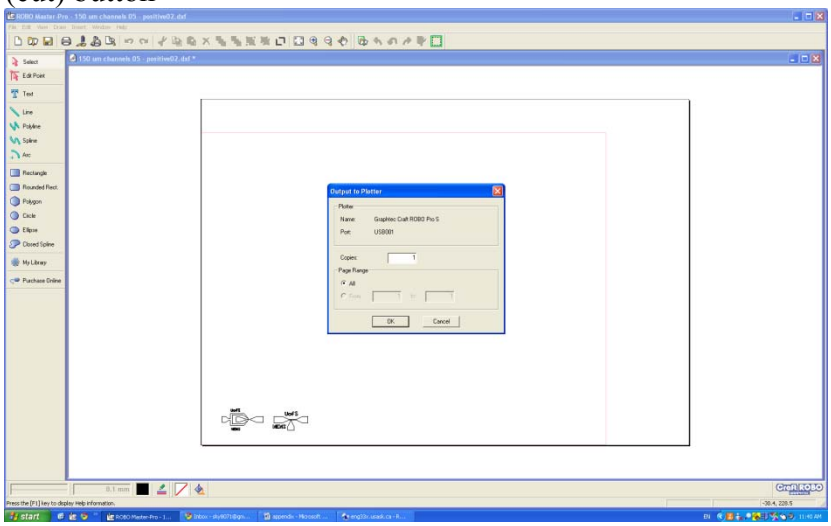

6. Press ‘OK’

7. Press ‘Edit Conditions…’

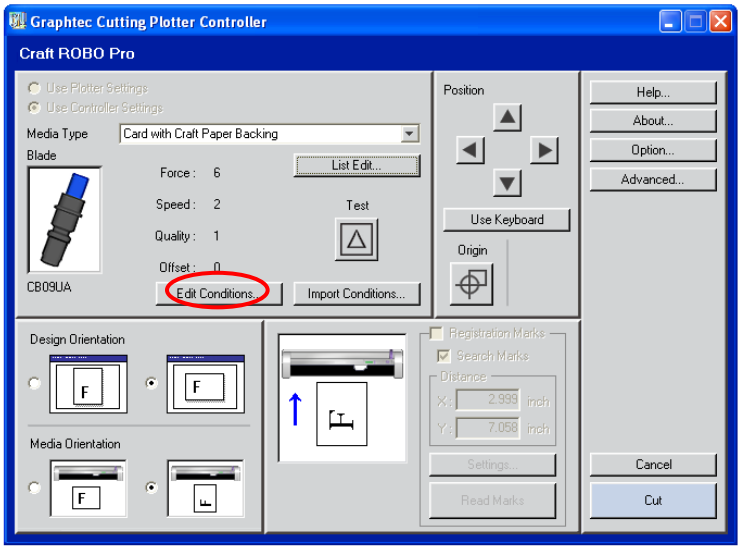

8. Adjust ‘Force’ and ‘Speed’, then press ‘OK’
    a. 10-20 for force, depending on the material
    b. 1-2 for speed (lower speed for better quality)

9. Press ‘Cut’ button for operation

10. Turn off the machine

11. Disconnect the cables

C.3. Taking images and videos from Microscope

1. Cable connections for microscopic images and videos

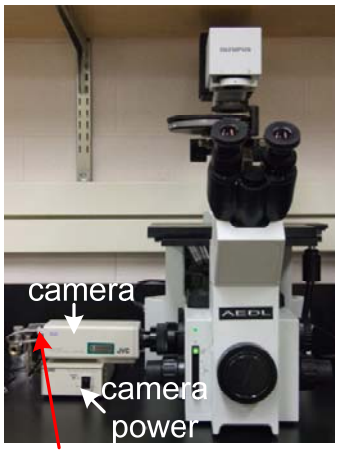

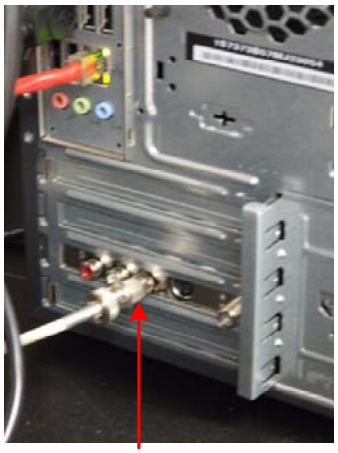

2. Turn on the main light switch on the microscope (back side)

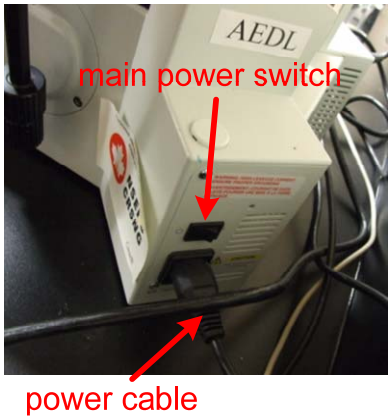

3. Turn on camera view mode by changing view mode (handle on the right side), and push light off indicator (on the left side). The LED of light off indicator will be off, and the light will be on the stage. Avoid too bright light. It damages the camera.

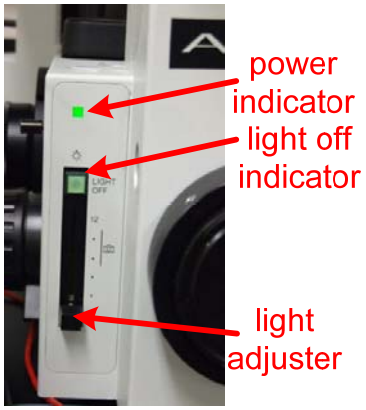

4. Turn on the camera power switch

5. Run AverQuick program in computer

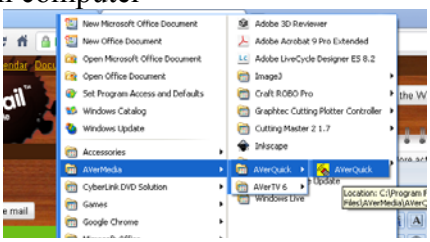

6. Select ‘composite’ video source

7. Select an objective (x5, x10, x20, and x40) for an image

8. Click ‘snap shot’ button after right-clicking mouse. For saving a video, click ‘record’ button.

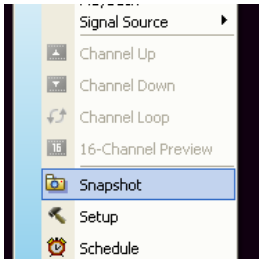

9. Choose ‘save as’ to locate and name the image file

10. Select the options and click ‘OK’

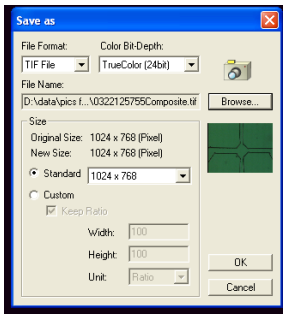

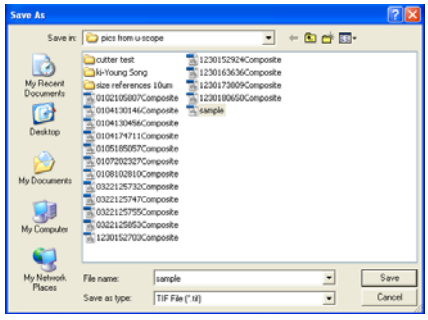

C.4. Measurement

1. Run ‘ImageJ’. It takes some time to run this program.

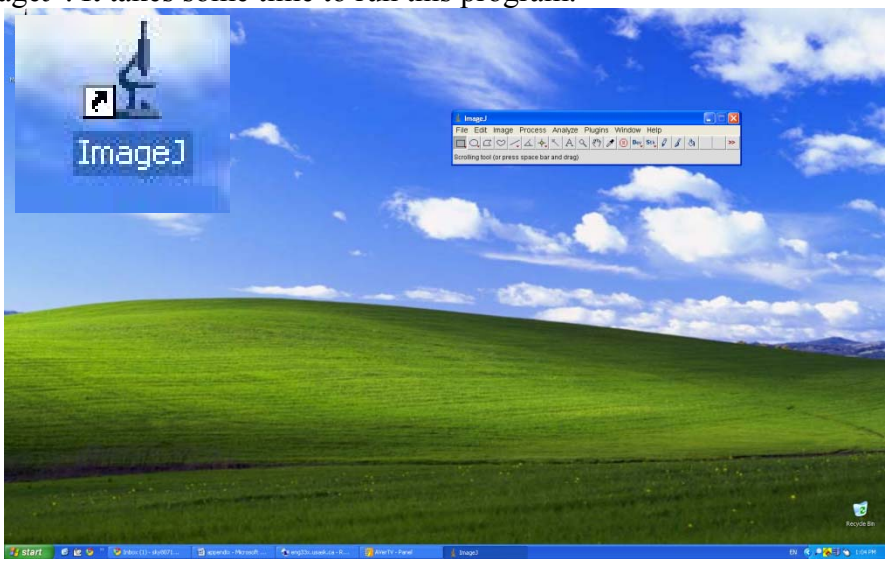

2. Select ‘Scale bar Tool for Microscope’ after clicking ‘>>’ button

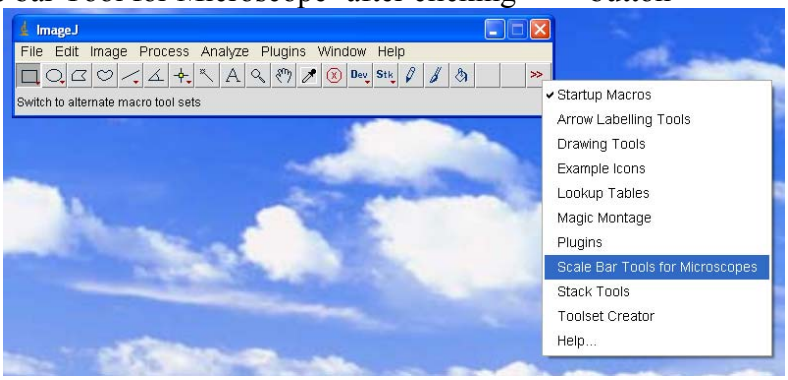

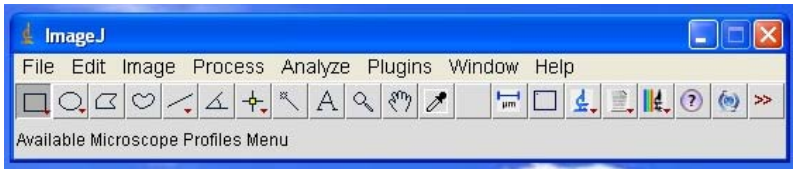

3. Click ‘  ’, then select ‘Olympus 1’ (if you use 1.5x function on the microscope, you should select ‘Olympus 1.5x’)

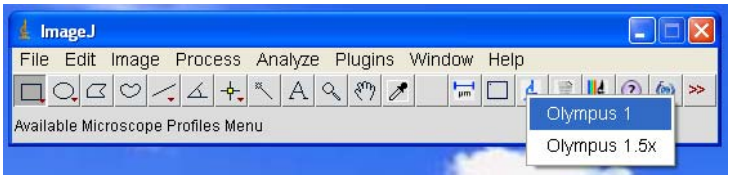

4. Open the saved file

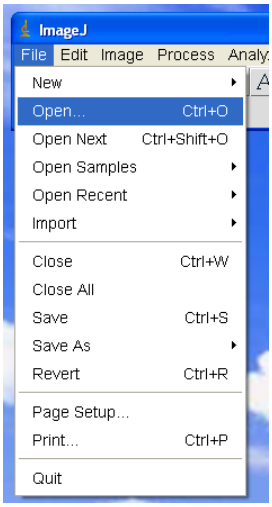

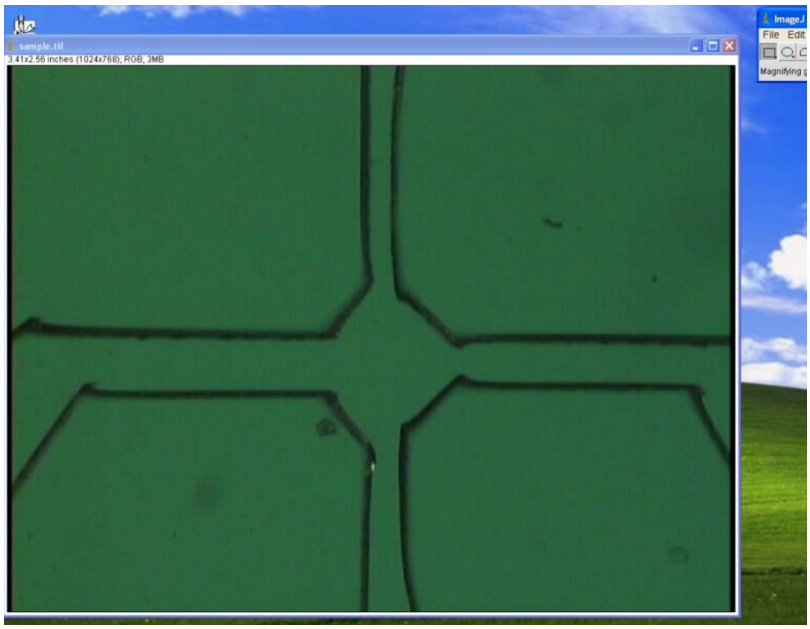

5. Select 'Scale bar' button, and select the objective to take the image (in this example, x5 of objective was used.). Then, 'OK'

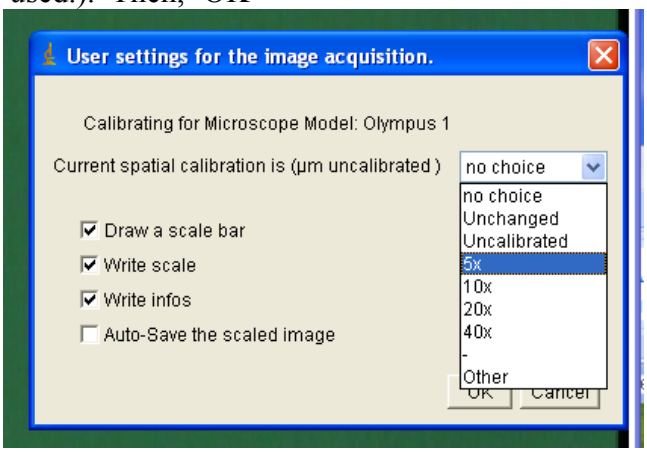

6. Choose scale bar size (In this example, the size of the scale bar will be 50 µm).

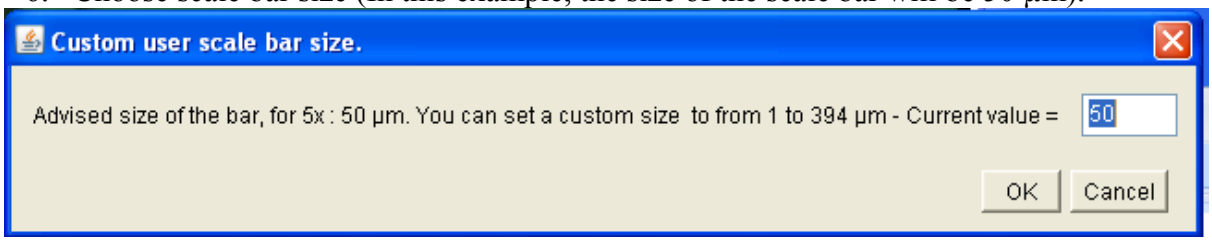

7. Select shapes to measure the object (In this example, line shape was selected)

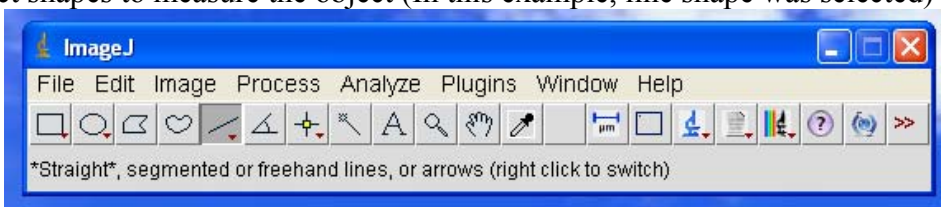

8. Apply the shape by clicking on the image

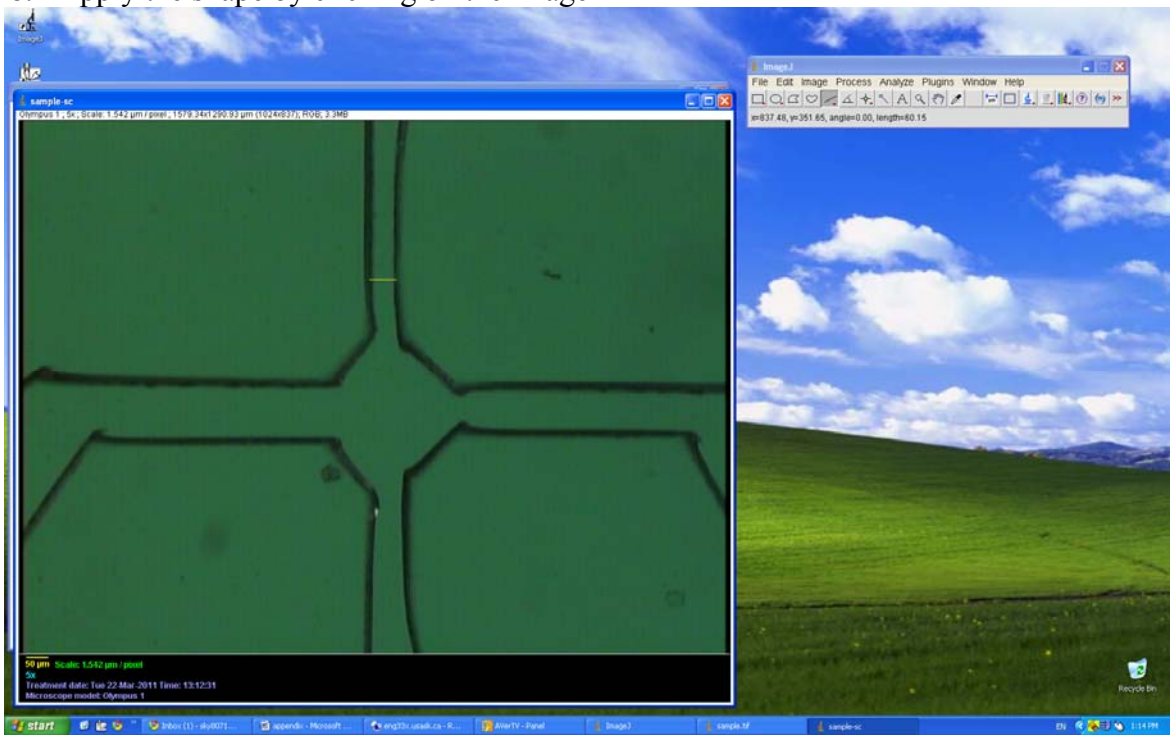

9. Select 'Analyze' → 'Measure' to read the results. In this example, the width of the channel was 60.151µm

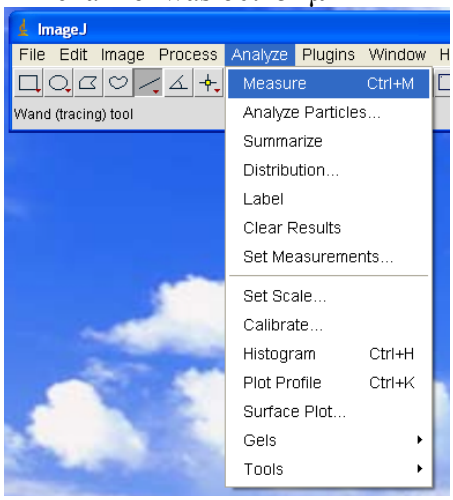

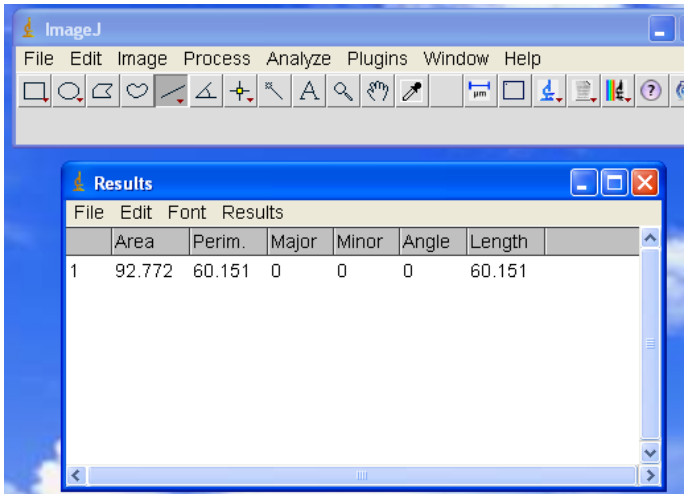

C.5. Connections for Experiment